

**Fine-tuning the properties of
hybrid hydrogels to modulate their
interactions with biological fluids:
A systematic study at different
length scales**

eman ta zabal zazu



Universidad
del País Vasco

Euskal Herriko
Unibertsitatea

2022

Autor:

David Esporrín Ubieta

Supervisor:

Prof. Marcelo Calderón

Tutor:

Prof. José M. Asua

Fine-tuning the properties of hybrid hydrogels to modulate their interactions with biological fluids: A systematic study at different length scales

Thesis submitted to obtain the Doctorate Degree in Applied Chemistry and Polymeric Materials at the University of the Basque Country (UPV/EHU)

By

David Esporrín Ubieta

San Sebastián-Donostia, 2022

Responsive Polymer Therapeutics Group

Department of Applied Chemistry

Thesis Supervisor: **Prof. Marcelo Calderón** (Responsive Polymer Therapeutics Group, Polymat)

University Mentor: **Prof. José M. Asua** (Polymerization Processes Group, Polymat, UPV/EHU)

POLYMAT

Basque Center for
Macromolecular Design and Engineering



Universidad del País Vasco Euskal Herriko Unibertsitatea



*A mi familia, amigos y en especial a
Teresa, por el apoyo constante durante
estos cuatro años*

“Nobody ever figures out what life is all about,
and it doesn't matter. Explore the world. Nearly
everything is really interesting if you go into it
deeply enough”

- Richard P. Feynman

Acknowledgements / Agradecimientos

Podríamos definir una tesis doctoral como una montaña rusa de emociones sumada a una carrera de fondo. No solo hay que aguantar de manera constante durante unos 3 – 4 años, sino que además se suman las grandes frustraciones que tienden a reiterarse cada cierto tiempo. No obstante, tras meses dándote contra una pared, los experimentos acaban funcionando, lo que te genera un éxtasis de emoción que engancha. Desde luego, si hay una cosa clara, es que todas estas sensaciones que hacen que un día estes en lo más alto y otro a nivel del suelo, no hay persona que pueda soportarlo por si mismo. Toda la tesis doctoral que se va a detallar a lo largo de las siguientes páginas es fruto de haber estado rodeado tanto cerca como lejos de las personas más maravillosas del mundo. Su constante apoyo, su capacidad de transmitirme alegría y hacerme seguir adelante ha dado como fruto que haya podido concluir este trabajo. No me cabe la menor duda de que, de haber estado solo, no habría aguantado ni el primer mes! Por ello, todas estas personas se merecen una mención, pues una parte de esta tesis doctoral les pertenece. Estamos acostumbrados a ver charlas en diversos ámbitos en las que la diapositiva final muestra al conjunto de personas que han trabajado duramente en sacar esos resultados adelante. Sobre el escenario, una persona hablando unos minutos, detrás de cada gráfica, el sudor de mucha gente. Esa diapositiva final termina siendo la más importante, pues sin ella, no habría charla, no habría ciencia, no habría desarrollo. Aquí ocurre lo mismo, el trabajo que se va a relatar a continuación es la suma de muchas colaboraciones y de infinitas horas de discusiones científicas con investigadores seniors. Pero, sobre todo y más importante, es el resultado alcanzado de haber recibido un grandísimo apoyo, amistad y amor por parte de muchos amigos, familia y compañeros.

En primer lugar, quiero dar las gracias a mi supervisor y mentor, el Prof. Marcelo Calderón. A **Marcelo** tengo que agradecerle el haberme dado la oportunidad de formar parte de su grupo actual y pasado. Tras un paso excepcional por Berlín, el grupo cambio de rumbo para situarse de manera permanente en Polymat, San Sebastián. Y como “primera” tesis de esta nueva década, he tenido el placer de haberla empezado en Berlín y haber podido conocer a los que me precedieron. Por todo ello, quiero darte enormemente las gracias. Me has permitido crecer como persona, trabajar unos meses en el extranjero, aprender algo de ciencia y sobre todo aprender mucho sobre gestionar la vida en general. Muchas gracias por haberme guiado a

comprender que es la ciencia, haberme permitido llevar adelante los proyectos y hacerlos míos dándome una gran libertad en el laboratorio y en las reuniones con los colaboradores. Gracias también por haber depositado tu confianza en mí a la hora de emprender un nuevo camino en otro país. Así como dejarme conocer de primera mano cómo se piensa la ciencia, como se plasma en un papel, como una idea de un café acaba siendo financiada y como gestionar de manera coherente el dinero de un laboratorio, en el que las cantidades a manejar acaban siendo desorbitadas... Jamás pensé poder sacar tanto conocimiento extra de una tesis, la cual me será muy útil en mi futuro tanto profesional como personal. Finalmente, muchas gracias por todas las reuniones científicas durante estos 4 años, desmenuzando los resultados, así como haber revisado y mejorado el manuscrito de esta tesis.

En segundo lugar, tengo mucho que agradecer a **Ana Beloqui**, que se nos unió al grupo con sus propias líneas de investigación en el aniversario de nuestra llegada a Donosti. Muchas gracias, primero de todo, ¡por haber traído dos UV-VIS al labo! Era una autentica tortura trabajar con NPs en el equipo del Korta, modelo que data del mismo año que la primera piedra que se puso al levantar la facultad de química. Y ahora hablando en serio, tengo que agradecerle Ana la cantidad de horas que hemos hablado en el laboratorio sobre ciencia y carrera científica. Muchas gracias por haber compartido en reiteradas ocasiones tu experiencia profesional conmigo, me ha permitido conocer más de cerca la realidad que nos rodea y el foco de los problemas. También agradecerte tus consejos sobre cómo enfocar entrevistas, cover letters, etc, me han hecho mejorar en muchos aspectos tanto a nivel profesional como personal. En la parte científica, agradecerte el grandísimo apoyo, sobre todo en las etapas iniciales y discusión de resultados ya maduros del capítulo 3 de esta tesis. Tus conocimientos y gran experiencia en polimerizaciones han sido imprescindibles para que ese capítulo haya existido. Te agradezco enormemente las horas que me has dedicado tanto en discusiones de resultados como en trabajo experimental cuando las reacciones nunca salían... y al igual que a Marcelo, muchas gracias por haber revisado parte de este manuscrito y haber contribuido a su mejora! *Eskerrik asko!*

Neha & Tracy, my partners in crime since day 1! I have so so so many things to thanks to you two! First of all, you have seen with me how much desperate can be to go day after day to the lab and... there is no lab! And like that for around half a year! Quite crazy! Anyway, thank you so much to you two for the enormous support during the worst and best moments! Without you two I would have quit the PhD for sure! **Neha**, with your great research

experience, being an extraordinary mentor and friend for us make it possible that today I am finishing my PhD. **Tracy**, your inexhaustible positivism has made us all happy day after day. It is extraordinary to see how you face everything in life! I have learned a lot from you. I couldn't have had a better thesis partner/friend! Thank you so much to you two and see you soon in India and China! 非常感謝

Cata, muchas gracias por haber sido la primera cara de mi tesis y haberme dedicado los últimos 3 meses de tu postdoc. Tengo que darte millones de gracias por haber asentado en mí las bases de lo que luego se ha convertido en esta tesis. Por enseñarme que es un nanogel, como se prepara, cómo se encapsula plata... irradiar con un láser... y que es eso de jugar con imanes y que las partículas te sigan! Pero, sobre todo, millones de gracias por haberme acogido tan sumamente bien en Berlín! La verdad es que llegué bastante desubicado, fueron muchos cambios que transcurrieron como un pestañeo. Pero ahí estabas tú para acogerme, invitarme a vuestras quedadas, cenas, lo que es un buen asado argentino, lomititos y el mate como forma de vida! Fueron 3 grandes meses que nunca olvidaré. Muchas gracias también por haber seguido formando parte de mi vida después de ese tiempo. Irme preguntando como iban las cosas, la tesis, la vida... en fin, muchas gracias por todo! Sin duda eres un ejemplo a seguir de superación, persistencia y aguante, y no me cabe la menor duda de que conseguirás todo lo que te propongas! Y ojalá pueda estar ahí para compartir tus éxitos contigo!

Siguiendo con Berlín, también tengo que agradecerles mucho a **Lucila** y a **Mati**. Ellos también me acogieron y compartieron muchos momentos conmigo, desde el festival de las luces, pasando por comer juntos todos los días hasta cenas asiáticas. Muchas gracias por haberme acogido tan bien y haberme hecho sentir como uno más desde el minuto 0. Fue una auténtica suerte habernos cruzado en el camino con vosotros. Unos científicos excepcionales de los que también aprendí mucho y unas personas maravillosas. Con Mati he tenido la suerte de reencontrarme en la etapa final de la tesis, y espero que no sea la última. Con Lucila, aún lo tengo pendiente, pero seguro que volvemos a vernos! Mientras tanto, no me cabe la menor duda de que os seguirá yendo todo genial!

Ana Sonzogni, o más conocida como "Anisha". Creo que yo y todos los que estuvimos en el labo en la época de tu estancia en Donosti tenemos que darte las gracias por la positividad que transmitías. Llegaste al grupo en un momento delicado con los ánimos un poco bajos y supiste sacarlo a flote! La positividad y energía que llevas siempre contigo es digna de admirar, si todos

fuéramos un poquito más como tú, el mundo sería un lugar mejor. Muchas gracias por haber sido la “experta” del grupo en hidrogeles. A ti te debo la existencia del capítulo 4 de esta tesis! Muchas gracias por haberle dado forma conmigo, por la cantidad de horas y reuniones para asentar las bases de lo que hoy es y de lo que mañana serán esos parches oculares! Gracias por haber sido una investigadora de 10 y haberme transmitido tu forma de ver la ciencia y enfocar proyectos. Igualmente, muchas gracias por haber revisado los borradores del artículo de hidrogeles, cuyo parte del texto ahora forma esta tesis doctoral! Gracias por haber sido compañera de trabajo y amiga! Y por el apoyo durante todo este tiempo.

A **Dani** quiero agradecerle los grandes momentos que hemos pasado dentro y fuera del labo! Desde pasarnos horas delante del HPLC sin entender ninguno de los picos que veíamos, hasta hacer un brainstorming de un material que casi se ve a escala macroscópica (fancy para una ERC pero coagula en la sangre nada más pincharlo). Y sobre todo pasando por grandes cenas, fiestas, granada... También quiero agradecerle el que haya estado ahí en algunos de los peores momentos de mi tesis, tendiéndome su mano y recordándome que tras un día viene le siguiente. Si hoy las cosas no salen y el mundo parece que se acaba... al día siguiente se vuelve a intentar y listo! Gracias por el apoyo constante y te veo por en algunos cafés del TEM a media noche.

Irene, que llegó como un soplo de aire fresco para el labo, enseguida (esta mesetarian) se convirtió en una más que parecía que llevaba ahí desde los inicios. Con su energía incansable, puso el labo “patas arriba”, pero ese soplo de novedad y energía han sido decisivos para juntarnos más, hacer más planes juntos, mejorar la convivencia y hacer el día a día más bonito y llevadero! Quiero agradecerte enormemente la ayuda durante mi último año de tesis, en lo profesional y más aún en lo persona, y que me haya aguantado mientras hacía electroforesis... también los grandes momentos vividos (culminando con el concierto de Fito en San Mamés! Y todos los que nos quedan por vivir! Una lástima no haber coincidido más tiempo en la tesis, pero no me cabe duda de que te irá genial y que seguiremos en contacto para celebrarlo juntos (hay que seguir creando historias)!!

To **Maria Angela**, *grazie mille per il tuo supporto in questi anni*. It has been a long way in which your foot has suffered a “little bit”. Thank you so much for being a very great support during this journey, Mary. For the long conversations and effort to make every day a little bit better. Also thank you a lot for feeding us with so many desserts, for the dinners, trips along the

mountain/sea, Granada and the coming ones! It has been a pleasure sharing this time with you!

A **Jakes**, te vi llegar como un TFM a un laboratorio que no terminaba de arrancar y en nada vas a ser doctor! El tiempo vuela, y no me sorprendería que un día consigas curar el cáncer! Muchas gracias por tu grandísima predisposición a ayudar desde el minuto uno, por las innumerables series comentadas en el labo. Por haber creado historias con fotografías, escapadas a conciertos planificadas en pocas horas, cenas y las que estén por venir! Ha sido un auténtico placer haber compartido todos estos años contigo y todas las charlas que hemos tenido. Tu apoyo en los momentos buenos y no tan buenos, han servido para seguir tirando hacia delante. Gracias por haber estado ahí desde el inicio y por el apoyo constante que me has dado. No tengo duda de que te va a ir genial y espero que podamos seguir creando historias con cada celebración que venga! *Eskerrik asko!*

Podría decir que a **Andoni** le debo la mitad de las caracterizaciones de esta tesis! Ya que ha sido la persona que me ha abierto las puertas de Nanogune, que tiene más equipos de los que alguien puede siquiera recordar! Quiero agradecerte tu gran predisposición siempre a ayudar! No solo es eres un científico brillante, sino que además eres una grandísima persona que está dispuesta a echarte un cable en cualquier situación, ya sea medir un FTIR, enfocar el SEM o aparecer en el momento clave para mover a pulso a Dani! Gracias por la semana de oro en Granada y la resaca a la vuelta! *Eskerrik asko!*

Nikos ha sido mi gurú en la vida personal, científica y cinéfila. Tengo que agradecerte la cantidad de series vistas y comentadas durante todos estos años así como la guía por los mejores restaurantes donostiarras! También agradecerte mucho que hayas compartido tus experiencias profesionales conmigo, gracias a ti he aprendido y reflexionado mucho sobre el mundo académico y gastronómico! Espero que disfrutes mucho de las mesoporosas, del liofilizador y que te acuerdes de alimentar a los conejos en mi ausencia! Te deseo lo mejor siempre. Muchas gracias por haberme apoyado todos estos años, ha sido un gran placer contar contigo! Nos vemos de visita por alguna isla griega. *Ευχαριστώ πολύ*

Sole se nos unió hace poco más de año y medio. Me habría encantado compartir contigo todos los momentos de la tesis, eres una persona increíble y una gran profesional! Lo bueno de este trabajo es que siempre te pone al lado a gente maravillosa y de la que se aprende siempre mucho, como tú! Gracias por habernos guiado, ayudado y orientado en los momentos buenos y en los no tan buenos! Y, sobre todo, por hacerlo siempre con una gran sonrisa

y dedicación. También por haber luchado a mi lado intentando que el oro penetre tejidos de animales!

To **Oli**, thank you so much for being part of any plan, hiking, dinners, night parties, house party, bbq...he has contributed a lot to “make stories” from this period, which has been extraordinary to enjoy the PhD life! From the professional part, thank you a lot for printing the device! And for doing sooo many trials until we got it! Kinetic release from chapter IV has been possible thanks to you! Thank you so much for your general support! *Vielen Dank*

A **Brunito**, yo y todos, tenemos que agradecerle su buena onda constante! Es una maravilla hacer cualquier cosa con este chico que hasta desde la otra punta del mundo te manda una postal porque se acuerda de nosotros! Muchas gracias Bruno por las medidas en Biomagune, por tu buena predisposición siempre ha ayudado y los grandes momentos vividos de sidrería, cenas, y los que nos quedan por vivir! Próxima parada: casa rural! *Merci beaucoup*

A **Pablo**, tengo que agradecerte las grandes conversaciones en el labo sobre la vida y la ciencia. Hablar con alguien que lee tanta bibliografía como tú siempre te hace ver el foco del problema, y es algo que todos deberíamos aprender. Pero, sobre todo, muchas gracias por los grandísimos momentos que hemos vivido hace nada en Granada! Has hecho de ese vieje un recuerdo imborrable contribuyendo a rebajar el estrés final de la tesis! Muchas gracias! *Eskerrik asko!*

A **Sandris**, esta grandísima persona llegó al labo en los meses finales de mi tesis... ojalá hubiéramos podido coincidir antes, pero el constructo espacio-temporal de la sociedad no nos lo ha permitido... Muchas gracias por haber construido historias juntos! Por apuntarte a todos los planes, ya sean cerves playeras, concierto exprés o escapadas rurales! Pero, sobre todo, por contribuir al conocimiento cultural (nunca antes se sabía que la sidra se guarda en recubrimiento de queso). Ahora sé que las fake news las dejo en buenas manos. Conocer gente nueva es uno de los mayores regalos de la ciencia, te hacen crecer como persona, y tu llegada ha sido uno de esos grandes momentos. Gracias por tu apoyo en estos meses y espero que podamos seguir compartiendo cervecitas con esta pequeña gran mesetarian.

A **Garazi**, la mayor fan del liofilizador! Aunque nos hayamos conocido en estos últimos meses y no hayamos podido compartir mucho tiempo juntos, es un gran placer charlar un rato cada vez que nos encontramos! Gracias por preguntarme como iban las cosas en estas últimas semanas críticas y por las

cervezas playeras entre perritos a los que quieres muchísimo! Espero que a partir de ahora podemos crear muchos más momentos y cuadremos los futuros congresos para reencontrarnos! *Eskerrik asko!*

A **Sergio**, ha sido un gran placer conocerte, aunque haya sido en los meses finales de mi tesis. Sin embargo, en el poco tiempo que hemos coincidido hemos podido tener unas muy buenas conversaciones en las que compartimos muchos puntos de vista. Sin duda he aprendido mucho de ti en este corto periodo, tanto de biología, como de ciencia y a nivel personal. Muchas gracias por tu apoyo y ayuda desde que nos conocimos!

Me gustaría agradecer también a **Marcos**, por los buenos momentos de cenas caseras entre pizzas y pollo al curro, y conversaciones poliméricas.

A **Oihana**, muchísimas gracias por todos los consejos que me has dado durante este tiempo. Todo el mundo debería tener un doctorando mayor que le ayude a entender como son las cosas, y eso has sido tu para mí. De ti he podido aprender de donde se saca la fuerza para superar las adversidades y tengo que agradecerte que hayas estado siempre ahí para echarme una mano. Ya sea para dejarme un destornillador, ayudarme con el papeleo, tomar un café o hablar sobre la vida. Has hecho mi camino más fácil y una parte de esta tesis te la debo a ti (además de por haberme enseñado que es la fisisorción). Para mi has sido un gran ejemplo como investigadora y como persona y eso ha sido una gran ayuda en el día a día. *Eskerrik asko!*

Muchas gracias a todos los colaboradores que con su trabajo, dedicación y múltiples reuniones científicas han contribuido al desarrollo y calidad de esta tesis doctoral. **Nora, Merche, Itxaso, Alejandro, Eider, Ruth, Aitor, Arantxa y Ayla**. Quiero agradecer también a todos los expertos en microscopías que tantas horas han pasado frente a los equipos para caracterizar algunas muestras de este trabajo: **Loli** (en la parte de AFM, DSC y TGA), **Ana** y **Maite** (en la parte de TEM). Muchas gracias también a **Oihane**, por haberme enseñado un poquito de ingeniería con la fisisorción y habernos ayudado en el montaje del laboratorio bajo el papel de proveedor oficial de ferretería. Quiero agradecer también al **Prof. Asua**, por formar parte de esta tesis en carácter de tutor, facilitando la parte burocrática con la universidad.

Quiero agradecer a mis compañeros del pisito pepito (**Jose y Elena**) por haber sido los mejores compañeros de piso que alguien puede tener durante su tesis! Por las grandes series que hemos compartido (descubriendo Community). Por las frustraciones investigadoras compartidas y las grandes divagaciones sobre el universo (nunca es buena idea juntar a 3 doctorandos

en un mismo piso). Sobre todo, tengo que agradecerles su apoyo durante toda mi tesis y que hayan soportado mi mal humor cuando no deja de llover en Donosti durante infinitos días! Gracias por todo amigos!

Todas las etapas de la vida vienen precedidas de unos pilares sólidos. En mi caso, esos pilares han sido el paso por el grupo NAP. Hay una serie de personas que marcaron de forma muy importante el rumbo que tomó mi vida profesional, y en parte, que esta tesis lleve mi nombre también es gracias a ellos.

A veces en la vida hay que tomar caminos que nos alejan de las personas pero que nunca se van de tu vida! Yo en esa vida personal y científica he tenido la maravillosa suerte de encontrarme con **Héctor**. A él tengo mucho que agradecerle, lo primero que me haya enseñado como se trabaja en un laboratorio, ya que tuve la suerte de estar codo con codo con uno de los mejores (si no el mejor) químico de mi tiempo. Los que lo conocemos sabemos que le espera un futuro brillante y yo me siento muy afortunado de haber aprendido de él. Muchas gracias por las horas que me has dedicado durante el TFG y TFM, muchas gracias por haber seguido ahí después. Con nuestras charlas filosófica para “arreglar el mundo” tanto a nivel personal como profesional. Pero, sobre todo, tengo que agradecerle que sea una de las personas que más papers me ha enviado en la vida (creo que ni los editores leen tantos artículos como él!) así como recomendado grupos/IP, etc. Sin duda una gran parte de mi éxito, pasado, presente y futuro se la deberé siempre a él. Eres una persona admirable y un ejemplo a seguir para todos. Ojalá la vida vuelva a ponernos algún día a trabajar juntos, y ojalá siempre te vaya tan bien como hasta ahora y yo esté cerca para celebrar tus éxitos contigo!

A **Sonia García** tengo muchísimo que agradecerle! Si bien nos unió la qifi y nos hicimos amigos durante el TFG, tengo que agradecerle que nunca haya dejado de estar ahí! Es una de esas personas que aparecen en tu vida de repente y que no quieres que se marchen nunca! Nuestras largas horas de conversaciones sobre la vida, estar siempre actualizados mutuamente, aunque nos veamos poco, pero que llegue el verano y siempre saquemos tiempo de pasar unos días juntos es lo que más se agradece. Muchas gracias por haber sido un gran apoyo durante todos estos años y habernos enseñado a todos como se afrontan situaciones realmente difíciles, todos hemos y seguimos aprendiendo mucho de ti! Por todos los que quedan por venir! Todas esas quedadas anuales se las tengo que agradecer también a **Víctor**, ya sean para escalar picos, esquiar o... comernos un chuletón donostiarra (que todavía queda pendiente).

Teresa Sierra, mi querida amiga exiliada de zgz al país vasco. Tengo que agradecerte el apoyo durante todos estos años, el que nos hayamos ido a ver mutuamente Bilbo-Donosti, excursiones (aunque nos perdamos) y skypes infinitos (que siempre es mejor que una llamada por tfn, no?) Pese a que por horarios casi no coincidíamos en el labo, muchas gracias por haber formado parte de mi vida durante y después! Las penas investigadoras compartidas, son menos penas! Y compartirlas contigo es un alivio!! Siempre nos quedarán los cafés para que te eches unas risas de Carrefour y las actualizaciones por audio de whatsapp casi semanales! Mucho ánimo en el final de tu tesis! Seguro que va todo genial, y quien sabe... igual coincidimos en algún postdoc! Quedan pendientes varias cervezas, así que tendrás que venir a verme pronto!!

A **Marieta y Eva** tengo que agradecerles mucho durante la etapa en NAP. Pese a que a **Maria** le costó medio año saber quien era yo, terminamos siendo muy buenos amigos! Siempre nos quedarán esas charlas filosóficas sobre la vida y que camino seguir! A **Eva** tengo que agradecerle el apoyo durante todo ese tiempo en el labo y que fuera la única persona del mundo en leerse los boletines informativos de unizar! Gracias a eso nos enterábamos de todas las becas. Esperemos que pilares vuelva a unirnos este año!!

Rafa y Scott, a vosotros dos tengo que agradecerlos muchísimo que me dierais la oportunidad de formar parte del labo en uno de mis peores momentos académicos. Muchas gracias por haber apostado por mi y darme esa plaza! Gracias por haberme guiado en mi TFG y TFM, enseñado y asentado las bases de lo que ahora culmino con esta tesis. Sin todo lo que aprendí sobre inorgánicas y polímeros, y como es realmente un laboratorio de investigación, nunca habría llegado hasta aquí. Os deseo lo mejor en el futuro y tal vez la vida nos lleve a una colaboración algún día!

Como en verdad esta tesis doctoral supone el fin de una etapa no de 4 años, sino de 10, que empezó en 2012. También tengo que agradecerles toda esta evolución y haber estado a mi lado a mis grandes amigos de la carrera.

A **Isaac** por las innumerables llamadas por teléfono y las visitas exprés cada vez que me exilian, ya sea en Alemania o en el País Vasco, ahí está él. Siempre nos quedarán historias para seguir flipando amigo! Desde el día que nos conocimos ha sido un autentico placer haber contado contigo, ya van unos cuantos años y seguirán quedando otros tantos más! Muchas gracias por el apoyo durante todos esos 10 años (que se dicen pronto), las frustraciones compartidas cuando salían las notas y levantarlas con unas cervezas, san pp, veteri, conciertos fugaces a horas de depositar y las que vengan!

A **Pablo**, gran músico, mejor persona! mi compañero de fatigas y horas interminables de biblioteca, sufrimientos y alegrías! Muchas gracias amigo por haber estado ahí desde el principio y seguir! Siempre has sido un referente de lucha y constancia del que todos hemos aprendido muchísimo. Me has hecho alegrarme de tus éxitos más incluso que si fueran míos. Gracias por la cantidad de exámenes compartidos, por haber estado en las duras y en las maduras!

A **Javi**, la vida nos unió en Zgz y nos va reencontrando en Barcelona. Muchas gracias amigo por estar siempre ahí, por hacerte varios Km solo para tomarnos un café. Por las alegrías vividas durante la carrera, por no fallar nunca a la llamada Soriana, sanpp, veteri, conciertos de Fito... por todos los momentos vividos compartiendo alegrías y por haber estado siempre en los momentos malos! Gracias por tu apoyo durante todos estos años. En particular, agradecerte tus conocimientos en síntesis orgánica avanzada, gracias a los cuales pudimos calentar lo que había que enfriar.

A **Torcho**, que aunque siempre tiene la cabeza en mil sitios y verlo es realmente difícil, nunca falla en las importantes! Gracias por las largas horas en magisterio, fuego, etc. Por las escapadas a cerradura, sanpp, y apariciones estelares en la cuca! Gracias por la visita donostiarra para reencontrarnos! Por haber estado siempre en los momentos buenos y no tan buenos! Y habernos enseñado a todos que, pese a las adversidades de la vida, siempre se puede encontrar un motivo para sonreír.

A las tres mellizas, **Marina, Amelia y Pili**, que aunque nos veamos de vez en cuando parece que la vida no pasa cada vez que nos reencontramos! Gracias por el apoyo durante estos años y durante toda la carrera! Los penas vividas edulcoradas con un poquito de ron soriano, sanppero y cucarachero! Además, a Marina le quiero agradecer los grandes momentos que hemos pasado en Donosti en los 2 años que lleva ya aquí! Desde los desayunos en Ñam, hasta los días de playa, sin olvidarnos del día que por fin logramos ir al acuario a ver al tiburón!

A **Vanesa**, mi hermana en la química! Con pocas personas he debido de pasar más horas comiendo en la uni! Muchas gracias amiga por todos estos años, las innumerables horas al teléfono, biblio, fiestas y llamadas de domingo! Aunque la vida nos ha llevado por caminos distintos, se que nunca dejaremos de estar el uno para el otro, compartiendo alegrías y aprovechando cada minuto que nos veamos! Quiero agradecerte mucho todo el apoyo que me has dado para completar esta etapa de mi vida! Y más aún por el apoyo que fuiste durante toda la carrera! Un brindis a las que vengan!

A **Paulita**, ni se la de veces que me has recogido en coche y la de horas que hemos compartido en la biblio durante toda la carrera... Sobre todo, tengo muchísimo que agradecerte del último año de carrera, nuestro año negro! Fuiste la pieza clave, el apoyo más necesitado en ese momento para que todo saliera bien, aunque pendiera de un hilo. Muchas gracias por estar siempre ahí (aunque te cueste infinito responder a un whatsapp), todo esto no habría sido tan fácil sin tu ayuda. Por las escapadas al monte, a conciertos exprés, a chupinazos y a donde haga falta con tal de vernos! Especial mención a mi otra Azcarate favorita, **Lucia**, que tuvo mucho que aguantarnos a su hermana y a mi cuando nuestro amor a unizar brillaba por su ausencia, pero que conseguíamos pailar con un pincho de tortilla bañado en aceite del London! Gracias por vuestro apoyo!

Dicen que durante tu niñez y adolescencia se forma la persona que terminarás siendo. Yo le debo todo a haberme rodeado de los mejores! Quiero agradecer en especial a **Carlos y Goby**, mis amigos oscenses del alma, por haber crecido a mi lado, haber tropezado en el camino y haber aprendido de nuestros errores juntos. Con Gob además he superado infinitos veranos de recus! Una parte de todo lo que he conseguido os lo debo a vosotros. También tengo que agradecerles mi evolución como persona a **Bellosta, Santi, Sonia, María, Buisan, Laura y Alba** por haber estado siempre ahí.

A mi segunda familia, **Paula, Guillermo, Tere, Juan** y la futura **Julia**, por haberme hecho sentir como uno más desde el principio y velar siempre por mi bienestar, habéis contribuido mucho a hacerme crecer como persona y por consiguiente a lograr cerrar esta etapa de mi vida.

Mis últimas y más preciadas palabras van para las personas más importantes de mi vida, las que me han hecho crecer y ser quien soy.

A mis **padres**, mi **hermana** y mis **abuelos**, ellos me han educado desde niño, me han hecho entender la vida, me han dejado cometer errores y siempre me han tendido su mano para recuperarme de ellos. Muchas gracias a mis padres por haber dado rienda suelta a las decisiones de mi vida, las cuales con sus aciertos y sus tropiezos me han hecho ser a día de hoy quien soy. Por todo lo que habéis tenido que aguantar estos años. Sin su apoyo permanente, hoy esta tesis no llevaría mi nombre.

Finalmente, a **Teresa**, no tendría espacio suficiente en estas líneas para agradecerte todo lo que has hecho y haces por mi cada día. Has sido mi amiga, mi confidente, un hombro en el que llorar y una mano a la que agarrar para salir a flote. La persona que me ha enseñado cuanto puedes llegar a

querer a alguien y la que ha estado ahí en cada segundo del día. Muchas gracias por todo, por caminar a mi lado, por aguantar los interminables viajes en tren, por soportar la distancia, por sacarme de cada agujero en el que me caía en los altibajos de la tesis y la vida. Que hayamos compartido la etapa de la tesis nos ha hecho comprender muy bien el uno al otro, y no todo el mundo puede contar con esa suerte. Así que siempre te estaré eternamente agradecido por ser como eres, por aguantarme y por hacerme ver la vida un poco más bonita cada día. Gracias por los viajes, las cenas, las fiestas, los cumpleaños. Gracias por todo lo vivido y aún más por todo lo que nos queda por vivir.

Muchas gracias a todos por haberme acompañado en esta etapa de mi vida! Thank you so much to all of you! Eskerrik asko!

Resumen

Durante los últimos años, la calidad de vida ha mejorado notablemente. Ha tenido lugar un desarrollo tecnológico sin precedentes, que ha permitido llevar un ordenador en el bolsillo cuando hace apenas 50 años ocupaban casi un edificio entero. Este salto exponencial de conocimiento científico también ha dejado huella en la medicina. El primer registro de un tratamiento médico data del año 800 D.C. Después, en torno al año 1220 aparecieron las primeras universidades que formaban personal cualificado capaz de tratar los problemas de salud de la sociedad. Apenas unos años después, la invención del primer microscopio permitió aumentar el conocimiento en el campo de la anatomía humana. Ya en el siglo XIX, el gran desarrollo de la sociedad, exigió la aparición de centros sanitarios, lo que desencadenó la creación de los primeros hospitales públicos. Todo ello vino de la mano del desarrollo de nuevas formulaciones de antibióticos que catapultaron al estrellato el conocimiento que se tenía sobre la medicina y el cuerpo humano. Además, los grandes avances en química, genética, rayos X, etc, permitieron asentar los pilares de lo que hoy en día se conoce como ciencia biomédica.

Dentro de la química biomédica, los polímeros han experimentado una gran evolución desde que en el siglo XX se empezó a modificarlos. En la década de los 50, Staudinger (conocido como el padre de la química de los polímeros) obtuvo el premio nobel por su trabajo en “el descubrimiento de la química macromolecular”. Sus investigaciones han alentado el desarrollo de tecnologías que permiten la modificación de los polímeros, alumbrando en la década de los 60 el primer tratamiento clínico, conocido como “co-polímero pirano”. El compuesto estaba basado en una combinación de divencil éter y anhídrido maleico. Pese a que en sus inicios ostentaba unos efectos anticancerosos alentadores, dicho ímpetu quedó mermado en sus primeros ensayos clínicos, tras reportarse una gran toxicidad desencadenada de su alto peso molecular. Sin embargo, todo lo que se aprendió durante su desarrollo ha permitido que hoy en día se cuente con un amplio espectro de dispositivos médicos poliméricos en el mercado. Tales como, bolsas de sangre (basadas en policloruro de vinilo), mallas para hernia (basadas en polifenilén éter) o prótesis vasculares (basadas en politetrafluoroetileno). Además, uno de los polímeros sintéticos más relevantes en medicina de los últimos tiempos es el polietilenglicol. Este compuesto presenta poca adhesión a proteínas, lo que,

combinado con una baja toxicidad, ha permitido su utilización en diversas aplicaciones; ingeniería de tejidos o el desarrollo de vehículos para el transporte de principios activos. Recientemente, el progreso de nuevas tecnologías para modificar posiciones terminales de las cadenas de polímeros, han permitido la aparición de polímeros “inteligentes”. Estas estructuras presentan respuesta frente a cambios en su entorno (pH, temperatura, etc), y logran adaptar sus propiedades físico-químicas o estructurales en consonancia.

En los últimos años, las cadenas poliméricas han sido entrecruzadas entre sí para dar lugar a materiales novedosos con propiedades mejoradas. Dicho entrecruzamiento puede tener lugar mediante interacciones físicas o enlaces químicos. El primer caso, se centra en el desarrollo de interacciones intermoleculares reversibles, tales como, puentes de hidrógeno, metales de coordinación o fuerzas π - π . La principal ventaja que aporta este entrecruzamiento polimérico es la ausencia de enlaces químicos, lo que permite garantizar una mejor biocompatibilidad al eliminar la posibilidad de que persistan sustancias sin reaccionar. Además, en el caso de utilizar polímeros ya aprobados por agencias reguladores (EMA, FDA), existe la posibilidad de unir las cadenas poliméricas mediante entrecruzamientos físicos evitando la creación de una nueva entidad química. El resultado final es una reducción notable en el tiempo que conllevaría la aprobación de esta nueva mezcla, garantizando un salto agilizado al mercado. Por el contrario, los entrecruzamientos químicos han permitido la unión de cadenas poliméricas mediante enlaces covalentes, bastante fuertes y en muchos casos irreversibles. Ambas estrategias han permitido la aparición de nuevos materiales conocidos como hidrogeles, microgeles y nanogeles (NGs), los cuales se presentan como estructuras tridimensionales, basadas en la combinación de cadenas poliméricas capaces de retener agua en su estructura. La complejidad de los hidrogeles también ha ido evolucionando a lo largo de los años, pasando de cadenas poliméricas entrecruzadas entre sí (primera generación) a redes dobles híbridas. Esta última generación ha permitido el entrecruzamiento de polímeros naturales y sintéticos, confiriendo a los sistemas inteligencia a estímulos a nivel de reconocimiento enzimático.

En 1959, el desarrollo de la nanociencia vino de la mano del Dr. Feynman, el cual esbozó la idea de diseñar nanorobots capaces de nadar por la sangre y reparar células a niveles moleculares. Las sucesivas investigaciones alumbraron la aparición en 1995 del Doxil[®], la primera formulación aprobada para el tratamiento de cáncer y basada en nanotecnología. Esta consiste en la

encapsulación de la droga antitumoral doxorubicina en liposomas PEGilados. Desde entonces, se han desarrollado múltiples capsulas poliméricas (micelas, vesículas, dendrímeros, NGs) y nanopartículas inorgánicas. De estas últimas, las basadas en oro (AuNPs) han suscitado especial interés en biomedicina. Pese a que se han investigado recientemente, en verdad datan de tiempos romanos, donde los primeros registros se observaron en la copa Lycurgus. Actualmente, dicha vasija se encuentra en el museo británico. Es capaz de cambiar su color en función de donde le incide la luz. Cuando el haz de luz incide desde fuera de la vasija, esta es de color verde, sin embargo, si el foco de luz se encuentra en su interior, el color de la copa cambia a rojo. Este efecto es una consecuencia de la presencia de AuNPs que se formaron en la superficie de la copa durante el secado de su pintura. Hoy en día, numerosos protocolos han sido optimizados para permitir sintetizar AuNPs con diversas formas y tamaños (esferas, bastones, estrellas, cajas, etc.). Todas estas partículas presentan diversas propiedades ópticas, modulables con el tamaño y la forma, como consecuencia de un efecto físico conocido como resonancia de plasmones de superficie. Se trata de un fenómeno que describe oscilaciones de electrones libres conductores a lo largo del metal. Cuando las NPs tienen un tamaño menor a la longitud del fotón, la oscilación del plasmón se esparce a lo largo de la partícula, creando una nube de electrones. Este fenómeno se ve reflejado en la capacidad que tienen las NPs de absorber radiación en el espectro Ultravioleta-infrarrojo cóncavo (UV-NIR). En el caso de las AuNPs isotrópicas (esferas), estas absorben en 530 nm. Sin embargo, las AuNPs anisotrópicas (bastones, estrellas o cajas) presentan una absorción en la zona NIR del espectro, donde también se localiza la ventana biológica en la que la luz no es adsorbida ni reflejada por los tejidos. Por todo ello, las AuNPs resultan de especial atención en aplicaciones biomédicas.

Todos los sistemas orgánicos e inorgánicos descritos previamente, cuentan con una gran sofisticación y versatilidad en aplicaciones biomédicas. Sin embargo, también presentan ciertos inconvenientes, ya que sufren una pérdida de estabilidad cuando están en contacto con fluidos biológicos. Todo ello ha desembocado en la necesidad plausible de preparar nuevos materiales todavía más rompedores, conocidos como sistemas híbridos. Para ello, la química orgánica (polímeros) se combina con la inorgánica (NPs metálicas) para dar lugar a la formación de materiales de nueva generación que combinan lo mejor de los dos mundos. Además, una nueva subcategoría de materiales híbridos, basados únicamente en química orgánica, ha surgido de la combinación de polímeros de origen natural con sintéticos. En definitiva, todo ello permite la coexistencia de una gran variedad de sistemas que

permiten el diseño customizado de tratamientos terapéuticos capaces de adaptarse a cada escenario.

La tesis doctoral que se va a detallar a lo largo de la presente memoria, explora la posibilidad de afinar las propiedades que presentan los geles cuando interactúan con medios biológicos. Además, la investigación se lleva a cabo en distintas escalas de longitud. El trabajo desarrollado se va a presentar en dos secciones diferenciadas que convergen en el estudio de la biointerfase. La sección A se centra en la escala nanométrica, profundizando en la influencia que tienen los NGs cuando actúan de manta protectora de AuNPs frente a interacciones con fluidos biológicos. Para ello, se han preparado nanoesferas, nanobastones y nanoestrellas de oro. Posteriormente, mediante una tecnología completamente novedosa, estas AuNPs han sido encapsuladas dentro de NGs, los cuales aportan al conjunto del sistema un espesor extra de tan solo 2 – 6 nm. Además, la cubierta polimérica ha logrado mantener la forma original de las AuNPs. Es decir, los NGs adquieren la forma de los núcleos inorgánicos. Cabe citar que el pequeño espesor que incrementan respecto al diámetro original de las AuNPs, garantiza que las propiedades ópticas de estas se mantengan y no se vean mermadas, como ocurre en sistemas de estabilización con NGs tradicionales. Por otro lado, es bien sabido que la carga superficial y los grupos hidrofóbicos juegan un papel fundamental en la interacción de los sistemas sintéticos con las biomoléculas. Por ello, se ha modulado la carga superficial y la hidrofobicidad de los NGs utilizando diversos polímeros. Por ejemplo, se han preparado NGs basados en poli(acrilamida (como polímero neutro), otros basados en poli-[2-(metacriloyloxy)etil]dimetil-(3-sulfopropil)amonio hidróxido (p-DMAPS), (como polímero zwitterionico), NGs basados en polivinilimidazol (polímero con cierto carácter hidrofóbico) y, finalmente, NGs basados en poli-isopropilacrilamida (p-NIPAM) (polímero inteligente con capacidades termoresponsivas). La combinación de estos polímeros entre sí, o por separado, ha permitido contar con una amplia familia de materiales capaces de encapsular AuNPs e interactuar de formas diversas con medios biológicos. De hecho, al entrar en contacto estos materiales con sales o proteínas, se ha reportado un incremento general de la estabilidad de las AuNPs en comparación con sistemas tradicionales de estabilidad de las AuPs. Cabe destacar que los NGs preparados a partir de poli(acrilamida o polivinilimidazol han logrado incrementar la estabilidad de las AuNPs en presencia de BSA evitando el desplazamiento de la banda plasmónica, lo que indica que no hay agregación entre las partículas. Por otro lado, cuando estos sistemas se han enfrentado a escenarios biológicos más avanzados (mucina dispersada en tampón fosfato), los NGs basados en poli-DMAPS han demostrado, en el caso de las esferas una notable reducción de su interacción

con la mucina. Es probable que esto se deba a la doble carga, positiva y negativa, presente en este polímero zwitterionico. Dicha doble carga es capaz de neutralizar la carga negativa de la mucina, reduciendo las interacciones. Al final, una reducción de interacción conlleva un incremento en la estabilidad de las AuNPs, así como una mayor probabilidad de penetrar la mucosa. De hecho, se podría esperar que estos sistemas permitan penetrar la mucosa de tejidos con mayor facilidad. Por el contrario, los NGs basados en polivinil imidazol, debido a su carácter hidrofóbico, incrementan la interacción con la mucina, lo que podría traducirse en una mayor capacidad de estos sistemas para adherirse a tejidos mucosos. Todo ello pone de manifiesto la capacidad que tiene esta tecnología para adaptarse a las circunstancias requeridas, en donde se puede jugar con la estabilidad de las AuNPs y modular sus capacidades de interacción a biomoléculas. Finalmente, estos NGs también han servido para incrementar la estabilidad de AuNPs cuando estas actúan de transductores de luz NIR en calor. Previamente, se ha reportado en la bibliografía un cierto porcentaje de átomos de oro (que conforman las AuNPs) que suelen sublimarse durante la irradiación. Como consecuencia, aparecen pequeños clústeres de oro cerca de las AuNPs, lo que disminuye su estabilidad y capacidad fototérmica. Mediante los NGs finos que se han preparado entorno a las AuNPs, se ha logrado mantener cuasi-constantes las capacidades fototérmicas durante periodos de irradiación de 3 h. Por todo ello, estos NGs prometen ser una verdadera revolución en la estabilidad de AuNPs en aplicaciones biomédicas.

La sección B de esta tesis doctoral profundiza en la influencia que tienen los polímeros Eudragits cuando forman parte de la estructura tridimensional de hidrogeles entrecruzados físicamente. Una amplia gama de estos polímeros se ha entremezclado con otros que también tienen propiedades mucoadhesivas (polivinilpirrolidona, alcohol de polivinilo y polietilenglicol) para conformar un total de cinco hidrogeles con diferencias estructurales. El objetivo final estriba en la realización de una caracterización exhaustiva de los materiales en términos de relación estructura-actividad, estabilidad de la matriz polimérica, capacidad de encapsulación y liberación proteica. Con el fin de ensalzar el potencial de estos materiales, se ha desarrollado una metodología que permite cuantificar el trabajo de adhesión entre los hidrogeles y la conjuntiva ocular mediante un reómetro. Este ensayo permite hacer un mapeo de varios materiales localizando los posibles candidatos más prometedores. Seguidamente, los materiales más prometedores se han ensayado en modelos de animales (conejos) en dos fases. La primera de ellas ha consistido en colocar, durante unos minutos, hidrogeles vacíos y comprobar si estos presentaban una buena adhesión a la

conjuntiva ocular. Posteriormente, el material final ha sido cargado con proteínas capaces de ayudar en la reepitelización ocular. De manera controlada, bajo los protocolos y permisos pertinentes, se han realizado úlceras en la superficie ocular de los ojos de los conejos con sosa caustica. Seguidamente, se ha aplicado el tratamiento (con hidrogel) durante un periodo de dos semanas, colocando un parche cada 12 horas. Los resultados adquiridos han sido comparados con el tratamiento médico actual, el cual requiere cirugía, para poner de manifiesto la capacidad de estos hidrogeles como alternativa real. Cabe citar que los resultados logrados todavía han sido algo preliminares, con peores resultados que los obtenidos en el tratamiento actual, el cual consiste en trasplantar membrana amniótica (rica en proteínas) alrededor del ojo. No obstante, los hidrogeles también han sido capaces de cerrar la úlcera ocular, pese a que a lo largo del tratamiento esta se ha vuelto a abrir. Se ha especulado que la “dureza” del hidrogel, sumado a la necesidad de aplicar un nuevo hidrogel cada 12 horas, ha dado como consecuencia adversa la reapertura de dicha úlcera, la cual aún era bastante inestable. Por todo ello, en futuros trabajos se intentará optimizar la formulación para erradicar este resultado imprevisto. No obstante, cabe destacar que la facilidad de colocar un hidrogel en pocos minutos en la misma consulta del oftalmólogo, frente a la necesidad de que el paciente vaya a un quirófano, ya supone un gran avance en el tratamiento. Es decir, se puede considerar estos hidrogeles como un primer grano de arena en la montaña que será la oftalmología del mañana.

Todo lo anterior demuestra que es posible modular las interacciones entre materiales híbridos y las biomoléculas, independientemente de la escala en la que se trabaje. De hecho, a escala nanométrica, se ha logrado proteger AuNPs mediante su encapsulación en NGs muy finos que apenas incrementan el diámetro total del sistema. Además, la forma del núcleo inorgánico, así como sus propiedades ópticas se han preservado. Por otro lado, a escala macroscópica, los hidrogeles entrecruzados físicamente han demostrado una gran robustez y capacidad de adhesión a la mucosa ocular que se ha visto reforzada con su capacidad de liberar proteínas que ayudan en la reepitelización de la superficie ocular. Si bien aún queda mucho trabajo por hacer, esta tesis doctoral ha asentado las bases de futuras líneas de investigación mediante la creación de pilares sólidos que se sustentan sobre un gran marco de caracterizaciones y protocolos sintéticos a la vanguardia de la ciencia del mañana.

Abstract

During the last decades, materials in nano- and microscales have attracted the attention of the scientific community. The methodologies that have emerged during the XX century for the functionalization of polymers, combined with the great impetus of inorganic nanoparticles (NPs) in the XXI century, have made possible the development of novel and sophisticated materials for biomedicine. However, the lack of stability that they suffer while being in contact with biological fluids, has promoted the appearance of hybrid systems capable of facing many scenarios. Hence, organic chemistry (polymers) and inorganic chemistry (metallic NPs) came to terms to give birth to a new generation of materials that combine the best of both worlds. By comparison, natural and synthetic polymers have been combined as well for the preparation of a new branch of hybrid organic materials. All of the above has given rise to the fact that today there is a wide variety of systems that allow custom-designed therapeutic treatments.

The PhD thesis here presented, explores how to tune the properties of gels at different length scales to moderate their interactions with biological fluids. The work has been divided in two sections. In section A, devoted to the nanometric scale, the influence that thin nanogels (NGs) shells have on the stability of gold nanoparticles (AuNPs) in biological media is being studied. Nano-spheres, -rods and -stars have been synthesized and protected with a thin polymeric mantle, increasing their total diameter in just 2 – 6 nm, while keeping their original shape. Furthermore, NGs' surface charge and hydrophilicity have been modulated using monomers with different reported interactions towards biological molecules. In the end, this will affect the stability of the AuNPs. Besides, a deep understanding of the laser into heat transducer capacity and stability of the materials, in this scenario, has been extensively studied.

Lastly, in section B the influence of Eudragits as building blocks in the preparation of physically cross-linked hydrogels is being screened. This type of polymer has been mixed with other mucoadhesive-reported polymers for the preparation of the materials. The final goal will be the determination of the structure-activity relationship in terms of hydrogel formulation, matrix stability, protein encapsulation, and release profiles. To highlight the potential of these materials, a methodology to quantify the adhesion work between the hydrogel and the conjunctiva by a rheometer was optimized. Additionally, pre-

clinical studies, using rabbits as an animal model have been addressed, to demonstrate the eye-mucus adhesion of the materials and their potential benefits as ocular smart carriers, achieving with them an improvement in the actual surgical treatments.

Altogether, this doctoral thesis demonstrates that it is possible to modulate the interactions between hybrid polymeric-based materials and biomolecules at different length scales. In fact, at the nanometric scale, it has been possible to prepare thin NGs to protect AuNPs preserving their size, shape and optical properties in presence of biological fluids. At higher scale, hydrogels have demonstrated their capacity to attach ocular mucosa and release proteins that help into ocular re-epithelization.

Table of contents

Chapter I: General Introduction

1.1	Introduction	3
1.2	Polymers in biomedical applications.....	3
1.2.1	Cross-linking polymers to improve their properties for biomedicine.....	5
1.3	Nanomedicine: A new trend of working at the atomic level	8
1.3.1	Organic nanoparticles for biomedical applications.....	9
1.3.2	Inorganic nanoparticles for biomedical applications	14
1.3.3	Hybrid systems: In a rush to achieve reinforced materials combining different sources of polymers and inorganic elements	18
1.4	The biointerface: When nanoparticles meet biological systems	21
1.4.1	The protein corona effect. An undesired effect of nanomaterials in biological media.	22
1.4.2	Mucosa interactions of synthetic materials.....	24
1.5	References – Chapter I	28

Chapter II: General objectives

2.1	Objectives.....	35
-----	-----------------	----

Chapter III: Design of thin nanogels to stabilize gold nanoparticles in presence of biological fluids

3.1	Introduction	43
3.2	Objectives.....	52
3.3	Results and discussion.....	53
3.3.1	Synthetic methodology for the preparation of thin mantle nanogels to protect gold nanoparticles	53
3.3.2	Structural and physicochemical characterizations of the materials	56

3.3.2.1	UV-Vis spectra	56
3.3.2.2	Hydrodynamic diameters (DLS) and surface charge of the materials (Z-Potential).....	60
3.3.2.3	Gel permeation chromatography as another proof of the presence of the NG shell protection around AuNPs	63
3.3.2.4	Transmission electron microscopy (TEM)	65
3.3.2.5	Atomic force microscopy (AFM).....	69
3.3.2.6	Differential scanning calorimetry (DSC)	71
3.3.3	A comprehensive study of the interactions between AuNPs and their biological surroundings	74
3.3.3.1	Evolution of the gold-based materials stabilities in presence of salts and proteins at the normal body temperature.....	74
3.3.3.2	Interactions between gold-based materials and mucin.....	84
3.3.4	Improving the stabilization of anisotropic AuNPs while they are acting as NIR light-into-heat transducers. A new hope in Au NPs photothermal applications.....	92
3.4	Materials and methods	100
3.4.1	Synthesis of gold nanoparticles.....	100
3.4.2	Ligand exchange for gold nanoparticles.....	102
3.4.3	PEG ending group modification to add acryl groups to the surface of gold nanoparticles.....	103
3.4.4	Synthesis of the thin NGs	103
3.4.5	Dynamic light scattering (DLS) and Z-Potential measurements	104
3.4.6	Gel permeation chromatography (GPC).....	104
3.4.7	Transmission electron microscopy (TEM)	105
3.4.8	Atomic force microscopy (AFM).....	105
3.4.9	Differential scanning calorimetry (DSC)	105
3.4.10	Scanning electron microscope (SEM).....	106
3.4.11	Interactions study between biological fluids and AuNPs (I): Salts and proteins.	106
3.4.12	Interactions study between biological fluids and AuNPs (II): Mucin interactions followed by rheology.	106

3.4.13	Laser irradiation of AuNPs. Photothermal conversion assays.	107
3.5	Main remarks, conclusions and future perspective.....	108
3.6	References – Chapter III.....	110

Chapter IV: Screening of Eudragits as building blocks in the preparation of physically cross-linked hydrogels

4.1	Introduction	115
4.2	Objectives.....	119
4.3	Results and discussion.....	121
4.3.1	Hydrogel preparation	121
4.3.2	Hydrogels pore sizes in dried state	123
4.3.3	Determination of matrix stability (I): Moisture uptake and moisture content.....	125
4.3.4	Determination of matrix stability (II): Kinetic of dissolution by NMR.....	128
4.3.5	Mechanical properties of the hydrogels without hydration: Tensile strain analysis.....	135
4.3.6	Rheological characterization	138
4.3.6.1	Dynamic oscillatory shear rheological analysis	138
4.3.6.2	Mucoadhesive properties of hydrogels towards ocular conjunctiva	140
4.3.7	Thermal and X-ray diffraction characterization for hydrogels' opacity comprehension.....	143
4.3.7.1	Thermogravimetric analysis (TGA)	144
4.3.7.2	Differential Scanning Calorimetry (DSC)	149
4.3.7.3	Wide-angle X-ray scattering (WAXS).....	154
4.3.8	Encapsulation and release of bovine serum albumin	156
4.3.9	Encapsulation and release of growth factors (GF)	161
4.3.10	Metabolic activity of MRC-5 cells in presence of hydrogels A.	165
4.3.11	Metabolic activity of WKD ocular conjunctiva cells in presence of hydrogels A – E.....	166

4.3.12	<i>In-vivo</i> eye-adhesion study.....	167
4.3.13	Hydrogels optimization: Improvement of their mucoadhesion properties.....	169
4.3.14	Material candidate: GF release, matrix stability and efficacy studies.....	173
4.3.14.1	Matrix stability followed by NMR	174
4.3.14.2	GF release profile from hydrogel C modified with HA	175
4.3.14.3	Efficacy assays of final hydrogel candidate	176
4.4	Materials and methods	180
4.4.1	Hydrogel preparation	180
4.4.2	Hydrogels pore sizes in dried state	181
4.4.3	Matrices stability under several conditions	181
4.4.3.1	Moisture uptake	181
4.4.3.2	Moisture content	181
4.4.3.3	Kinetic of dissolution by NMR	182
4.4.4	Hydrogel's mechanical properties: Tensile strain	182
4.4.5	Hydrogel's rheological characterizations	183
4.4.5.1	Dynamic oscillatory	183
4.4.5.2	Mucoadhesive rheological characterization	183
4.4.6	Thermal and X-ray diffraction characterization for hydrogels' opacity comprehension.....	183
4.4.6.1	Thermogravimetric analysis (TGA)	183
4.4.6.2	Differential Scanning Calorimetry (DSC)	184
4.4.6.3	Wide-angle X-ray scattering (WAXS).....	184
4.4.7	Bovine Serum Albumin as a model for encapsulation and release studies.....	184
4.4.8	Growth Factors encapsulation and release studies	185
4.4.9	Metabolic activity of MRC-5 cells. <i>In-vitro</i> studies.....	185
4.4.10	Metabolic activity of WKD conjunctiva cells. <i>In-vitro</i> studies ..	185
4.4.11	<i>In-vivo</i> assays (I): Eye-adhesion study	186
4.4.12	<i>In-vivo</i> assays (II): Efficacy studies.....	186

4.5	Main remarks, conclusions and future perspective.....	187
4.6	References – Chapter IV.....	188

Chapter V: General remarks and conclusions

5.1	General remarks and conclusions.....	195
-----	--------------------------------------	-----

Annexes

Annex I: UV-VIS spectra showing the plasmon band evolution of AuNPs at 37 °C.....	201
Annex II: UV-VIS spectra showing the plasmon band evolution of AuNPs at 37 °C in presence of NaCl.....	203
Annex III: UV-VIS spectra showing the plasmon band evolution of AuNPs at 37 °C in presence of PBS.....	205
Annex IV: UV-VIS spectra showing the plasmon band evolution of AuNPs at 37 °C in presence of BSA.....	207
Annex V: Curriculum Vitae.....	209

List of figures and tables

Chapter I: General Introduction

Figure 1.1. (A) Scheme showing several strategies to prepare hydrogels. (B) Physical and chemical cross-linkers to join polymeric chains during the preparation of hydrogels.....	7
Figure 1.2. Scheme of organic and inorganic nanoparticles.....	9
Figure 1.3. Different classes of ordered mesoporous micelle in the function of the architecture level.	10
Figure 1.4. Scheme of the divergent synthesis of dendrimers.	11
Figure 1.5. Scheme of a smart nanogel releasing a drug under a change of temperature, enzyme overexpression, magnetic field and pH.....	13
Figure 1.6. Lycurgus cup. On the left, cup with the light coming from inside the vessel. On the right, the cup with light coming from outside.....	14
Figure 1.7. Some different shapes of AuNPs. (A) nanospheres, (B) nanocubes, (C) nanobranches, (D - F) different sized nanorods, (G – J) several sized nanobipyramids.....	16
Figure 1.8. Scheme showing the surface plasmon resonance effect.....	17
Figure 1.9. (A) Scheme of hybrid thermoresponsive nanogel based on magnetic NPs as cross-linkers and their capacity of releasing a drug under the presence of NIR-laser irradiation. (B) Scheme and TEM pictures of hybrid nanogels with gold NPs grown inside.	20
Figure 1.10. Scheme of the protein corona effect where several proteins are absorbed and desorbed from the surface of the nanoparticle.....	23
Figure 1.11. Scheme of AuNPs decorated with polymers that can be adhesive to the intestine mucus layer and gold nanoparticles encapsulated onto nanogels that can penetrate the mucus layer.	27

Chapter II: General objectives

Figure 2.1. Scheme that summarizes the work included in this PhD thesis and the global objectives.	39
----------------------------------------------------------------------------------------------------------------	----

Chapter III: Design of thin nanogels to stabilize gold nanoparticles in presence of biological fluids

Figure 3.1. AuNPs TEM images and optical properties. (A) Au Nanospheres. (B) Au Nanorods. (C) Au Nanodumbbells. (D) Au Nanoprism. (E) Au Nanowires. (F) Au Nanostars. (G) Au Nanodendrites. (H) Au Nanocubes. (I) AuNanorods' colour changes while increasing the axial axis. (J) Au Nanoshells' colour changes while reducing the shell thickness. 43

Figure 3.2. Scheme of UV-VIS spectra obtained from the measurements of an aqueous dispersion of Au nanospheres, nanorods and nanostars. 44

Figure 3.3. (A) Infrared thermal image of the tumour after irradiation with a laser, with $\lambda = 808$ nm, from 0 to 30 s. (B) Heating curve of the silica-rod NPs vs. time. (C) Tumour weight for: (I) untreated mouse; (II) NIR laser; (III) doxorubicin; (IV) silica-rod after laser irradiation; (V) doxorubicin and silica-rod after laser irradiation. 45

Figure 3.4. Scheme of the most used stabilization strategies for colloidal Au NPs. These are the functionalization of the particles with surfactants, ligands, organic and metallic shells or biomolecular ligands. 47

Figure 3.5. (A) TEM pictures of Au nanorods absorbed into silica nanospheres with a p-NIPAM nanogel shell around. (B) AFM microscopy pictures of the same material. (C) DLS measurement in a ramp of temperature from 25 to 38 °C. (D) photothermal conversion efficiency of Au nanorods and Au nanorods absorbed into silica nanospheres covered with a p-NIPAM nanogel shell. 49

Figure 3.6. (A) Scheme showing the developed nanogel shell with AuNPs as a core. (B) TEM pictures of the prepared material. (C) Scheme showing the degradation of the NG at acid conditions. (D) Fluorescence intensity released at different pH. (E) Protein absorption and Au concentration for AuNPs protected with a peptidic shell, a peptidic/PEG shell or a nanogel. 50

Figure 3.7. Scheme of the AuNPs shielded by a thin layer of NGs and chemical structure of the monomers used for the synthesis of the NGs. 51

Table 3.1. Graphical design, sample codes, chemical composition and the molar ratio of the Au-based materials prepared. 54

Figure 3.8. Synthetic scheme followed for the preparation of thin mantle NGs with AuNPs as core. 55

Figure 3.9. UV-VIS spectra of (A) 13 nm Au Nanospheres with citrate, PEG-NH₂, PEG-acryl ligands and NGs shells 1 – 4. (B) 40 nm Au Nanospheres with citrate, PEG-NH₂, PEG-acryl and NGs shells 5 – 6. (C) 40 nm Au Nanorods with citrate,

PEG-NH₂, PEG-acryl and NG shell 9. (D) 40 nm Au Nanorods with citrate, PEG-NH₂, PEG-acryl and NG shell 10. (E) 40 nm Au Nanorods with citrate, PEG-NH₂, PEG-acryl and NG shell 11. (F) 40 nm Au Nanorods with citrate, PEG-NH₂, PEG-acryl and NG shell 12. (G) 40 nm Au Nanostar with PEG-acryl and NG shell 13. (H) 40 nm Au Nanostar with PEG-acryl and NG shell 14. (I) 40 nm Au Nanostar with PEG-acryl and NG shell 15. (G) 40 nm Au Nanostar with PEG-acryl and NG shell 16. 57

Table 3.2 Max. absorption for the most relevant spectra showed in Figure 3.9. 58

Figure 3.10. (A, B) Z average and PDI of 13 nm AuNSs grafted with PEG-acryl and NG 1 - 4. (C) Z-potential of 13 nm AuNSs grafted with PEG-acryl and NG 1 - 4. (D) Agarose gel electrophoresis of 13 nm AuNSs grafted with PEG-acryl and NG 1 - 4. (E, F) Z average and PDI of 40 nm AuNSs grafted with PEG-acryl and NG 5 - 8. (G) Z-potential of 40 nm AuNSs grafted with PEG-acryl and NG 5 - 8. (H, I, J) Z average and PDI of 40 nm AuNRs grafted with PEG-acryl and NG 9 - 12. (K) Z-potential of 40 nm AuNRs grafted with PEG-acryl and NG 9 - 12. (L, M) Z average and PDI of 40 nm AuNSTs grafted with PEG-acryl and NG 13 - 16. (K) Z-potential of 40 nm AuNSTs grafted with PEG-acryl and NG 13 - 16. 60

Figure 3.11. GPC chromatographs, all of them have been measured at the mentioned wavelength with confidence interval of 100 nm. (A) Au nanospheres 13 nm. (B) Au nanospheres 40 nm. (C) Au nanorods 40 nm. (D) Au nanostars 40 nm. 63

Figure 3.12. TEM images of 13 nm Au nanospheres. (A, B) Au nanospheres grafted with PEG_{5k}-acryl. (C) Au nanospheres covered with a thin mantle NG shell. (D, E) Au nanospheres with thin mantle NG shell, samples stained..... 65

Figure 3.13. TEM images of 40 nm Au nanospheres. (A) Au nanospheres grafted with PEG_{5k}-acryl. (B) Au nanospheres covered with a thin mantle NG shell. 66

Figure 3.14. TEM images of 40 nm Au nanorods. (A) Au nanorods grafted with PEG_{5k}-acryl. (B, C) Au nanorods covered with thin mantle NG shell..... 67

Figure 3.15. TEM images of 40 nm Au nanostars. (A, B) Au nanostars grafted with PEG_{5k}-acryl. (C, D) Au nanostars covered with thin mantle NG shell..... 68

Figure 3.16. AFM images and data obtained from their posterior analysis of 13 nm Au nanospheres. (A-I) Height AuNPs grafted with PEG-acryl. (A-II) Height AuNPs encapsulated inside NG4. (B-I) Adhesion AuNPs grafted with PEG-acryl. (B-II) Adhesion AuNPs encapsulated inside NG4. 70

Figure 3.17. DSC heating curves of AuNPs grafted with PEG (blue) and encapsulated inside of a p-NIPAM thin NG (red). (A) 13 nm Au nanospheres. (B) 40 nm Au nanospheres. (C) 40 nm Au nanorods. (D) 40 nm Au nanostars.	72
Table 3.3. Peak of temperature corresponding to the heat flow and enthalpy of crystallisation for each AuNPs material. Data obtained from the DSC heating curves shown in Figure 3.17.....	72
Figure 3.18. Stability evolution along the time for 13 nm Au nanospheres. (A) Particles incubated at 37 °C. (B) Particles incubated at 37 °C in presence of NaCl 2M. (C) Particles incubated at 37 °C in presence of PBS 10 mM. (D) Particles incubated at 37 °C in presence of BSA (2 mg/mL in PBS 10 mM). (E) Comparative summary between materials.....	75
Figure 3.19. Stability evolution along the time for 40 nm Au nanospheres. (A) Particles incubated at 37 °C. (B) Particles incubated at 37 °C in presence of NaCl 2M. (C) Particles incubated at 37 °C in presence of PBS 10 mM. (D) Particles incubated at 37 °C in presence of BSA (2 mg/mL in PBS 10 mM). (E) Comparative summary between materials.....	77
Figure 3.20. Stability evolution along the time for 40 nm Au nanorods. (A) Particles incubated at 37 °C. (B) Particles incubated at 37 °C in presence of NaCl 2M. (C) Particles incubated at 37 °C in presence of PBS 10 mM. (D) Particles incubated at 37 °C in presence of BSA (2 mg/mL in PBS 10 mM). (E) Comparative summary between materials.....	79
Figure 3.21. Stability evolution along the time for 40 nm Au nanostars. (A) Particles incubated at 37 °C. (B) Particles incubated at 37 °C in presence of NaCl 2M. (C) Particles incubated at 37 °C in presence of PBS 10 mM. (D) Particles incubated at 37 °C in presence of BSA (2 mg/mL in PBS 10 mM). (E) Comparative summary between materials.....	80
Figure 3.22. SEM pictures of (A) Au nanostars and after 10 days of incubation with BSA (1 mg/mL in PBS) at 37 °C. (B) grafted with PEG-acryl. (C) encapsulated in p-acrylamide NG. (D) encapsulated in p-vinylimidazole NG. (E) encapsulated in p-DMAPS NG. (F) encapsulated in p-NIPAM NG.....	82
Figure 3.23. Scheme of the four results cases that can be obtained after the measurement.....	85
Figure 3.24. Evolution of the G' and G'' modulus along the time for 13 nm Au nanospheres mixed with mucin. In green, AuNPs grafted with linear PEG-acryl. (A) NG1 based on p-Acrylamide. (B) NG2 based on p-vinylimidazole. (C) NG3	

based on p-DMAPS. (D) NG4 based on p-NIPAM at 37 °C. (E) NG4 based on p-NIPAM at 20 °C..... 86

Figure 3.25. Evolution of the G' and G'' modulus along the time for 40 nm Au nanospheres mixed with mucin. In green, AuNPs grafted with linear PEG-acryl. (A) NG5 based on p-Acrylamide. (B) NG6 based on p-vinylimidazole. (C) NG7 based on p-DMAPS. (D) NG8 based on p-NIPAM at 37 °C. (E) NG8 based on p-NIPAM at 20 °C..... 88

Figure 3.26. Evolution of the G' and G'' modulus along the time for 40 nm Au nanorods mixed with mucin. In green, AuNPs grafted with linear PEG-acryl. (A) NG9 based on p-Acrylamide. (B) NG10 based on p-vinylimidazole. (C) NG11 based on p-DMAPS. (D) NG12 based on p-NIPAM..... 89

Figure 3.27. Evolution of the G' and G'' modulus along the time for 40 nm Au nanostars mixed with mucin. In green, AuNPs grafted with linear PEG-acryl. (A) NG13 based on p-Acrylamide. (B) NG14 based on p-vinylimidazole. (C) NG15 based on p-DMAPS. (D) NG16 based on p-NIPAM..... 90

Figure 3.28. Graphical summary showing the mucin interaction tendencies from less (left) to more (right) for 13 nm Au nanospheres, 40 nm Au nanospheres, 40 nm Au nanorods and 40 nm Au nanostars..... 91

Figure 3.29. (A) Laser irradiation heating curves in triplicate for 13 nm Au nanospheres. (B) UV-VIS spectra before and after the irradiation of Au nanospheres. (C) Laser irradiation heating curves in triplicate for 40 nm Au nanospheres. (D) UV-VIS spectra before and after the irradiation of Au nanospheres..... 93

Figure 3.30. (A) Laser irradiation heating curves in triplicate for Au nanorods@PEG-acryl. (B) UV-VIS spectra before and after the irradiation of Au nanorods@PEG-acryl. (C) Laser irradiation heating curves in triplicate for Au nanorods@NG9 (p-acrylamide). (D) UV-VIS spectra before and after the irradiation of Au nanorods@NG9 (p-acrylamide). (E) Laser irradiation heating curves in triplicate for Au nanorods@NG10 (p-vinylimidazole). (F) UV-VIS spectra before and after the irradiation of Au nanorods@NG10 (p-vinylimidazole). (G) Laser irradiation heating curves in triplicate for Au nanorods@NG11 (p-DMAPS). (H) UV-VIS spectra before and after the irradiation of Au nanorods@NG11 (p-DMAPS). (I) Laser irradiation heating curves in triplicate for Au nanorods@NG12 (p-NIPAM). (J) UV-VIS spectra before and after the irradiation of Au nanorods@NG12 (p-NIPAM)..... 95

Figure 3.31. (A) Laser irradiation heating curves in triplicate for Au nanostars@PEG-acryl. (B) UV-VIS spectra before and after the irradiation of Au nanostars@PEG-acryl. (C) Laser irradiation heating curves in triplicate for

Au nanostars@NG13 (p-acrylamide). (D) UV-VIS spectra before and after the irradiation of Au nanostars@NG13 (p-acrylamide). (E) Laser irradiation heating curves in triplicate for Au nanostars@NG14 (p-vinylimidazole). (F) UV-VIS spectra before and after the irradiation of Au nanostars@NG14 (p-vinylimidazole). (G) Laser irradiation heating curves in triplicate for Au nanostars@NG15 (p-DMAPS). (H) UV-VIS spectra before and after the irradiation of Au nanostars@NG15 (p-DMAPS). (I) Laser irradiation heating curves in triplicate for Au nanostars@NG16 (p-NIPAM). (J) UV-VIS spectra before and after the irradiation of Au nanostars@NG16 (p-NIPAM). 98

Table 3.4. Centrifugation conditions used for the different AuNPs. 102

Chapter IV: Screening of Eudragits as building blocks in the preparation of physically cross-linked hydrogels

Figure 4.1. Scheme of a hydrogel composition and GF encapsulated inside the matrix (Epidermal, Nerve, Hepatocyte and Insuline GF). 118

Table 4.1. Polymers used in the hydrogel's formulations and their chemical structure. 122

Figure 4.2. Pictures of the 5 prepared hydrogels and their average thickness (mm) measured with a caliper. 123

Figure 4.3. (A - E) SEM pictures and histogram distribution for the pores in the transversal cut of the five hydrogels after their freeze-drying. (F) Summary plot with the average pore diameter for the five materials. Scale bars 50 μm . . 124

Figure 4.4. Samples of 1 x 1 cm from hydrogels A - E inside of a desiccator. Moisture uptake assay (with a saturated solution of K_2SO_4 , 95% relative humidity) and moisture content (with silica gel). 126

Figure 4.5. (A) Percentage of moisture uptake for all hydrogels vs. time. (B) Percentage of moisture content for all hydrogels vs. time. W_i represents initial weight; W_f is referred to the final weight. 126

Figure 4.6. $^1\text{H-NMR}$ (300 MHz, BSS/ D_2O 90/10) spectra of all the polymers that are involved in the different hydrogels. A) Eudragit RSPO, B) Eudragit RL100, C) Eudragit S100, D) Eudragit L100, E) Eudragit L100-55, F) Polyvinylpyrrolidone, G) Polyvinyl alcohol, H) Polyethylene glycol and I) Glycerol. 130

Figure 4.7. $^1\text{H-NMR}$ (300 MHz, BSS/ D_2O 90/10) spectra were obtained during the dissolution of hydrogel A (A) and hydrogel B (B). For hydrogel A (A), spectra 150 min, 180 min and 230 min have been shifted -0.24 ppm to improve signals

observation. For hydrogel B (B), spectra 70 and 75 min have been shifted -0.24 ppm to improve signals observation..... 131

Figure 4.8. $^1\text{H-NMR}$ (300 MHz, BSS/ D_2O 90/10) spectra were obtained during the dissolution of hydrogel C (A) and hydrogel D (B) and hydrogel E (C). For hydrogel C (A), spectrum 145 min has been shifted -0.24 ppm to improve signals observation. For hydrogel D (B), spectrum 130 min has been shifted -0.24 ppm to improve observation. For hydrogel E (C), spectrum 105 min has been shifted -0.24 ppm to improve observation. 134

Figure 4.9. The scheme shows the dogbone stands for the hydrogel and the different information that is possible to obtain with the tensile strain analysis. 136

Figure 4.10 Plots of tensile stress versus percentage of tensile strain applied for hydrogels A - E. 136

Figure 4.11 Plots showing (A) the maximum tensile strength applied until the material breaks, (B) the tensile break and (C) Young's modulus for hydrogels A – E. 137

Figure 4.12 Scheme of compression dynamic oscillatory rheology analysis and the information that can be obtained. Storage modulus (G'), loss modulus (G'') and glass transition temperature ($\text{Tan } \delta$)..... 139

Figure 4.13 Evolution of storage modulus G' , loss modulus G'' and $\text{tan } \delta$ loss tangent at different temperatures and a constant 1 Hz oscillatory frequency compression. 139

Table 4.2 Tg values for hydrogels A – E obtained from Figure 4.13C after compression dynamic oscillatory rheology analysis. 140

Figure 4.14 Scheme of the hydrogel's mucoadhesive measurements using an Ares instrument. (I) Conjunctiva approximates hydrogel. (II) Conjunctiva and hydrogel together during a certain time. (III) Separation conjunctiva from the hydrogel. Work of adhesion is determined with the formula shown in the figure. 141

Figure 4.15 Work of adhesion obtained for hydrogels A – E. Day 0 means without hydration, after 3 days hydration being in a 95% of relative humidity, after 5 days hydration being in a 95% of relative humidity, after 10 min of hydration with 20 μL of BSS solution, after 30 min of hydration with 20 μL of BSS solution. 142

Figure 4.16. TGA plots for Hydrogels A – E in three scenarios. (A) Empty hydrogels. (B) Hydrogels with BSA. (C) Hydrogels with BSA-FITC. (D) Eudragits

as controls. (E) Rest of the polymers and proteins used for hydrogel preparation. 145

Table 4.3 Summary of the temperatures at which 5, 10 and 50% of the total weight has been lost. Data is shown for Hydrogels A – E in the three scenarios. 1) Empty hydrogels. 2) Hydrogels with BSA. 3) Hydrogels with BSA-FITC. .. 145

Figure 4.17. (A – E) First derivative of the TGA curve for hydrogels A – E. (X_1) Empty hydrogels. (X_2) Hydrogels with BSA. (X_3) Hydrogels with BSA-FITC. (F) First derivative of the TGA curve for Eudragits pure polymers. (G) First derivative of the TGA curve for the rest of polymers and proteins used for hydrogel's preparation..... 147

Table 4.4 Summary of the temperatures from the maximum peak obtained from the first derivative of the TGA curve. 148

Figure 4.18 (A) DSC results of the first heating for hydrogel A. A_1 empty hydrogel A. A_2 hydrogel A with BSA. A_3 hydrogel A with BSA-FITC. (B) DSC of the cooling curve. (C) DSC of the second heating curve. (D) DSC of the first heating curve after 24 hours. (E) DSC of the cooling curve in the second experiment. (F) DSC of the second heating curve in the second experiment. The heating and cooling rate for all the cases are 20 °C..... 149

Table 4.5 Summary of the endothermic peak T_p and the enthalpy of the melting endotherms for hydrogels A. A_1 empty hydrogel. A_2 hydrogel A with BSA. A_3 hydrogel A with BSA-FITC. Data obtained from DSC analysis. 150

Table 4.6 Summary of the crystal fractions obtained by DSC for hydrogel A, scenarios 1 – 3..... 151

Figure 4.19. X_1 empty hydrogel A. X_2 hydrogel A with BSA. X_3 hydrogel A with BSA-FITC. (A, D, G, J) DSC of the first heating for hydrogels B, C, D and E respectively. (B, E, H, K) DSC of the cooling curve for hydrogels B, C, D and E respectively. (C, F, I, L) DSC of the second heating curve for hydrogels B, C, D and E respectively. The heating and cooling rate for all the cases are 20 °C. 152

Table 4.7 Summary of the temperatures at maximum peak, the enthalpy of the melting endotherms and the crystals fraction for hydrogels B - E. X_1 empty hydrogel. X_2 hydrogel with BSA. X_3 hydrogel with BSA-FITC. Data obtained from DSC analysis..... 153

Figure 4.20 WAXS analysis of (A) empty hydrogel A. (B) hydrogel A with BSA. (C) hydrogel A with BSA-FITC. (D) empty hydrogel C. (E) hydrogel C with BSA. (F) hydrogel C with BSA-FITC. 155

Table 4.8 Summary of PVA and PEG percentage of crystals presented in hydrogels A_1, A_3, C_1 and C_3.	156
Figure 4.21. Hydrogels A – E with BSA-FITC protein encapsulated inside the materials and their average thickness (mm). The aspect of the materials with direct observation (top) and aspect after irradiation with 254 nm wavelength (bottom).	157
Figure 4.22. BSA-FITC release kinetics obtained from hydrogels A – E. Results represented as a percentage of accumulative released (A, C, E, G, I) and as BSA μg released (B, D, F, H, J).	159
Table 4.9. Summary of the principal data obtained from the BSA-FITC release kinetic from hydrogels A – E.	160
Figure 4.23. Grow Factor release kinetics obtained from hydrogels A – E. Results represented as a percentage of cumulative release (A, C, E, G, I) and as BSA $\mu\text{g}/\text{mL}$ released (B, D, F, H, J). Table summarizing the time for 50%, 80%, 100% and max mg released is also represented for each hydrogel and compared with the value obtained from BSA release studies.	163
Figure 4.24. Metabolic activity of MRC-5 cells was obtained after 24 and 48 h of incubation with different dissolution degrees (25, 50 and 100%) of hydrogels A – E with the cells.	165
Figure 4.25. Metabolic activity of WKD Chang conjunctiva epithelial cells was obtained after 72 h of incubation of hydrogels A – E with the cells. (A) Summary of the cell viability. (B – G) Optical microscopy pictures of the cell's aspect.	167
Figure 4.26. (A) Hydrogel A with dimensions 0.4 x 0.4 x 0.1 cm onto the ocular surface. (B) Hydrogel A onto the ocular surface. (C) A few seconds after, the material is not attached to the conjunctiva and can be easily removed.	168
Figure 4.27. (A) Hydrogel C with dimensions 0.4 x 0.4 x 0.1 cm onto the ocular surface. (B) Hydrogel C outside ocular conjunctiva after closing and opening again the eyelid.	169
Figure 4.28. Chemical structures of (A) HA and (B) HPC.	170
Figure 4.29. Work of adhesion of the hydrogels to the ocular conjunctiva obtained after 15 and 30 min of hydrogels pre-hydration with BSS.	171
Figure 4.30. Mucoadhesion test <i>In-vivo</i> of hydrogel C with three composition modifications. (A) Hydrogel C + 2% HPC. (B) Hydrogel C + 10% HPC. (C) Hydrogel C + 30% HA. For all the cases, (I) placing the material. (II) closing the eyelid. (III) opening again the eyelid.	172

Figure 4.31. ¹H-NMR (300 MHz, BSS/D₂O 90/10) spectra were obtained during the dissolution of hydrogel C modified with (A) 30% of HA and (B) hydrogel C without modifications. 174

Figure 4.32. Grow Factor release kinetics obtained from hydrogels C modified with 30% of HA. (A) Percentage of cumulative release vs time. (B) µg of GF released vs time. 175

Table 4.10. Summary of the most relevant data obtained from GF release kinetics from hydrogel C modified with 30% of HA and hydrogel C without modifications..... 176

Figure 4.33. Evolution of the eye injury after 0, 7, 14, 21 and 28 days of two random rabbits treated with (A) Tobradex as a control. (B) AM and Tobradex as a positive control. (C) Hydrogel C + 30% HA and Tobradex..... 177

Figure 4.34. (A) Median epithelial defect area (mm²) after 0, 7, 14, 21 and 28 days of the injured eye with Tobradex (blue), AM and Tobradex (red) and hydrogel C + 30% HA candidate and Tobradex (green). (B) Ocular epithelial wound closure as a percentage of total rabbits' complete closure after 0, 7, 14, 21 and 28 days of the injured eye with Tobradex (blue), AM and Tobradex (red) and hydrogel C + 30% HA candidate and Tobradex (green)..... 178

Figure 4.35. Scheme of stability assays set-up. 182

Annexes

Figure Annex I. (Scenario I) Evolution of the UV-VIS spectra along the time obtained incubating the materials at 37 °C for NPs grafted with PEG-acryl and encapsulated into p-acrylamide, p-vinylimidazole, p-DMAPS and p-NIPAM. (A - E) 13 nm Au nanospheres. (F - J) 40 nm Au nanospheres. (K - O) 40 nm Au nanorods. (P - T) 40 nm Au nanostars. 202

Figure Annex II. (Scenario II) Evolution of the UV-VIS spectra along the time obtained incubating the materials at 37 °C with NaCl 2M for NPs grafted with PEG-acryl and encapsulated into p-acrylamide, p-vinylimidazole, p-DMAPS and p-NIPAM. (A - E) 13 nm Au nanospheres. (F - J) 40 nm Au nanospheres. (K - O) 40 nm Au nanorods. (P - T) 40 nm Au nanostars. 204

Figure Annex III. (Scenario III) Evolution of the UV-VIS spectra along the time obtained incubating the materials at 37 °C with PBS 10mM for NPs grafted with PEG-acryl and encapsulated into p-acrylamide, p-vinylimidazole, p-DMAPS and p-NIPAM. (A - E) 13 nm Au nanospheres. (F - J) 40 nm Au nanospheres. (K - O) 40 nm Au nanorods. (P - T) 40 nm Au nanostars. 206

Figure Annex IV. (Scenario IV) Evolution of the UV-VIS spectra along the time obtained incubating the materials at 37 °C with BSA 1 mg/mL (in PBS 10 mM) for NPs grafted with PEG-acryl and encapsulated into p-acrylamide, p-vinylimidazole, p-DMAPS and p-NIPAM. (A - E) 13 nm Au nanospheres. (F - J) 40 nm Au nanospheres. (K - O) 40 nm Au nanorods. (P - T) 40 nm Au nanostars..... 208

List of abbreviations and symbols

Abbreviation	Meaning
%	Percentage
°	Angle
°C	Celsius Degrees
µg	microgram
µL	Microliter
µm	Micrometer
AFM	Atomic Force Microscopy
AgNPs	Silver Nanoparticles
AM	Amniotic Membrane
APS	Ammonium persulfate
Au	Gold
AuNPs	Gold Nanoparticles
AuNRs	Gold Nanorods
AuNSs	Gold Nanospheres
AuNSts	Gold Nanostars
BSA	Bovine Serum Albumin
BSS	Balanced Salt Solution
cm	centrimetre
CTAB	Cetyl Trimethyl Ammonium Bromide
CuNPs	Copper Nanoparticles
D₂O	Deuterated Water
DLS	Dynamic Light Scattering
DMAPS	[2-(Methacryloyloxy)ethyl]dimethyl-(3-sulfopropyl)ammonium hydroxide
DMEM	Dubelcco's modified Eagle's medium
DSC	Differential Scannin Calorimetry
EGF	Epidermal Growth Factors
EMA	European Medicine Agency
FBS	Fetal Bovine Serum
FDA	Food and Drug Administration
FITC	Fluorescein isothiocyanate
G´	Storage/Elastic Modulus
G´´	Loss/Viscous Modulus
GF	Growth Factors
GPC	Gel Permeation Chromatography
GSH	Glutathione
h	Hours

H₂O	Water
HA	Hyaluronic Acid
H₂AuCl₄	Tetrachloroauric
HEPES	4-(2-hydroxyethyl)-1-piperazineethanesulfonic acid
HGF	Hepatocyte Growth Factors
HPC	Hydroxypropyl cellulose
IGF-1	Insulin-like Growth Factors
IPN	Interpenetrating
K₂SO₄	Potassium sulphate
kDa	Kilodalton
KPS	Potassium persulfate
kv	kilovoltage
LCST	Lower Critical Solution Temperature
Max.	Maximum
MC	Moisture Content
mg	Miligram
MHz	Megahertz
min	Minute
mL	Millileter
mm	milimetres
mm	Millimeter
mm²	Square meters
MRC-5	Human fetal lung fibroblast cells
MU	Moisture Uptake
MW	Molecular Weight
MΩcm	Million ohms per centimetre
N	Newton
NaBH₄	Sodium borohydride
NaCl	Sodium Chloride
NGF	Nerve Growth Factors
NGs	Nanogels
NIPAM	N-Isopropylacrylamide
NIR	Near Infrared
nm	Nanometer
NMR	Nuclear Magnetic Resonance
NPs	Nanoparticles
PAM	Polyacrylamide
PBS	phosphate-buffered saline
PC	Protein Corona
PCL	polycaprolactone
PDI	Polydispersity Index
PDMAEMA	poly(2(dimethylaminoethyl methacrylate)
PEG	Polyethylene glycol

PEI	Poly(ethyleneimine)
pHEMA	Poly(2-hydroxyethyl methacrylate)
PIS	Penicilin-streptomycin solution
PLGA	Poly(lactic acid-co-glycolic acid)
pNIPAM	Poly(N-isopropylacrylamide)
PPE	Polyphenyl ether
ppm	Parts Per Million
PTFE	Polytetrafluoroethylene
PVA	Polyvinyl alcohol
PVC	Polyvinyl chloride
PVP	Polyvinyl pyrrolidone
PVP	Polyvinylpyrrolidone
s	second
SEM	Scanning Electron Microscope
Tcp	Cloud-point temperature
TEM	Transmission Electron Microscopy
TEMED	Tetrametilendiamina
Tg	Glass Transition Temperature
TGA	Thermogravimetric analysis
Tm	Melting temperature
UCNPs	Upconverting Nanoparticles
UV-VIS	Ultraviolet–Visible
WAXS	Wide-angle X-ray scattering
W_f	Final Weight
W_i	Initial weight
WKD	Kibourne derivate of Chang conjunctiva epithelial cell line
ΔH_m	Enthalpy melting endotherms
ε₀	Molar Extinction Coefficient



CHAPTER I: General Introduction

1.1 Introduction

During the last years, the human lifestyle has changed dramatically in many aspects. We have experienced an exponential growth in technological development that let us pass from creating the first computer in 1970 to being able to wear one in our pocket just 30 years later.^[1] This big jump had also an effect on medicine, thanks to that, we have seen human life expectancy growing year by year. The first records of human wound treatment dates back to the year 800 BC. Around the year 1220, the first universities started training people to heal others. Some years later, the first microscope was created, letting us increase our knowledge of anatomy. During the XIX century, the development of society demanded sanitary measures and the first public health services appeared. They came hand-in-hand with the advance of antibiotics. Then, the curve of knowledge was skyrocketed with progress in chemistry, genetics, X-ray technology, etc., setting up the pillars of what we nowadays know as biomedical science.^[2] A well-understanding of the background is a must to promote progress. Therefore, in the following sections, the evolution of medical treatments linked to the evolution of chemistry will be reviewed.

1.2 Polymers in biomedical applications

Natural polymers have been used in medicine for several years, obtained from plants in healers' treatments.^[3] Later, the advance in synthetic chemistry has opened a new door, modifying natural polymers and even creating synthetic ones in the XX century. This milestone could not have been possible without the effort of thousands of researchers around the world. The "big bang" of modern polymer science is attributed to Staudinger,^[4] who is considered the father of polymer chemistry. In 1953, he received the Nobel prize "for his discovery in the field of macromolecular chemistry" as a conclusion of his work for more than 30 years. During that period, he sketched the post-polymerization technology that nowadays has evolved into the methodology that many of us are employing in laboratories. Some years later, the importance of synthetic polymers kept growing. In the 1960s, a polymer was used in clinical trials for the first time. It was called pyran co-polymer,^[5] and it was based on divinylether and maleic anhydride. It was considered a biologically active polymeric drug, and the idea was to test its promising anticancer effects. Unfortunately, all the hope was lost during the first round of assays due to its high toxicity related to its high molecular weight. Nevertheless, this experiment was a turning point and several optimizations

took place in the following years. Nowadays, we can find many polymers in the market as medical devices, like blood bags, made of low molecular weight polyvinyl chloride (PVC), hernia meshes from polyphenyl ether (PPE) or vascular prostheses from polytetrafluoroethylene (PTFE).^[6] Besides, polymers are also widely used for wound dressing, tissue engineering, drug delivery, cosmetics, water treatment, food preservation, among others.^[7]

There are plenty of tools to modify the chemical structure of polymers, which triggers the emergence of neutral, negative and positive charged polymers coming from natural or synthetic sources.^[8] Furthermore, it is possible to tune the physical and chemical properties of materials and increase their biocompatibility based on controlled synthetic strategies, monomers nature and combination of polymeric ratios.^[9] Scientists have modified polymers to let them interact with cells and even whole tissues. For instance, one of the most relevant synthetic polymers in medicine is polyethylene glycol (PEG). It is frequently used in tissue engineering and for drug delivery platforms. This polymer is non-adhesive to proteins and also exhibits very low cell toxicity. Furthermore, the technology to modify their chains to add functional groups at the terminal positions is well established, allowing it to be used in plenty of polymerization reactions and surface decoration.^[10] More recently, several polymer modifications have let appeared a new world of structures known as smart polymers.^[11] In this scenario, polymers are sensitive to their environment (pH, temperature, etc.) changing their molecular structure or physiochemical properties accordingly.^[12] In addition, they can self-assembly forming nanometer-sized systems. One can find in the literature many examples that show how this smart behaviour can be actively used for biomedical applications. For example, poly(lactic acid-co-glycolic acid) (PLGA) have been modified with methyl groups to implement changes in their thermo-mechanical, swelling and degradation properties as a consequence of pH response.^[13] This pH sensitivity has a very important role in medicine as the pH in tumour cells is more acid than in normal ones.^[14] Therefore, smart devices that can change their conformation in function of a variation of pH, can be used as intelligent drug carriers. The cargo release from this type of device is controlled by the environmental stimulus (pH), improving their therapeutic efficiency and targetability to the target tissue. Smart pH-sensitive polymers have also found similar applications in wound healing,^[15] where the pH also turns to acidic. Consequently, smart pH-sensitive nanocarriers based on polymers can be used for skin treatments.

As the average normal body temperature is 37 °C, polymers that undergo a phase transition around that temperature are particularly useful because their chains can contract or elongate allowing a controlled drug release. Furthermore, this also allows a decrease of the undesired adverse side effects. The cloud-point temperature (T_{CP}) is the temperature at which phase separation starts, which means that the solubility of thermoresponsive polymers starts decreasing. Poly(N-isopropylacrylamide) (pNIPAM)^[16] is the most broadly studied. It has a lower critical solution temperature (LCST) in water of around 32 °C. In other words, when the temperature is above 32 °C, the polymeric chains contract. In contrast, the chains expand when the temperature is below 32 °C. This polymer can be prepared by radical polymerization of N-isopropylacrylamide (NIPAM). Additionally, the transition temperature can be easily tuned by co-polymerizing this monomer with another acrylic one. If the co-monomer is hydrophilic, the LCST temperature will increase. Otherwise, if the co-monomer is hydrophobic, the LCST will decrease. In biomedicine, this strategy has been applied for the preparation of smart nanocarriers^[17] that can release the cargo only when the temperature is about the T_{CP} .

1.2.1 Cross-linking polymers to improve their properties for biomedicine

A cross-link is referred to a short bond between two or more polymeric chains that end in a modification of the physical and chemical properties of the material. The two main strategies for linking polymeric chains with each other are by physical or chemical cross-links.^[18] Physical cross-linking is generally created by intermolecular reversible interactions, hydrogen bonds, different polar/apolar interactions, the appearance of crystals, metal coordination and π - π forces. The main benefit of this type of interaction is the absence of chemical cross-linkers, which guarantees better biocompatibility as there is no risk of the presence of unreacted chemical hazardous linkers in the final product. Besides, this strategy allows the use of already approved polymers by regulations agencies (e.g., European Medicines Agency, EMA, and Food and Drug Administration, FDA) that can be mixed and joined by physical interactions without creating a new synthetic identity. Furthermore, physically cross-linked hydrogels are often further processed with many treatment methods to reinforce their matrix stability. As example, freeze-thaw cycling, heat, self-assembly, ionic interactions and hydrophobic interactions with other polymers have been used.

On the other side, mixing polymers with chemical cross-linkers involves the formation of covalent bonds between chains. This junction is fairly strong and, in many cases, permanent. Nevertheless, reversible covalent bonds are as well prepared by chemical cross-linking strategies. To this point, cross-linking strategies have yielded in the appearance of hydrogels, microgels and nanogels (NGs), allowing the development of carriers at the micro and nanoscale respectively.^[19]

The complexity of hydrogel has evolved over the years. The first generation of reported hydrogels dates from the 1960s and it was just simple polymeric chains combined between them with physical or chemical cross-linkings. For the second case, it can be used a cross-linker molecules that can join two polymeric chains or a tetra functional monomer, that can join four polymeric chains. Then, in the 1970s the second generation appeared including stimuli-responsive behaviours. The third generation was based on physically cross-linked stereo-complexed structured, which gained importance in the 1980s. Nowadays, the fourth generation exhibits double networks matrices based on a combination of natural and synthetic polymers and the stimulus behaviour has changed until the level to recognize enzymes.

According with their composition, hydrogels can be split into five classes.^[20] (I) Homopolymers, that only contain one monomer forming the whole hydrogel matrix. They can also be prepared with a pre-polymer, which is a monomer that have been reacted into an intermediate molecular mass. (II) Copolymers, based on two or more monomers. (III) Interpenetrating networks (IPN), where two different precursors can be polymerized at once (simultaneous polymerization). (IV) Semi-IPN, which is form in two steps. First, a polymeric network is prepared based on one monomer and then, a second polymeric chain is embedded inside the initial network (sequential polymerization). This second chain, based on another monomer, swells in the polymeric network without the presence of a cross-linker. The main benefit of semi-IPN is that their mechanical strength and swelling capacities are higher than homo- or co-polymer hydrogels. (V) Ionic polymers, which are pH-sensitive polymers, are used to modify the polymeric charges inside the hydrogel. **Figure 1.1** summarises the different strategies for preparing hydrogels and the type of cross-linkers that can be used for stabilizing the matrices.

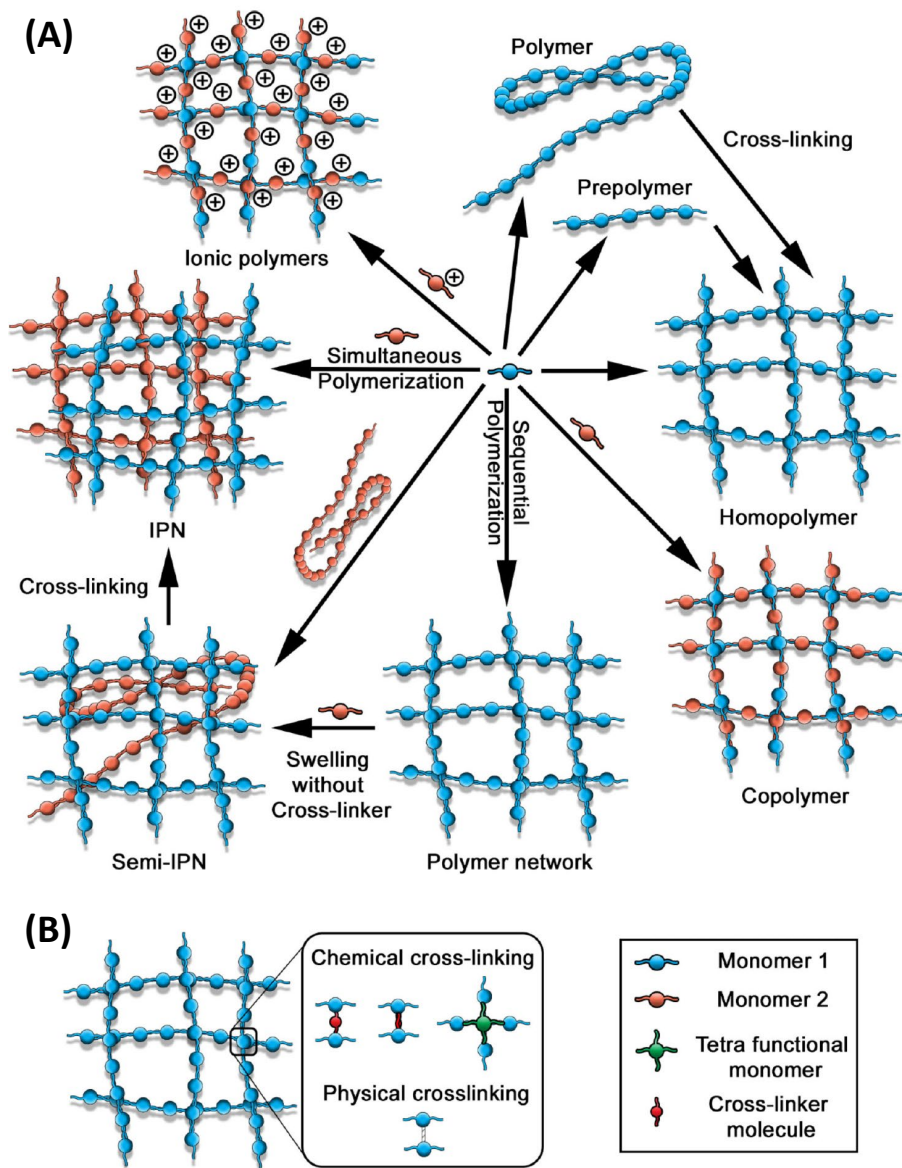


Figure 1.1. (A) Scheme showing several strategies to prepare hydrogels. (B) Physical and chemical cross-linkers to join polymeric chains during the preparation of hydrogels. Figure adapted with permissions from *Journal of Applied Polymer Science*, 2021.^[20]

The presence^[21] of several hydrophilic groups, like, $-\text{COOH}$, $-\text{OH}$, $-\text{NH}_2$, $-\text{CONH}-$, $-\text{CONH}_2$, $-\text{SO}_3\text{H}$, allow hydrogels to retain high amounts of water and physiological liquids (more than 20% from its dry weight), as hydrogen bonds can be formed.^[22] Besides, they also exhibit good permeability to low and high molecular weight molecules and extraordinary swelling properties. For drug

delivery,^{[23][24]} they have in their matrices regions that can be used for drug storage, controlling and driving the drug release rate. They have been used to deliver drugs via oral, nasal, buccal, rectal, vaginal, ocular and intravenous routes, improving the therapeutic outcome of the cargo. In general, hydrogels have been used to overcome the poor solubility, stability and dispersion drawbacks of lipophilic drugs. *In-situ* forming thermo-sensitive hydrogels^[25], which are materials that gel directly in the site of action, have been applied to deliver anti-tumour drugs directly into the tumour mass, avoiding drug leak into healthy organs and decreasing undesired side effects.

For wound healing,^[26] they have been adapted to have adhesiveness, antimicrobial, anti-inflammatory and pro-angiogenic properties. The aforementioned, together with the pre-encapsulation of wound healing therapeutic agents makes them perfect candidates for this treatment. Hydrogels for ocular drug delivery,^[27] have also been explored for several years. Soft contact lenses, based on poly(2-hydroxyethyl methacrylate) (pHEMA) and silicone, have been used to increase the corneal residence time of drugs by 15 folds compared with the typical eye drops. Besides, *In-situ* gels have also been used for dry eye syndrome, glaucoma and retinal diseases.^[28] Other hydrogel applications in the field of medicine behold tissue engineering,^[29] in food science,^[30] food packaging, adsorption and removing metals heavy metals from food; and as biosensors,^[31] through plasmonic nanostructures, fluorescence sensing or by electrochemical methods.

1.3 Nanomedicine: A new trend of working at the atomic level

Since Dr. Feynman said “There’s plenty of room at the bottom”^[32] during his speech at the annual meeting of the American Physical Society in 1959, the boom of nanotechnology has emerged. He sketched the idea that tiny nanorobots could be designed and introduced into the human body to perform cellular repairs at the molecular level. At present, nanotechnology^[33] is known as the area of science that studies materials with dimensions in the range of 1 – 100 nm. Operating the matter at the nanometric scale has assumed enormous challenges.^[34] From self-assembly structures, that mimic the properties of DNA, to positional assembling complex structures that set fragments into the appropriate area of the body. The first approval of a nanomedicine by the FDA took place in 1995. It was commercialized under the name of Doxil®.^[35] It is mainly formed by the encapsulation of doxorubicin, a

widely used anticancer drug, inside of PEGylated nano-liposomes. After Doxil, over the last 20 years, nanomedicine has pushed pharmaceuticals, medical imaging, diagnosis, cancer treatment, tissue regeneration, among others, to be developed quicker.^[36] The development of materials for all these applications, have been possible thanks to a new level of analytical tools^[37] that have encompassed a better understanding of the materials. Thanks to the development of nanotechnology, novel therapies are emerging day by day (drug and gene delivery, imaging, etc), improving cost-effective healthcare and decreasing hazardous effects like toxicity.^[38] Indeed, different particles based on organic or inorganic elements have been prepared recently. **Figure 1.2** shows a scheme of several types of nanoparticles of interest in nanomedicine.

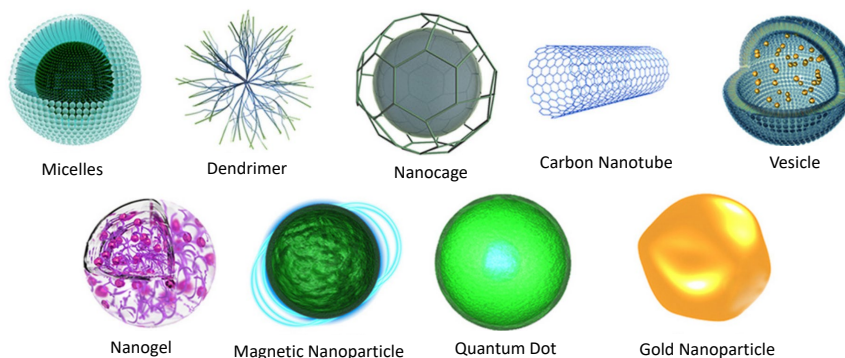


Figure 1.2. Scheme of organic and inorganic nanoparticles. Figure adapted with permission from IORScience, 2015.[39]

As it can be seen from **Figure 1.2**, many types of nanoparticles can be synthesized through different routes to achieve monodisperse organic or inorganic nanoparticles. The most relevant are going to be described in the following sections.

1.3.1 Organic nanoparticles for biomedical applications

Since the appearance of NPs, the use of the carbon element has been explored in several forms to be used in novel therapeutics treatments. Micelles, vesicles and dendrimers are the most studied ones. In fact, they have found their place in the market already. More recently, microgels and nanogels have appeared as a novel and intelligent class of material with promising applications. In this section, the most relevant organic NPs and their evolution along the time are going to be reviewed.

Polymeric micelles and vesicles have emerged as promising nanocarriers. They are mesoporous nanomaterials that can be structured at three different dimensions (**Figure 1.3**), with pore sizes in the range of 2 – 50 nm. Selecting the appropriate block copolymers, micelles can also be biodegradable. This particular branch of organic NPs has the benefit of loading hydrophobic drugs, which allows an increase on their lifetime durability in presence of a biological fluid. Furthermore, they can be prepared with diameters in the range of 20 – 200 nm, a perfect size to let them swim in the blood vessels for longer times, as compared with small molecules, and to be accumulated in the diseased tissues and be eventually excreted. As they are mainly composed of organic materials, it turns out quite easy to modify their functional groups to actively target the site of action.^[40]

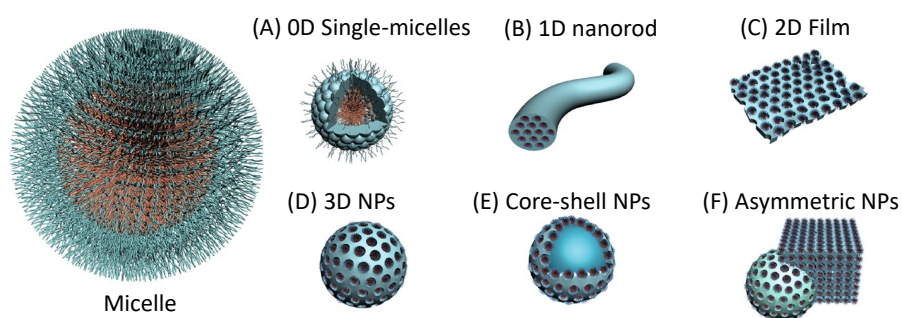


Figure 1.3. Different classes of ordered mesoporous micelle in the function of the architecture level. Figure adapted with permission from Nature Reviews Materials, 2019.^[41]

Polymeric micelles can be fabricated by the hard-templating and soft-templating methods. The first one involves the preparation of pre-synthesized mesoporous solids. Meanwhile, the second method let the preparation of polymeric micelles by self-assembly of amphiphilic block copolymers.^[41] Every year is more and more frequent to find commercial formulations of drugs encapsulated onto micelles NPs. An example is Genexol-PM[®],^[42] based on a di-block copolymer of PEG and polylactic acid (PLA), with an active ingredient called paclitaxel encapsulated inside, for breast and lung cancer treatment. Nevertheless, micelles have also found applications as biosensing,^[43] catalysis^[44], pesticides,^[45] and others.

Dendrimers are another kind of organic nanoparticles that were reported for the first time in 1978. Afterwards, many different types of dendrimers were prepared, given more complex structures with multiple reactive sites that let the dendrimer grow layer-by-layer in different concentric generations. The third and fourth generation allows the

appearance of internal cavities giving the dendrimers a circular shape.^[46] Their divergent preparation^[47] starts from a multifunctional core where the dendrimer can be developed through the sequential attachment of monomers as shown in **Figure 1.4**.

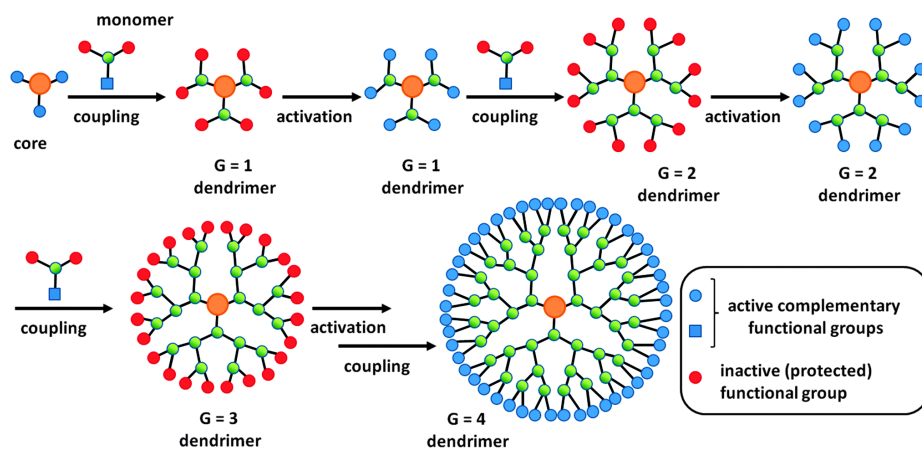


Figure 1.4. Scheme of the divergent synthesis of dendrimers. Figure adapted with permission from *New Journal of Chemistry*, 2014.^[47]

Dendrimers have been used in medicine since their first preparation. Due to their functional terminal groups, the applications are almost unlimited. For instance, adding thiol groups^[48] to the surface have been used as a strategy to increase their mucoadhesion properties, thanks to the junction of thiol with cysteine domains typically found in mucosa. Likewise, their used as drug nanocarriers have also been explored. Thanks to their porous structure, the gaps between polymeric chains can be used to load drugs. This behaviour is optimal for gene delivery towards tumours even in the brain,^[49] overcoming the blood-brain barrier. In addition, dendrimers have also found their purpose in analytical extractions (solid phase, capillary, etc).^[50]

The knowledge achieved over the last years with all this variety of organic nanoparticles, settled the fundamentals for more advanced nanoparticles, called nanogels that were reported for the very first time in 1999.^[51] Nevertheless, in 1988 Antonietti^[52] reported similar structures, but they were called microgels. In that study, the authors created a hydrophilic network by crosslinking PEG. In the following year,^[53] a second study appeared with the preparation of a nanogel based on poly(ethyleneimine) (PEI) to be used as nanocarrier of antisense oligonucleotides. Essentially, nanogels are hydrogels developed at the nanometric scale. They have a three-dimensional structure stabilized by physically or chemically cross-linkers of natural or synthetic polymeric chains. Due to the hydrophilicity of their chains, they can

swell in aqueous media, retaining a large amount of water inside their matrix.^[54] At the very beginning, the degree of cross-linker was controlled by adding surfactants to the reaction. Nevertheless, one of the main drawbacks of this strategy was the increase of cytotoxicity if the surfactants were not properly removed.^[55] At present, “click chemistry”^[56] has emerged as an alternative route to prepare cross-linked nanogels thanks to azide-alkyne, nucleophilic and radical thiol-ene reactions. This technology allows the preparation of nanogels with different dimensions, good reactivity, excellent selectivity and soft reaction conditions. Besides, the by-products that could appear as a consequence of the synthesis can be easily removed by centrifugation or dialysis. This, avoids the traditional and complex chromatography purification strategies. Moreover, click chemistry is also stereospecific, highly reproducible and works well in benign solvents. Nanogels have met a whole set of applications,^[57] ranging from smart nanogels in stimuli-responsive drug nanocarriers to imaging, like MRI contrast agents, PET imaging, optical and multimodal imaging.

Smart nanogels^{[58][59]} have emerged as a sub-category that can interact with their environment, having a response towards a modification in the pH, temperature, enzyme overexpression and electro-magnetic fields. For instance, the pH^[60] of healthy tissue is normally 7.4, but, in tumour environments, the production of excess of lactic acid, decrease the pH to around 6.5. In addition, the pH of intracellular endolysosomes can decrease even to around 5. A smart nanogel can be easily designed to recognize this decrease of pH, to deliver the cargo only under this particular conditions. The main benefit of this technology, in comparison to normal nanocarriers, is that non-intelligent ones can be easily degraded due to the acidic conditions, releasing the drug in a non-controlled manner, while in a smart nanogel the release is controlled. To add this pH-responsive capacity into the nanogels, it is just requested the presence of a pH-responsive polymer. Such as Gong, et al.,^[61] who used poly(2-(hexamethyleneimino) ethyl methacrylate) as a pH-responsive polymer in the preparation of a nanogel for the delivery of DNA. Another strategy is to add pH-sensitive bonds into the cross-linked network. For instance, Lee, et al.^[62] used a disulfide-bond linker to prepare a pH-sensitive nanogel based on hyaluronic acid for lung cancer therapy. Conversely, thermoresponsive^[63] nanogels can respond to temperature changes in their environment. They can be prepared similarly to the pH-sensitive ones, incorporating temperature-sensitive polymers to the structure or the bonds. Nevertheless, there is an alternative strategy to prepare this type of material, which includes the incorporation of hydrophobic moieties to side groups of the network. The moieties have the ability to decrease the LCST

of the polymer, letting adjust the critical solution temperature of the nanogel. pNIPAM is one of the most well-known polymers for the preparation of thermoresponsive nanogels. Lu, et al.,^[64] prepared a di-block copolymer nanogel based on a combination of pNIPAM and vinylphenylboronic acid to be used as an eye glucose detector. They achieved high monodispersed nanogels that respond towards temperature, pH and glucose, displaying a colour change in function of the glucose concentration. In another recent example, Calderón et al.^[65] analyzed the effect that the crosslinking degree has on the release kinetics of a protein that was previously encapsulated within the thermoresponsive nanogels. They prepared nanogels based on pNIPAM as thermoresponsive polymer and dendritic polyglycerol as cross-linker with a range of diameter of 70 – 210 nm. They concluded that an increase in the pNIPAM ratio was directly correlated to an increase in protein retention at a temperature above LCST. This result highlights the importance of adjusting properly the thermoresponsive polymer ratio into the desired application. All these examples evidence that smart nanogels can be modified for many target applications in biomedicine, including the addition of end groups to recognize enzymes or magnetic fields variation.^[66] **Figure 1.5**, shows a scheme of a nanogel releasing a drug by different responsive mechanisms.

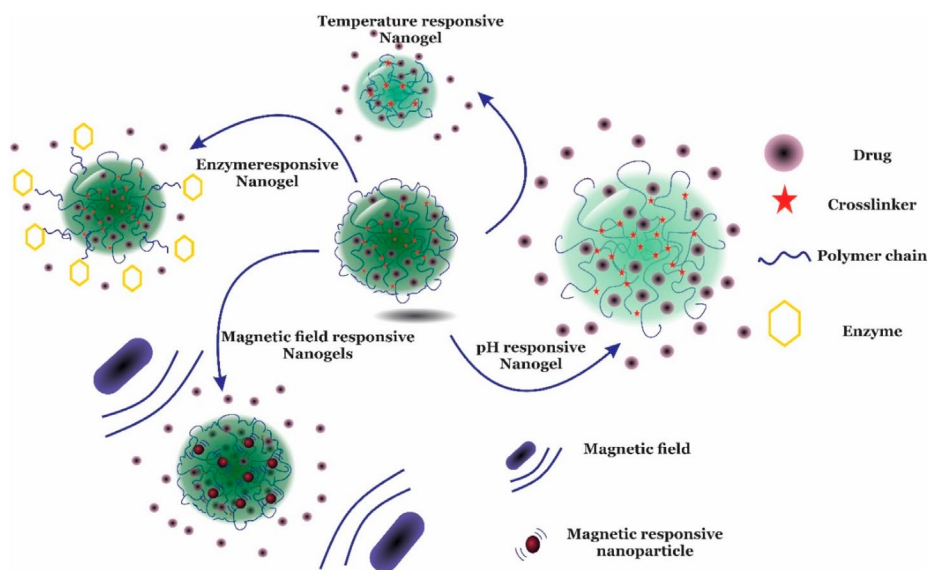


Figure 1.5. Scheme of a smart nanogel releasing a drug under a change of temperature, enzyme overexpression, magnetic field and pH. Figure reproduced with permission from *Gels*, 2020.^[63]

1.3.2 Inorganic nanoparticles for biomedical applications

Gold, silver, copper and iron are the most typical metals used for the preparation of inorganic nanoparticles (NPs). Most recently, quantum dots or up-converting nanoparticles have emerged as promising inorganic nanoparticles based on rare earth elements for diagnostic applications in biomedicine. In this section, the evolution of these kinds of particles and their main advantages in comparison with organic nanoparticles are going to be explored.

Nanomaterials based on gold, silver and copper are considered to be the oldest ones. During Romans times, fifth century AD, a crystal cup was created, known as the Lycurgus cup^[67] (**Figure 1.6**). This cup was considered “magic” for several centuries as to when it is illuminated from outside, the cup is green, but when the light comes from inside, the cup turns purple. The explanation of this phenomenon went public in 1990 after a deep analysis with atomic force microscopy (AFM). It was determined that the cup was formed by silver nanoparticles (AgNPs) (66%), gold nanoparticles (AuNPs) (31.2%) and copper nanoparticles (CuNPs) (2.6%). Most probably, the artist used a metal aqueous solution for the preparation of the glass, and during the drying process, these metals were reduced letting the appearance of inorganic nanoparticles. Nowadays, this cup is part of the permanent exhibition of the British Museum.



Figure 1.6. Lycurgus cup. On the left, cup with the light coming from inside the vessel. On the right, the cup with light coming from outside. Figure adapted with permission from *Nature*, 2000.^[68]

In the 1850s, Michael Faraday^[69] gave a lecture at the Royal Institution of Great Britain sharing with the scientific community his impressive discoveries about gold. He mixed an aqueous gold salt solution with phosphorous, observing a change in the colour varying the ratios until

achieving a transparent solution. Afterwards, he also observed that the gold solution could interact with light-emitting different colours. What he didn't know by that time was that he prepared for the very first time, a colloidal solution of gold nanoparticles dispersed in water.

More than a hundred years later, thanks to the work done by Faraday and colleagues, the inorganic nanoparticles started being understood and several synthetic methodologies were established. Au NPs^[70] emerged in the 1990s as a talented platform for drug delivery. Their surface can be conjugated with thiolated molecules through a combined interaction of 35% covalent and 65% electrostatic. This functionalization rises the properties of the Au NPs to effective cellular uptake, controlled payload and cell targeting. Moreover, Au NPs can be prepared in the range of $< 2 - 150$ nm, which allows the delivery of small drugs and big biomolecules. Varying the size and shape, it is possible to tune their physio-chemical, pharmacokinetic, optical properties, high X-ray absorption coefficient and electronic properties. They can be prepared^[71] by several approaches like γ -irradiation, microwave, sonochemical, ultraviolet, laser ablation, photochemical process, reduction chemical process and biological synthesis. Furthermore, Au NPs can have different shapes; **Figure 1.7** shows a few of them, (A) nanospheres, (B) nanocubes, (C) nanobranched, (D - F) different sized nanorods, (G - J) several sized nanobipyramids. Their applications in biomedicine cover all the areas, from diagnosis used in chemical sensing,^[72] to drug delivery. In between, they are also used for imaging, as MRI contrast agents,^[73] and in therapy for their capacity of converting light into heat.^[74] Many characteristics and properties of AuNPs are going to be described in more detail in chapter IV.

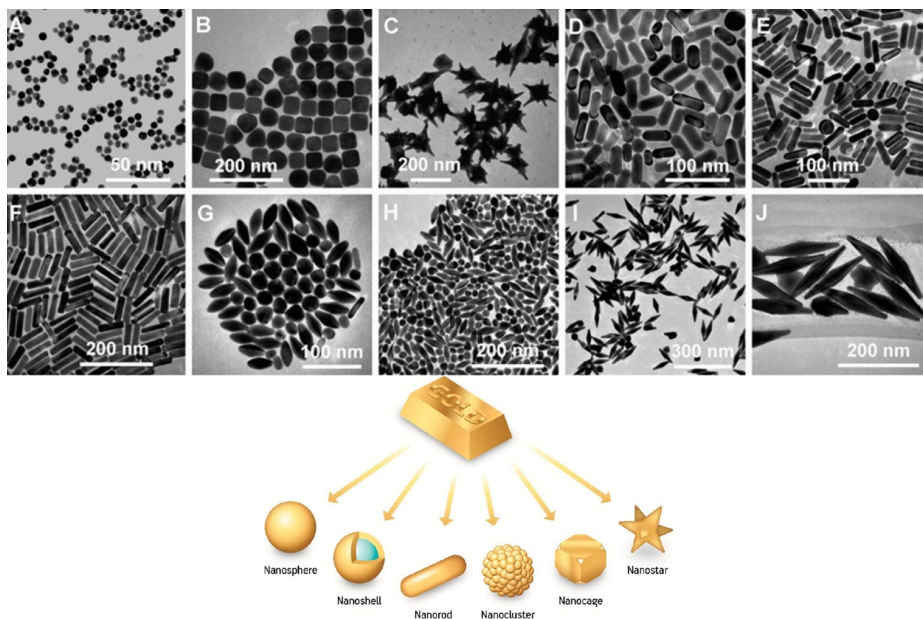


Figure 1.7. Some different shapes of AuNPs. (A) nanospheres, (B) nanocubes, (C) nanobranched, (D - F) different sized nanorods, (G – J) several sized nanopyramids. Figure adapted with permissions from *Chemistry – An Asian Journal*, 2021.^[75]

Parallel to the development of AuNPs, silver atoms were reduced letting the preparation of colloidal AgNPs suspensions.^[76] In particular, AgNPs have gained interest for their strong antimicrobial activity, as they can cause microbial membrane damage by attaching to the cell surface and performing some structural modifications. Similarly, the release of Ag^+ ions and reactive oxygen species cause microbial sub-cellular structure damage,^[77] with some important differences in function of the NPs morphology.^[78] In general, there is a strong correlation between the specific surface area and the dissolution kinetics. In fact, the oxidation of Ag to Ag^+ is the key to understand the process. It has been found that particles with a higher specific surface area dissolved faster than the rest increasing the toxicity behaviour of the material. In a recent study, M. Epple *et al.*^[78] reported the effect of the release of Ag^+ ions in the function of the different particle morphology, with the help of *S. Aureus* as a bacterial model. They concluded that the trend of the dissolution rate is: platelets > spheres glucose synthesis > spheres microwave synthesis \approx rods > cubes. Likewise, biomedical materials based on AgNPs have appeared in the literature with applications as anticancer agents,^[79] drug-delivery nanocarriers,^[80] orthopaedic materials,^[81] among others.

The wide range of possible uses of silver and gold NPs is mainly due to their unique optical properties, which can be tuned by changing their size and

shape. Essentially, this is possible thanks to an effect called surface plasmon resonance.^[82] It is a physical phenomenon that describes the collective oscillation of free conduction electrons in a metal. When the NPs size is smaller than the wavelength of a photon, the resulting plasmon oscillation is spread along the whole particle, creating an electron cloud.^[83] This effect is reflected into an absorption in the UV-NIR spectrum with a tuneable maximum peak in function of the metal, size and shape of the NPs. For instance, some anisotropic NPs have the absorption band in the NIR region,^[84] where is located the biological window. This, increase the safety use of NPs for biomedical applications. **Figure 1.8** shows a scheme of this effect in a gold nanosphere.

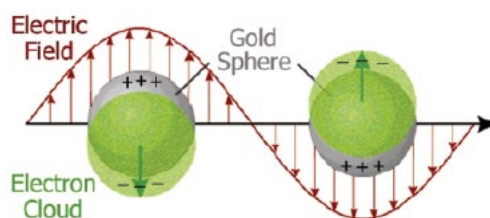


Figure 1.8. Scheme showing the surface plasmon resonance effect. Figure adapted with permission from *MRS Bulletin*, 2005.^[82]

In the 1950s, the interest in inorganic NPs was enormous after the boom of gold and silver NPs. By that time, scientists wanted to explore every single metal to unravel its nanometric potential. During the 50s, Néel^[85] reported for the first-time structures in the range 1 – 100 nm with magnetic behaviour. In the beginning, Fe, Co, Ni and ferrites ($\text{Mn}_{0.6}\text{Zn}_{0.4}\text{F}_2\text{O}_4$ and CoFe_2O_4) were used for the synthesis of highly stable colloidal magnetic NPs. Thanks to the rapid popularization of synthetic methods, their interest in biomedicine started growing. Nevertheless, as soon as the first studies in magnetic hyperthermia or magnetic resonance imaging took place, the toxicity levels reported expressed the necessity of an optimization of magnetic NPs for this aim. To solve this drawback, iron oxides (Fe_3O_4 , $\gamma\text{-Fe}_2\text{O}_3$) have emerged as the optimal starting materials for the preparation of highly biocompatible magnetic NPs. The most advantage of these systems is that they are sensitive to an external magnetic field.^[86] Thanks to this property, it is very easy to purify them, to use them in bioseparations,^[87] to increase their localize temperature, known as photothermal therapy,^[88] and to use them as imaging contrast agents.^[89] All this is possible just by applying an external magnetic field, which stands out the great potential of magnetic NPs. Nowadays, the interest and knowledge around magnetic NPs are growing exponentially. Proof of this can be seen in many clinical trials^[90] that have been

completed using magnetic NPs for the treatment of cancers with hyperthermia applications. Subsequently, even though magnetic NPs are not yet available in the clinical routine, it would not be surprising to see their rise in the coming years.

More recently, in the 1990s, inorganic NPs based on rare earth elements (Yb, Er)^[91] started to be studied for biomedical applications. In 2004, Yi et al.^[92] reported the first synthesis for NaYF₄-Upconverting NPs (UCNPs) with narrow distribution and good shape control. The main benefit of using rare-earth-doped-UCNPs is that these elements can convert low-energy photons into high-energy photons.^[93] The final application is that UCNPs can absorb NIR wavelength light and emit visible light. In other words, thanks to this property, UCNPs have a great value in biosensing.^[94] Besides, they have also been used for treatment as antimicrobial platforms,^[95] and in the food safety analysis.^[96]

Up to now, the continue evolution of inorganic NPs remains promising, with unique properties that are improving medicine day by day. Nevertheless, metals have high toxicity^[97] for cells even at very low concentrations. Moreover, inorganic NPs are generally recognized by the body as a foreign substance, and several biological mechanisms are used to remove them, decreasing their therapeutic activity. Recently, hybrid materials, as combinations of organic polymers with inorganic nanoparticles, have gained interest as a strategy to overcome these issues.

1.3.3 Hybrid systems: In a rush to achieve reinforced materials combining different sources of polymers and inorganic elements

By definition, a hybrid system is “the product of mixing two or more elements with different nature”. Therefore, it is possible to combine several characteristics from the systems previously described to end up with a better and reinforced material. For example, hydrogel-based on natural polymers^{[98][99]} have low toxicity and high biocompatibility. They have been used for tissue engineering or regenerative medicine thanks to their feature of promoting cell growth near wounds. Chitosan, collagen, starch, cellulose, sodium alginate, hyaluronic acid and guar gum are some of the most used natural polymers to build hydrogels. Even though all these good benefits, the main disadvantages are their low mechanical properties, high acquisition cost and the difficulty to modify their chemical structure.^[100] On the other side, a

hydrogel based on synthetic polymers^{[101][102]} can have good mechanical properties, the economic source of the polymer will be lower and the polymeric chain can be modified to increase functional groups for many applications. Nevertheless, their lack of biocompatibility and biodegradability results in by-products that could increase their toxicity. Some of typical synthetic polymers used are polyvinylpyrrolidone (PVP),^[103] PEG, PHEMA, polyacrylamide (PAM),^[104] polyvinyl alcohol (PVA),^[105] poly(2(dimethylamino)ethyl methacrylate) (PDMAEMA)^[106] and polycaprolactone (PCL),^[107] among others. To get over these challenges, hybrid hydrogels with a good balance of natural and synthetic polymers have appeared for several disease treatments in medicine. Many examples of hybrid materials can be found in the literature. To sum up some examples, Marra, et al.^[108] copolymerized aminated hyaluronic acid with pNIPAM for the preparation of a thermoresponsive and non-toxic hydrogel to be used as injectable scaffold in tissue engineering. In a similar study, pNIPAM was also used as thermoresponsive polymer to graft chitosan^[109] in the preparation of hydrogels with reversible soluble-insoluble properties, fast transition kinetics and big improvement into the mechanical chitosan strength thanks to the presence of pNIPAM. Besides, the obtained hydrogel can mimic the initial cell-cell interaction, which makes it promising for meniscus tissue engineering. Other studies have been published based on other thermoresponsive polymers. For example, thermoresponsive vinyl sulfonate was conjugated with thiolated-dextran via Michael addition for the preparation of injectable hydrogels.^[110] They found that the co-polymers gels in a short time with adaptive mechanical properties varying the feeding ratios. In addition, one can find in the literature studies that combine proteoglycans with PEG to enhance their mechanical properties by the preparation of bio-synthetic scaffolds for tissue engineering applications.^[111]

Hybrid systems have also been explored by the combination of polymers and inorganic nanoparticles. It has been shown previously, that one of the main drawbacks of the inorganic NPs are undesired effects, like an increase of toxicity. In the last years, several organic nanoparticles have been used to protect inorganic NPs when they are in a biological media. One recent example of the wonderful characteristics of organic-inorganic hybrid systems can be found in Biglione et al.'s^[112] work. They prepared thermoresponsive hybrid nanogels based on magnetic NPs combined with diethylene and oligoethylene glycol methacrylate monomers. In this study, magnetic nanospheres are used as cross-linkers, covalently joined to the global structure. This hybrid system can be used for theranostics, thanks to its dual capacity of MRI contrast agent and NIR-triggered chemotherapy properties.

With the help of a NIR laser, it could be possible to irradiate the hybrid nanogel letting the release of an anticancer drug pre-encapsulated inside them for anti-cancer therapy (**Figure 1.9A**).

Gold nanoparticles have also been set inside of a nanogel (**Figure 1.9B**).^[113] In this work, the nanogel was based on a triblock polypeptide (PC₁₀A-RGD) that can self-assemble into nanogels at a certain concentration.

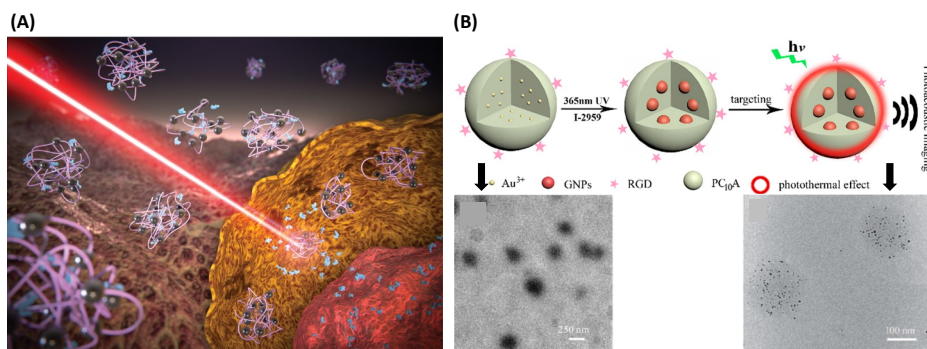


Figure 1.9. (A) Scheme of hybrid thermoresponsive nanogel based on magnetic NPs as cross-linkers and their capacity of releasing a drug under the presence of NIR-laser irradiation. (B) Scheme and TEM pictures of hybrid nanogels with gold NPs grown inside. Figures adapted with permissions from *Nanoscale*, 2020 (A) and *ACS Sustainable Chemistry & Engineering*, 2017 (B).^{[112][113]}

In the work presented in **Figure 1.9 B**, several ions of Au³⁺ were introduced inside the nanogel and reduced to Au⁰ thanks to the presence of a photoinitiator under 365 nm irradiation. The reduction of gold ion let the appearance of several AuNPs (GNPs) inside of each nanogel, where the size and shape of the NPs can be also controlled. The final nanogels had a diameter of 100 nm with a narrow size distribution. Thanks to the presence of AuNPs, the photoacoustic signal of the hybrid system was notably improved, being this nanogels perfect to be used for imagining diagnosis in nanomedicine.

Even though hybrid nanogels based on the combination of organic-inorganic materials are the most recently studied systems for biomedical applications, other organic NPs have been used as a cover of inorganic NPs. For instance, magnetic NPs have been encapsulated inside of micelles formed by β -cyclodextrin.^[114] The system allows the appearance of a host-guest interaction with bisphenol A,^[115] a hazardous organic molecule used in the industry for the synthesis of several plastics. As it can be found in wastes, it is normally removed from water consumption during the purification stages, which makes this hybrid micelles system a perfect strategy for its removal. Conversely, inorganic NPs, like the silver ones, have also been used for the

preparation of organic NPs to be used as emulsifiers in Pickering emulsion technology.^[116] The idea of this technology is to apply solid NPs as surfactants. Hybrid Ag-micelles have demonstrated long-time stability and pH sensitivity in the preparation of Pickering oil-in-water emulsions, being promising systems for coating industries.

Combining organic and inorganic elements have let researchers the potential of achieving better materials with improved properties for biomedical applications. Even though huge progress has been achieved in this field, there are still some challenges that need to be considered. For example, the reviewed studies have shown big organic NPs in comparison with the size of inorganic NPs, where the inorganic properties could be compromised for the used ratios when they are in a biological environment.

1.4 The biointerface: When nanoparticles meet biological systems

The immune system from biological entities is always in warning from the presence of foreign species that could damage their integrity. This includes bacteria, viruses, fungi and also any artificial material that is injected to be used as therapeutic to avoid undesired immune responses. A well-understanding of them is fundamental to have control over the design of the material. To achieve that, the study of the biointerface^[117] has emerged as a science that tries to elucidate the interaction between materials and biological structures. As the cell is considered the basic unit of living organisms, it is highly frequent to study the behaviour of materials in presence of different cell types. Endothelial, epithelial, antigen-presenting, T lymphocytes, Stem are the most frequent cells used in biolaboratories.^[118] The chemical nature of the material, its particle size, shape, rigidity, surface charge, hydrophilicity are some of the factors that influence the interaction between the material and the cell. The main mechanism that nanomaterials are followed for cell interaction is cellular uptake, where the NPs internalized inside the cells. Phagocytosis and micropinocytosis^[119] are other routes that NPs and the surface of the material can be modified to force follow, either one or another. The outcome of the path followed will determine the degree of internalization and the resultant biological therapeutic effect. However, not only the interactions with cells are determining the final therapeutic result and the stability of the material. When a material is in contact with a biological fluid,^[120] this contains a lot of salts and proteins that will start interacting with

it. In the particular case of salts, the typical concentration of sodium in the blood is in the range of 135 – 145 mEq/L. Phosphate-buffered saline (PBS) is generally used to mimic the biological fluid salts concentration. Therefore, it is quite frequent to incubate nanomaterials with a certain amount of PBS to analyse their stability in presence of salts. In the case of inorganic NPs, the colloidal stability is compromised in presence of salts, as they tend to aggregate losing their intrinsic properties. A hybrid system based on rods absorbed into high-density lipoprotein has been incubated in presence of PBS and sucrose to quantify their stability.^[1221] Along with the study, the stability of the materials was followed thanks to the NIR plasmonic absorption of the gold nanorods. In comparison to naked Au nanorods, the hybrid system reported an increase in their colloidal stability. Likewise, the incubation with sucrose demonstrated the appearance of a corona around the nanomaterial, which is responsible for the increase in the stability of the system. Similar strategies are followed in many hybrid systems. For example, Jurga, et al.,^[1222] protected copper oxide nanoparticles with a shell of hyaluronic acid (HA) and glutathione (GSH). After incubation of the materials with different biological fluids, they concluded that the modification with HA exhibited higher stability than the one with GSH. Besides, the interaction with HeLa cells was also less in both cases, thereby minimizing the effects of the normal cell grow. In comparison with non-protected copper oxide NPs, the release of copper atoms was less for the hybrid systems, decreasing the toxicological effect.

The human body is full of several biological complexities. Therefore, when (nano)materials are administered to a person, they find several biological barriers like mucosal membranes,^[123] blood-brain barriers,^[124] protein corona absorption,^[125] skin,^[126] among others. The development of the engineering techniques is contentiously evolving trying to overcome all of them. In the following sections, the protein corona effect and polymer-mucosa interaction will be described in more detail.

1.4.1 The protein corona effect. An undesired effect of nanomaterials in biological media.

When nanomaterials come into contact with biological media, the proteins that are swimming there create a halo around them trying to hide their synthetic identity. This phenomenon is known as protein corona formation, and it is a dynamic process, where proteins can be absorbed into the surface of the nanomaterial and later desorbed in function of the binding energy of the complex. It was first described in 2007 by Dawson et al.^[127] Over

the last 16 years, several studies have determined that protein corona is influenced by many parameters^[125] involved in the interaction between the system and the proteins. Such as dynamicity of the environment, physico-chemical properties from the nanomaterial and protein structure, among others. The interactions are driven by affinity proteins constants and their thermodynamics structure. In general, neutral nanomaterials interacts less than electrostatically charged ones, as proteins are always charged. Besides, pH also plays an important role, as it can neutralize the charges.

In function of the nature of the protein, the protein corona effect is classified as soft or hard.^[128] Hard protein corona exhibits an intensive affinity, being the exchange time more than the one required for cellular uptake. This protein-nanomaterial interaction is so strong that might cause damage to the secondary protein structure, making them lose their biological activity. On the other side, soft protein corona is based on low-affinity interactions including Van der Waals forces, ionic interactions, hydrophobic interactions and hydrogen bonding. In addition, in the function of the pH of the medium, the density of the soft protein corona can change, letting the appearance of a dynamic process in which the proteins are absorbing and desorbing all the time (**Figure 1.10**). Along with the pH, the size of the nanomaterial also matters,^[129] as it has been found less protein corona absorption of smaller particles than for bigger ones.

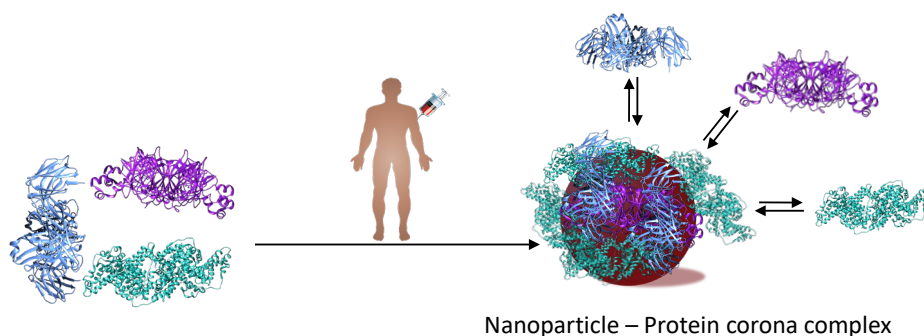


Figure 1.10. Scheme of the protein corona effect where several proteins are absorbed and desorbed from the surface of the nanoparticle.

A huge variety of analytical methods^[130] have been employed for the characterization of the soft and hard protein corona. Chromatography techniques allow the separation and identification of each protein. On the one hand, size-exclusion chromatography let the separation of large molecules and aggregated attending to their molar mass and size. On the other hand, reversed-phase chromatography allows the separation in the function of their

hydrophobic properties. Gel electrophoresis also allows the identification of proteins applying an external electric field. In function of the different protein charges, they will move at different speeds along the gel. When electrophoresis is combined with mass spectrometry, comes one of the more well-established strategies for the quantification of nanoparticle-protein corona complex.

Several studies have analyzed in detail the protein corona effect in hybrid nanosystems. Glitscher, et al.,^[131] prepared four shapes of AuNPs (spheres, rods, stars and cages) and they stabilized all of them with a PEG ligand. After a deep analysis of the protein corona effect onto the different systems, by LC-MS/MS chromatography, they concluded that the total amount of proteins adsorbed onto the Au nanocages were less than in the rest of the shapes. This result can be explained by attending to their smallest surface area and strong surface curvatures at the edges. In a similar study, Kostarelos, et al.,^[132] prepared gold nanorods and nanostars with 40 and 70 nm of diameter stabilized with PEG ligand and then injected intravenously in rodents. Their in-vivo analysis of protein corona through electrophoresis gel determined that larger gold nanostars were covered with an extra number of proteins than the other systems.

1.4.2 Mucosa interactions of synthetic materials

Mucosa^[133] is a mucus membrane, where mucus is referred to as a viscoelastic secretion formed by electrolytes, lipids and proteins. It is mainly formed by glycoproteins, proteoglycans and lipids diluted into an aqueous environment. Its main purpose is to protect organs that could be exposed to external damage as part of the advanced immune systems. This excretion can be found in the mouth,^[134] vagina,^[135] eye,^[136] stomach,^[137] intestine,^[138] among other digestive, breathing and urologic organs.

Synthetic materials can be designed to be attached to mucosa layers or even to penetrate them without so much interaction. Knowing the mucoadhesion mechanism followed by nanomaterials is essential to have control over it. Therefore, the main mechanisms^[139] are three: (I) adsorption, (II) diffusion and (III) electronic interactions.

In the first mechanism, adsorption, the driving forces are hydrogen bonding and van der Waals interactions. Polymers with -OH and -COOH groups are the best candidates to interact with mucin through this strategy. Such as PVA and poly(methacrylic acid). In the diffusion processes (mechanism II), the

adhesion is driven by shape, architecture, diffusion coefficient mobility, contact time and flexibility of the polymer. An example of this is the PEG polymer, which can easily penetrate the mucus. The III mechanism, electronic interactions, is based on the negatively charged mucin. Therefore, positively charged molecules will interact with it. For example, chitosan that is positively charged has been reported as a strong mucosa-adhesion polymer.

Taking into account the different mechanisms for mucosa adhesion, many strategies have been followed to improve the residence time of delivery vehicles into the mucosa membranes. For instance, a hybrid polymeric film was prepared by Khytoryanski and co-workers.^[140] It is based on poly(acrylic acid) and modified cellulose with hydroxypropyl groups. The final material, prepared by physically cross-linking chains, was tested in presence of buccal mucosa. It reported a good mucosa adhesion during 30 – 110 minutes until it was dissolved. Some other natural polymers have been used to improve mucoadhesive properties. For example, hyaluronic acid^[141] has been used in clinical trials to increase mucoadhesive properties. It has been demonstrated that it can preserve the adhesion properties even when the saliva is trying to wash it in buccal applications.

In the particular case of the eye, the high-water degree that this organ contains increases the difficulty of developing materials with good mucoadhesive capabilities. Until now, it was quite frequent to use eye-drop for ocular treatments, but their poor retention time in the eye decreases considerably their efficacy. Hydrogels are being currently developed as ocular inserts to solve this issue. But even though contact lenses are hydrogels that appeared in the market in 1958, it is not so common to find them as drug carriers. Recent studies have carried this technology, from vision-correcting to loading a drug and letting it pass through the mucosa layer. For example, PHEMA cross-linked with PEG dimethacrylate have been used to load ofloxacin delivering it into the posterior segment of the eye.^[142] Nevertheless, the use of biopolymers in hydrogels formulations have been used recently to increment their adhesion. Chitosan and cellulose derivatives are the more common ones. However, HA,^[143] which is a biodegradable polymer present in the human body, has seen its interest increase for ophthalmology application in the last years. It is highly presented in the aqueous vitreous of the eye, which guarantees the no activation of the immune system response. In addition, it has been reported that the presence of HA in the formulations increase the mucoadhesion properties of the materials in several orders of magnitude.^[144]

The surface of hybrid systems based on inorganic NPs have also been modified to adhere or penetrate the mucus layer (**Figure 1.11**). For instance, the mucin interactions of Au nanospheres with two modification were analyzed by Boisselier et al.,^[145] They modified the surface of the NPs with two PEGs, one with a methoxy ending group and the other one with thiolated ending groups. On the one hand, they showed that the methoxy functionalized PEG exhibited higher interaction with the internal amino acids of the mucin. On the other hand, when the ending group of PEG was modified with thiol groups, the weaker interaction with mucin allows the particles to penetrate deeper into the mucin layer. Similar results have been observed in mesoporous silica NPs,^[146] where cover their surface with thiolated PEG also decrease the adhesion to the mucus layer in comparison with non-thiolated NPs.

It is important to highlight that inorganic NPs can be toxic if they are not well-protected. Therefore, understanding their mucoadhesion mechanism remains important to avoid possible side effect. In a very recent toxicology study, Filon, et al.,^[147] became aware of the potential hazards of AgNPs for kids. These NPs are presented in many products that children can put into their mouths by mistake. To understand better their potential nanotoxicology, they analyse the mucosa penetration of the particles into baby porcine buccal mucosa with vertical Franz diffusion cells. The conclusions were that when polyvinylpyrrolidone is stabilizing AgNPs, they can penetrate the mucus layer in around 3 h of the experiment. Also, the particles remained stable after their incubation with mucin. The results reveal the potential toxicity of AgNPs for children and the importance of keeping some products out of their reach.

Overcoming the mucus barrier have been a great challenge during the last few years. Control over the synthetic strategies of nanoparticles is a key parameter to modulate the adhesion mechanisms between the system and the mucus layer. Moreover, decorating nanoparticles with mucoadhesive polymers allow the immobilization of the vehicle letting a better drug release control. In contrast, mucopenetrating materials enhance drug uptake. As mucosa is presented in several organs, its structure is highly complex. Therefore, a well-understanding of the target tissue and disease is a must to optimize the synthesized material. Although much progress has been made in recent years, there is still a long way to improve the adhesion of hybrid systems at the mucosal biointerface.

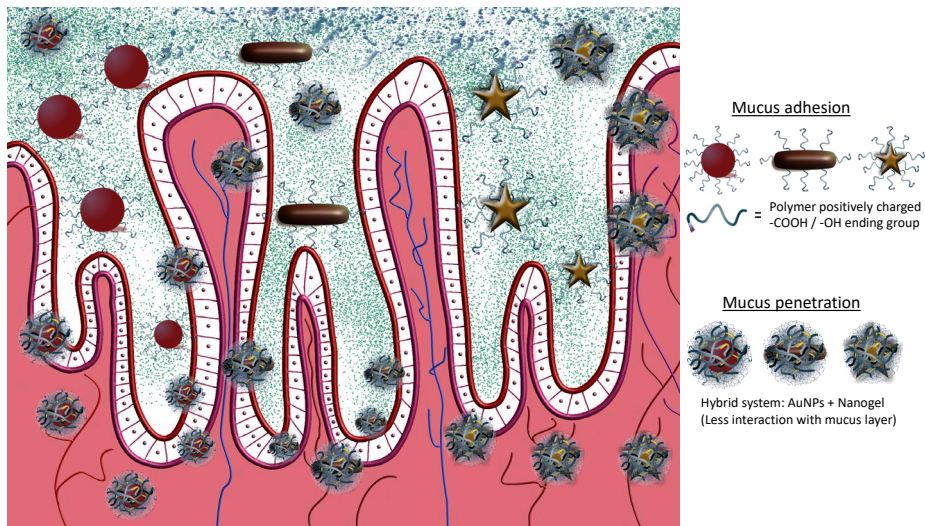


Figure 1.11. Scheme of AuNPs decorated with polymers that can be adhesive to the intestine mucus layer and gold nanoparticles encapsulated onto nanogels that can penetrate the mucus layer.

1.5 References – Chapter I

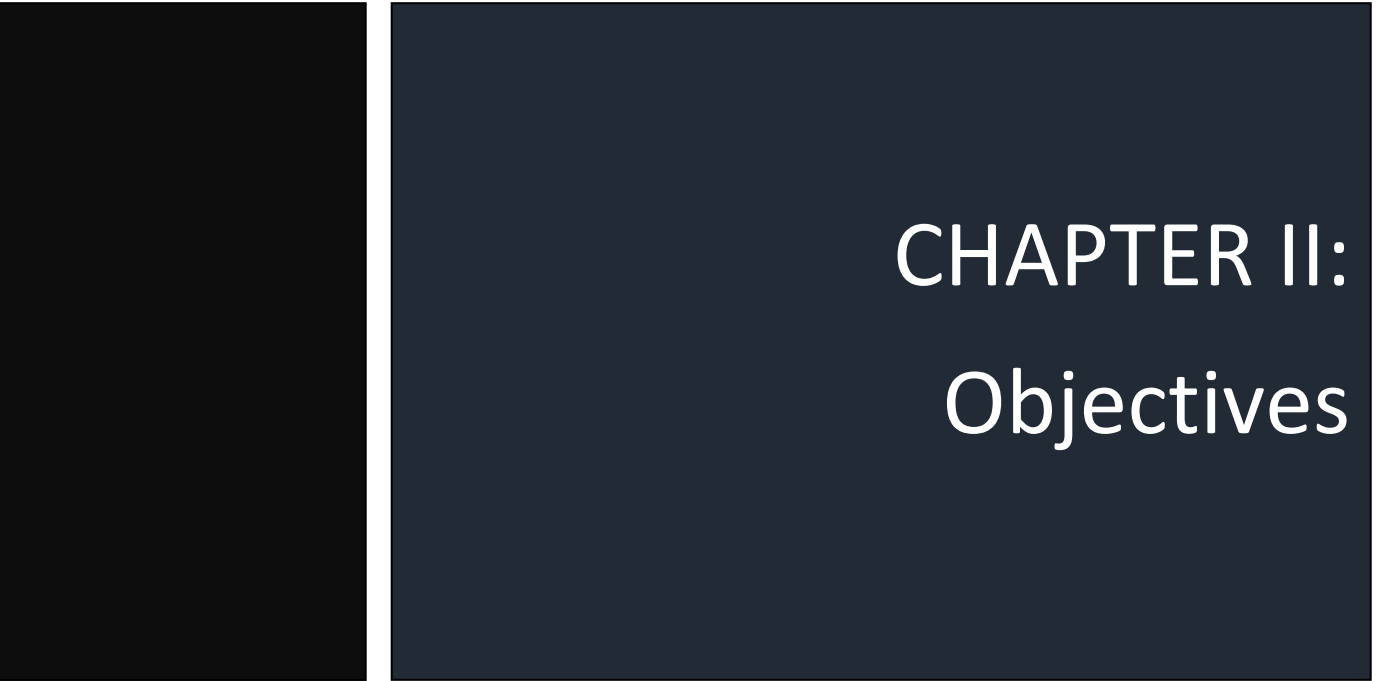
- [1] R. R. Schaller, *IEEE Spectr.* **1997**.
- [2] D. Koutsouris, *Health Technol. (Berl)*. **2017**, 7, 3.
- [3] V. Kulkarni, K. Butte, S. Rathod, *Int. J. Res. Pharm. Biomed. Sci.* **2012**, 3, 1597.
- [4] K. A. Günay, P. Theato, H. A. Klok, *J. Polym. Sci. Part A Polym. Chem.* **2013**, 51, 1.
- [5] L. Seymour, *J. Bioact. Compat. Polym.* **1991**, 6, 178.
- [6] A. Lendlein, M. Rehahn, M. R. Buchmeiser, R. Haag, *Macromol. Rapid Commun.* **2010**, 31, 1487.
- [7] M. Kouhi, M. P. Prabhakaran, S. Ramakrishna, *Trends Food Sci. Technol.* **2020**, 103, 248.
- [8] Y. Li, H. Y. Yang, T. Thambi, J. H. Park, D. S. Lee, *Biomaterials* **2019**, 217, 119299.
- [9] M. F. Maitz, *Biosurface and Biotribology* **2015**, 1, 161.
- [10] S. Drotleff, U. Lungwitz, M. Breunig, A. Dennis, T. Blunk, J. Tessmar, A. Göpferich, *Eur. J. Pharm. Biopharm.* **2004**, 58, 385.
- [11] N. A. Peppas, J. Z. Hilt, A. Khademhosseini, R. Langer, *Adv. Mater.* **2006**, 18, 1345.
- [12] S. Baudis, M. Behl, A. Lendlein, *Macromol. Chem. Phys.* **2014**, 215, 2399.
- [13] J. Cui, J. Iturri, J. Paez, Z. Shafiq, C. Serrano, M. D'Ischia, A. Del Campo, *Macromol. Chem. Phys.* **2014**, 215, 2403.
- [14] G. Hao, Z. P. Xu, L. Li, *RSC Adv.* **2018**, 8, 22182.
- [15] L. A. Wallace, L. Gwynne, T. Jenkins, *Ther. Deliv.* **2019**, 10, 719.
- [16] J. Bergueiro, M. Calderón, *Macromol. Biosci.* **2015**, 15, 183.
- [17] F. F. Sahle, M. Giulbudagian, J. Bergueiro, J. Lademann, M. Calderón, *Nanoscale* **2017**, 9, 172.
- [18] W. Hu, Z. Wang, Y. Xiao, S. Zhang, J. Wang, *Biomater. Sci.* **2019**, 7, 843.
- [19] S. H. Aswathy, U. Narendrakumar, I. Manjubala, *Heliyon* **2020**, 6.
- [20] U. S. K. Madduma-bandarage, S. V. Madihally, *J. Appl. Polym. Sci.* **2021**, 138, 1.
- [21] Z. Zhang, W. Jiang, X. Xie, H. Liang, H. Chen, K. Chen, Y. Zhang, W. Xu, M. Chen, *ChemistrySelect* **2021**, 6, 12358.
- [22] R. Darvishi, H. Moghadas, A. Moshkriz, *Korean J. Chem. Eng.* **2021**, 38, 1.
- [23] K. Wang, Y. Hao, Y. Wang, J. Chen, L. Mao, Y. Deng, J. Chen, S. Yuan, T. Zhang, J. Ren, W. Liao, *Int. J. Polym. Sci.* **2019**, 2019.
- [24] E. Caló, V. V. Khutoryanskiy, *Eur. Polym. J.* **2015**, 65, 252.
- [25] Y. Yu, Y. Cheng, J. Tong, L. Zhang, Y. Wei, M. Tian, *J. Mater. Chem. B* **2021**, 9, 2979.
- [26] I. Firlar, M. Altunbek, C. McCarthy, M. Ramalingam, G. Camci-Unal, *Gels* **2022**, 127, 1.
- [27] C. Torres-luna, X. Fan, R. Domszy, N. Hu, N. S. Wang, A. Yang, *Eur. J. Pharm. Sci.* **2020**, 154, 105503.
- [28] G. Fang, X. Yang, Q. Wang, A. Zhang, B. Tang, *Mater. Sci. Eng. C* **2021**, 127, 112212.
- [29] B. S. Kaith, A. Singh, A. K. Sharma, D. Sud, *J. Polym. Environ.* **2021**, 29, 3827.
- [30] J. Li, X. Jia, L. Yin, *Food Rev. Int.* **2021**, 37, 313.
- [31] Z. Wang, Y. Liu, Z. Wang, X. Huang, W. Huang, *View* **2021**, 2, 20200165.

- [32] R. P. Feynman, *There's Plenty of Room at the Bottom*, **1960**, pp. 22–36.
- [33] F. Caruso, T. Hyeon, V. M. Rotello, *Chem. Soc. Rev.* **2012**, *41*, 2537.
- [34] D. F. Emerich, C. G. Thanos, *Expert Opin. Biol. Ther.* **2003**, *3*, 655.
- [35] R. Zingg, M. Fischer, *Wiley Interdiscip. Rev. Nanomedicine Nanobiotechnology* **2019**, *11*, 1.
- [36] M. L. Etheridge, S. A. Campbell, A. G. Erdman, C. L. Haynes, S. M. Wolf, J. McCullough, *Nanomedicine Nanotechnology, Biol. Med.* **2013**, *9*, 1.
- [37] J. Yao, M. Yang, Y. Duan, *Chem. Rev.* **2014**, *114*, 6130.
- [38] E. H. Chang, J. B. Harford, M. A. W. Eaton, P. M. Boisseau, A. Dube, R. Hayeshi, H. Swai, D. S. Lee, *Biochem. Biophys. Res. Commun.* **2015**, *468*, 511.
- [39] M. Karimi, P. S. Zangabad, A. Ghasemi, M. R. Hamblin, *Smart External Stimulus-Responsive Nanocarriers for Drug and Gene Delivery*, **2015**.
- [40] A. S. Manjappa, P. S. Kumbhar, A. B. Patil, J. I. Disouza, V. B. Patravale, *Crit. Rev. Ther. Drug Carrier Syst.* **2019**, *36*, 1.
- [41] T. Zhao, A. Elzatahry, X. Li, D. Zhao, *Nat. Rev. Mater.* **2019**, *4*, 775.
- [42] Y. Yi, G. Lin, S. Chen, J. Liu, H. Zhang, P. Mi, *Mater. Sci. Eng. C* **2018**, *83*, 218.
- [43] U. Nayanathara, S. S. Kermaniyan, G. K. Such, *Macromol. Rapid Commun.* **2020**, *41*, 1.
- [44] M. N. Khan, I. I. Fagge, *Prog. React. Kinet. Mech.* **2018**, *43*, 1.
- [45] T. Rasheed, S. Shafi, M. Bilal, T. Hussain, F. Sher, K. Rizwan, *J. Mol. Liq.* **2020**, *318*, 113960.
- [46] S. S. Gillani, M. A. Munawar, K. M. Khan, J. A. Chaudhary, *J. Iran. Chem. Soc.* **2020**, *17*, 2717.
- [47] M. Sowinska, Z. Urbanczyk-Lipkowska, *New J. Chem.* **2014**, *38*, 2168.
- [48] A. S. Chauhan, *Molecules* **2018**, *23*, 1.
- [49] N. Dwivedi, J. Shah, V. Mishra, M. C. I. Mohd Amin, A. K. Iyer, R. K. Tekade, P. Kesharwani, *J. Biomater. Sci. Polym. Ed.* **2016**, *27*, 557.
- [50] M. Sajid, *Trends Anal. Chem.* **2018**, *98*, 114.
- [51] S. Vinogradov, E. Batrakova, A. Kabanov, *Colloids Surfaces B Biointerfaces* **1999**, *16*, 291.
- [52] M. Antonietti, H. Sillescu, W. Germany, H. Schuch, *Macromolecules* **1988**, 736.
- [53] P. Lemieux, S. V. Vinogradov, C. L. Gebhart, N. Guerin, G. Paradis, H. K. Nguyen, B. Ochietti, Y. G. Suzdaltseva, E. V. Bartakova, T. K. Bronich, Y. St.-Pierre, V. Y. Alakhov, A. V. Kabanov, *J. Drug Target.* **2000**, *8*, 91.
- [54] I. Neamtu, A. G. Rusu, A. Diaconu, L. E. Nita, A. P. Chiriac, *Drug Deliv.* **2017**, *24*, 539.
- [55] V. M. Vijayan, P. N. Vasudevan, V. Thomas, *Curr. Nanosci.* **2020**, *16*, 392.
- [56] Y. Jiang, J. Chen, C. Deng, E. J. Suuronen, Z. Zhong, *Biomaterials* **2014**, *35*, 4969.
- [57] B. Sierra-Martin, A. Fernandez-Barbero, *Soft Matter* **2015**, *11*, 8205.
- [58] H. Wu, C. Wang, *Langmuir* **2016**, *32*, 6211.
- [59] L. Zha, B. Banik, F. Alexis, *Soft Matter* **2011**, *7*, 5.
- [60] Z. Li, J. Huang, J. Wu, *Biomater. Sci.* **2021**, *9*, 574.
- [61] M. Ye, Y. Wang, Y. Zhao, R. Xie, N. Yodsanit, K. Johnston, S. Gong, *ACS Appl. Mater. Interfaces* **2019**, *11*, 42865.
- [62] Z. Khatun, M. Nurunnabi, M. Nafiujjaman, G. R. Reeck, H. A. Khan, K. J. Cho, Y. K. Lee, *Nanoscale* **2015**, *7*, 10680.
- [63] S. Ghaeini-Hesaroeiye, H. R. Bagtash, S. Boddohi, E. Vasheghani-Farahani, E. Jabbari, *Gels* **2020**, *6*, 1.

- [64] M. Peng, S. Yuan, X. Shi, X. Lu, *J. Appl. Polym. Sci.* **2019**, 47933, 6.
- [65] L. Navarro, L. E. Theune, M. Calderón, *Eur. Polym. J.* **2020**, 124, 109478.
- [66] G. Sang, G. R. Bardajee, A. Mirshokraie, K. Didehban, *Iran. Polym. J.* **2018**, 27, 137.
- [67] B. Karmakar, *Fundamentals of Glass and Glass Nanocomposites*, Elsevier Inc., **2016**.
- [68] F. E. Wagner, S. Haslbeck, L. Stievano, S. Calogero, Q. A. Pankhurst, K. P. Martinek, *Nature* **2000**, 407, 691.
- [69] R. D. Tweney, *Perspect. Sci.* **2006**, 14, 97.
- [70] D. C. Luther, R. Huang, T. Jeon, X. Zhang, Y. Lee, H. Nagaraj, V. M. Rotello, *Adv. Drug Deliv. Rev.* **2020**, 156, 188.
- [71] N. Elahi, M. Kamali, M. H. Baghersad, *Talanta* **2018**, 184, 537.
- [72] M. Falahati, F. Attar, M. Sharifi, A. A. Saboury, A. Salihi, F. M. Aziz, I. Kostova, C. Burda, P. Priel, J. A. Lopez-Sanchez, S. Laurent, N. Hooshmand, M. A. El-Sayed, *Biochim. Biophys. Acta - Gen. Subj.* **2020**, 1864, 129435.
- [73] D. Luo, X. Wang, C. Burda, J. P. Basilion, *Cancers (Basel)*. **2021**, 13, 1.
- [74] A. S. C. Gonçalves, C. F. Rodrigues, A. F. Moreira, I. J. Correia, *Acta Biomater.* **2020**, 116, 105.
- [75] N. Sarfraz, I. Khan, *Chem. - An Asian J.* **2021**, 16, 720.
- [76] B. Khodashenas, H. R. Ghorbani, *Arab. J. Chem.* **2019**, 12, 1823.
- [77] A. C. Burduşel, O. Gherasim, A. M. Grumezescu, L. Mogoantă, A. Fici, E. Andronescu, *Nanomaterials* **2018**, 8, 1.
- [78] J. Helmlinger, C. Sengstock, C. Groß-Heitfeld, C. Mayer, T. A. Schildhauer, M. Köller, M. Epple, *RSC Adv.* **2016**, 6, 18490.
- [79] A. Deep, M. Verma, R. K. Marwaha, A. K. Sharma, B. Kumari, *Curr. Cancer Ther. Rev.* **2020**, 16, 145.
- [80] S. Ghosh, U. Anand, S. Mukherjee, *Analyst* **2013**, 138, 4270.
- [81] S. Castiglioni, A. Cazzaniga, L. Locatelli, J. A. M. Maier, *Nanomaterials* **2017**, 7, 1.
- [82] Y. Xia, N. J. Halas, *MRS Bull.* **2005**, 30, 338.
- [83] V. Amendola, R. Pilot, M. Frascioni, O. M. Maragò, M. A. Iatì, *J. Phys. Condens. Matter* **2017**, 29, 203002.
- [84] W. Yingxin, Z. Qianqian, *Mater. Res. Express* **2020**, 7.
- [85] P. M. Martins, A. C. Lima, S. Ribeiro, S. Lanceros-Mendez, P. Martins, *ACS Appl. Bio Mater.* **2021**, 4, 5839.
- [86] D. A. Alromi, S. Y. Madani, A. Seifalian, *Polymers (Basel)*. **2021**, 13, 1.
- [87] H. Fatima, K. S. Kim, *Korean J. Chem. Eng.* **2017**, 34, 589.
- [88] J. G. Ovejero, F. Spizzo, M. P. Morales, L. Del Bianco, *Materials (Basel)*. **2021**, 14, 1.
- [89] M. G. M. Schneider, M. J. Martín, J. Otarola, E. Vakarelska, V. Simeonov, V. Lassalle, M. Nedyalkova, *Pharmaceutics* **2022**, 14, 1.
- [90] S. Shirvalilou, S. Khoei, A. J. Esfahani, M. Kamali, M. Shirvaliloo, R. Sheervalilou, P. Mirzaghavami, *J. Neurooncol.* **2021**, 152, 419.
- [91] M. F. Torresan, A. Wolosiuk, *ACS Appl. Bio Mater.* **2021**, 4, 1191.
- [92] G. Yi, H. Lu, S. Zhao, Y. Ge, W. Yang, D. Chen, L.-H. Guo, *Nano Lett.* **2004**, 4, 2191.
- [93] M. K. Mahata, R. De, K. T. Lee, *Biomedicines* **2021**, 9, 1.
- [94] H. Montaseri, C. A. Kruger, H. Abrahamse, *Pharmaceutics* **2021**, 13, 1.

- [95] N. Kandoth, S. Barman, A. Chatterjee, S. Sarkar, A. K. Dey, S. K. Pramanik, A. Das, *Adv. Funct. Mater.* **2021**, *31*, 1.
- [96] D. Abdul Hakeem, S. Su, Z. Mo, H. Wen, *Crit. Rev. Food Sci. Nutr.* **2021**, 1.
- [97] N. Tiwari, E. R. Osorio-Blanco, A. Sonzogni, D. Esporrín-Ubieto, H. Wang, M. Calderón, *Angew. Chemie - Int. Ed.* **2022**, *61*, 1.
- [98] F. S. El-banna, M. E. Mahfouz, S. Leporatti, M. El-Kemary, N. A. N. Hanafy, *Appl. Sci.* **2019**, *9*, 1.
- [99] Z. Bao, C. Xian, Q. Yuan, G. Liu, J. Wu, *Adv. Healthc. Mater.* **2019**, *8*, 1.
- [100] J. Su, J. Li, J. Liang, K. Zhang, J. Li, *Life* **2021**, *11*, 1.
- [101] Y. Tu, S. G. Wise, A. S. Weiss, *Micron* **2010**, *41*, 268.
- [102] F. Khan, M. Atif, M. Haseen, S. Kamal, M. S. Khan, S. Shahid, S. A. A. Nami, *J. Mater. Chem. B* **2022**, *10*, 170.
- [103] P. Franco, I. De Marco, *Polymers (Basel)*. **2020**, *12*, 18.
- [104] L. Xu, X. Zhang, C. Zhu, Y. Zhang, C. Fu, B. Yang, L. Tao, Y. Wei, *J. Biomater. Sci. Polym. Ed.* **2013**, *24*, 1564.
- [105] P. Yusong, D. Jie, C. Yan, S. Qianqian, *Mater. Technol.* **2016**, *31*, 266.
- [106] G. A. Mahmoud, M. A. Abdel Khalek, E. M. Shoukry, M. Amin, A. H. Abdulghany, *Egypt. J. Chem.* **2019**, *62*, 1537.
- [107] M. Chen, Z. Feng, W. Guo, D. Yang, S. Gao, Y. Li, S. Shen, Z. Yuan, B. Huang, Y. Zhang, M. Wang, X. Li, L. Hao, J. Peng, S. Liu, Y. Zhou, Q. Guo, *ACS Appl. Mater. Interfaces* **2019**, *11*, 41626.
- [108] H. Tan, C. M. Ramirez, N. Miljkovic, H. Li, J. P. Rubin, K. G. Marra, *Biomaterials* **2009**, *30*, 6844.
- [109] J. P. Chen, T. H. Cheng, *Macromol. Biosci.* **2006**, *6*, 1026.
- [110] C. Lin, P. Zhao, F. Li, F. Guo, Z. Li, X. Wen, *Mater. Sci. Eng. C* **2010**, *30*, 1236.
- [111] T. P. Appelman, J. Mizrahi, J. H. Elisseeff, D. Seliktar, *Biomaterials* **2011**, *32*, 1508.
- [112] C. Biglione, J. Bergueiro, S. Wedepohl, B. Klemke, M. C. Strumia, M. Calderón, *Nanoscale* **2020**, *12*, 21635.
- [113] R. M. Jin, M. H. Yao, J. Yang, D. H. Zhao, Y. Di Zhao, B. Liu, *ACS Sustain. Chem. Eng.* **2017**, *5*, 9841.
- [114] W. Yuan, J. Shen, L. Li, X. Liu, H. Zou, *Carbohydr. Polym.* **2014**, *113*, 353.
- [115] K. Czarny, B. Krawczyk, D. Szczukocki, *Chemosphere* **2021**, *263*, 128299.
- [116] J. Zhou, X. Zha, *React. Funct. Polym.* **2019**, *137*, 46.
- [117] H. Meng, W. Leong, K. W. Leong, C. Chen, Y. Zhao, *Biomaterials* **2018**, *174*, 41.
- [118] C. Cortez-Jugo, E. Czuba-Wojnilowicz, A. Tan, F. Caruso, *Adv. Healthc. Mater.* **2021**, *10*, 1.
- [119] R. Augustine, A. Hasan, R. Primavera, R. J. Wilson, A. S. Thakor, B. D. Kevadiya, *Mater. Today Commun.* **2020**, *25*, 101692.
- [120] L. Guerrini, R. A. Alvarez-Puebla, N. Pazos-Perez, *Materials (Basel)*. **2018**, *11*, 1.
- [121] T. Nobeyama, M. Mori, K. Shigyou, K. Takata, G. N. Pandian, H. Sugiyama, T. Murakami, *ChemistrySelect* **2018**, *3*, 8325.
- [122] M. J. Woźniak-Budych, B. Maciejewska, Ł. Przysiecka, D. Wieczorek, K. Staszak, J. Jencyk, T. Jesionowski, S. Jurga, *J. Mol. Liq.* **2020**, *319*, 1.
- [123] R. W. McCullough, *Transl. Gastroenterol. Hepatol.* **2021**, *6*, 1.
- [124] J. M. Provenzale, S. Mukundan, M. Dewhirst, *Am. J. Roentgenol.* **2005**, *185*, 763.

- [125] R. García-álvarez, M. Vallet-Regí, *Nanomaterials* **2021**, *11*, 1.
- [126] F. D. Cojocar, D. Botezat, I. Gardikiotis, C. M. Uritu, G. Dodi, L. Trandafir, C. Rezus, E. Rezus, B. I. Tamba, C. T. Mihai, *Pharmaceutics* **2020**, *12*, 1.
- [127] D. Baimanov, R. Cai, C. Chen, *Bioconjug. Chem.* **2019**, *30*, 1923.
- [128] R. K. Mishra, A. Ahmad, A. Vyawahare, P. Alam, T. H. Khan, R. Khan, *Int. J. Biol. Macromol.* **2021**, *175*, 1.
- [129] P. Breznica, R. Koliqi, A. Daka, *Med. Pharm. Reports* **2020**, *93*, 342.
- [130] A. L. Capriotti, G. Caracciolo, C. Cavaliere, V. Colapicchioni, S. Piovesana, D. Pozzi, A. Laganà, *Chromatographia* **2014**, *77*, 755.
- [131] T. Bewersdorff, E. A. Glitscher, J. Bergueiro, M. Eravci, E. Miceli, A. Haase, M. Calderón, *Mater. Sci. Eng. C* **2020**, *117*, 1.
- [132] R. García-Álvarez, M. Hadjidemetriou, A. Sánchez-Iglesias, L. M. Liz-Marzán, K. Kostarelos, *Nanoscale* **2018**, *10*, 1256.
- [133] S. Pinzón Martín, P. H. Seeberger, D. Varón Silva, *Front. Chem.* **2019**, *7*, 1.
- [134] J. Hao, P. W. S. Heng, *Drug Dev. Ind. Pharm.* **2003**, *29*, 821.
- [135] R. R. De Araújo Pereira, M. L. Bruschi, *Drug Dev. Ind. Pharm.* **2012**, *38*, 643.
- [136] L. S. Chan, *Clin. Dermatol.* **2012**, *30*, 34.
- [137] A. F. Goddard, *Aliment. Pharmacol. Ther.* **1998**, *12*, 1175.
- [138] M. J. Dar, H. Ali, A. Khan, G. M. Khan, *J. Drug Target.* **2017**, *25*, 582.
- [139] R. S. Dave, T. C. Goostrey, M. Ziolkowska, S. Czerny-Holownia, T. Hoare, H. Sheardown, *J. Control. Release* **2021**, *336*, 71.
- [140] A. V. Dubolazov, Z. S. Nurkeeva, G. A. Mun, V. V. Khutoryanskiy, *Biomacromolecules* **2006**, *7*, 1637.
- [141] A. Z. Abo-shady, H. Elkammar, V. S. Elwazzan, M. Nasr, *J. Drug Deliv. Sci. Technol.* **2020**, *55*.
- [142] R. C. Cooper, H. Yang, *J. Control. Release* **2019**, *306*, 29.
- [143] C. R. Lynch, P. P. D. Kondiah, Y. E. Choonara, L. C. du Toit, N. Ally, V. Pillay, *Front. Bioeng. Biotechnol.* **2020**, *8*, 1.
- [144] A. Graça, L. M. Gonçalves, S. Raposo, H. M. Ribeiro, J. Marto, *Pharmaceutics* **2018**, *10*.
- [145] M. Ouellette, F. Masse, M. Lefebvre-demers, Q. Maestracci, P. Grenier, R. Millar, N. Bertrand, M. Prieto, É. Boisselier, *Sci. Rep.* **2018**, *8*, 1.
- [146] E. A. Mun, A. C. Williams, V. V. Khutoryanskiy, *Int. J. Pharm.* **2016**, *512*, 32.
- [147] I. Zaroni, M. Crosera, E. Pavoni, G. Adami, M. Mauro, A. L. Costa, J. R. Lead, F. Larese Filon, *Nanotoxicology* **2021**, *15*, 1005.



CHAPTER II: Objectives

2.1 Objectives

Over the last years, the number and complexity of polymers for biomedical applications have been tremendously raised. Powerful synthetic strategies have emerged for the combination of polymeric chains giving the emergence of nano- and micro-gels. This, coupled with the preparation of inorganic NPs with “*à la carte*” shapes, has been the engine that let researchers prepare hybrid materials with functions that were believed of science fiction. This PhD thesis, divided in two sections, aims to develop novel hybrid polymeric-based materials with tunable properties with regard to their interaction with biomolecules at the nano- and micro-scale. It is expected that by modulating the polymeric chain junctions with physical or chemical cross-linkers, the interactions between the material and the biological media will change.

Figure 2.1 summarizes in a scheme the general objectives. **Section A** is devoted to the preparation of thin mantle nanogels that can be used to protect different AuNPs while keeping their original shape. The section has been entitled “Design of thin nanogels to stabilize AuNPs in presence of biological fluids”, and is described in detail in **Chapter III**. Au nanospheres, nanorods and nanostars will be prepared and stabilized with PEG for a posterior functionalization with terminal vinyl groups. These functional groups will allow the preparation of chemically cross-linked NGs around the inorganic NPs through free-radical polymerization. It is hypothesised that this novel strategy will increase the stability of the AuNPs in presence of biological fluids and will also reinforce their intrinsic properties such as optical and photothermal. The specific objectives addressed in this first section can be divided in scientific and technical ones, and they are summarized as follows.

Section A. Scientific objectives:

- AuNPs suffers a lack on their stability while meeting biological fluids. It has been hypothesized that this issue could be solved by encapsulating them into a thin NG. Therefore, it is expected that the AuNPs stability will be improved in presence of several biological media when the NG is present in comparison with traditional stabilization strategies.
- This technology should be easily adapted to different AuNPs shapes, while maintaining their original shape and size. Therefore, it is mandatory to find a proper relationship between the monomer feed ratio and the size of the AuNPs.

- The synthetic technology developed along this work should be stable and easy to apply to a variety of monomers (neutral, charged, hydrophilic, hydrophobic, etc.).
- If this synthetic route allows the preparation of thin NGs around AuNPs with controlled thickness, it can be hypothesized that the modification of the surface charge would play an important role in the interaction with proteins, salts, mucus layer, etc.
- AuNPs can be used in photothermal applications acting as light-into-heat transducers. However, they use to have a lack of stability that decrease the photothermal capacity. It is hypothesized that the NGs will provide higher stability, which will result in a better photoconversion.

Section A. Technical objectives:

- Prepare very thin NGs (2 – 6 nm) around AuNPs based on four different structural monomers. p-Acrylamide, as a neutral polymer, p-vinylimidazole as a partially hydrophobic polymer, [2-(Methacryloyloxy)ethyl]dimethyl-(3-sulfopropyl)ammonium hydroxide (p-DMAPS) as zwitterionic polymer and N-isopropylacrylamide (p-NIPAM) as thermoresponsive polymer, will be assayed.
- Improve the stability into more than 1 day of AuNPs upon exposure to salts, proteins and mucin thanks to the NG cover.
- Improve the photothermal conversion efficacy, in terms of avoiding plasmon band shift, of AuNPs thanks to the nanogel cover.
- Decrease the mucus adhesion of AuNPs to improve their tissue penetration which could end up in an enhancement of their therapeutic properties. To demonstrate this, G' and G'' rheological modulus will be analyzed to quantify the interaction between the AuNPs and the mucin.

The second section of the PhD thesis, **Section B**, explores the influence that the polymer composition has on the stability, mechanical properties and mucoadhesion of physically cross-linked hydrogels. It has been entitled “Screening of Eudragits as building blocks in the preparation of physically cross-linked hydrogels”, and is going to be explained in detail in **Chapter IV**. Its main focus is the understanding of the material’s behaviour at the ocular

biointerface, attending to their mucoadhesion with the ocular conjunctiva. Besides, their stability in presence of tear fluids and mechanical, rheological and crystallographic properties in function of the hydrogel composition will be addressed to end up with *In-vitro* and *In-vivo* analysis. Furthermore, it is expected that several optimizations will be required until the achievement of a final material with the desired characteristics to be used as an ocular insert. Besides, their protein encapsulation and release capacity will be addressed, as the ultimate objective is to use the hydrogels for ocular protein release.

Similar to the previous section, the specific objectives approached in this second section can be divided into scientific and technical ones, and they are summarized as follows.

Section B. Scientific objectives:

- The main goal is the reproducible preparation of physically cross-linked hydrogels with different stabilities in function of the selected Eudragit. The ones used in this project are versatile polyacrylates polymer with a broad range of hydrophilicities. It is hypothesized that by adding hydrophobic Eudragit to the formulation, the dissolution of the matrix will be slower than using hydrophilic Eudragits.
- It can be hypothesized that the preparation of hydrogels with Eudragits with different hydrophilicity could play an effect on the release kinetics of the encapsulated proteins. Therefore, several formulations will be investigated to try to adjust the release kinetics to the final application.
- Achieving a good adhesion towards the ocular conjunctiva remains challenging. Therefore, it has been hypothesized that applying polymers with well-reported mucoadhesion, the hydrogel's mucoadhesion could be improved.
- Ideally, the developed technology should enable a fast translation from the lab to the clinics. Hence, polymers and reagents already approved by regulation agencies (FDA, EMA) will be investigated to determine the potential preparation of the materials on a large scale.

Section B. Technical objectives:

- Reproducibly prepare physically cross-linked hydrogels based on polyvinylpyrrolidone (PVP), polyvinyl alcohol (PVA) and polyethylene

glycol (PEG) as common polymers and Eudragits with different water-soluble properties.

- Reinforce the mucoadhesive properties of the hydrogels up to 12 h guarantee that they could stay on the eye's surface for long periods.
- Achieve a homogeneous encapsulation of proteins inside the hydrogel matrix.
- Have control over the release kinetics that can assure a constant flow of proteins during the whole therapeutic dose time.
- Achieve a biocompatible hydrogel that promotes healthy growth of ocular cells by analysing the metabolic activity of the cells and comparing them with their metabolic activity without hydrogels. Both measurements should report similar results to conclude that the materials are biocompatible.
- Demonstrate in pre-clinical studies that the material can promote the re-epithelialization of the eye by measuring the epithelial defect area of an ocular wound. The obtained results will be compared with the re-epithelization obtained with amniotic membrane transplanted around the epithelial defect area (gold standard).
- End up with a clear alternative option that can face the actual surgical treatment for eye recovery.

More specific and detailed objectives of each section will be addressed in each chapter. In addition, general conclusions and future perspectives of the PhD thesis will be summarized in **Chapter V**.

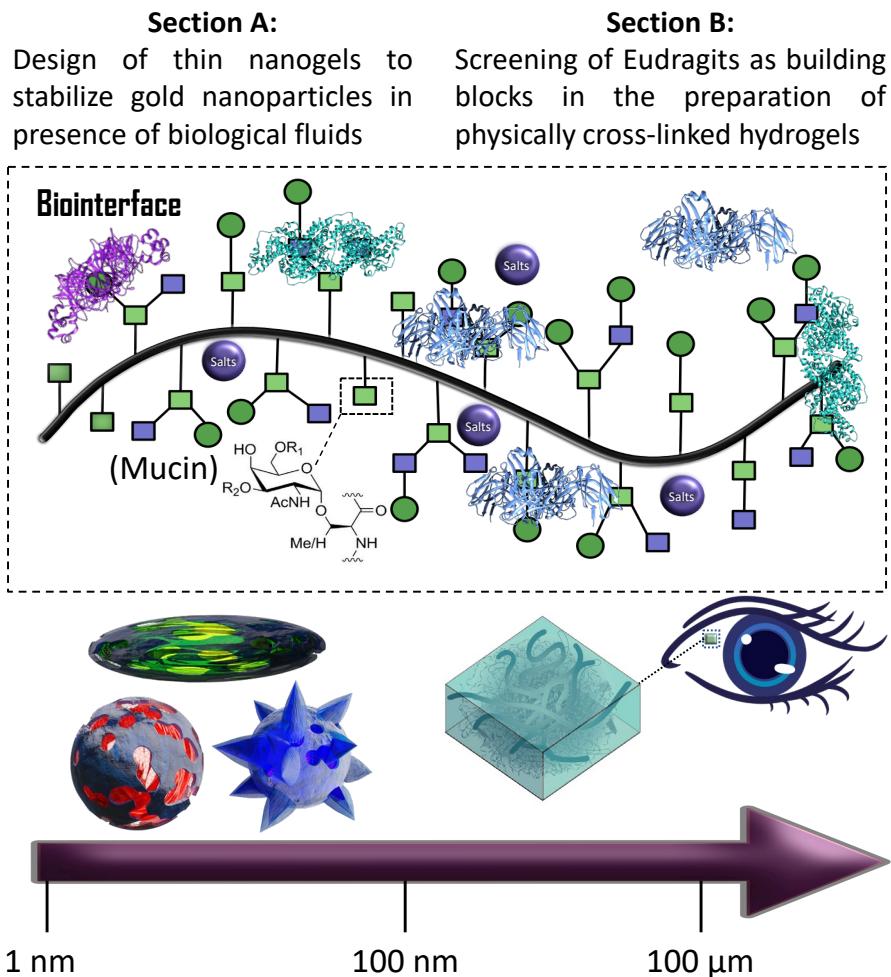


Figure 2.1. Scheme that summarizes the work included in this PhD thesis and the global objectives.

SECTION A

CHAPTER III:

Design of thin nanogels
to stabilize gold
nanoparticles in
presence of biological
fluids

3.1 Introduction

Inorganic NPs are promising materials that have met their place in biomedicine for a broad range of applications thanks to their high surface area to volume ratio.^{[1][2]} In particular, AuNPs have emerged as one of the most interesting nanomaterials up to date due to their use in diagnostics, drug delivery, therapy and imaging.^[3] Since the first AuNPs were prepared by accident in the fifth century A.D., during the roman times,^[4] or by Michael Faraday^[5] in the 1850s, a lot of work have been done by researchers to understand their synthetic mechanism and their powerful applications. Their unique optical properties, with resonance in the visible range, and local field enhancement of light interaction, have roused the interest of AuNPs allowing the appearance of hundreds of synthetic protocols. Turkevich et al., brought to the scientific community one of the most frequently applied methodologies to prepare Au nanospheres in high concentrations and with different diameters.^[6] It consists of the reduction of Au³⁺ to Au⁰ by citrate, which also acts as a ligand to stabilize the particles while they are forming. The stability in water achieved with this methodology is up to one year, which was a big jump from previous methodologies. Nowadays, Turkevich's work can be considered as a turning point in the AuNPs synthetic strategies. Since then, it is possible to find protocols that have allowed the preparation of AuNPs "à la carte" with multiple shapes and sizes.

According to their shape, AuNPs can be divided into isotropic NPs (spheres) or anisotropic ones. The last ones can be also divided into 1D (e.g. nanorods, nanowires, nanotubes, nanobelts), 2D (e.g. nanostars, nanopentagons, nanohexagon, nanocubes) and 3D (e.g. nanotadpoles, nanodumbbells, nanodendrimers).^[7] **Figure 3.1** shows the aspect of several AuNPs revealed by TEM microscope and the variety of their optical properties in aqueous dispersion.

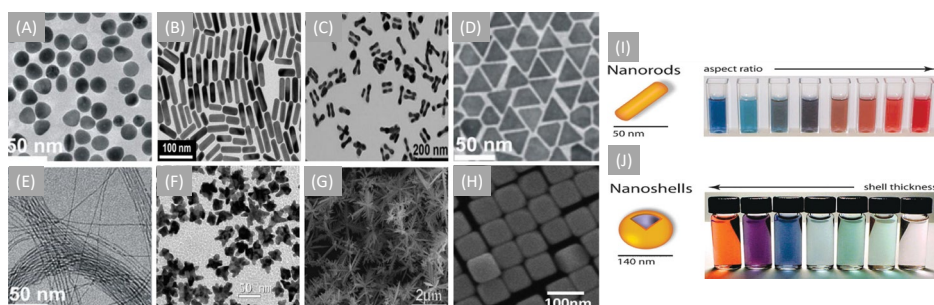


Figure 3.1. AuNPs TEM images and optical properties. (A) Au Nanospheres. (B) Au Nanorods. (C) Au Nanodumbbells. (D) Au Nanoprism. (E) Au Nanowires. (F) Au

Nanostars. (G) Au Nanodendrites. (H) Au Nanocubes. (I) Au Nanorods' colour changes while increasing the axial axis. (J) Au Nanoshells' colour changes while reducing the shell thickness. Figures adapted with permissions from *Talanta*, 2018.^[7]

In fact, as a consequence of the interaction between the incident light with the electrons located in the AuNPs surface (known as surface plasmon resonance) the nanoparticles' colour in aqueous dispersions changes with the shape and size of the nanomaterials (**Figure 3.1 I and J**). This phenomenon allows the appearance of a UV-Vis spectrum, which has a double benefit.^[8] First, it can be used as a quick characterization after the synthesis of any AuNPs. Second, it is possible to irradiate the particles at the wavelength of their maximum (max.) absorption to get an efficient light-into-heat transducer capacity. **Figure 3.2** shows a schematic of the UV-Vis spectra that can be collected from the measurement of Au nanospheres, nanorods and nanostars.

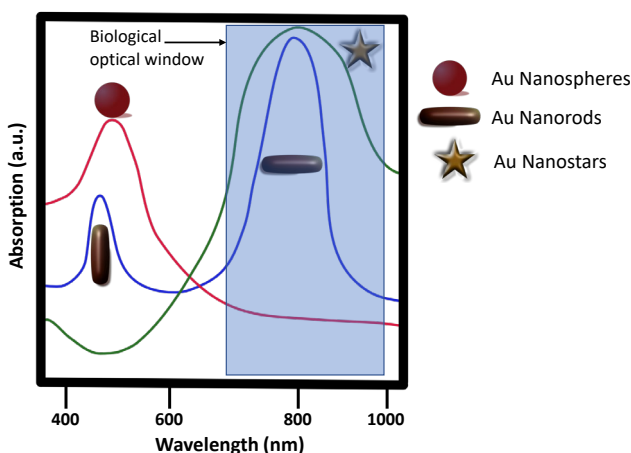


Figure 3.2. Scheme of UV-VIS spectra obtained from the measurements of an aqueous dispersion of Au nanospheres, nanorods and nanostars.

As can be seen in **Figure 3.2**, Au nanospheres have a peak of absorption at around 550 nm. By contrast, anisotropic Au NPs can have their peak absorptions in the range from 700 to 1200 nm.^[9] It is remarkable the particular case of Au nanorods. They exhibit two peaks, one at around 500 nm and another one at around 800 nm, as a consequence of the transversal and longitudinal orientation of these NPs.^[10] By controlling the aspect ratio of the Au nanorod, the second peak can be further shifted to the NIR region. This, along with the capacity of Au anisotropic NPs to absorb in the NIR region, makes them useful for biomedical applications at the biological optical transparent window (700 – 1100 nm).^[11] At this range of wavelengths the light

has its maximum depth of penetration in tissue without damaging any organ.^[12]

Since the publication of many reproducible protocols for the preparation of AuNPs, with isotropic and anisotropic shapes, the number of applications in biomedicine has exploded. For instance, AuNP's surface has been modified to recognize and attach biomolecules for the fabrication of diagnosis devices. This has allowed the recognition of nucleic acids, proteins, etc., in lateral flow assays, microfluidics, printed electrodes, etc., following the optical properties of AuNPs.^[13] Moreover, AuNPs have been also used in diagnosis as enhancement contrast of imaging. They can be modified to accumulate in infections, tumours, etc. to later, with the help of a laser, improve the tumour observation in many organs.^{[14][15][16]} In the treatment of diseases, AuNPs have been mainly used in photothermal, radiation and drug delivery therapy. For instance, Yang, et al. reported the use of silica-coated Au nanorods for the *In-vivo* cancer treatment in an animal model (**Figure 3.3**).^[17] As it can be seen, mice were irradiated with 808 nm NIR laser for 30 s after 2 h post-intravenous injection of the NPs. The obtained results concluded that the tumour weight decreased from 1 g (untreated mouse) to less than 0.5 g for the silica-nanorods treated animals. Furthermore, an extra material that combined the anticancer drug doxorubicin with the Au nanorods, allowed a decrease in the tumour weight to around 0.2 g.

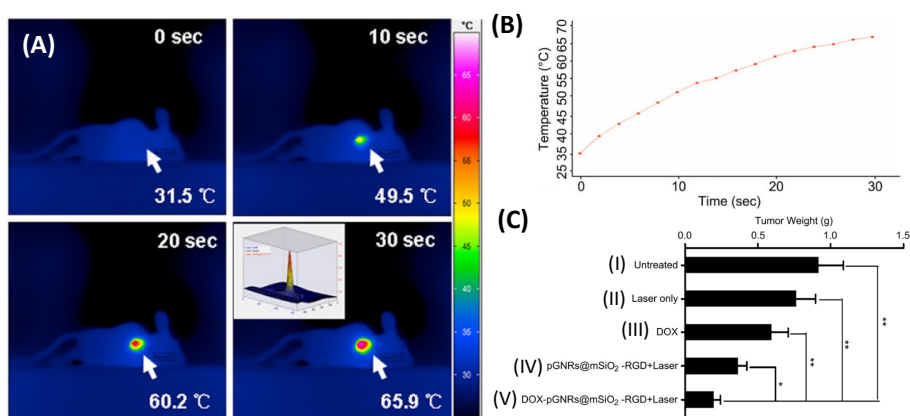


Figure 3.3. (A) Infrared thermal image of the tumour after irradiation with a laser, with $\lambda = 808$ nm, from 0 to 30 s. (B) Heating curve of the silica-rod NPs vs. time. (C) Tumour weight for: (I) untreated mouse; (II) NIR laser; (III) doxorubicin; (IV) silica-rod after laser irradiation; (V) doxorubicin and silica-rod after laser irradiation. Figures adapted with permissions from *Biomaterials*, 2013.^[17]

More recently, Vo-Dinh, et al. developed a novel technology to treat cancer called “synergistic immune photothermal nanotherapy”. This technology is based on the combination of Au nanostars with checkpoint inhibitor immunotherapy. The AuNPs were combined with anti-PD-1, which is an already approved antibody for a variety of solid tumours treatment. Their results demonstrated that the combination of the AuNPs with laser and Anti-PD-L1 was the only treatment with a 40% of mouse survival rate. Therefore, it can be concluded a high therapy success. They concluded that this novel technology has two benefits, it can treat the primary tumour and also it can trigger systemic anticancer immune responses to treat cancer metastasis. The Au nanostars could amplify the laser light and convert it into heat, which killed the tumoral cells. Besides, these targeted NPs demonstrated their capacity to improve checkpoint blockade immunotherapy. They foresee that with some optimization, this technology could be easily translated into clinical assays for melanoma and breast cancer.^[18]

Several years of pre-clinical research has resulted in the appearance of one of the first big successes in human trials for prostate cancer treatment with AuNPs, published in PNAS in 2019.^[19] In this study, 16 men were treated with auro-shell NPs, which are AuNPs protected with a layer of silica around them. One patient could not finish the treatment as a consequence of epigastric pain. The other 15 completed the treatment. The results concluded that 14 of the 16 patients had eradicated the tumour after 12 months. In the other two, for the one that couldn't complete the treatment, cancer grew 9 mm after 1 year and for the other one, cancer grew 3 mm after 1 year. Nevertheless, the study was completed with 87% of success, which represents a notable advance over current chemotherapy and a halo of hope for the future of nanomedicine.

There is no denying that the previously described applications of Au NPs are simply extraordinary. Inorganic NPs, and more specifically AuNPs have appeared in our lives to revolutionize current medicine. However, “not all that glitters is gold” (never has it been said better), as AuNPs suffers a lack in their stability when they are in presence of biomolecules. Therefore, protecting them (e.g., with organic shells or silica NPs) from hazardous interactions with biological fluids is a must for their use in biomedicine. Several strategies have been addressed to eradicate that issue, **Figure 3.4** summarize the most typical ones.^[20]

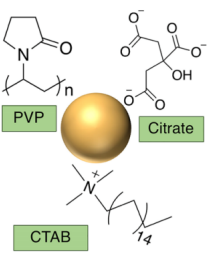
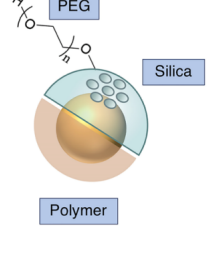
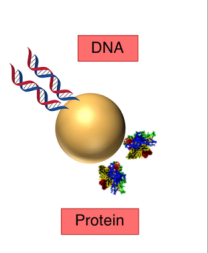
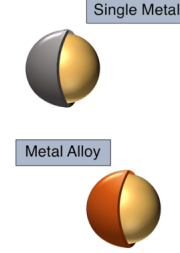
Conventional Surfactants and Ligands	Organic/Inorganic Shells	Biomolecular Ligands	Metal Shells
 <ul style="list-style-type: none"> • Reversibility • Morphology guide 	 <ul style="list-style-type: none"> • High colloidal stability • Facile functionalization 	 <ul style="list-style-type: none"> • High biocompatibility • Programmable assembly 	 <ul style="list-style-type: none"> • Core-shell chemical interaction

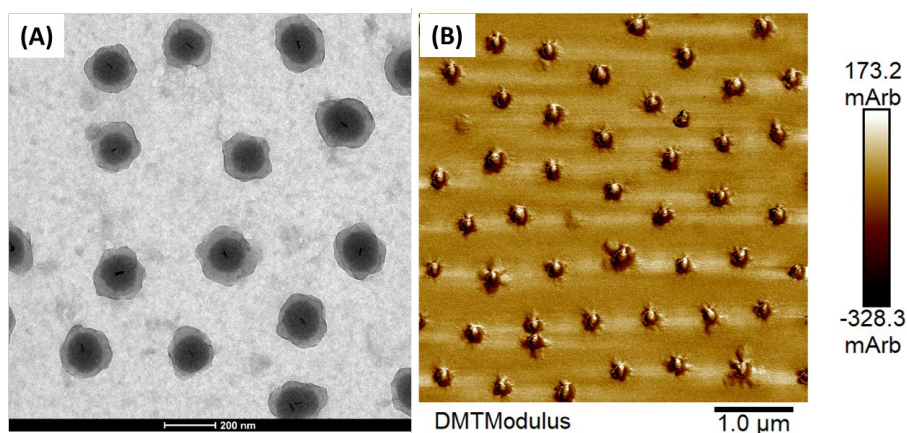
Figure 3.4. Scheme of the most used stabilization strategies for colloidal Au NPs. These are the functionalization of the particles with surfactants, ligands, organic and metallic shells or biomolecular ligands. Figure adapted with permissions from *Chemical Reviews*, 2019.^[20]

Stabilization strategies mentioned in **Figure 3.4** consider several scenarios. For instance, coupling ligands like PVP, citrate or CTAB to AuNPs have been respectively used to stabilize Au nanocages, nanospheres and nanorods during their synthesis.^{[21][22]} The main benefit of these ligands, besides of guiding the formation of the desired morphology, is that they can be easily exchanged for other ones, like thiolated PEG. Besides, the creation of a polymeric or silica shell around the AuNPs can increase the colloidal stability while adding extra surface functionalization to the material. For instance, the porosity of silica shells, together with the functionalization of their surface, has been used to improve catalytic reactions.^[23] Furthermore, the incorporation of biomolecular ligands can camouflage the synthetic identity of AuNPs letting the recognition of the material as a biological identity by the immune response. Besides, the functionalization of AuNPs with ligands, like DNA, have a reported improvement on their stabilization towards salts.^[24] Finally, a metallic core shell allows the interaction of the material with several chemical molecules while preserving their integrity.

In essence, many of methodologies are emerging day by day to keep improving the life stability of AuNPs in biological fluids. During the last years, thanks to the development of NGs, these organic 3D structures have been used as core-shell protection for AuNPs. For instance, Marzán et al. prepared p-NIPAM thermoresponsive NGs around AuNPs as a core-shell material.^[25] In that study, they prepared CTAB-coated Au nanospheres with a few polystyrene units that are used afterwards for the post-polymerization of

NIPAM. The resulting material is a NG, with a diameter of around 300 nm, that is acting as a shell of Au nanospheres with a diameter of 90 nm. Even though the material has good thermoresponsive behaviour, the optical properties of the AuNPs are being reduced as a consequence of the polymer shell being 3 times bigger than the inorganic core. More recent studies prepared thermoresponsive NGs with several AuNPs as a core of the material.^[26] Even though these materials were highly biocompatible, and could encapsulate hydrophobic drugs and release them into cells, they have lack into the photothermal capacity of the AuNPs. In fact, they could only increase the solution temperature in around 10 centigrade degrees after 12 min of laser irradiation. As was happening in the previously cited study, the main reason for that is to have a 200 nm NG shell with 20 nm AuNPs inside of them. Therefore, the optical properties of the AuNPs are inevitably undermined. In another study, Shi et al. developed a 100 nm NG that contains a combination of Au and Gd spheres inside of them.^[27] They applied the material into tumours for imaging enhancement. Even though the final NG had good cytocompatibility and aqueous stability, to improve notably the tumour imaging it was required to add several NPs per NG, to avoid to lose the optical effect of the inorganic NPs. In a very recent study from Marzán, et al., they also explored the encapsulation of several AuNPs in spherical organic shells as a good approach to increase their biocompatibility for bioimaging. They were forced to add several AuNPs to each organic shell to preserve the optical properties coming from the Au as a contrast imaging.^[28]

Figure 3.5, shows preliminary results in the framework of the current thesis. As it can be observed, these results highlight similar issues to the ones previously reported in the literature.



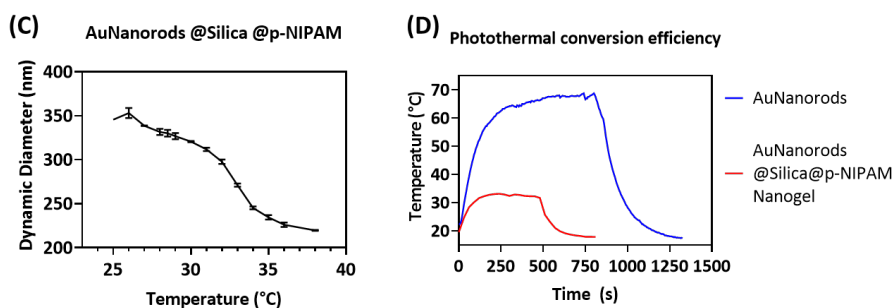


Figure 3.5. (A) TEM pictures of Au nanorods absorbed into silica nanospheres with a p-NIPAM nanogel shell around. (B) AFM microscopy pictures of the same material. (C) DLS measurement in a ramp of temperature from 25 to 38 °C. (D) photothermal conversion efficiency of Au nanorods and Au nanorods absorbed into silica nanospheres covered with a p-NIPAM nanogel shell.

In **Figures 3.5A** and **B**, it can be seen the good homogeneity of the NGs and the presence of one single Au nanorod inside of each mesoporous silica nanosphere. Then, the p-NIPAM thermoresponsive NGs can decrease their hydrodynamic diameter from 350 nm to around 200 nm while increasing the temperature from 25 to 38 °C (**Figure 3.5 C**). Hence, a priori, the material's behaviour is optimal. Nevertheless, the photothermal conversion efficiency (**Figure 3.5 D**) demonstrated that, with similar concentrations, the Au nanorods can heat up to 70 °C. However, when they are protected by a mesoporous silica NPs and a p-NIPAM NGs, this temperature can reach only 30 °C. It can be hypothesized that the photothermal conversion capacity of the AuNPs is being reduced as a consequence of the two shells. Therefore, probably the silica and the NGs are absorbing part of the heat. In an attempt to reduce the thickness of the NGs and improve the thermo-optical properties of the AuNPs, new protocols are emerging nowadays. In a very recent study, Liu, et al. prepared a multifunctional NG that can contain a single Au nanosphere with a reduced thickness of the shell.^[29] Their material was based on vinyl-peptides-PEG chemically linked to a 20 nm Au nanosphere. Then, the polymerization took place in deoxygenated phosphate buffer with the monomers 2-dimethylaminoethyl methacrylate, 2-methacryloyloxyethyl phosphorylcholine and glycerol dimethacrylate. The final material required overnight dialysis purification. The formed NGs were characterized in presence of several proteins, determining that the NG shell protection decreases notably the PC absorption. **Figure 3.6** show the most relevant results from Liu et al.

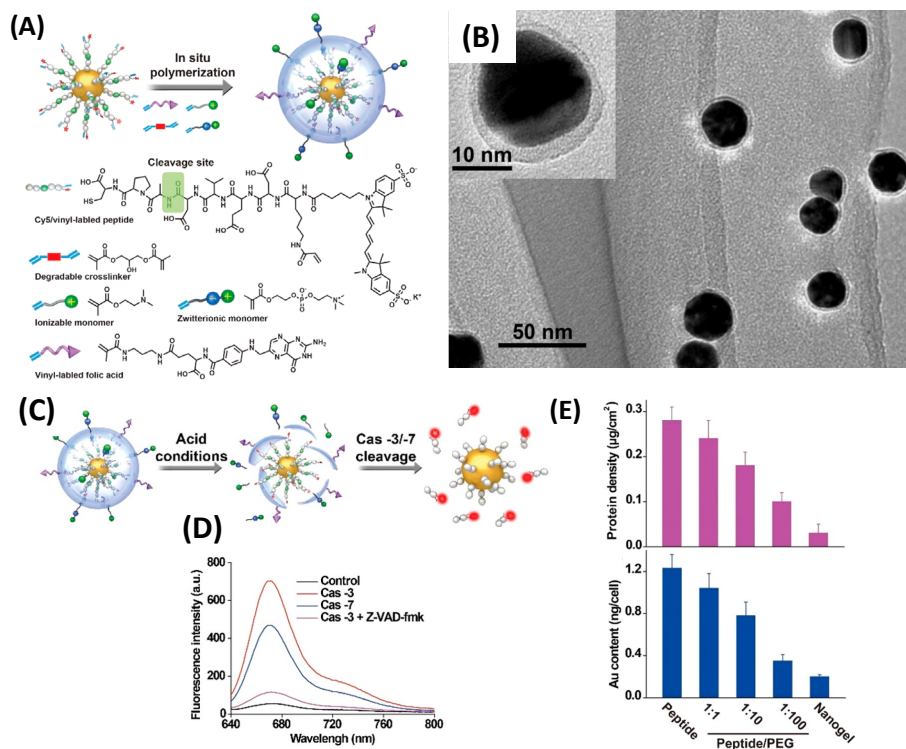


Figure 3.6. (A) Scheme showing the developed nanogel shell with AuNPs as a core. (B) TEM pictures of the prepared material. (C) Scheme showing the degradation of the NG at acid conditions. (D) Fluorescence intensity released at different pH. (E) Protein absorption and Au concentration for AuNPs protected with a peptidic shell, a peptidic/PEG shell or a nanogel. Figures adapted with permission from *Analytical chemistry*, 2019.^[29]

The work summarized in **Figure 3.6** demonstrated the possibility to create a thin NG around AuNPs. Nevertheless, the system prepared here required complex peptidic sequences and the use of deoxygenated solvents. In addition, the synthetic methodology has been applied only to isotropic NPs, which calls into question the possibility of preparing these NGs with good yield in anisotropic NPs. Conversely, even though the protein amount absorbed onto the NG is very low in comparison with the AuNPs protected with peptide or peptide/PEG linear sequences, the concentration of Au presented in the NG is also quite low. Therefore, the optical Au properties can still be greatly diminished.

In the present work, a completely novel synthetic strategy has been optimized for the preparation of very thin cross-linked NGs to act as a shell of isotropic and anisotropic AuNPs. The chemistry behind is a new branch of the

single-enzyme NGs technology developed by Beloqui, et al. during the last years.^{[30][31]} Their work allowed the encapsulation of a single protein into a chemically cross-linked NG that can be used for catalysis applications. In the case of the AuNPs, their diluted concentration in colloidal dispersions have required to adapt the chemical reactions. New molar ratios, polymer stabilization and characterization techniques have been applied for the preparation of thin mantle NGs to protect Au nanospheres, nanorods and nanostars while preserving their size and shape. The final material only increases the total thickness by around 2 – 4 nm. To provide various functionalities, neutral, hydrophobic, zwitterionic and antifouling polymers have been used during the preparation of the materials here reported. Finally, all of them will be exposed towards biological fluids to test their stabilities. **Figure 3.7** shows a general scheme of the materials that will be prepared along with Chapter III.

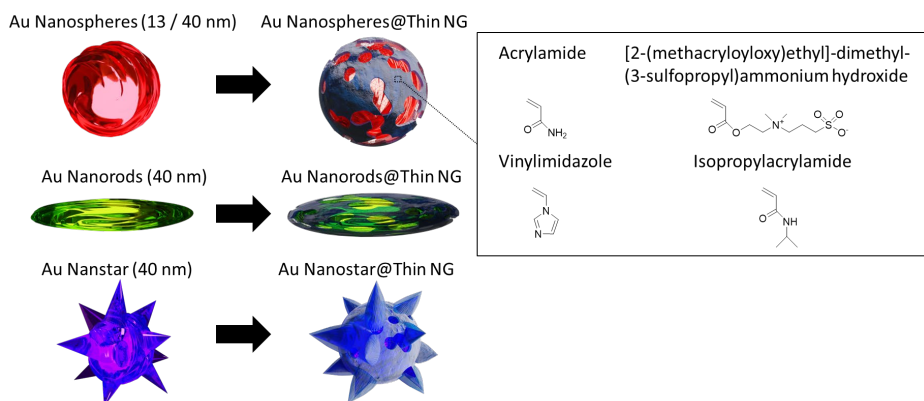


Figure 3.7. Scheme of the AuNPs shielded by a thin layer of NGs and chemical structure of the monomers used for the synthesis of the NGs.

3.2 Objectives

The general objectives of Chapter III were addressed in Chapter II. Here, some specific objectives of the project are going to be remarked.

The project aims to synthesize very thin NGs that can be used to protect AuNPs while keeping their size and shape. The global objective is to develop chemically cross-linked NGs that increase the size of the Au nucleus by a few nm, in which the surface charge and the hydrophobicity can be modulated. These NGs should enhance the stability of the AuNPs when they face biological fluids, containing salts, proteins and mucus. The main objectives are listed as follows:

- The optimization of a protocol that allows the synthesis of very thin NGs around AuNPs that can polymerize *In-situ* while maintaining the size and shape of the core.
- The optimized technology should be easily transferred to any shape of AuNPs and work with different monomers. This will allow tuning the surface charge and hydrophobicity of the materials.
- Due to the small thickness of the organic NGs, the correct characterization of these materials remains quite challenging. Hence, another objective is to tune the parameters in electronic microscopies, chromatography techniques and thermal analysis to demonstrate the presence of the NG on the surface of AuNPs.
- AuNPs have met many applications in biomedicine. Therefore, a good design and control over the synthetic materials are crucial to modulate their interactions with biological fluids. Thus, it is expected to improve the stability of AuNPs in presence of proteins and salts using different monomers for the preparation of the NGs.
- Finally, it is also expected that the thin NGs could improve the stability of AuNPs during their irradiation with laser light. Thanks to the good relationship between the size of the inorganic core and the small thickness of the NGs, the thermal conversion efficacy is expected to be high.









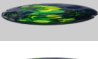
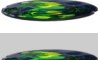
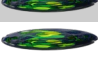





3.3 Results and discussion

3.3.1 Synthetic methodology for the preparation of thin mantle nanogels to protect gold nanoparticles

A total of sixteen materials have been prepared based on isotropic and anisotropic AuNPs covered with thin NGs. In a first step, Au nanospheres (AuNSs), Au nanorods (AuNRs) and Au nanostars (AuNSTs) were synthesized following reported protocols from the literature.^{[6][22][32]} Then, high excess (around 2 mM per 10 mL AuNPs solution) of thiolated-PEG_{5k}-NH₂, has been used as an exchange ligand for the AuNPs. As the PEG has been added in high excess, the surface of the AuNPs is presumably fully covered by this linear polymer. Particles have been centrifuged between each step to remove the non-reacted materials. The final pellet has been redispersed in 4-(2-hydroxyethyl)-1-piperazineethanesulfonic acid (HEPES) buffer 10 mM, pH 8.02, to guarantee that the amine groups are not protonated. The third step of the protocol is a reaction with N-acryloylsuccinimide during 2 h. This reagent attacks the amine groups to generate an acryl-amide. Therefore, now AuNPs are functionalized with acryl groups on the surface that can be used to perform a free radical polymerization. In a final step, the free radical polymerization of the thin mantle NGs takes place with a very diluted concentration of the monomers, cross-linker, initiator and catalyst. It is worth it to mention that the molar ratio and the reaction time change in function of the size and shape of the AuNPs. More details about the synthetic conditions are given in the experimental section (3.4). To modify the hydrophilicity and surface charge of the NGs, different monomers have been used. For the preparation of a neutral NG, acrylamide has been the selected monomer. Another neutral NG with zwitterionic properties has been prepared using the monomer [2-(methacryloyloxy)ethyl]-dimethyl-(3-sulfopropyl)ammonium hydroxide (DMAPS). Then, vinylimidazole has been used as a monomer with a certain character of hydrophobicity coming from a nitrogenated cycle located in its chemical structure. For the preparation of these two last NGs (p-vinylimidazole and p-DMAPS), the respective monomers have been copolymerized with acrylamide. Nevertheless, to simplify the manuscript, the acrylamide will not be referred together with the other monomers in the text. Finally, a thermoresponsive NG has been developed using NIPAM as monomer. All of them have been chemically cross-linked with methylenbisacrylamide, and the polymerization has been started with ammonium persulfate (APS) and accelerated with the catalyst tetrametiletilendiamina (TEMED). It is invaluable to notice that the technology developed has allowed the preparation of chemically cross-linked thin NGs

around AuNPs that increase the total diameter by 2 – 6 nm while keeping the original shape of AuNPs. **Table 3.1** summarizes the materials developed in this work and the chemical structure of the used reagents. In addition, **Figure 3.8** shows a schematic of the synthetic methodology applied.

Table 3.1. Graphical design, sample codes, chemical composition and the molar ratio of the Au-based materials prepared.

Graphical design	Sample Code	Sample composition	Thin mantel NG composition	AuNPs concentration (M)	Molar Ratio AuNPs:monomers (Cross-linker:Initiator:Catalyst)
	AuNSs@NG 1	Au Nanospheres 13nm @NG 1	p-Acrylamide (Bisacrylamide:APS:TEMED)	10 ⁻⁸	1:30,000 (3,300:4,000:5)
	AuNSs@NG 2	Au Nanospheres 13nm @NG 2	p-Acrylamide-co-Vinylimidazole (Bisacrylamide:APS:TEMED)	10 ⁻⁸	1:10,000:30,000 (4,500:5,600:7)
	AuNSs@NG 3	Au Nanospheres 13nm @NG 3	p-Acrylamide-co-DMAPS (Bisacrylamide:APS:TEMED)	10 ⁻⁸	1:10,000:30,000 (4,500:5,600:7)
	AuNSs@NG 4	Au Nanospheres 13nm @NG 4	p-NIPAM (Bisacrylamide:APS:TEMED)	10 ⁻⁸	High excess, protocol at r.t.
	AuNSs@NG 5	Au Nanospheres 40nm @NG 5	p-Acrylamide (Bisacrylamide:APS:TEMED)	10 ⁻¹⁰	1:30,000 (10,000:12,000:15)
	AuNSs@NG 6	Au Nanospheres 40nm @NG 6	p-Acrylamide-co-Vinylimidazole (Bisacrylamide:APS:TEMED)	10 ⁻¹⁰	1:10,000:30,000 (13,000:16,000:20)
	AuNSs@NG 7	Au Nanospheres 40nm @NG 7	p-Acrylamide-co-DMAPS (Bisacrylamide:APS:TEMED)	10 ⁻¹⁰	1:10,000:30,000 (13,000:16,000:20)
	AuNSs@NG 8	Au Nanospheres 40nm @NG 8	p-NIPAM (Bisacrylamide:APS:TEMED)	10 ⁻¹⁰	High excess, protocol at r.t.
	AuNRs@NG 9	Au Nanorods 40 nm @NG 9	p-Acrylamide (Bisacrylamide:APS:TEMED)	10 ⁻⁹	1:30,000 (10,000:12,000:15)
	AuNRs@NG 10	Au Nanorods 40 nm @NG 10	p-Acrylamide-co-Vinylimidazole (Bisacrylamide:APS:TEMED)	10 ⁻⁹	1:10,000:30,000 (13,300:16,000:20)
	AuNRs@NG 11	Au Nanorods 40 nm @NG 11	p-Acrylamide-co-DMAPS (Bisacrylamide:APS:TEMED)	10 ⁻⁹	1:10,000:30,000 (13,300:16,000:20)
	AuNRs@NG 12	Au Nanorods 40 nm @NG 12	p-NIPAM (Bisacrylamide:APS:TEMED)	10 ⁻⁹	High excess, protocol at r.t.
	AuNSTs@NG 13	Au Nanostars 40 nm @NG 13	p-Acrylamide (Bisacrylamide:APS:TEMED)	10 ⁻⁹	1:30,000 (10,000:12,000:15)
	AuNSTs@NG 14	Au Nanostars 40 nm @NG 14	p-Acrylamide-co-Vinylimidazole (Bisacrylamide:APS:TEMED)	10 ⁻⁹	1:10,000:30,000 (13,300:16,000:20)
	AuNSTs@NG 15	Au Nanostars 40 nm @NG 15	p-Acrylamide-co-DMAPS (Bisacrylamide:APS:TEMED)	10 ⁻⁹	1:10,000:30,000 (13,300:16,000:20)
	AuNSTs@NG 16	Au Nanostars 40 nm @NG 16	p-NIPAM (Bisacrylamide:APS:TEMED)	10 ⁻⁹	High excess, protocol at r.t.

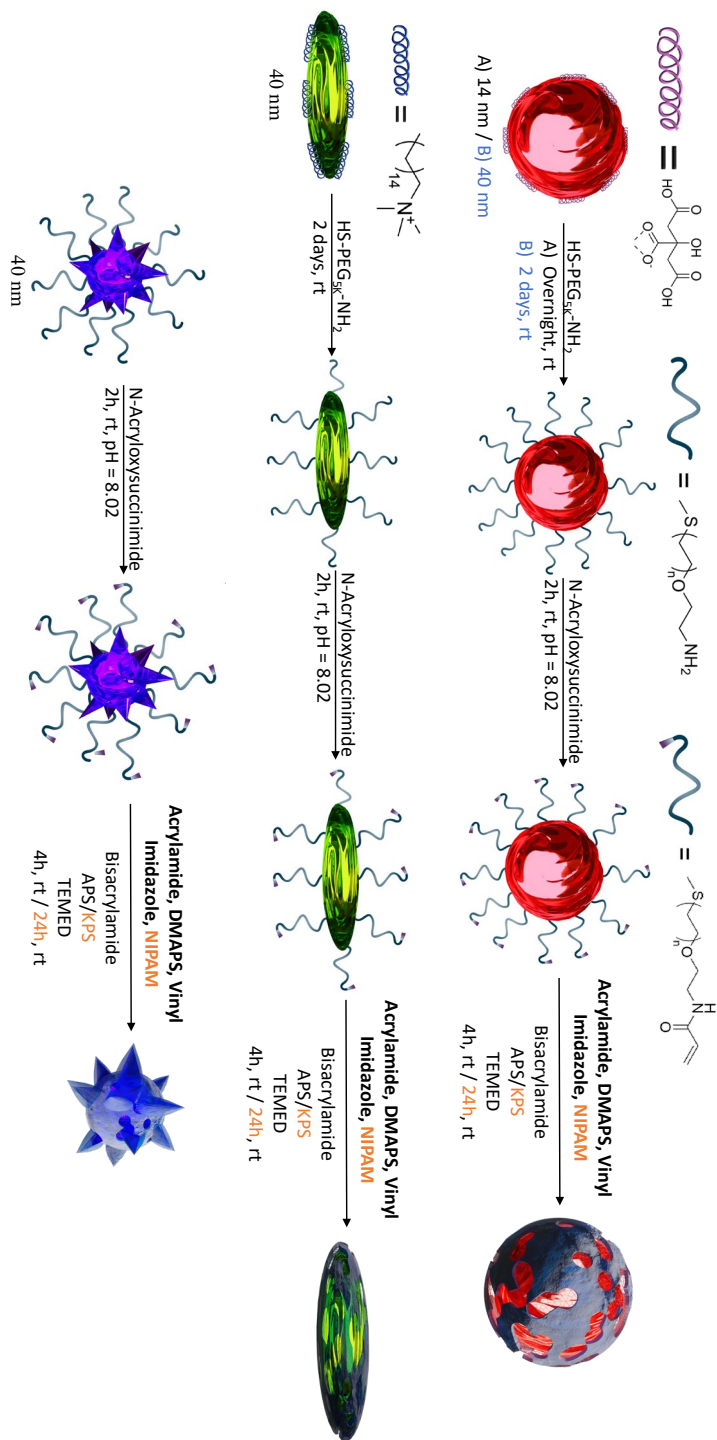


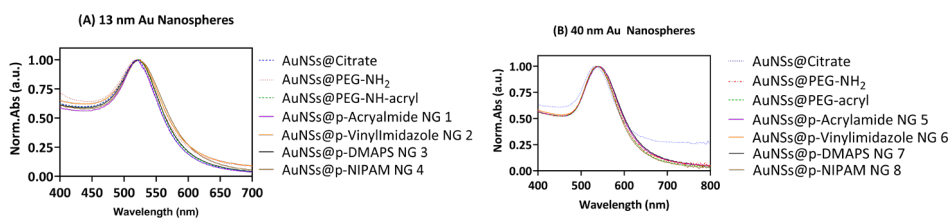
Figure 3.8. Synthetic scheme followed for the preparation of thin mantle NGs with AuNPs as core.

3.3.2 Structural and physicochemical characterizations of the materials

3.3.2.1 UV-Vis spectra

Thanks to the presence of the plasmonic behaviour typical of AuNPs, the characterization of these materials by UV-VIS is always the first characterization step while working with AuNPs. The plasmonic absorption bands spectra have been widely explored by many researchers in the past. Therefore, nowadays it is quite easy to compare the UV-Vis spectrum obtained after AuNPs synthesis with the ones available in the literature. Besides, this characterization can be used to corroborate if, after a surface modification of the AuNPs, they are still stable, maintaining their original size and shape. Conversely, the molar concentration from AuNPs in the colloidal dispersion can be obtained by applying the Beer-Lambert law (**equation 3.1**). The extinction molar coefficient " ϵ_0 " required to apply the formula is tabulated for each size and shape of AuNPs. The rest of the parameters from the equation are given by the UV-Vis spectrophotometer, where "Abs" is the measured absorbance and "l" the optical path length. According to the literature, Au nanospheres show a maximum absorption peak at 520 – 530 nm for the range of 10 – 45 nm diameters and ϵ_0 are $1.76 \cdot 10^8$ and $4.92 \cdot 10^9 \text{ M}^{-1} \text{cm}^{-1}$ at 450 nm for 14 and 40 nm Au nanospheres, respectively.^[33] In the case of Au nanorods, the UV-Vis absorption spectrum exhibits two peaks, in function of the longitudinal or axial orientation of the NPs. Besides, 40 nm Au nanorods have an intense peak around 800 nm and a reported ϵ_0 of $20 \cdot 10^8 \text{ M}^{-1} \text{cm}^{-1}$.^[34] Last, but not least, Au nanostars with 40 nm of size have been reported to have a ϵ_0 of $24.4 \cdot 10^8 \text{ M}^{-1} \text{cm}^{-1}$ and a max. absorption in the NIR region (around 800 nm).^[35] This information taken from the literature has been used for the correct characterization of the here developed materials. **Figure 3.9** collects the spectra for all the products and **Table 3.2** shows the main data obtained from the spectra.

$$Abs = \epsilon_0 c l \quad (\text{Equation 3.1})$$



Design of thin nanogels to stabilize gold nanoparticles in presence of biological fluids

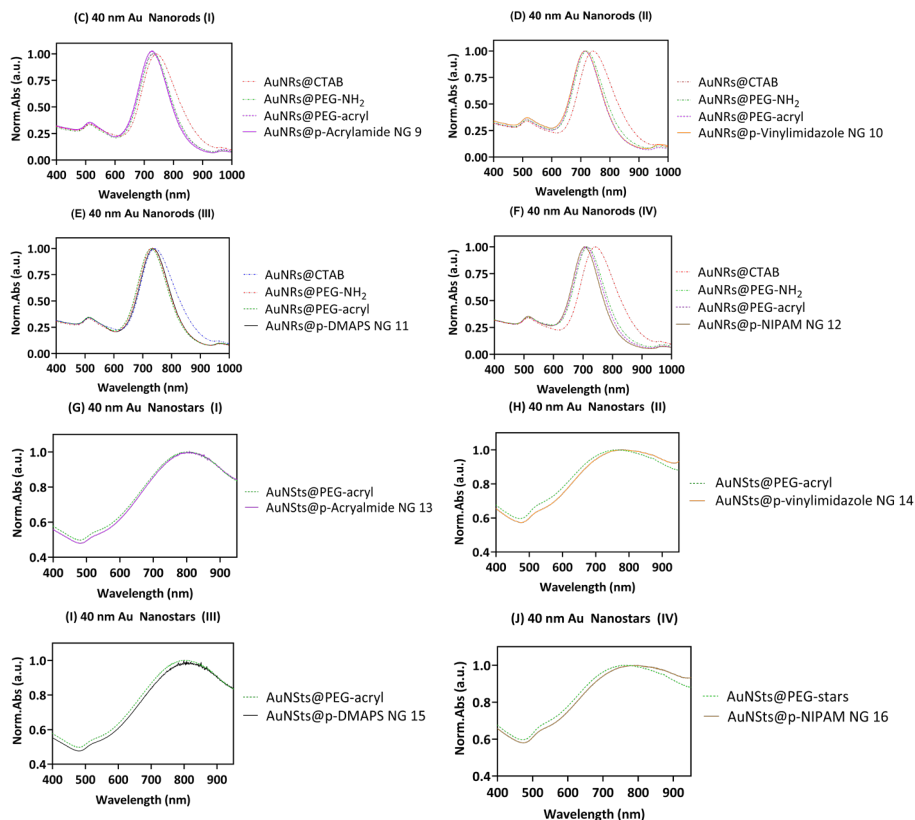


Figure 3.9. UV-VIS spectra of (A) 13 nm Au Nanospheres with citrate, PEG-NH₂, PEG-acryl ligands and NGs shells 1 – 4. (B) 40 nm Au Nanospheres with citrate, PEG-NH₂, PEG-acryl and NGs shells 5 – 6. (C) 40 nm Au Nanorods with citrate, PEG-NH₂, PEG-acryl and NG shell 9. (D) 40 nm Au Nanorods with citrate, PEG-NH₂, PEG-acryl and NG shell 10. (E) 40 nm Au Nanorods with citrate, PEG-NH₂, PEG-acryl and NG shell 11. (F) 40 nm Au Nanorods with citrate, PEG-NH₂, PEG-acryl and NG shell 12. (G) 40 nm Au Nanostar with PEG-acryl and NG shell 13. (H) 40 nm Au Nanostar with PEG-acryl and NG shell 14. (I) 40 nm Au Nanostar with PEG-acryl and NG shell 15. (J) 40 nm Au Nanostar with PEG-acryl and NG shell 16.

Table 3.2 Max. absorption for the most relevant spectra showed in Figure 3.9.

Sample Code	Max. Absorption (UV-VIS)	Sample Code	Max. Absorption (UV-VIS)	
13 nm Au NSs@PEG-acryl	521	40 nm Au NRs@PEG-acryl	(I) 731	(II) 711
AuNSs@NG 1	521		(III) 731	(IV) 710
AuNSs@NG 2	520	AuNRs@NG 9		716
AuNSs@NG 3	523	AuNRs@NG 10		714
AuNSs@NG 4	525	AuNRs@NG 11		736
		AuNRs@NG 12		705
40 nm Au NSs@PEG-acryl	539	40 nm Au NSts@PEG-acryl	(I) 797	(II) 768
AuNSs@NG 5	541		(III) 797	(IV) 768
AuNSs@NG 6	541	AuNSts@NG 13		799
AuNSs@NG 7	541	AuNSts@NG 14		780
AuNSs@NG 8	535	AuNSts@NG 15		799
		AuNSts@NG 16		781

Figure 3.9 A shows the spectra for 13 nm Au Nanospheres prepared with citrate ligand and their posterior modifications. It can be seen and corroborated in **Table 3.2** that the posterior modification of the spheres with linear PEG or with the four varieties of NGs, maintain the max. absorption in the range 520 – 525 nm. The slight varieties in the number are a consequence of surface modifications. According to literature, graft Au nanospheres surface with linear PEG causes a bathochromic effect on the plasmonic band, shifting it in about 2 nm, but it maintains the size of the precursor AuNPs.^[36] Nevertheless, the creation of the thin NG shell around the AuNPs has shifted the abs. peak in around 1 – 4 nm, which indicates that the core of Au Nanospheres preserves its integrity in terms of size and shape.

For the case of 40 nm Au nanospheres, **Figure 3.9 B** and **Table 3.2**, it can be observed a similar tendency. For this case, the max. peak absorption for the surface grafted with linear PEG appeared at 539 nm. Moreover, the creation of the thin NG around the 40 nm Au nanospheres, barely shifts the peak, which indicates the preservation of the size and shape of the NPs.

Attending now to the Au nanorods, **Figures 3.9 C-F** and **Table 3.2**, these NPs have the limitation that the synthetic protocol is a bottleneck in the amount of material that can be prepared. Therefore, it is necessary to prepare a full sequence batch (**Figure 3.8**) for each NG. As it is quite tricky to replicate the protocol without any single modification, the preparation of two or more batches of AuNRs with CTAB could have a max. absorption peak shifted some nm. In the end, all the prepared AuNRs have an average diameter of around 40 nm. Nevertheless, small variation could happen between batches, which is the reason why the UV-VIS spectra for every NG is plotted in an individual graph. Graphs C – F show that after the CTAB is exchanged by PEG-NH₂, the peak shifts to the blue. Nonetheless, the preparation of the NG as a shell just shifts slightly the peaks, maintaining it in the NIR region (> 700 nm), which indicates that the size and shape of the AuNRs are maintained.

Finally, a similar situation is happening for the Au nanostars. In general, the anisotropic AuNPs can be prepared in very diluted conditions. Hence, as it was happening with the rods, it is necessary to prepare a new batch of AuNanostars for the synthesis of each NG. It is also worth it to mention that the synthetic protocol of Au nanostars has a crucial step, where two reagents must be added at the same time to avoid shifting the plasmon band. One might mention that anisotropic AuNPs are more sensitive than isotropic ones to surface grafting. As it can be seen, now the plasmonic bands are more shifted, after grafting the surface with PEG, than in the case of the spheres. However, it has been corroborated by electronic microscopies (section **3.3.2.4**) that the size and shape of the stars are maintained during the NGs formation. Also, as it can be corroborated in **Table 3.2**, from one batch to another of the AuNSts grafted with PEG-NH₂, the peak has been shifted around 30 nm. Nevertheless, both are in the NIR region.

In a partial conclusion, it can be confirmed that the optimized protocols allow the preparation of NGs around 13, 40 nm Au nanospheres, 40 nm Au nanorods and 40 nm Au nanostars maintaining their size, shape and optical properties. Nevertheless, more characterizations are required to confirm the thickness and the presence of the polymeric layer around.

3.3.2.2 Hydrodynamic diameters (DLS) and surface charge of the materials (Z-Potential)

The hydrodynamic diameter of the AuNPs and surface charge have been measured in a Malvern Z-sizer. The data obtained is shown in **Figure 3.10**.

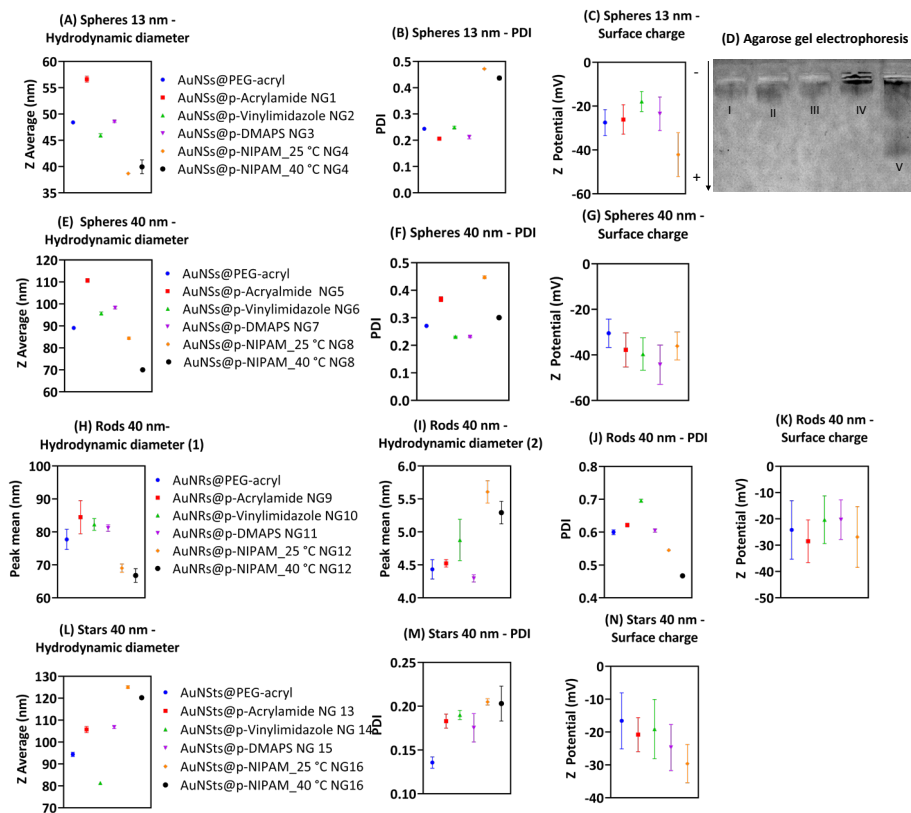


Figure 3.10. (A, B) Z average and PDI of 13 nm AuNSs grafted with PEG-acryl and NG 1 - 4. (C) Z-potential of 13 nm AuNSs grafted with PEG-acryl and NG 1 - 4. (D) Agarose gel electrophoresis of 13 nm AuNSs grafted with PEG-acryl and NG 1 - 4. (E, F) Z average and PDI of 40 nm AuNSs grafted with PEG-acryl and NG 5 - 8. (G) Z-potential of 40 nm AuNSs grafted with PEG-acryl and NG 5 - 8. (H, I, J) Z average and PDI of 40 nm AuNRs grafted with PEG-acryl and NG 9 - 12. (K) Z-potential of 40 nm AuNRs grafted with PEG-acryl and NG 9 - 12. (L, M) Z average and PDI of 40 nm AuNSTs grafted with PEG-acryl and NG 13 - 16. (N) Z-potential of 40 nm AuNSTs grafted with PEG-acryl and NG 13 - 16.

Isotropic and anisotropic AuNPs are never totally homogenous. Actually, many reports have called Au nanospheres, as quasi-spheres which indicates that their shape is not perfect.^[37] In the case of anisotropic particles, the heterogeneity between particles increases. As a consequence of these, a

proper measurement of the hydrodynamic diameter of AuNPs, by dynamic light scattering (DLS), remains challenging. In fact, it is quite frequent to find in the bibliography bigger hydrodynamic diameters (with high polydispersity index, PDI) of AuNPs than the ones reported by electronic microscopies (like TEM or SEM).^[38] In **Figure 3.10**, it is reported the hydrodynamic diameter of AuNPs with very thin shells. Due to the small thickness of the organic shell, the measured values may be underestimated. The information reported in this section can be interpreted as qualitative and non-quantitative.

For the case of 13 nm Au nanospheres, as the Au core of the materials is quite small, there are no clear tendencies from the point of view of the size. Also, the PDI for all the 13 nm materials is 0.2 – 0.3, which do not allow the differentiation in 2 nm organic thickness. By contrast, the surface charge (**Figure 3.10C**) indicates that the most negative one is the p-NIPAM NG (NG4, -42.1 ± 10 mV), followed by p-acrylamide NG (NG1, -26.1 ± 6.73 mV), then p-DMAPS NG (NG3, -23.5 ± 7.67 mV) and finally p-acrylamide NG (NG2, -17.9 ± 4.58). Nevertheless, all of them reported negative surface charges. This tendency has been corroborated with an agarose gel electrophoresis (**Figure 3.10D**) obtaining similar tendencies. Hence, it can be concluded that even in the case of a high value of PDI (higher than 0.2), the Z-potential tendencies can be estimated correctly.

The big size of the prepared Au nanospheres should have a Au core of 40 nm diameter. The AuNSs grafted with PEG-acryl have reported a 90 nm of Z-average hydrodynamic diameter and a PDI of around 0.25. As was described in the literature, this value is bigger than the one obtained by UV-VIS and TEM microscopy (section 3.3.2.4.). Nevertheless, the NG5, 6 and 7 (p-acrylamide, vinylimidazole and DMAPS) have reported 110, 95 and 98 nm of hydrodynamic diameters, respectively. All of them are bigger values than the material with linear PEG. Therefore, the growing tendency indicates the creation of a polymeric cross-linked shell. On contrast, the NG based on p-NIPAM attracts attention as it reports a smaller diameter than the linear PEG-acryl. It shows 84 nm (PDI = 0.44) at 25 °C and 70 nm (PDI = 0.3) at 40 °C. In fact, it can be speculated that the PEG is contracting during the formation of the p-NIPAM NG. Nevertheless, the thermoresponsive behaviour of the p-NIPAM is present, as the hydrodynamic diameters decrease at higher temperatures. Attending now to the surface charge of the 40 nm sphere materials, it can be seen in **Figure 3.10G** that all of them exhibit negative values, in the range of – 30 to – 40 mV. This tendency is similar to the one observed in the smaller spheres.

Au nanorods show two different diameters as a consequence of their double orientation (axial or longitudinal), the PDI of these materials is too high for the same reason (**Figure 3.10J**). For the longitudinal diameters, **Figure 3.10H**, NG9, 10 and 11 (based on p-acrylamide, p-vinylimidazole and p-DMAPS respectively) have reported 84, 82 and 81 nm respectively. These three values are bigger than 77 nm which has been reported for the Au nanorods grafted with linear PEG. As was happening with the big spheres, the p-NIPAM NG has reported a smaller diameter than the material with linear PEG. For this case, the hydrodynamic diameter is 69 (25 °C) and 66 (40 °C). The conclusion is similar to the previous case. The thermoresponsive behaviour of the p-NIPAM is correct and the smaller value could be a consequence of the PEG contraction while it is being polymerized with NIPAM. Nevertheless, in the axial diameters (**Figure 3.10I**), the p-NIPAM NG12 show the biggest Z-average among all the materials. This is irrefutable proof of the presence of the NG around the Au nanorods.

The surface charges of the Au nanorods (**Figure 3.10K**) are -28, -20, -20 and -26 mV for NG 9 – 12 respectively. Even though all the surfaces are negative, they are less negative than the spheres. It is expected that this will play an important role in their interaction with biological fluids, as it will be explained in detail later.

Finally, the Au nanostars also show a tendency with bigger Z-average diameters (**Figure 3.10L**), which indicates the presence of the NGs. The thermoresponsive behaviour of p-NIPAM (NG16) is also present. The surface charge (**Figure 3.10N**) of these materials is -20 mV for NG13 (p-acrylamide), -19 mV for NG14 (p-vinylimidazole), -24 mV for NG15 (p-DMAPS) and -30 mV for NG16 (p-NIPAM). In other words, all these NGs have a negative surface charge.

It can be concluded that the negative values of the Z-potential observed for all the systems are probably influenced by the high amount of PEG that is bonded to the surface of the NPs. However, in many cases, when this PEG is polymerized with other monomers (e.g., vinylimidazole), the average surface charge becomes more positive.

3.3.2.3 Gel permeation chromatography as another proof of the presence of the NG shell protection around AuNPs

Size-exclusion gel permeation chromatography (GPC) has been developed to separate and purified molecules with different MW.^[39] Besides, polymers can interact with the column and change their retention time in function of their ending functional groups. Hence, this methodology has been applied to NG 1 – 16 and compared with the same characterization applied to AuNPs grafted with linear PEG. The objective is to obtain slightly different retention times as another proof of the presence of the thin NG shell around the AuNPs. To guarantee that any shift in the gaussian peaks corresponds to the presence of a NG shell, all the samples have been diluted to the same concentration. **Figure 3.11** shows the obtained data.

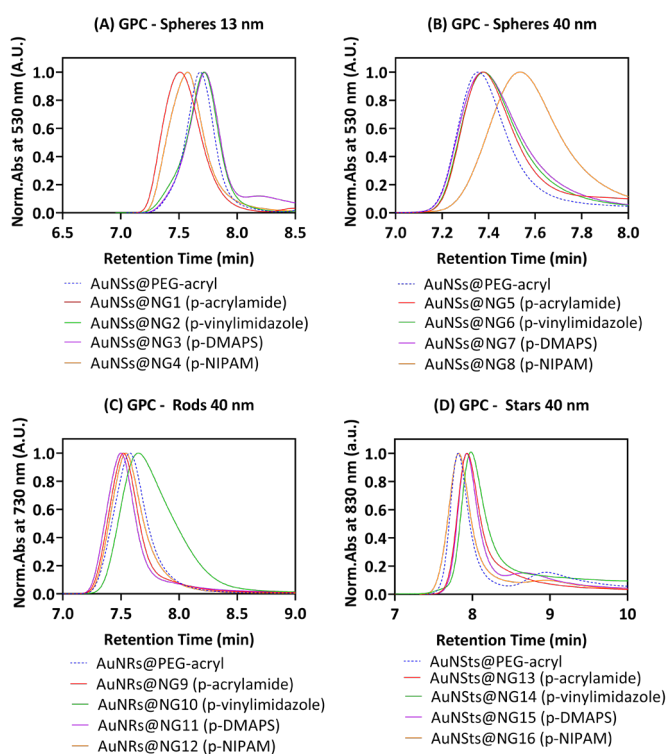


Figure 3.11. GPC chromatographs, all of them have been measured at the mentioned wavelength with confidence interval of 100 nm. (A) Au nanospheres 13 nm. (B) Au nanospheres 40 nm. (C) Au nanorods 40 nm. (D) Au nanostars 40 nm.

As can be seen in **Figure 3.11**, all the gaussian peaks from NG 1 – 16 are sifted in comparison with the corresponding AuNPs grafted with linear PEG. The column used for the separation of the compounds is the OHPak SB-

806MHQ shodex column. It is made of polyhydroxy methacrylate, which makes it perfect to separate water-soluble polymers. The elution has taken place in ultra-pure water.

In the case of 13 nm Au nanospheres (**Figure 3.11A**), NGs 1 and 4 elute before the spheres that are grafted with PEG-acryl. One might mention that in GPC chromatography, higher molecular weight molecules elute before. Therefore, it makes sense that both of these NGs appeared before in the chromatogram. Moreover, p-acrylamide and p-NIPAM have similar chemical structures. In contrast, NG 2 and NG3 (p-vinylimidazole and p-DMAPS, respectively) are a little bit more retained in the column than the control with linear PEG-acryl. The explanation for this behaviour is their chemical structures. Vinylimidazole contains a nitrogenated cycle with vinyl groups. This polymer is the most hydrophobic among all of them. Therefore, probably it is interacting more with the column. In the case of p-DMAPS, it is a zwitterionic polymer. The charges and the positively charged group could interact with the column as well.

In the case of the 40 nm spheres, **Figure 3.11B**, the bigger surface-to-volume relation, in comparison with the small spheres, implies that there is more polymer amount per NG. Therefore, the interactions with the GPC column are also intensified. The consequence is that the NGs are more retained in the column and they elute later. Nevertheless, the most retained one is the thermoresponsive p-NIPAM NG (NG8). Considering that the column temperature is 25 °C, this NG would be expected to swell during the GPC characterization, which may explain the higher retention.

The GPC chromatograms for Au nanorods, **Figure 3.11C**. In this case, NGs 9, 11 and 12 (p-acrylamide, p-DMAPS and p-NIPAM respectively) are eluted before the rods that are grafted with linear PEG-acryl. This result matches with the increment on the MW. In the plot, it can be seen that the NG10 (p-vinylimidazole) is more retained than the others. Hence, it can be concluded that the nitrogenated cycles with vinyl that is forming this polymer increments notably its hydrophobicity, which ends in a major interaction with the column.

The last case of study is Au nanostars, **Figure 3.11D**, here all the NGs are more retained than the control with linear PEG-acryl. In other words, the interaction between these materials with the GPC column is stronger for all the cases. Nevertheless, NG14, based on vinylimidazole is also eluting the last one, which reinforces the previous results and conclusions. The shape of this anisotropic Au NPs is a “sphere” where peaks have been grown around. This

increments notably the surface area that can be polymerized, increasing the amount of polymer per NG. The results obtained here are quite similar to the 40 nm spheres, and the shape is quite similar as well. Therefore, it is not a surprise to observe longer elution times for the NGs than for the particles with linear PEG-acryl.

In general, it can be concluded that all the NGs show elution times shifted from their corresponding controls (surface grafted with PEG-acryl). Therefore, these results are an irrefutable proof indicating that the polymerization of the NGs around the Au has been a success.

3.3.2.4 Transmission electron microscopy (TEM)

The methodology reported in this chapter has allowed the preparation of very thin mantle NGs that can act as a shell of the AuNPs. Due to the very low polymeric density achieved on the prepared NGs, obtaining a good result in electron microscopy has been very challenging. **Figures 3.12** show TEM pictures corresponding to the 13 nm Au nanospheres materials, obtained with a TITAN high-resolution TEM microscope.

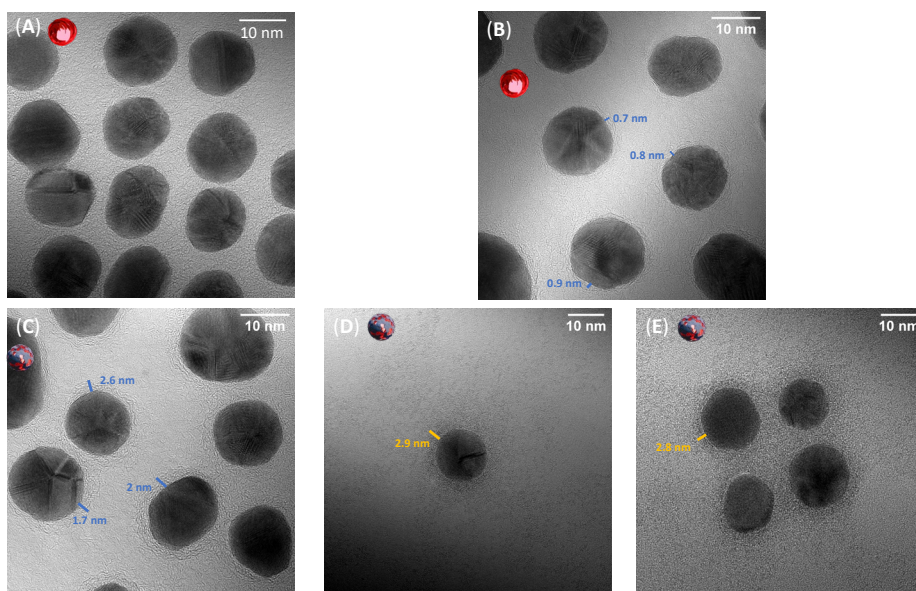


Figure 3.12. TEM images of 13 nm Au nanospheres. (A, B) Au nanospheres grafted with PEG_{5k}-acryl. (C) Au nanospheres covered with a thin mantle NG shell. (D, E) Au nanospheres with thin mantle NG shell, samples stained.

Figure 3.12 represents the TEM pictures obtained at high-resolution TEM microscopy for the quasi-sphere AuNPs, which exhibit a narrow distribution with an average diameter of 14 nm. The graphical design of each material is also accompanying each picture to facilitate its understanding. The material that belongs to **Figures 3.12 A** and **B**, is the 13 nm spheres grafted with linear PEG_{5k}-acryl. It can be observed (particularly in picture B) a very thin layer of around 0.7 – 0.9 nm, which belongs to the linear PEG that is attached to the particles. This observation has been previously reported for other molecules with similar sizes.^[40] After the preparation of the thin NGs around the AuNSs (**Figures 3.12 C, D** and **E**) it can be observed a layer of around 2 – 3 nm, chemically cross-linked, that is indicating the presence of the NG. Thanks to these TEM pictures, it can be corroborated that the formed NG is very thin, observed with (**Figures 3.12D** and **E**) and without (**Figure 3.12C**) staining the samples. As all the NGs prepared with the other polymers look equal to the microscope. Therefore, it is only shown the one obtained with p-acrylamide.

The following **Figure 3.13**, shows the TEM images obtained for the 40 nm Au nanospheres materials.

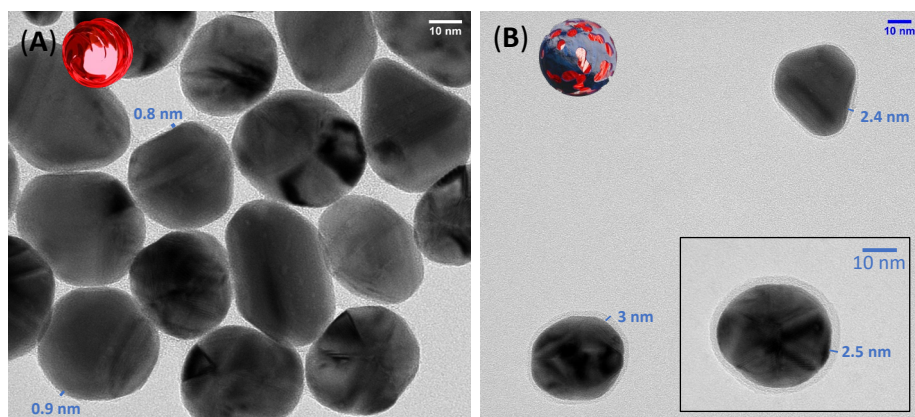


Figure 3.13. TEM images of 40 nm Au nanospheres. (A) Au nanospheres grafted with PEG_{5k}-acryl. (B) Au nanospheres covered with a thin mantle NG shell.

Similar results have been obtained for the case of 40 nm Au nanospheres. **Figure 3.13A** show Au nanospheres grafted with PEG_{5k}-acryl. As was happening in the previous case, using a very powerful TEM microscope, it is possible to observe a thin layer of linear PEG of around 0.8 – 0.9 nm. Nevertheless, when the NGs are being created around the particles, it can be seen very clear (**Figure 3.13 B**). Thanks to the increment in the size of the AuNPs, now it is very easy to observe a thin NG of 2 – 3 nm around the particles. The pictures shown here correspond to the thermoresponsive NG

based on p-NIPAM. Similar results have been observed with the other polymers.

The next **Figure 3.14** shows TEM images obtained from the preparation of Au nanorods protected with thin NGs shell and its control with linear PEG_{5k}-acryl.

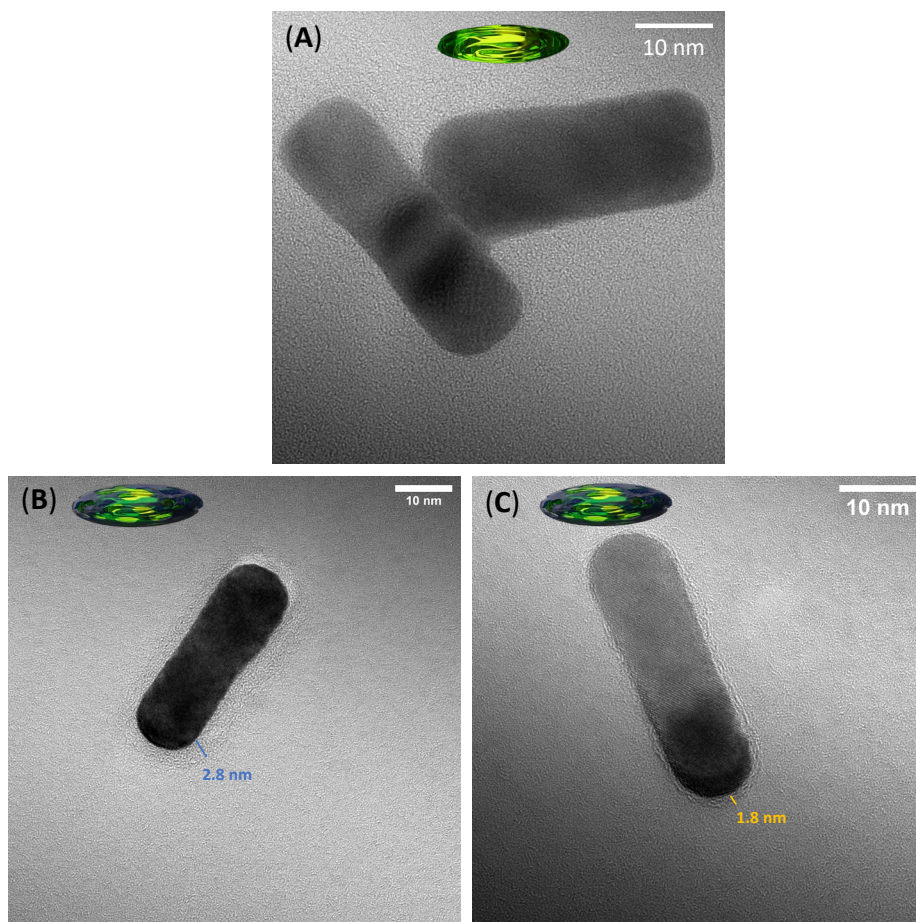


Figure 3.14. TEM images of 40 nm Au nanorods. (A) Au nanorods grafted with PEG_{5k}-acryl. (B, C) Au nanorods covered with thin mantle NG shell.

In the case of the 40 nm Au nanorods, it was not possible to observe clearly the linear PEG (**Figures 3.14 A**). Nevertheless, the NG around with a thickness between 1.6 – 3 nm can be seen (**Figures 3.14 B and C**). Furthermore, these NGs adopt the shape of the nanorod, which maintains its integrity, size and shape more optimally than spherical NGs containing rods previously reported in the literature.^{[41][42]}

The last shape of AuNPs analyzed in this work is shown in **Figure 3.15**, which correspond to Au nanostars.

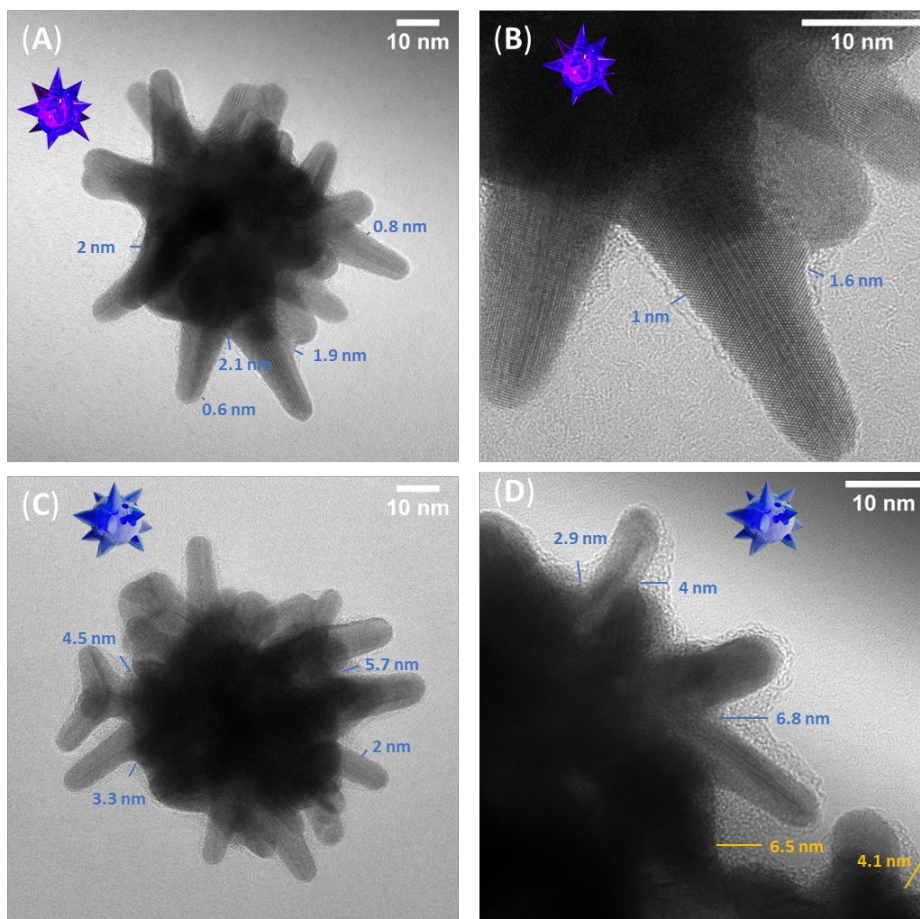


Figure 3.15. TEM images of 40 nm Au nanostars. (A, B) Au nanostars grafted with PEG_{5k}-acryl. (C, D) Au nanostars covered with thin mantle NG shell.

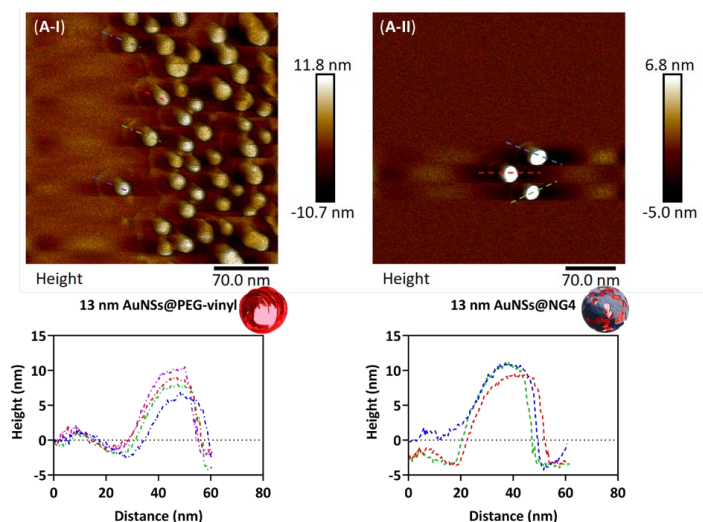
In the case of the 40 nm Au nanostars, it can be seen the linear PEG_{5k}-acryl for the grafted materials (**Figures 3.15 A and B**). It can be observed 0.6 – 1 nm of PEG shell that grows until 2 nm at the junctions of the star’s peaks. When the thin NG shell is created encapsulating a single Au nanostar inside it (**Figures 3.15 C and D**), the polymeric thickness shell is around 2 nm in the peaks and 4 – 6 nm in the junctions of the peaks. Similar to the case with rods, many reports have prepared NGs to protect Au nanostars, but with spherical shape.^[43] However, in the materials here reported, the NG is adapting its shape to the star. This guarantees the maintenance of the star shape, its original size and good optical properties as the NG is quite thin.

From the TEM pictures shown in **Figures 3.12 – 3.15**, it can be concluded that the desired thin NGs preserving the size and shape of the AuNPs, for isotropic and anisotropic particles, have been achieved. The optimized technology has demonstrated its potential to polymerize the NG around the inorganic NP in a few hours and in a water solvent, which is optimal for biomedicine applications. In addition, this technology represents a significant improvement over the current NG protocols for the protection of inorganic NPs.

3.3.2.5 Atomic force microscopy (AFM)

AFM in peak force mode was used to analyse the mechanical properties of the NPs. Some studies have used this microscope and mode to obtain some structural information like deformation, modulus elasticity, etc.^[44] Here, this technology has been applied to some Au-based NGs and compared with their counterpart version stabilized with lineal PEG-acryl. Several mechanical properties have been compared between systems, measured one after the other to guarantee that the cantilever has been used with the same calibration and that the equipment is being used under the same voltage parameters and with the same tip.

13 nm Au nanospheres grafted with linear PEG_{5k}-acryl and encapsulated into p-NIPAM thin NG (NG4) have been analyzed at the AFM to determine how much the NG could affect the mechanical properties of the material at the nanoscale. **Figure 3.16** show the obtained data for height, adhesion and DMT modulus.



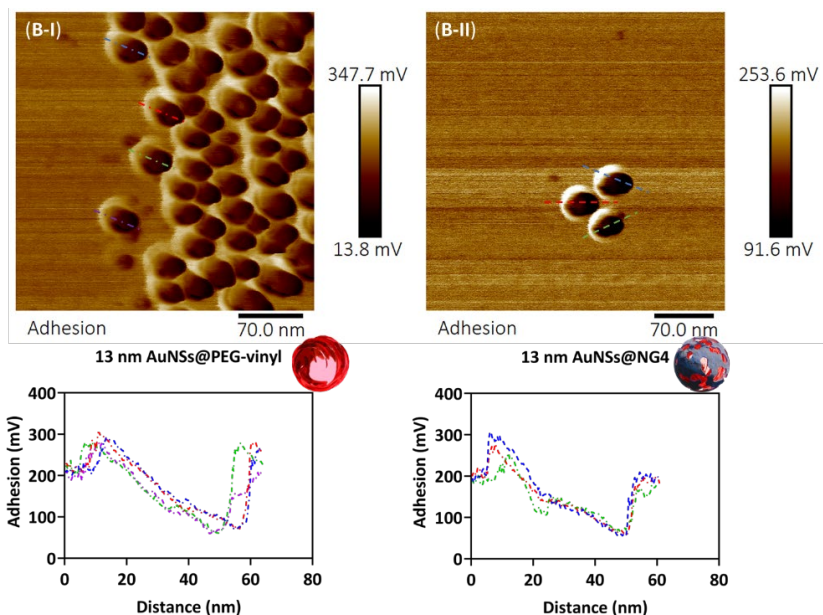


Figure 3.16. AFM images and data obtained from their posterior analysis of 13 nm Au nanospheres. (A-I) Height AuNPs grafted with PEG-acryl. (A-II) Height AuNPs encapsulated inside NG4. (B-I) Adhesion AuNPs grafted with PEG-acryl. (B-II) Adhesion AuNPs encapsulated inside NG4.

It has to be considered that the materials compared in **Figure 3.16 (I vs II)** only differ in the creation of a thin NG shell that increases the total thickness by 1 – 3 nm. Therefore, the differences found in the mechanical properties are quite subtle. Nevertheless, they are sufficient to, together with the previously shown characterization, reveal the presence of the thin NGs. In **Figure 3.16 A** is shown the height, which is the most sensitive one. As it can be appreciated in the plot, the NG4 has a wider height vs distance than the material with linear PEG. This can be interpreted as in the case of the NGs, the tip can penetrate deeper during more distance. In the case of the particles stabilized with PEG, the distance analyzed is 28 – 30 nm (in the four samples analyzed). Besides, it can be observed that now the curve is narrower. In the case of the NG, the curve is wider and with higher height. For the three analyzed NPs, the measured distance is 30 – 33 nm.

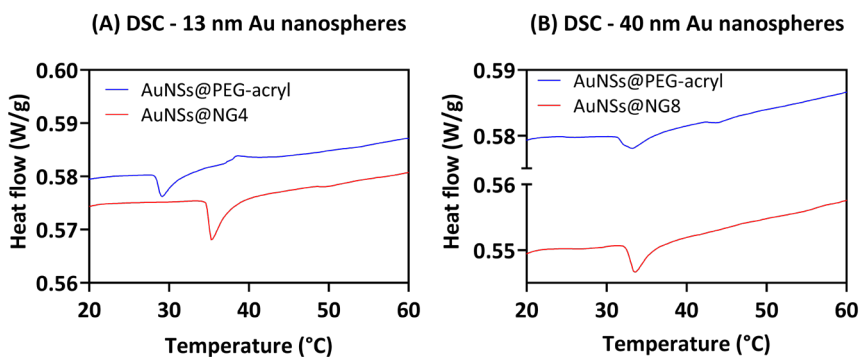
In the adhesion, **Figure 3.16 B**, it can be appreciated that the NGs (**II**) are orientated, as a consequence of their adhesion to the tip. Hence, the plot shows higher adhesion during the first 20 nm distance and in the last 10 nm the adhesion cannot achieve the same value. Also, in the AFM picture, it can be observed a lighter area that corresponds with an accumulation of the NGs that have been attached to the tip. In contrast, the particles with linear PEG

show a similar value of adhesion at the two ends of the NP, indicating a better distribution of the linear polymer. Besides, the non-stick capacity from PEG also reduces the attraction between these materials with the AFM tip.

It can be concluded that these results obtained from the mechanical properties, measured by AFM, have proved the existence of the NG around the AuNPs.

3.3.2.6 Differential scanning calorimetry (DSC)

Differential scanning calorimetry (DSC) is a technique in which the heat required to increase the temperature of a sample is determined by the function of the temperature. In the case of AuNPs, this technique allows a better understanding of their thermodynamic parameters when they are combined with several polymers. For example, p-NIPAM has a reported LCST at 33 – 34 °C measured by DSC.^[45] Nevertheless, many reports have demonstrated that this polymer increases its transition temperature in presence of AuNPs. Besides, it also changes in function of the concentration and shape of the AuNPs.^[46] Conversely, non-thermoresponsive polymers, also exhibit abrupt peaks at a certain temperature as a consequence of polymer chains from their coil form to globular one. This is the case of PEG, in which the melting point differs in function of its MW. For 3k – 4k PEG, it has been described the presence of a DSC peak in the range of 33 – 34 °C.^[47] DSC heating curves of AuNPs modified with linear PEG and encapsulated inside p-NIPAM NGs are reported in **Figure 3.17** for nanospheres, nanorods and nanostars. **Table 3.3** show the most relevant information obtained from the DSC heating curves.



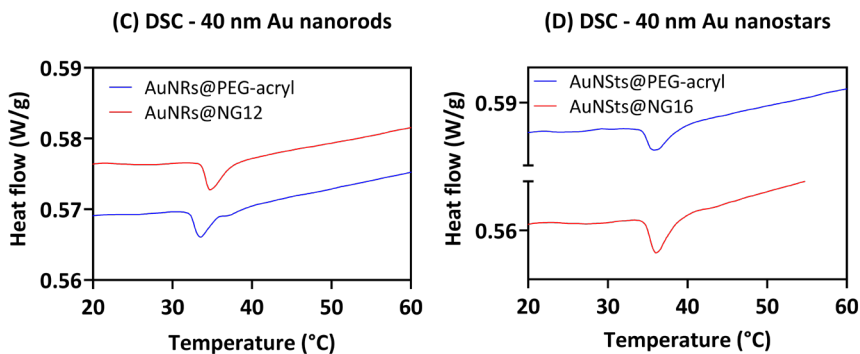




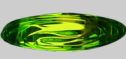
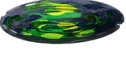




Figure 3.17. DSC heating curves of AuNPs grafted with PEG (blue) and encapsulated inside of a p-NIPAM thin NG (red). (A) 13 nm Au nanospheres. (B) 40 nm Au nanospheres. (C) 40 nm Au nanorods. (D) 40 nm Au nanostars.

Table 3.3. Peak of temperature corresponding to the heat flow and enthalpy of crystallisation for each AuNPs material. Data obtained from the DSC heating curves shown in Figure 3.17.

Graphical design	Sample Code	Sample composition	Peak (°C)	Enthalpy of crystallisation (mJ/g) [Normalized]
	AuNSs@PEG	Au Nanospheres 13 nm @PEG-acryl	29.14	-48.68
	AuNSs@NG 4	Au Nanospheres 13nm @p-NIPAM	35.28	-87.43
	AuNSs@PEG	Au Nanospheres 40 nm @PEG-acryl	33.17	-31.37
	AuNSs@NG 8	Au Nanospheres 40nm @p-NIPAM	33.49	-58.89
	AuNRs@PEG	Au Nanospheres 40 nm @PEG-acryl	33.49	-57.71
	AuNRs@NG 12	Au Nanorods 40 nm @p-NIPAM	34.64	-50.04
	AuNSts@PEG	Au Nanospheres 40 nm @PEG-acryl	35.96	-77.11
	AuNSts@NG 16	Au Nanostars 40 nm @p-NIPAM	35.98	-58.80

The AuNPs prepared for this study have their surface grafted with linear PEG_{5k}. From the data shown in **Figure 3.17** and **Table 3.3**, it can be observed that the peak corresponding to the Au nanospheres (13 and 40), nanorods and nanostars shifts to red when the p-NIPAM is co-polymerized with PEG. The smallest AuNPs, 13 nm spheres, are the ones that report bigger differences. When they are only grafted with PEG, the DSC peak appears at 29 °C with an enthalpy of crystallisation of -48 mJ/g. After the encapsulation of the spheres into the p-NIPAM NG, the transition temperature increases to 35 °C and the enthalpy grows to -87 mJ/g. The negative values of the enthalpies indicate an exothermic process. Therefore, it is expected that the NG will shrink at around 35 °C, which is 3 °C higher than previously reported NGs.^[48] Hence, this novel thin NG containing small Au nanospheres could be very promising for biomedical applications, as the transition temperatures obtained are close to the human body ones. In the end, this can enhance their penetrability through many physiological barriers thanks to the shrinking size of the NGs.

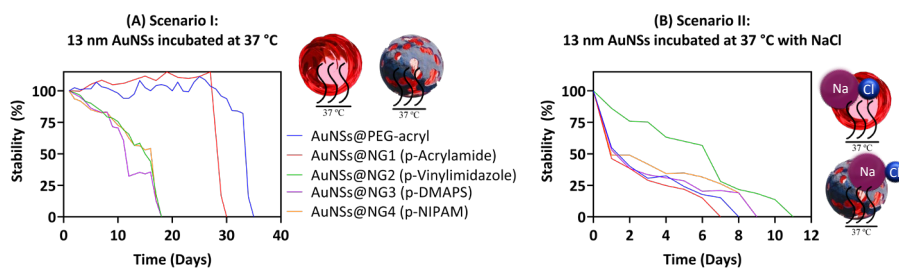
Bigger Au nanospheres have only shifted the DSC peak a few tenths of degrees centigrade. However, the enthalpy of crystallisation has changed from -31 to -58 mJ/g which brings out the presence of the p-NIPAM NG. It can be hypothesized that the big surface area allows the location of more amount of PEG, which increases the enthalpy net value already in comparison with the smaller AuNPs.

Au anisotropic NPs (rods and stars) have reported fewer negative enthalpies than their corresponding materials with linear PEG. Au nanorods, with a peak shifted from 33.49 to 34.64 °C, have reported an enthalpy of -57 mJ/g for the materials grafted with PEG and -50 mJ/g for the rods encapsulated into the p-NIPAM NG. As it was happening with the spheres, when the p-NIPAM is co-polymerized with the PEG the transition temperature increase. Nevertheless, for this material, the process is less exothermic in comparison with the rods grafted only with PEG. Finally, in the case of the Au nanostars, the enthalpy 20 mJ/g is less exothermic when the p-NIPAM NG is absorbing the AuNPs (it changes from -77 to -58 mJ/g). However, the peak of the DSC does not shift, being 35.96 °C when the particles are covered with PEG and 35.98 °C when they are encapsulated into the NG. Nevertheless, the increment in enthalpy is further irrefutable evidence of the presence of the thin mantle NGs.

3.3.3 A comprehensive study of the interactions between AuNPs and their biological surroundings

3.3.3.1 Evolution of the gold-based materials stabilities in presence of salts and proteins at the normal body temperature.

The interaction between inorganic NPs and biological fluids has been one of the main points of interest over the last few years. As was discussed in Chapter I, when a synthetic identity gets into contact with biological fluids, the biomolecules start interacting with them, which results in a lack of stability of the synthetic identity. Besides, inorganic NPs use to interact with proteins and physiological saline in such a way that they end up aggregating.^[49] Hence, novel methodologies are emerging daily to protect inorganic NPs and keep improving their stability so they can complete their therapeutic goal. To quantify the stability of the Au-based materials summarized in this chapter, AuNPs have been exposed to four scenarios and their plasmonic bands have been quantified every 24 h. In the first one (I), aqueous dispersions of the materials have been incubated at 37 °C to determine their maximum stability at the normal body temperature. Then, in a second scenario (II) the materials have been incubated at 37 °C in NaCl 2 M (ratio 1:1). Following, in a third scenario (III) the materials have been incubated at 37 °C in PBS 10 mM (ratio 1:1). Finally, in the fourth scenario, the AuNPs have been incubated at 37 °C together with BSA (2 mg/mL in PBS 10 mM) at a ratio of 1:1. The UV-VIS spectra evolution can be found in **Annex I – IV**. The absorption peaks have been followed to determine the AuNPs stability evolution along the time. **Figure 3.18** shows the obtained results for 13 nm AuNPs spheres.



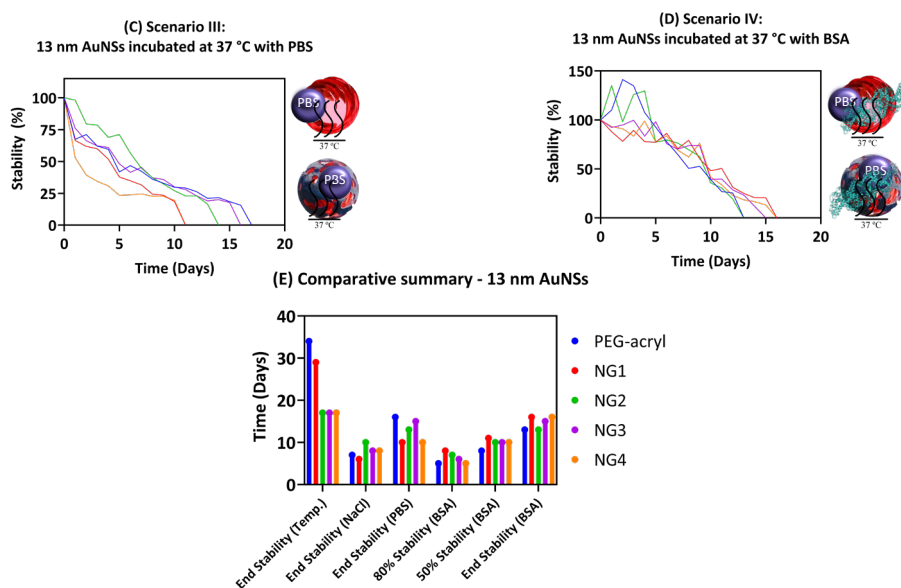


Figure 3.18. Stability evolution along the time for 13 nm Au nanospheres. (A) Particles incubated at 37 °C. (B) Particles incubated at 37 °C in presence of NaCl 2M. (C) Particles incubated at 37 °C in presence of PBS 10 mM. (D) Particles incubated at 37 °C in presence of BSA (2 mg/mL in PBS 10 mM). (E) Comparative summary between materials.

As can be seen in **Figure 3.18A**, testing the thermal stability at normal body temperature (37 °C) of AuNPs has been the first approach to quantify their firmness for biomedical applications. The evolution of the plasmon band peak (at 520 nm) has been followed every 24 h to track the stability of the materials. As can be observed in the comparative summary (**Figure 3.18 E**), the nanospheres grafted with PEG-acryl are the most stable ones, followed by NG1 (based on p-acrylamide). NGs 2, 3 and 4 (based on p-vinylimidazole, p-DMAPS and p-NIPAM, respectively) have demonstrated similar tolerance to the temperature with stabilities up to 17 days. However, when the NPs are exposed to biological media, like salts or proteins, the NGs protection increases significantly the overall systems' stability. For instance, it has been previously reported that a very high concentration of NaCl produces an aggregation of AuNPs.^[50] As can be observed in **Figure 3.18 B** and **E**, NGs 2, 3 and (based on p-vinylimidazole, p-DMAPS and p-NIPAM) have improved the stability of Au nanospheres in presence of NaCl. It is worth it to highlight that p-vinylimidazole-based NG has demonstrated robust stability with around 30% more stability than the rest of the materials. As this polymer has a certain degree of hydrophobicity, it can be expected that it is repelling the interaction

with salts. Conversely, in presence of PBS 10 mM, all the materials have reported better stabilities than the ones observed with NaCl. Probably, as the concentration of the PBS is lower, the number of interactions between salts and AuNPs is also lower. It is remarkable that even though the total stability (**Figure 3.18 E**) of PEG-acyl-grafted AuNPs is higher in comparison with the other materials. NG2, based on p-vinylimidazole, (**Figure 3.18 C**) is the one that has demonstrated better stabilities during the first 10 days. That is, the versatility of p-vinylimidazole to repeal interactions with salts is revealed.

Finally, **Figures 3.18 D** and **E** show the benefit of encapsulating the AuNPs in NGs to increase their stability in presence of proteins. These biomolecules often create a corona layer (PC) around the AuNPs, which can reduce the gold particles' stability. The influence of PC on AuNPs has been widely studied in many systems and under different conditions. It has been reported that the large surface-to-volume ratio of NPs is ideal for protein binding. For instance, Chakrabarti et al. analyzed the stability of Au nanospheres and nanorods in presence of different concentrations of BSA.^[51] They observed that the visible absorption peak of rods (located around 520 nm) decreased while increasing the concentration of BSA as a consequence of the adsorption between the Au and the protein. Also, when the rods (grafted with CTAB ligand) were exposed to 50 μ M of BSA, both peaks at VIS and NIR region disappeared after 4 h, which indicates the destruction of the particles as a consequence of their strong binding with the protein. They found a similar tendency in Au nanospheres, where their binding forces with proteins are even stronger. In another study, they analyzed how different concentrations of BSA induce aggregation on AuNPs.^[52] From their study, it can be concluded that a small concentration of protein (0.0005 – 0.001 mg/mL) induces aggregation between particles. In contrast, a high concentration of BSA (> 0.02 mg/mL) creates a corona around the AuNPs that increase the interparticle distance. This corona does not shift so much the absorbance peak but it decreases the lifetime of the particles. This last effect is the one investigated in this section. In fact, it can be observed that the stability of the spheres has been improved when they are encapsulated within NGs 1 – 4 in comparison with the PEG-acyl grafted material. During the first 5 days of the experiment, it can be seen in the plot shown in **Figure 3.18 D** that the percentage of stability, for the materials AuNPs grafted with PEG-acyl and NG2 (based on p-vinylimidazole), is higher than 100%. The reason for this is that a protein corona is being created around these materials increasing the absorbance. In contrast, NGs 1, 3 and 4 (based on p-acrylamide, p-DMAPS and p-NIPAM, respectively) do not increase the absorbance, which indicates that these materials reduce the protein corona effect. Besides, it can be emphasised that

NG1 (based on p-acrylamide) is the one with the best stability capacity towards protein interactions, as it slows down the aggregation of Au nanospheres. In fact, with this NG, the AuNPs have lost 20% of their stability after 8 days, which means a stability improvement of over 60% more compared to the PEG-acryl-based material. Half of the stability has been lost after 11 days, which suppose a 37% improvement in comparison with the PEG-acryl-based material. This improvement trend is followed by NG2 (based on p-vinylimidazole), NG3 (based on p-DMAPS) and NG4 (based on p-NIPAM).

The same stability experiments have been applied to bigger spheres (40 nm). The results of stability obtained by following the absorbance peak at around 540 nm, are summarized in **Figure 3.19**.

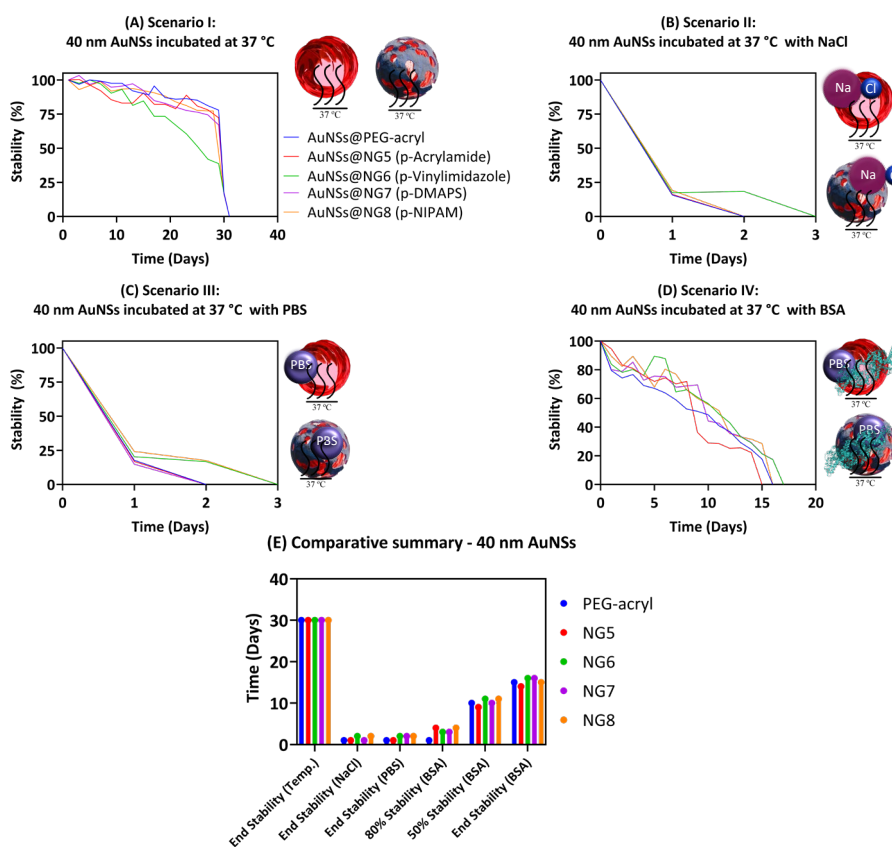
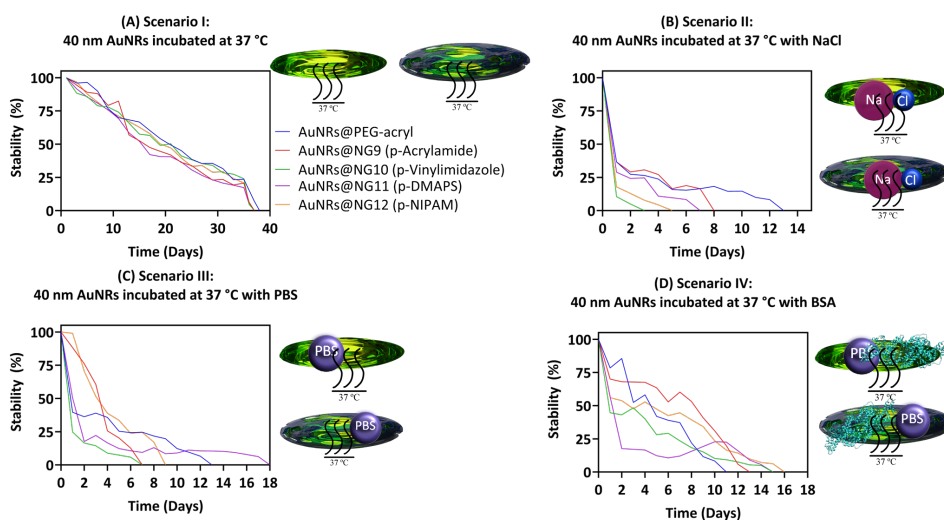


Figure 3.19. Stability evolution along the time for 40 nm Au nanospheres. (A) Particles incubated at 37 °C. (B) Particles incubated at 37 °C in presence of NaCl 2M. (C) Particles incubated at 37 °C in presence of PBS 10 mM. (D) Particles incubated at 37 °C in presence of BSA (2 mg/mL in PBS 10 mM). (E) Comparative summary between materials.

In the case of the bigger spheres, the thermal stability (**Figures 3.19 A and E**) has raised to 30 days, which represents, for the NGs, almost double stability than the ones achieved by the 13 nm spheres. In contrast, the stability of materials when facing biomolecules has been notably reduced in comparison with the smaller nanospheres. Nevertheless, the 40 nm spheres encapsulated within the thin NGs, have demonstrated better stability, in presence of salts and proteins (**Figure 3.19 E**), than the PEG-acryl grafted material. In particular, NG6 (based on p-vinylimidazole) have proved the best stability in presence of NaCl (**Figure 3.19 B**) and PBS (**Figure 3.19 C**) among the rest materials, following a similar tendency than the one observed for 13 nm spheres. In other words, the hydrophobicity of the p-vinylimidazole, reduces the interaction with salts, improving the stability of the AuNPs. Lastly, in the case of the interactions between 40 nm Au nanospheres and BSA (**Figures 3.19 D and E**), the NGs have demonstrated a slightly improve in the stability of the AuNPs along the time. It should be noticed that a big difference has been observed after losing the 20% of their stability, where the NGs have improved the stability by 3 – 4 times more. However, the global stability, until the total aggregation of AuNPs, has been just slightly improved thanks to the presence of the NGs, being NG6 (based on p-vinylimidazole) the one with the best stability.

Similar experiments have been applied to anisotropic AuNPs. **Figure 3.20** summarises the results obtained for Au nanorods after following the peak absorbance at around 730 nm.



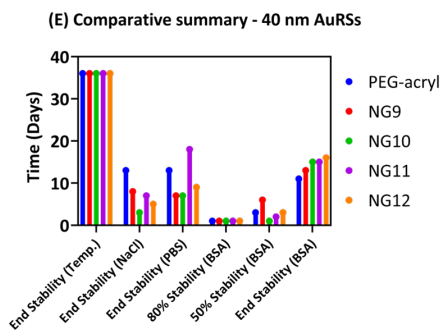


Figure 3.20. Stability evolution along the time for 40 nm Au nanorods. (A) Particles incubated at 37 °C. (B) Particles incubated at 37 °C in presence of NaCl 2M. (C) Particles incubated at 37 °C in presence of PBS 10 mM. (D) Particles incubated at 37 °C in presence of BSA (2 mg/mL in PBS 10 mM). (E) Comparative summary between materials.

As can be observed in **Figure 3.20 A** and **E**, Au nanorods have been the most thermally stable ones. These AuNPs have shown stoutness up to 36 days, which is almost the double of stability than the ones achieved by 13 nm Au nanospheres. One might mention that Au nanorods-based NGs, have not been allowed to increase, remarkably, the steadiness of the systems in presence of salts (**Figures 3.20 B, C** and **E**). However, some promising results have been achieved in the case of Au nanorods encapsulated within p-DMAPS NGs (NG 11), which has reported an increase in their stability to 1.5 times more, in presence of salts, compared to PEG-acryl grafted material. Lastly, similar results have been observed when the nanorods have been in contact with BSA (**Figures 3.20 D** and **E**). At half of their lifetime, NG9 (based on p-acrylamide) has demonstrated an improvement in the AuNPs stability of the double in comparison with the PEG-acryl grafted counterpart. Furthermore, NGs 9 – 12 have proved an improvement in the total stability of the rods, in comparison with the PEG-grafted material. It is important to highlight that the curve shown for NG11 (based on p-DMAPS) shows a recovery into stability after 8 days. As the stability has been obtained by analysing the evolution of the plasmon band, an improvement in the stability percentage means an improvement in the absorption band. This might be attributed to the formation of a BSA corona around this NG after 8 days, which maintains the stability of the material for more days.

Finally, the same fourth scenario has been applied to Au nanostars. **Figure 3.21** shows the stability collected results obtained by following the peak absorbance at 760 – 790 nm.

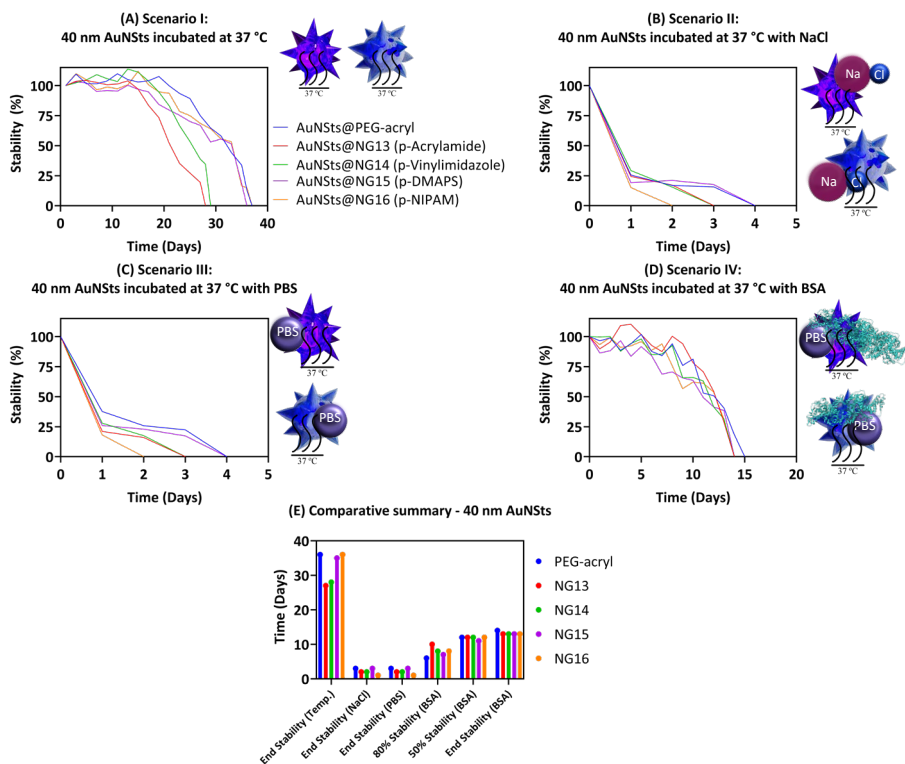
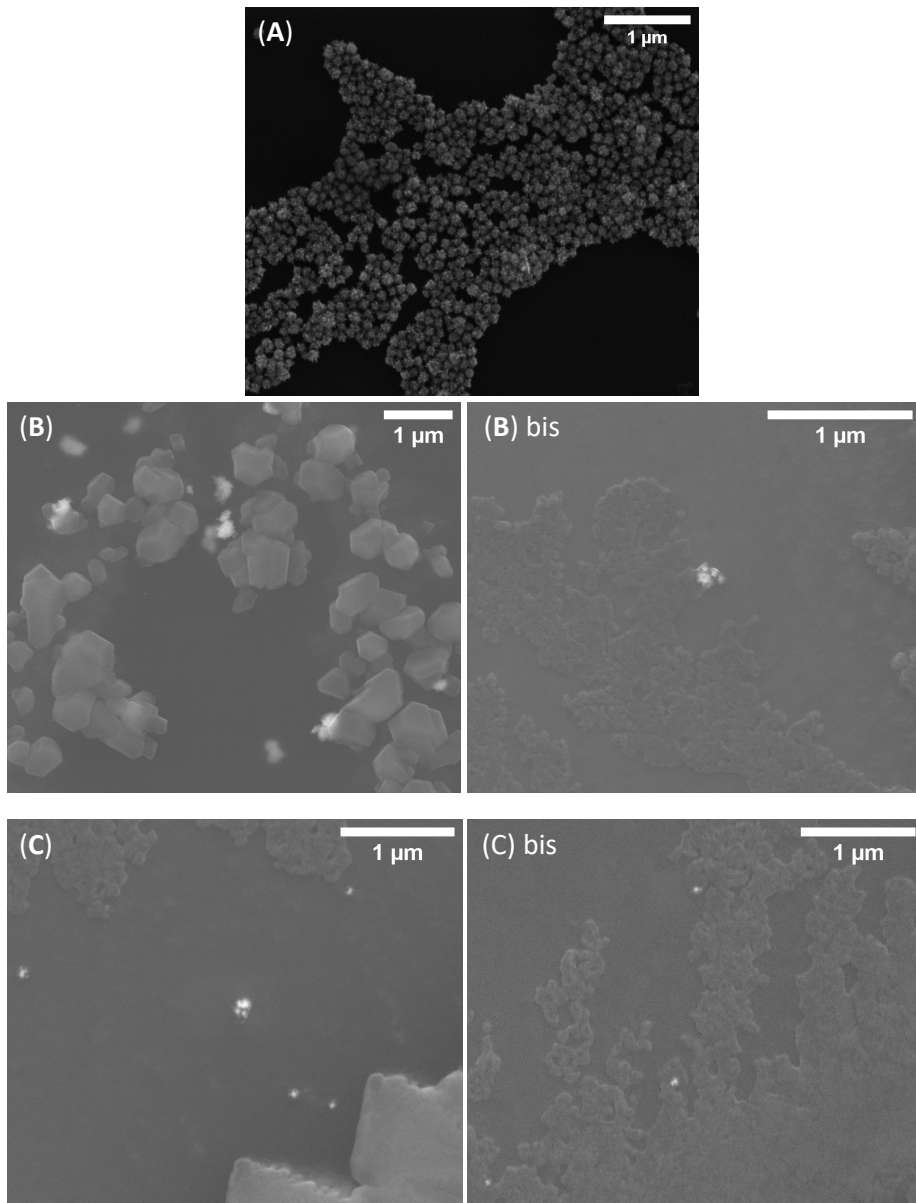


Figure 3.21. Stability evolution along the time for 40 nm Au nanostars. (A) Particles incubated at 37 °C. (B) Particles incubated at 37 °C in presence of NaCl 2M. (C) Particles incubated at 37 °C in presence of PBS 10 mM. (D) Particles incubated at 37 °C in presence of BSA (2 mg/mL in PBS 10 mM). (E) Comparative summary between materials.

The last morphology investigated is the Au nanostars. In this case, improvements in stability of AuNPs, achieved thank to the NGs shells, are observed only in the presence of BSA (**Figures 3.21 A, B and E**). NG13 (based on p-acrylamide) has improved the stability of the stars at 80% of their lifetime in 40% more compared with its PEG-grafted counterpart. Similarly, at 80% of their stability, NG14 and NG16 (based on p-vinylimidazole and p-NIPAM, respectively) have improved the stability by 25% more than the PEG-acryl material. Similarly, NG15 (based on p-DMAPS) in 15%. The tendencies at 50% and 0% of their stabilities are similar for the five materials. Nevertheless, attending to **Figure 3.21D**, it can be observed that NG13 (based on p-acrylamide) has stronger stability than the rest of the materials for the whole experiment, which highlights the great potential of this polymer to stabilize anisotropic AuNPs in presence of biological fluids.

To clarify the aggregation that is happening in the AuNPs, the complete set of nanostars systems (with the same concentration) have been incubated with BSA for 10 days. Then, the resulting materials have been analyzed by SEM (**Figure 3.22**) to observe their morphological changes.



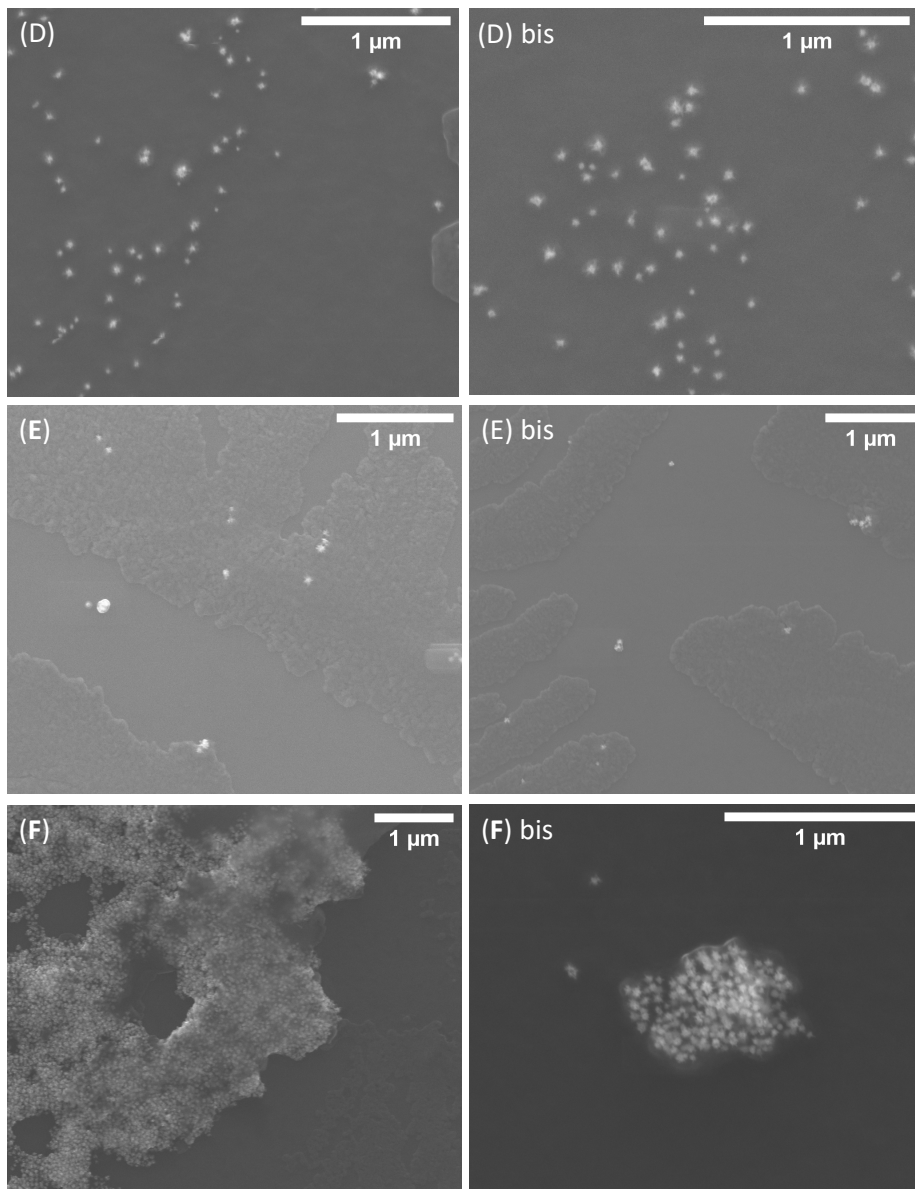


Figure 3.22. SEM pictures of (A) Au nanostars and after 10 days of incubation with BSA (1 mg/mL in PBS) at 37 °C. (B) grafted with PEG-acryl. (C) encapsulated in p-acrylamide NG. (D) encapsulated in p-vinylimidazole NG. (E) encapsulated in p-DMAPS NG. (F) encapsulated in p-NIPAM NG.

Some clear tendencies can be extracted from **Figure 3.22**. In figure **A**, it can be seen the original star-like shape of the NPs as a control. In contrast, in figure **B**, it is easy to observe that the star shape is not present anymore. Particles have aggregated and a deformed shape can be seen in between salts

and proteins. In contrast, figure **D**, which is based on p-vinylimidazole NGs, shows individual stars that maintain their original aspect almost unchanged. Figures **C** and **E** based on p-acrylamide and p-DMAPS NGs respectively show aggregated particles with more spherical aspects than p-vinylimidazole NGs. Therefore, it can be concluded that the stability of the Au nanostars encapsulated inside p-vinylimidazole NGs is the highest. The last material, figure **F**, based on p-NIPAM NGs, show a huge number of stars that maintain their shape but with a big PC that is containing several NPs. So, even though the stability of the AuNPs (in terms of size and shape) is very good, this thermoresponsive NG does not decrease the protein corona effect.

In the results summarized in this section, it can be observed that for all the morphologies and shapes of AuNPs, the materials encapsulated inside the NGs have reported better stabilities in presence of salts and proteins. In particular, NGs-based on p-vinylimidazole have turned out to be one of the most promising materials for the stabilisation of AuNPs in biological fluids. The hydrophobicity of this polymer has reduced the interactions between the material and the biomolecules, rising the stability of the AuNPs. Additionally, p-acrylamide-based NGs have also increased notably the stability of AuNPs, mostly anisotropic ones. Nevertheless, p-vinylimidazole NGs avoid a shift in the plasmon peaks of anisotropic AuNPs. This tendency has been only observed with this polymer, which indicates that even if the stability (in terms of concentration) is lower than the one obtained with p-acrylamide, the particles do not aggregate. In other words, the hydrophobicity of the p-vinylimidazole decreases the interactions with the BSA preserving the integrity of the AuNPs. This behaviour makes the presence of vinylimidazole especially interesting. Considering that the NG of vinylimidazole is also co-polymerized with p-acrylamide, it could be possible to balance the ratio of both polymers to keep increasing the stability of the AuNPs while preserving their integrity.

In summary, it can be concluded that thin NGs developed in this work reduce the binding between AuNPs and BSA, which make them suitable for biomedical applications. In fact, p-vinylimidazole-based NGs have demonstrated by SEM that can keep the original shape of Au nanostars while they are in presence of proteins and salts. Besides, the hydrophobicity of this polymer repels the interactions with biomolecules, which is shown in the plasmon band, that is not shifted. In other words, this polymer remains the most promising one for improving the stability of AuNPs in presence of biological fluids to move towards the next step *In-vitro* and/or *In-vivo*. For the time being, to take a step ahead in the AuNPs interactions with the biological surrounding, in complex systems, the materials have been exposed to mucin

and their behaviour analyzed by rheology. These results are going to be described in detail in the next section; **3.3.3.2**.

3.3.3.2 Interactions between gold-based materials and mucin

Many of the body entry routes (mouth, vagina, eye, stomach, intestine, etc.), followed by NPs, have mucosa layers that act as a physical barrier. NPs need to pass over them to achieve their target place, which supposes the development of complex mechanisms and advance synthetic designs.^[53] Polymers have sorted out the enhancement of mucus penetration. Since PEG became the gold standard for NPs functionalization in biomedicine, it has been used to enhance the mucus penetration of NPs with promising results.^[54] Moreover, AuNPs have been modified to modulate their physicochemical properties to let them penetrate mucin. Some studies have played with their size, surface charge and rigidity to let them penetrate intestinal mucosa.^[55] Non-rigid materials, combined with slightly negatively surface charged NPs, seem to be the key to achieving a moderate interaction with mucin.^[56] However, a good balance between particles stability and mucin interactions remains challenging, as there are not so many studies in the field. In general, the interaction between AuNPs and mucin has been characterized by UV-VIS, following the mucin absorption band, where the mucin increases its absorption indicating the formation of a complex. Then, this interaction has been ratified by fluorescence, observing the quenching of mucin.^[57] In contrast, during the last years, viscometric rheology characterization has emerged to quantify the mucin-polymer strength interactions. The experiment consists on applied a certain force (constant frequency) over the material and evaluating the evolution of the loss and storage modulus along the time.^[58] In the following section, Au-NGs-based materials have been mixed with mucin solution to analyze their interaction with a rheometer by following the evolution of the viscous mixture behaviour.

Commercialized mucin from the porcine stomach has been dispersed in PBS obtaining a mixture of 10 % w/w. According to reported literature, this is the minimum percentage required to measure the viscosity by rheology.^[59] For the experiment, 1 g of this mucin dispersion has been mixed with 100 μL of AuNPs (10^{-9} M for 13 nm spheres, 40 nm rods and 40 nm stars and 10^{-11} M for 40 nm spheres). The resulting products have been analyzed in a rheometer at a constant share strain of 1 Hz and a set temperature of 37 °C. Previously, it has been corroborated that at this constant strain, the moduli are in a linear viscoelastic regime, which means that this force is not affecting the viscous

behaviour of the materials.^[60] Therefore, the interactions observed during the experiment belong to interactions between AuNPs and the mucin. Plotting the moduli G' (storage or elastic modulus) and G'' (loss or viscous modulus) versus time, four different cases can be obtained. **Figure 3.23** shows a schematic of the experiment set-up and the results cases that can be obtained.

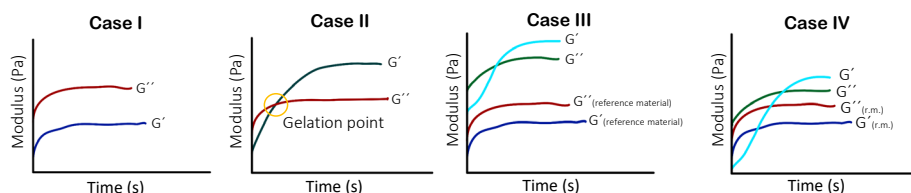


Figure 3.23. Scheme of the four results cases that can be obtained after the measurement.

The four possible cases that can be obtained from the material's measurement in the rheometer are described in **Figure 3.23**. Case I shows the typical behaviour from a viscous material, where it can be observed the G' and G'' moduli. As G'' is above G' , this means that there is no interactions along the time and the viscosity of the sample remains constant. Case II shows the opposite effect. Hereafter certain time, G' is higher than G'' which indicates that the material has changed its viscosity and now it has more solid behaviour than at the beginning of the experiment. The point at which G' and G'' meets is called "gelation point" and it is considered the turning point in which the properties of the material change. In the third case, there are a material with a gelation point and higher G' and G'' moduli than the reference material. Assuming that the reference material is also present in the other material, it can be concluded that the non-reference one has changed the viscosity of the reference (as both moduli are higher). Besides, after the gelation point, the material turns to be more solid. The final case (IV), shows a material with fewer interactions than the reference in the initial times (with a G' modulus very small). But, after a certain time, this material also shows more solid behaviour than the reference. With this explanation in mind, **Figure 3.24** show the obtained results for the 13 nm Au nanospheres. Each NG is shown in an independent plot that contains mucin as reference material and AuNPs grafted with PEG-acryl as comparative material.

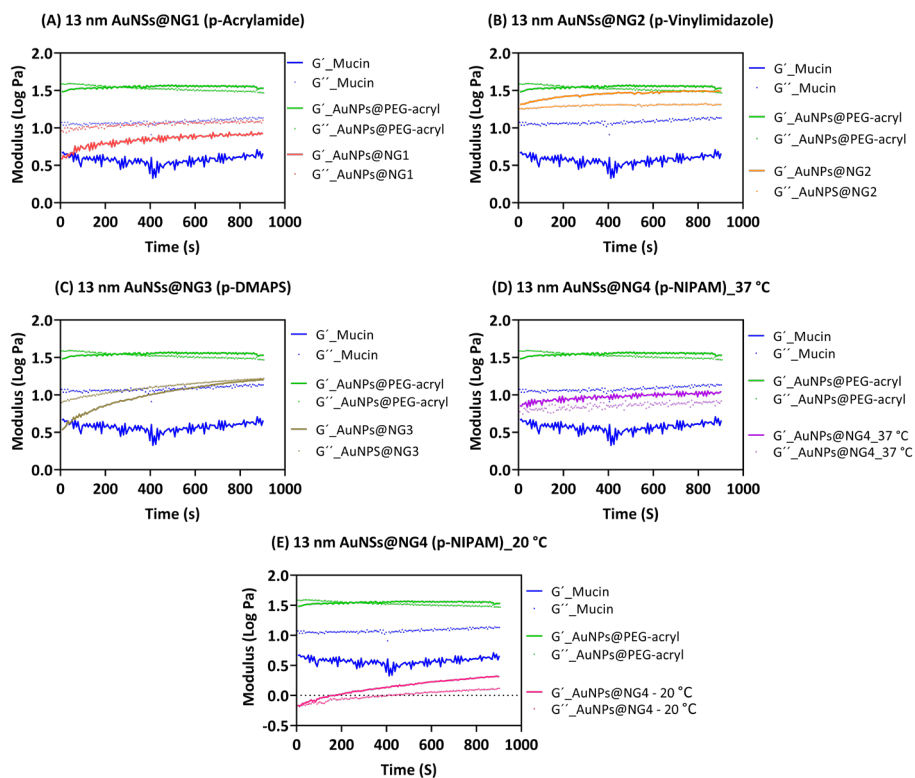
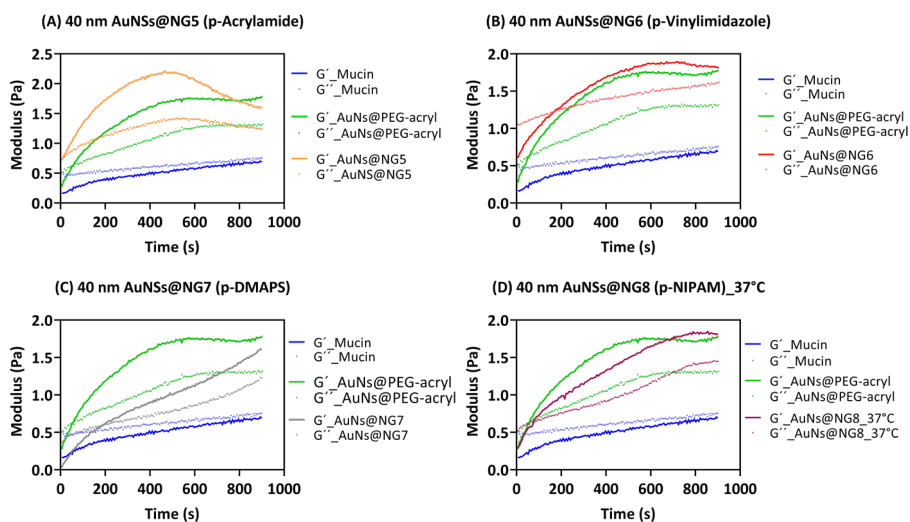


Figure 3.24. Evolution of the G' and G'' modulus along the time for 13 nm Au nanospheres mixed with mucin. In green, AuNPs grafted with linear PEG-acryl. (A) NG1 based on p-Acrylamide. (B) NG2 based on p-vinylimidazole. (C) NG3 based on p-DMAPS. (D) NG4 based on p-NIPAM at 37 °C. (E) NG4 based on p-NIPAM at 20 °C.

From **Figure 3.24** it can be seen that the interactions between the Au-based NGs with the mucin are different in function of the surface charge and hydrophilicity. Nevertheless, all the NGs have lower G' and G'' moduli than the nanospheres grafted with PEG-acryl. Presumably the hydrophobic acryl groups located at the end of the PEG structure are reacting quite strong with the mucin. Plot **A** shows the p-acrylamide NG results. It can be seen in the figure that there is no gelation point, which means that the mucin is not changing its viscosity behaviour in this case. Similar results have been obtained in plot **C**, p-DMAPS NG. In that case, the gelation point is about to happen at the end of the experiment (after 15 min). Probably the zwitterionic behaviour of these polymers makes it interact stronger with the negative charges from the mucin. Which turns slowly the viscoelastic behaviour of the mucin into solid. The NG2, based on p-vinylimidazole (plot **B**), show a G' higher than G'' since $t = 0$ min. This indicates that NG2 interacts very strong with the mucin after mixing both. Then, the behaviour of the mixture is highly solid, similar to the particles

stabilized with PEG-acryl. Finally, the NG4 is a thermoresponsive p-NIPAM NG (plots **D** and **E**). This NG is shrunk at 37 °C and swelled at 20 °C, which is the reason why this one has been measured at two different temperatures. The results reported that even though the gelation point happens at $t = 0$ min, the G' and G'' values are less than half of the obtained with PEG-acryl. Then, it can be concluded that the material is changing the viscoelastic behaviour of the mucin to a more solid one, but less than PEG-acryl. In addition, when the NG is at 20 °C, these two moduli are even smaller, which indicates very low interactions with the mucin. Considering that weak interactions with the mucin could facilitate AuNPs to penetrate the mucus layer, it has been demonstrated that with the NGs is possible to decrease this interaction. Ordering the 13 nm Au nanospheres materials from weak to strong interactions with mucin, it can be found this trend: NG1 (p-acrylamide) < NG3 (p-DMAPS) < NG4 at 20 °C (p-NIPAM) < NG4 at 37 °C (p-NIPAM) < NG2 (p-vinylimidazole) < PEG-acryl.

The same experiments have been performed with 40 nm Au nanospheres, and **Figure 3.25** shows the obtained results.



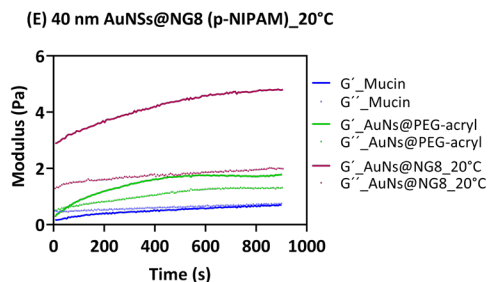


Figure 3.25. Evolution of the G' and G'' modulus along the time for 40 nm Au nanospheres mixed with mucin. In green, AuNPs grafted with linear PEG-acryl. (A) NG5 based on p-Acrylamide. (B) NG6 based on p-vinylimidazole. (C) NG7 based on p-DMAPS. (D) NG8 based on p-NIPAM at 37 °C. (E) NG8 based on p-NIPAM at 20 °C.

For the big spheres (**Figure 3.25**), only NG7 (plot **C**) based on p-DMAPS exhibits less interaction with mucin than the AuNPs grafted with PEG-acryl. In fact, the G' and G'' are lower and the gelation point takes more time to be achieved. Therefore, this material has less interaction with mucin. On the other side, NG5 and NG6 (based on p-acrylamide and p-vinylimidazole respectively) exhibit higher values of moduli than the particles grafted with PEG. In the case of the p-vinylimidazole, the result is the same as the one found for the 13 nm spheres. However, p-acrylamide has reported the opposite effect. It can be hypothesized that the increase in the surface area of the AuNPs increases the amount of polymer in the NG, which in the case of p-acrylamide increases also the interactions with the mucin. Finally, the NG8 (p-NIPAM) now has more size to exhibit better thermoresponsive properties. At 37 °C (plot **D**), the NG is shrunk as it shows fewer values of G' and G'' moduli than the PEG-acryl and the gelation point took some more seconds to be achieved, which indicates lower interactions with mucin. In contrast, at 20 °C (plot **E**) the p-NIPAM NG is swollen and the gelation point is achieved at the very beginning of the experiments. Besides, the G' and G'' moduli are more than one unit higher than the PEG-acryl which indicates very strong interactions with mucin. In summary, the thermoresponsive behaviour of this NG is evidenced, where the one that is swollen at 20 °C shows a greater interaction with the mucin. Therefore, a lower ability to penetrate the mucosa would be expected from the swollen form of the NG. Ordering the 40 nm Au nanospheres materials from weak to strong interactions with mucin, it can be found this trend: NG7 (p-DMAPS) < NG8 at 37 °C (p-NIPAM) < PEG-acryl < NG6 (p-vinylimidazole) < NG5 (p-acrylamide) < NG8 at 20 °C (p-NIPAM).

Figure 3.26 reports the mucin interaction studies achieved by rheology for the Au nanorods.

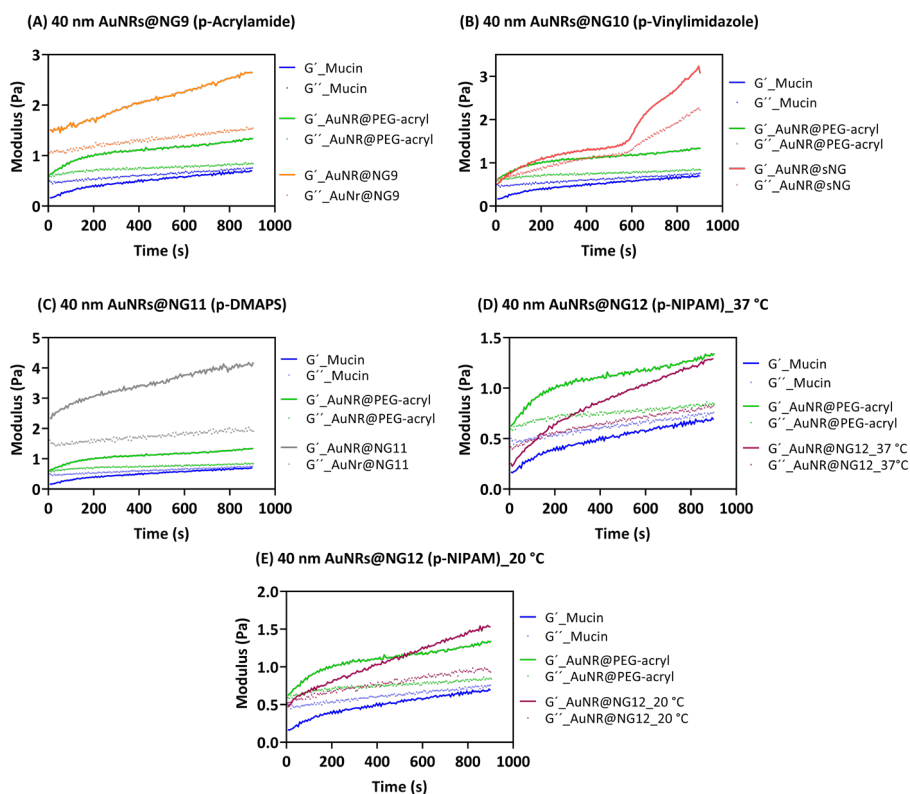


Figure 3.26. Evolution of the G' and G'' modulus along the time for 40 nm Au nanorods mixed with mucin. In green, AuNPs grafted with linear PEG-acryl. (A) NG9 based on p-Acrylamide. (B) NG10 based on p-vinylimidazole. (C) NG11 based on p-DMAPS. (D) NG12 based on p-NIPAM.

Au nanorods are a particular morphology due to their extended form. For this anisotropic AuNPs, NG9 (p-acrylamide), plot **A**, 10 (p-vinylimidazole), plot **B**, and 11 (p-DMAPS), plot **C**, have been reported to interact stronger with the mucin than the rods grafted with PEG-acryl. However, the thermoresponsive NG12, plots **D** and **E**, (p-NIPAM) have shown lower interactions with mucin than the PEG-acryl counterpart at 37 and 20 °C. Nevertheless, at 37 °C the NG is swollen, the interaction is lower than the one observed at 20 °C and the gelation point is achieved after a long time. One might mention that in general 40 nm Au nanorods exhibit bigger moduli than the 40 nm spheres. Hence, it could be expected that rods would attach to the mucosa better than the spheres, and spheres would penetrate the mucosa better than the rods. Ordering the 40 nm Au nanorods materials from weak to strong interactions with mucin would follow the following trend: NG12 at 37

$^{\circ}\text{C}$ (p-NIPAM) < NG12 at 20°C (p-NIPAM) < PEG-acryl < NG10 (p-vinylimidazole) < NG9 (p-acrylamide) \leq NG11 (p-DMAPS).

The interaction between the last morphology, Au nanostars, and the mucin is shown in **Figure 3.27**.

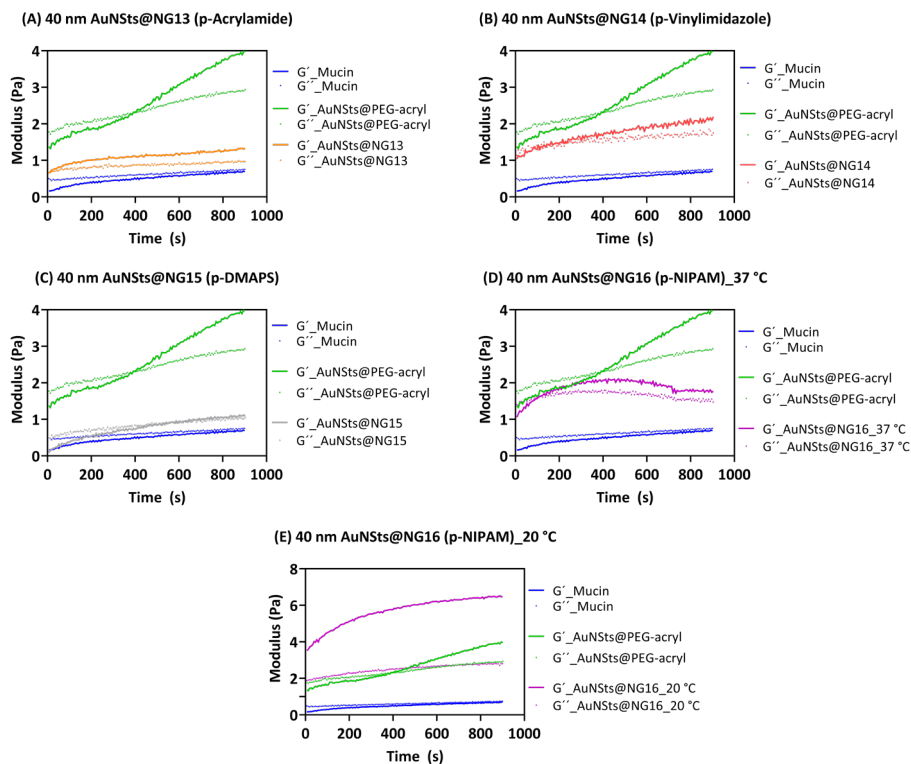


Figure 3.27. Evolution of the G' and G'' modulus along the time for 40 nm Au nanostars mixed with mucin. In green, AuNPs grafted with linear PEG-acryl. (A) NG13 based on p-Acrylamide. (B) NG14 based on p-vinylimidazole. (C) NG15 based on p-DMAPS. (D) NG16 based on p-NIPAM.

The last morphology analyzed in this chapter is the star. These anisotropic AuNPs are more similar to the sphere in size and form than the rods. Here, it has been observed that the Au nanostars encapsulated inside of any NG show less interaction with mucin than the stars grafted with PEG-acryl at 37°C . The NG that has reported less interaction with mucin is NG15, plot C, (p-DMAPS), probably as a consequence of its zwitterionic behaviour. The negative charge of the mucin will interact less with the positive charge of the p-DMAPS as a consequence of the negative charge presented as well in this polymer. Then, the NG13, 14 and 16 have similar interactions. P-Acrylamide NG (NG13, plot A) has the lowest G' and G'' moduli among the three.

However, the gelation point is achieved before NG14 or 16 (p-vinylimidazole and p-NIPAM respectively, plots **B** and **D**). Finally, the thermoresponsive behaviour of the p-NIPAM is demonstrated even more for this morphology. At 20 °C, the NG16 shows higher G' and G'' moduli with gelation point achieved at the very beginning. Ordering the 40 nm Au nanostar materials from weak to strong interactions with mucin would follow the following trend: NG15 (p-DMAPS) < NG13 (p-acrylamide) \leq NG16 at 37 °C (p-NIPAM) \leq NG14 (p-vinylimidazole) < PEG-acryl < NG16 at 20 °C (p-NIPAM).

To facilitate the general overview of the tendencies observed, **Figure 3.28** summarises visually the trends for each AuNPs shape.

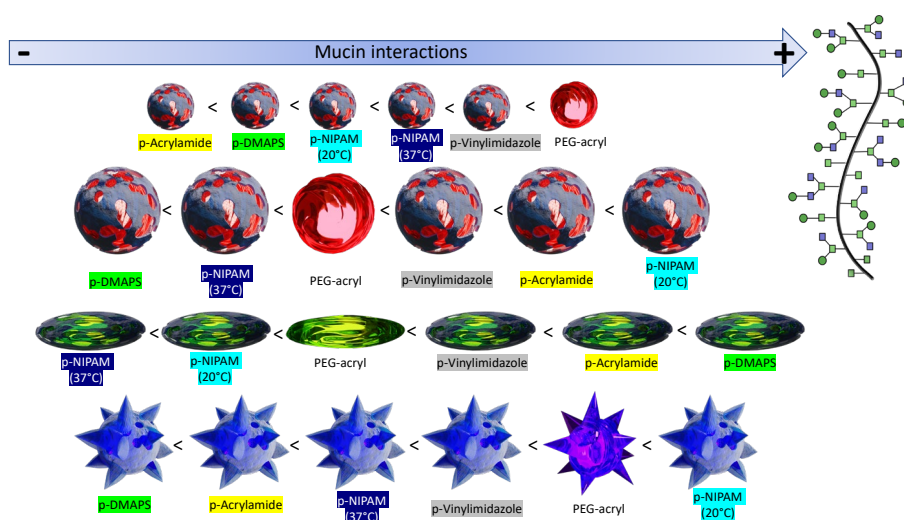


Figure 3.28. Graphical summary showing the mucin interaction tendencies from less (left) to more (right) for 13 nm Au nanospheres, 40 nm Au nanospheres, 40 nm Au nanorods and 40 nm Au nanostars.

As a general tendency, it can be concluded, from **Figure 3.28**, that Au-based p-DMAPS NGs exhibit a lower tendency to interact with mucin as a consequence of its zwitterionic behaviour. In the case of Au nanorods, it can be hypothesized that there is a synthetic issue in the NG11 (based on p-DMAPS), as it cannot be expected such a higher interaction between this material and the mucin. In contrast, p-vinylimidazole-based NGs are the ones that always report stronger interactions with mucin. Probably, the reason for this behaviour is the higher hydrophobicity of this polymer coming from its nitrogenated cyclic group presented in its chemical structure. Finally, the thermoresponsive behaviour is observed in the bigger NPs (40 nm). When the p-NIPAM NG is at 37 °C, the NG is shrunk and the affinity towards mucin is

always lower than the one observed at 20 °C where the NG is swollen. In other words, translating this into a hypothetical real application in biomedicine, p-DMAPS and p-NIPAM would be promising candidates for the preparation of thin NGs to protect AuNPs if the idea is to penetrate a mucin layer. In contrast, if the idea is to prepare a material that can attach the mucin layer, Au-based NGs with p-vinylimidazole would be an interesting candidate. Even so, further experiments with *Ex-vivo* mucin and/or *In-vivo* models would be required to elucidate if these tendencies are correct or not.

3.3.4 Improving the stabilization of anisotropic AuNPs while they are acting as NIR light-into-heat transducers. A new hope in Au NPs photothermal applications.

AuNPs have been used in photothermal applications at laboratory and clinical scales. These particles can absorb light coming from a laser source and transduce it into heat. This effect is possible thanks to the presence of the localized surface plasmon resonance typical from AuNPs. The process takes part in four sequences. First, the laser light is absorbed by the AuNPs, then a thermal electron equilibrium is reached at the Fermi distribution. Afterwards, an electro-phonon coupling is formed and the energy is transferred from the electron to the inorganic NP. Finally, there is a phonon-medium interaction process that transfers the thermal energy to the surrounding media.^[61] This process has been applied in biomedicine to kill cancer cells. AuNPs are designed to penetrate tumoral cells and then a laser is applied to increase the localized temperature of the NPs.^[62] Subsequently, throughout the described mechanism, the cells are heated to reduce their growth and propagation. The biological window is known as the spectrum area (600 – 1200 nm) in which the light can penetrate deeper into the tissue without damaging them. Particularly, in the 750 – 900 nm, the laser can penetrate 3 – 4 cm, which makes this range the most widely used one for tissue treatment. Isotropic AuNPs have maximum absorption of around 520 nm, which is in the visible region. Therefore, these NPs are not suitable for photothermal applications. Nevertheless, anisotropic NPs (like rods and stars) have their maximum absorption in the range of 700 – 900 nm, which makes them perfect candidates to be used in photothermal therapies.^[63] However, there is a lack in the stability of AuNPs while applying the laser. Many reports have demonstrated a decrease in the absorbance of the plasmon band of the NPs and a shift of these bands after applying a laser onto the NPs. Anisotropic NPs tend to shift to the visible region, losing their shapes and turning into more

spherical ones.^[64] This results in a decrease in their photothermal capacities, as particles cannot adsorb the same amount of laser light after a certain time due to the shift of the plasmon band. Other studies have demonstrated, by TEM microscopy, that by heating AuNPs, they lose their original shapes. Also, small spherical particles appeared as a consequence of the eruption of evaporated atoms and Au clusters. As a consequence of this, the size of the original AuNPs are also decreased and the photothermal conversion capacity reduced.^[65]

A colloidal dispersion of the AuNPs shown in this chapter has been irradiated with a 785 nm laser, applying a power of 1980 mW/cm² onto the particles. The increase in the solution temperature has been recorded with a thermal camera and the laser has switched on/off every 30 min for 3 h. As a negative control, Au nanospheres (13 and 40 nm) have been irradiated verifying that the temperature of the solution only increases a few Celsius degrees. **Figure 3.29** shows the set-up used for this experiment and the photothermal conversion efficiency achieved for the Au nanospheres.

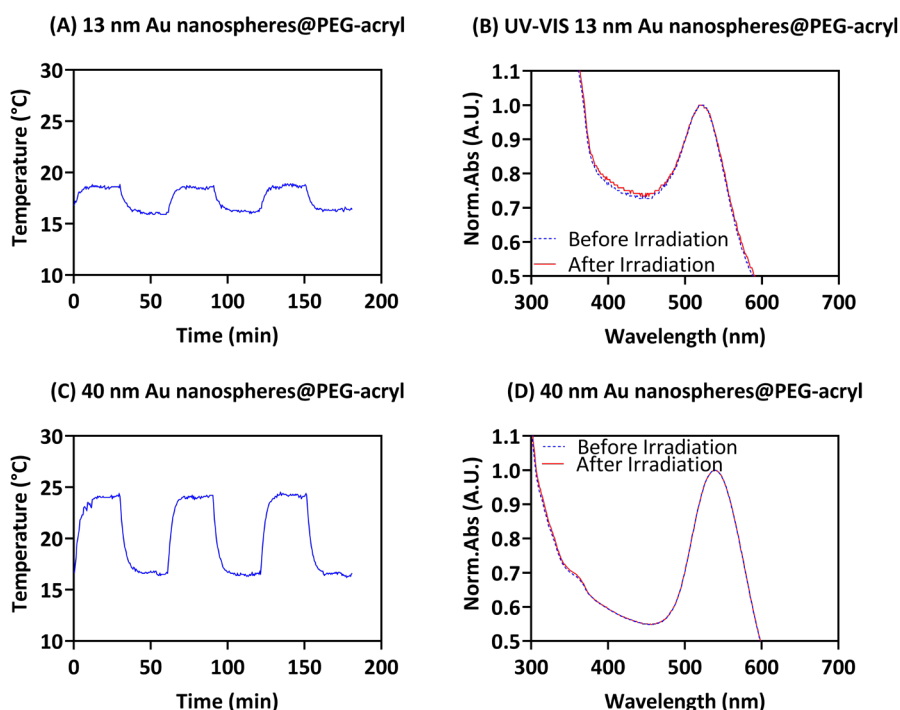
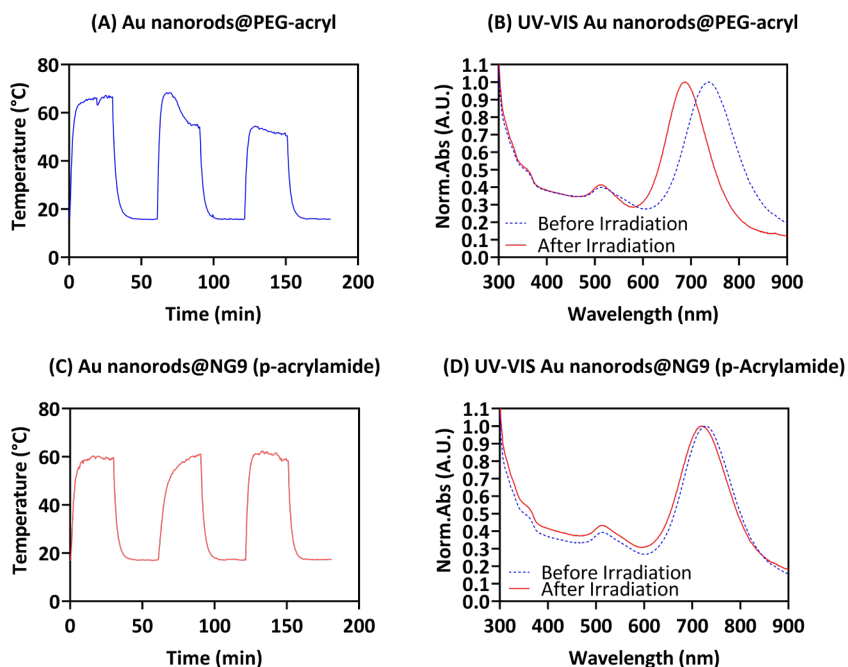


Figure 3.29. (A) Laser irradiation heating curves in triplicate for 13 nm Au nanospheres. (B) UV-VIS spectra before and after the irradiation of Au nanospheres.

(C) Laser irradiation heating curves in triplicate for 40 nm Au nanospheres. (D) UV-VIS spectra before and after the irradiation of Au nanospheres.

In plots **B** and **D** from **Figure 3.29** can be observed that isotropic 13 and 40 nm of Au nanospheres do not exhibit good photothermal conversion capacity upon irradiation with the laser with $\lambda = 785$ nm, as was expected. These two materials have been used as a negative control to corroborate that they cannot convert the NIR laser into heat, as there is no plasmon band in that region. In fact, the 13 nm spheres have increased the solution temperature to 2 °C and the 40 nm spheres have increased the solution temperature to 4 – 5 °C. Moreover, UV-VIS spectra before and after the irradiation have not changed for both AuNPs, which indicates that there is no aggregation. The minimum photothermal effect achieved is a consequence of the width of the plasmon bands and the laser may have a certain wavelength error. Nevertheless, an increase of 2 – 5 °C after 30 min can be neglected. In other words, it can be determined that isotropic AuNPs do not exhibit photothermal conversion properties in the NIR region.

Anisotropic AuNPs are the ones with real interest to act as NIR laser-into-heat transducers. The same methodology has been applied to rods and stars materials developed along with this chapter. **Figure 3.30** shows the laser irradiation heating curves and the UV-VIS spectra before and after irradiation for nanorods materials.



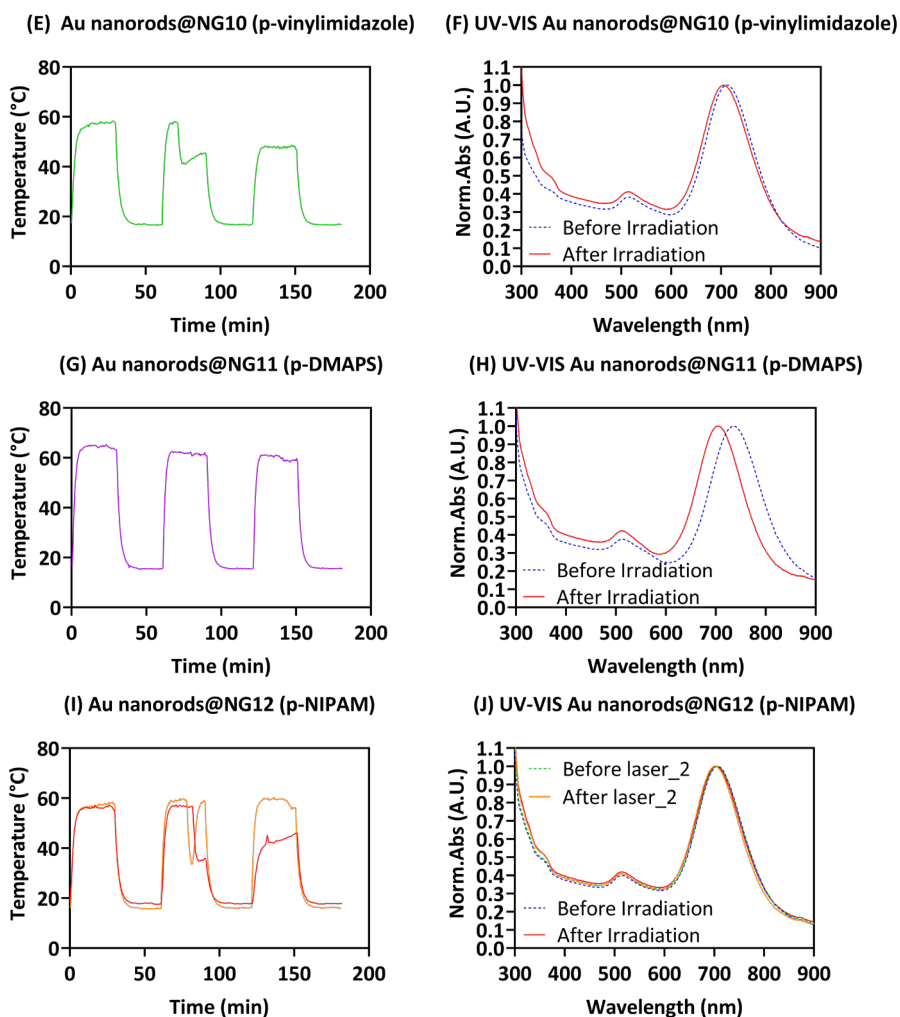


Figure 3.30. (A) Laser irradiation heating curves in triplicate for Au nanorods@PEG-acryl. (B) UV-VIS spectra before and after the irradiation of Au nanorods@PEG-acryl. (C) Laser irradiation heating curves in triplicate for Au nanorods@NG9 (p-acrylamide). (D) UV-VIS spectra before and after the irradiation of Au nanorods@NG9 (p-acrylamide). (E) Laser irradiation heating curves in triplicate for Au nanorods@NG10 (p-vinylimidazole). (F) UV-VIS spectra before and after the irradiation of Au nanorods@NG10 (p-vinylimidazole). (G) Laser irradiation heating curves in triplicate for Au nanorods@NG11 (p-DMAPS). (H) UV-VIS spectra before and after the irradiation of Au nanorods@NG11 (p-DMAPS). (I) Laser irradiation heating curves in triplicate for Au nanorods@NG12 (p-NIPAM). (J) UV-VIS spectra before and after the irradiation of Au nanorods@NG12 (p-NIPAM).

In **Figures 3.30 A** and **B**, it can be observed that the photothermal conversion efficacy obtained from the rods stabilized with PEG-acryl decreases

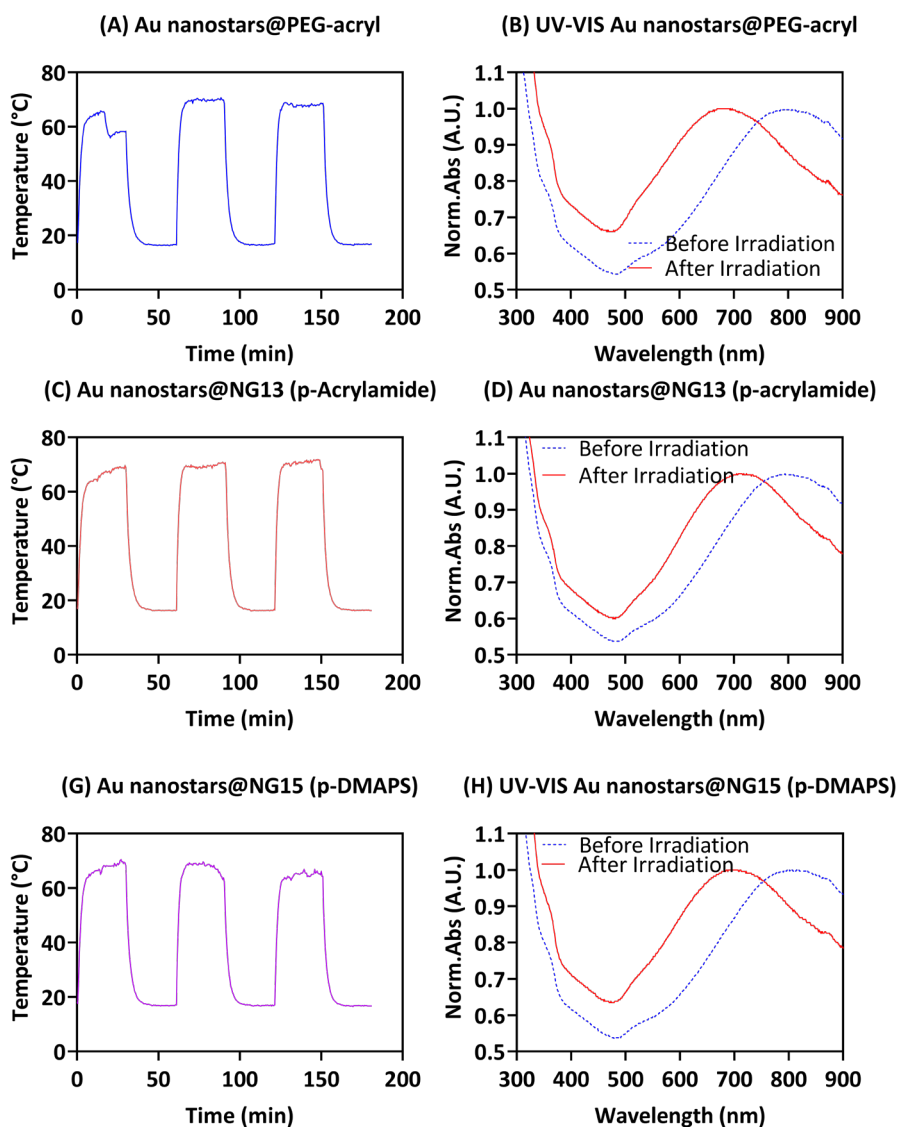
with each irradiation cycle (from 67 °C to 51 °C). In addition, the UV-VIS plasmon band has been shifted from 736 to 686 nm after the irradiation, which means that some nanorods have lost their size and shape, aggregating into spherical forms. On the contrary, the undesired aggregation effect has been reduced or even eradicated after the encapsulation of the rods into the NGs. For instance, NG9 (p-acrylamide) shown in plots **C** and **D** has reported an optimal and constant photothermal conversion during the three cycles. Moreover, the plasmon band has shifted from 728 to 721 nm, meaning an improvement in the stability of around 7 times more. Similar results have been achieved with p-DMAPS (NG11), plots **G**, **H**. For this case, the NG guarantees a good photothermal conversion efficacy that only drops from 64 to 59 °C. Even so, the stability registered is worse than the p-acrylamide NG. In this case, the plasmon peak has been moved from 734 to 707 nm. In any case, despite being worse stability than the one obtained with the other NG, it still supposes a double improvement concerning PEG.

The two remaining NGs show an intermediate behaviour between the previous discussions. The stability obtained after laser irradiation is quite high. With p-vinylimidazole, NG10 (plots **E** and **F**), the plasmon peak has shifted from 710 to 706 nm, which is an increment of 12 times more stability in comparison with the PEG-acryl. However, the photothermal conversion efficiency has dropped from 58 to 40 °C. To explain these results, it's necessary to understand the great ability of p-vinylimidazole to coordinate with metals.^[66] In fact, it has been used for the stabilization of Au nanoclusters.^[67] Therefore, it can be hypothesized that the vinylimidazole is stabilizing some of the clusters formed during the irradiation process, which could explain the lack of thermal conversion for the second and third cycles of irradiation.

Finally, the p-NIPAM NG (NG12), plots **I** and **J**, have been irradiated in two different samples because of the weird curve obtained during the second irradiation cycle. However, the same result was achieved in both samples, where in the middle of the second irradiation, the photothermal conversion capacity drops more than 20 °C. Even so, the plasmon peak has not shifted any single nm after the irradiation. One must have in mind that p-NIPAM is a thermoresponsive NG, and probably it is shrinking during the irradiation. Therefore, some of the thermal temperature released from the rods is being absorbed by the thermoresponsive NG, which could explain that the temperature in the aqueous solution is dropping and being recovered after a while.

It can be concluded that with the thin NGs, the aggregation of Au nanorods during their use in photothermal applications has been notably reduced. Besides, p-acrylamide and p-DMAPS have reported good photothermal conversion capacities that can be recovered after long periods of laser irradiation. Lastly, thin NGs are a very promising platform to stabilize Au nanorods for their use in biomedicine.

The same experiment has been applied to Au nanostars. **Figure 3.31** shows the collected heating curves and the UV-VIS spectra before and after the irradiation.



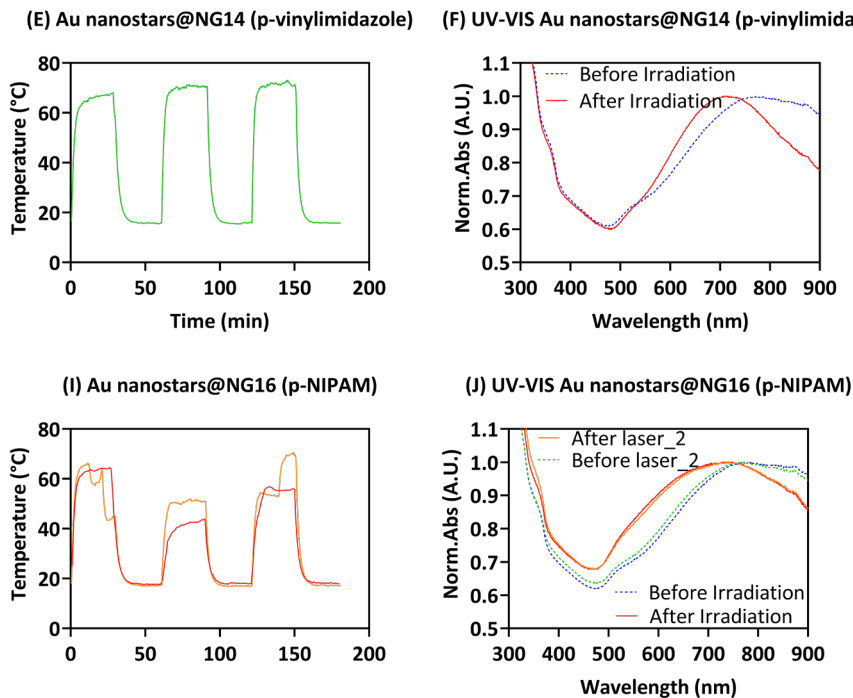


Figure 3.31. (A) Laser irradiation heating curves in triplicate for Au nanostars@PEG-acryl. (B) UV-VIS spectra before and after the irradiation of Au nanostars@PEG-acryl. (C) Laser irradiation heating curves in triplicate for Au nanostars@NG13 (p-acrylamide). (D) UV-VIS spectra before and after the irradiation of Au nanostars@NG13 (p-acrylamide). (E) Laser irradiation heating curves in triplicate for Au nanostars@NG14 (p-vinylimidazole). (F) UV-VIS spectra before and after the irradiation of Au nanostars@NG14 (p-vinylimidazole). (G) Laser irradiation heating curves in triplicate for Au nanostars@NG15 (p-DMAPS). (H) UV-VIS spectra before and after the irradiation of Au nanostars@NG15 (p-DMAPS). (I) Laser irradiation heating curves in triplicate for Au nanostars@NG16 (p-NIPAM). (J) UV-VIS spectra before and after the irradiation of Au nanostars@NG16 (p-NIPAM).

Au nanostars have a very broad plasmon band, which means that even if particles aggregate, they could maintain a good light into heat conversion. This can be observed (**Figure 3.31**) in plots **A** and **B**, which are based on Au nanostars grafted with PEG-acryl. In this material, the thermal conversion efficacy only drops 3 – 5 °C from one irradiation cycle to another. However, the maximum absorption in the plasmon band shifts from 796 to 697 nm. In other words, the shape of the stars is lost after three irradiation cycles. When the nanostars are encapsulated in NGs 13, 14 and 15 (p-acrylamide, p-vinylimidazole and p-DMAPS respectively) the thermal conversion efficacy is also maintained and the agglomeration is reduced. Contrary to the situation

observed for the nanorods, the p-vinylimidazole (plots **E** and **F**) has turned out to be the polymer that best stabilizes nanostars. For this case, the maximum absorption peak has been moved from 770 nm to 718 nm. In terms of sample stabilization, represents a double increase in comparison with the PEG-acryl ligand. Conversely, NG13 (p-acrylamide, plots **C** and **D**) has reported a plasmon shift from 794 to 723 nm, which can be translated into a stabilization 1.3 times higher than PEG, and NG15 (p-DMAPS, plots **G** and **H**) has reported a stability increase of 1.2 times higher than PEG.

Lastly, the thermoresponsive NG16 (p-NIPAM, plots **I** and **J**) shows similar heating curves to the nanorods. For this last material, the temperature in the solution is decreased and recovered many times in each cycle. As it was hypothesized before, the same applies here, probably the thermoresponsive capacity of the p-NIPAM is absorbing part of the heat to shrink and swell subsequently while the laser is on and off respectively. Furthermore, as was observed in TEM pictures (section **3.3.2.4**), the Au nanostar has areas with higher polymer density due to its particular shape. Thus, the NG has more space to shrink in comparison with the rod, which that there is more polymer that can absorb heat. Consequently, the heating curves experience steeper dips.

In conclusion, NGs13, 14 and 15 are good candidates to encapsulate Au nanostars and protect them during laser irradiations. In fact, p-vinylimidazole has turned out to be the best polymer for this particular application to encapsulate stars inside it.

3.4 Materials and methods

The starting materials were purchased from the following suppliers: Tetrachloroauric acid (HAuCl_4), silver nitrate (AgNO_3), sodium citrate, HS-PEG_{5k}-NH₂ and N-(2-hydroxyethyl)piperazine-N'-(2-ethanesulfonic acid) (HEPES), acrylamide, [2-(Methacryloyloxy)ethyl]dimethyl-(3-sulfopropyl)ammonium hydroxide (DMAPS), 1-vinylimidazole, N,N'-Methylenebisacrylamide, N,N,N',N'-tetramethylethylenediamine (TEMED), sodium dodecyl sulfate (SDS), N-isopropylacrylamide (NIPAM), potassium persulfate (KPS), phosphate-buffered saline (PBS), sodium chloride (NaCl), bovine serum albumin (BSA) and mucin from porcine stomach were obtained from Merck®. Hexadecyltrimethylammonium bromide (CTAB) was from Thermofisher®. Sodium borohydride (NaBH_4) and N-Acryloxysuccinimide were bought in Scharlab. Ascorbic acid was offered by Alfa Aesar. Ammonium persulfate (APS) was bought in VWR. The water used for the synthesis was type I quality (ultrapure water), obtained from a purification system (18.2 MΩcm). All the reagents were used as received, without any further purification.

3.4.1 Synthesis of gold nanoparticles

Au nanospheres of two sizes (13 and 40 nm), Au nanorods of 40 nm and Au nanostars of 40 nm were prepared following the described protocols from the literature. All the glass and magnetic stirrers used during the synthesis have been washed many times with aqua regia, rinsed with ultrapure water and finally dried in the oven at 120 °C before being used.

Au nanospheres were synthesized using the citrate reduction method, first described by Turkevich.^[6] For 13 nm size, HAuCl_4 (80.1 mg; 0.236 mmol) were dissolved in ultra-pure H₂O (195 mL). The mixture was heated under reflux at 100 °C. After the boiling point was achieved, sodium citrate was added to the system (200 mg; 0.93 mmol) previously dissolved in ultra-pure H₂O (5 mL). The synthesis took place at 100 °C for 30 min. The red aqueous solution containing the nanospheres was slowly cooled down to room temperature and kept at 4 °C protected from the light until their use without any further purification. The citrate act as a reducer and stabilizer ligand. As this ligand can be easily removed, particles were not centrifuged in this step to avoid aggregation. The final container was a low-biding plastic tube, that avoids particle aggregations.

Au nanospheres with 40 nm diameter were prepared with the same methodology adapting the amounts of the reagents. HAuCl_4 (39.4 mg; 0.1 mmol) was dissolved in ultra-pure H_2O (400 mL) and heated to 100 °C. Then, sodium citrate (2.36 mL; 1 wt.% in ultra-pure water; 0.08 mmol) was quickly added to the system. The product was stirred under reflux for 15 min. After completion of the reaction, the deep red solution was slowly cooled down to room temperature and kept at 4 °C without any further purification. The final container was a low-biding plastic tube, that avoids particles aggregation.

For the preparation of Au nanorods,^[22] seeds need to be synthesized in advance. For the preparation of the seeds, HAuCl_4 (25 μL ; 50 mM) were mixed with CTAB (4.7 mL; 0.1 M) at 27 – 30 °C during 5 min. Then, NaBH_4 (300 μL ; 10 mM) was rapidly injected under vigorous stirring of 1200 rpm. After 20 s, the solution was stirred at 400 rpm and maintained at 30 °C until its use.

For the preparation of the nanorods, HAuCl_4 (100 μL ; 50 mM) was mixed with CTAB (10 mL; 100 mM) at 27 °C for 10 min. Then, ascorbic acid (75 μL ; 100 mM) was added to the mixture and stirred for 1 min. Afterwards, AgNO_3 (80 μL ; 5 mM) is added to the mixture and stirred for another min. Finally, the seeds solution was added (120 μL) and the mixture was stirred for the last time during 1 min. Then, the synthesis is left undisturbed at 27 °C for 30 min. For the purification of the nanorods, the solution was centrifuged at 8000 rpm during 30 min and the supernatant was redispersed in ultra-pure water. The final product is kept at 4 °C protected from the light until used. The final container was a low-biding plastic tube, that avoids particles aggregation.

The last morphology, Au nanostars of 40 nm, were prepared as reported, with minimum modifications.^[32] They also required a first step for the preparation of seeds. Sodium citrate (5 mL; 34 mM) was added to a boiling solution of HAuCl_4 (95 mL 0.5 mM) under a magnetic stirrer. The mixture was stirred during 15 min at 100 °C. After that time, the product was cooled down to room temperature and stored at 4 °C until used. For the synthesis of the stars; HAuCl_4 (50 mL; 0.25 mM) was mixed with seeds (2.5 mL) under magnetic stirring for some min. AgNO_3 (500 μL ; 3 mM) and ascorbic acid (250 μL ; 100 mM) were injected simultaneously into the synthesis. This is a crucial step as if they are not injected together, the plasmon band of the stars can be shifted several nm. Some seconds after this, the colour of the materials turns greenish, indicating the formation of the desired shape. To preserve this shape along the time, HS-PEG_{5k}-NH₂ (500 μL , 0.1 mM) was added to the process and stirred for 15 min. The final product was purified at 6000 rpm, 10 °C for 45 min, twice. The pellet was redispersed in ultra-pure water and kept at 4 °C

protected from the light until their use. The final container was a low-binding plastic tube, that avoids particles aggregation.

The plasmon band of all the AuNPs has been registered using a NanoPhotometer NP80 from IMPLLEN® and BioTek Synergy Neo 2 multi-mode reader. The data were processed with the software GEO 5 3.1 and GraphPad Prism 9.3.

3.4.2 Ligand exchange for gold nanoparticles

The surface of Au nanospheres, nanorods and nanostars were saturated with PEG-NH₂ ligand. For that. A high excess of HS-PEG_{5k}-NH₂ (0.5 mL; 10 mg; 4 mM) were added to each of the AuNPs (10 mL; 10⁻⁸ M 13 nm spheres; 10⁻¹⁰ M 40 nm spheres; 10⁻⁹ M 40 nm rods; 10⁻⁹ M 40 nm stars). The mixture was placed in a low binding plastic tube and set in the thermoshaker (Termo agitador TR100-G from Optic ivymen system®) at room temperature and 800 rpm. The synthesis took place overnight for 13 nm spheres and 2 days for the rest of the samples. After the completion of the process, to purify the materials and remove the outgoing ligand, AuNPs were centrifugated in quadruple with the conditions shown in **Table 3.4**. The pellets were redispersed in HEPES buffer (10 mM; pH = 8.52) to protonate the amine ending group of the PEG. The materials were kept at 4 °C protected from the light until their use. The stability of these materials has been established in one week. Therefore, the step described in section 3.4.3 was done in tandem with this one.

Table 3.4. Centrifugation conditions used for the different AuNPs.

Sample	rpm	Temperature (°C)	Time (min)
Au 13 nm nanospheres	15000	10	45
Au 40 nm nanospheres	5000	10	50
Au nanorods	8000	20	45
Au nanostars	6000	10	45

3.4.3 PEG ending group modification to add acryl groups to the surface of gold nanoparticles

Prior to the synthesis of the NGs, the protonated ending amine group of the PEG needs to be converted into vinyl. For that, acryloylation reaction took place with the reagent N-Acryloxysuccinimide as previously described in the literature.^[68] A high excess of N-Acryloxysuccinimide (0.5 mL; 3 mg; 35 mM) was added to the previously prepared AuNPs@PEG_{5k}-NH₂ (10 mL; 10⁻⁸ M 13 nm spheres; 10⁻¹⁰ M 40 nm spheres; 10⁻⁹ M 40 nm rods; 10⁻⁹ M 40 nm stars) and incubated in the thermoshaker (Termo agitador TR100-G from Optic ivymen system[®]) at room temperature and 800 rpm for 2 h. The final product contains an acryl group at the edge of the PEG, which means that the surface of the AuNPs now is saturated with acryl groups. The final materials were purified by centrifuge, in quadruple, following the conditions described in **Table 3.4**. The ending pellets were redispersed in ultra-pure water and kept at 4 °C protected from the light until their use. The stability of these materials has been established for more than 6 months.

3.4.4 Synthesis of the thin NGs

The synthesis of the thin NGs around the AuNPs has been divided into two separate protocols.

The first one is a modification of the previously described technology for the synthesis of single-Enzyme NGs.^[30] This new methodology applies to the synthesis of p-acrylamide, p-vinylimidazole and p-DMPAS NGs (NGs 1, 2, 3, 5, 6, 7, 9, 10, 11, 13, 14 and 15 from **Table 3.1**). For the preparation of these NGs, solutions of acrylamide, vinylimidazole, DMAPS, methylenebisacrylamide, APS and TEMED were prepared according to the molar ratios described in **Table 3.1**. For each NGs, the previous prepared AuNPs@PEG_{5k}-NH-CO-CH₂=CH₂, the corresponding monomer(s) and methylenebisacrylamide as crosslinker were mixed in a low-binding plastic tube where Argon was bubbling during 1h to remove the oxygen. Individual solutions of APS and TEMED were also prepared and Argon was bubbled for 1h as well. After degassing was completed, APS and TEMED were added to the synthesis as polymerization initiator and catalyst respectively. The polymerization took place under an Argon atmosphere during 4 h at room temperature and 800 rpm in the thermoshaker (Termo agitador TR100-G from Optic ivymen system[®]). The polymerization process were done in a low-binding plastic tube to avoid aggregation and precipitation. The final products

were purified by centrifugation, in quadruple, following the conditions described in **Table 3.4**. The obtained pellets were redispersed in ultra-pure water and kept at 4 °C protected from light until their use.

The second protocol applies to the p-NIPAM thermoresponsive NGs (NGs 4, 8, 12 and 16 from **Table 3.1**). In a general protocol, p-NIPAM NGs took place at 70 °C to perform precipitation polymerization of the NGs. This high temperature could damage the AuNPs and in general, it is used for NGs with sizes 100 – 200 nm.^[48] Here, a similar protocol, with minimum modifications, has been applied but it took place at room temperature. This low temperature has allowed the polymerization of very thin thermoresponsive NGs creating a narrow layer and avoiding the precipitation of the NG. Briefly, the previously prepared AuNPs@PEG_{5k}-NH-CO-CH₂=CH₂ were mixed with methylenebisacrylamide, as a crosslinker, (3.9 mg; 0.025 mmol), SDS, as surfactant stabilizer, (1 mg; 3.46*10⁻³ mmol) and NIPAM, as a monomer, (56 mg; 0.5 mmol) and degassed for 1h with Argon. Individual solutions of KPS (1 mL; 0.1 M) and TEMED (1 mL; 6.66 mmol) were also prepared and Argon was bubbled for 1h as well. After 1 h, 65 µL of KPS and 10 µL of TEMED were added to the reaction and the polymerization took place for 24 h. The polymerization was done in a low-binding plastic tube at room temperature and 800 rpm in a thermoshaker (Termo agitador TR100-G from Optic ivymen system®). The final products were purified by centrifugation, in quadruple, following the conditions described in **Table 3.4**. The obtained pellets were redispersed in ultra-pure water and kept at 4 °C protected from light until their use.

3.4.5 Dynamic light scattering (DLS) and Z-Potential measurements

Hydrodynamic diameter (DLS) and surface charge (Z-potential) of the AuNPs-based materials were characterized on a Zetasizer Nano ZS Malvern® equipment. The measurements took place in water with polystyrene reference material at 25 °C and 37 °C. The settings were 3 runs with 15 accumulations each. Samples were analyzed in ultra-pure water. The data was processed with Zetasizer software and GraphPad Prism 9.3.

3.4.6 Gel permeation chromatography (GPC)

GPC chromatograms were obtained with the Shimadzu® Nexera series of ultra-high-performance liquid chromatography, used in GPC mode. AuNPS-

based materials (1 mL) were prepared in 2 mL GPC glass tubes and injected with an auto-injector. 10 μ L of each sample was injected and run for 1h. The mobile phase used was ultra-pure water. Samples passed through column OHpak SB-806MHQ shodex at a flow of 0.5 mL/min with a constant temperature of 25 °C. Then, the chromatograms were collected in a UV-VIS detector with the spectra ranging from 300 to 800 nm. The data has been processed LabSolution 5.1, Microsoft Excel 2021 and Gradpadh Prism 9.3 software.

3.4.7 Transmission electron microscopy (TEM)

TEM pictures from AuNPs-based materials were obtained in a Talos F200 i (from ThermoFisher®) and TITAN High-resolution transmission electron (HRTEM) from FEI Company®. 3 μ L of each material was drop-casting into Carbon coated TEM grids the day previous to the measurements. To avoid any damage to the samples, the drying process took place with the materials protected from the light. In the HRTEM, the samples were measured at 80 kV and in the Talos F200 I at 200 kV. Some samples were stained adding W atoms to the surface of the particles. The obtained pictures were processed with the software ImageJ 1.53s.

3.4.8 Atomic force microscopy (AFM)

Mechanical properties of AuNPs-based materials were characterized with AFM in PeakForce Tapping™ mode. The used equipment was Dimension ICON Nanoscope V from Bruker. 3 μ L of each sample was drop-casting into AFM mica discs and placed into the equipment. The materials were analyzed with the height, adhesion and DMT modulus sensors at the same time. The collected data were processed with NanoScope Analysis 1.9 and GraphPad Prism 9.3.

3.4.9 Differential scanning calorimetry (DSC)

DSC experiments of AuNPs-based materials were done in DSC3+ equipment, from Mettler Toledo®. 40 μ L of each sample were set into Al cresol, typically used for high-quality thermal analysis. The isotherms were run in a temperature range from 10 to 80 °C at a heating rate of 10 °C/min under

N₂ flow at 50 mL/min. The collected data have been processed with the software GraphPad Prism 9.3.

3.4.10 Scanning electron microscope (SEM)

AuNPs-based materials were drop-casting into silicon wafers and dried protected from the light. The samples were analyzed in an environmental scanning electron microscope (ESEM) model FEI Quanta 250. The equipment was used in a high vacuum at 30 KeV of electron acceleration. The obtained pictures were processed with the software ImageJ 1.53s.

3.4.11 Interactions study between biological fluids and AuNPs (I): Salts and proteins.

AuNPs (100 μ L; 10⁻⁸ M 13 nm spheres; 10⁻¹⁰ M 40 nm spheres; 10⁻⁹ M 40 nm rods; 10⁻⁹ M 40 nm stars) were incubated at (I) 37 °C; (II) with NaCl (100 μ L; 2M) at 37 °C; (III) with PBS (100 μ L; 10 mM) at 37 °C; (IV) with BSA (100 μ L; 1 mg/mL in PBS 10 mM) at 37 °C. The samples were incubated in a thermoshaker (Termo agitador TR100-G from Optic ivymen system[®]) and shaken at 400 rpm. The plasmon band were followed every 24 h with a BioTek Synergy Neo 2 multi-mode reader. The data were processed with the software GEO 5 3.1 and GraphPad Prism 9.3.

3.4.12 Interactions study between biological fluids and AuNPs (II): Mucin interactions followed by rheology.

AuNPs (100 μ L; 10⁻⁹ M 13 nm spheres; 10⁻¹¹ M 40 nm spheres; 10⁻¹¹ M 40 nm rods; 10⁻¹¹ M 40 nm stars) were mixed with mucin from the porcine stomach (1 g; 10 % wt. in PBS 10 mM) and immediately transferred into an ARES G2 rheometer. The analysis took place in soft motor mode, at 37 °C and 20 °C and constant frequency of 1 Hz for 15 min. The data were collected and processed in TRIOS software 5.1 and plotted in GraphPad Prism 9.3.

3.4.13 Laser irradiation of AuNPs. Photothermal conversion assays.

AuNPs-based materials (100 μ L; 10^{-8} M 13 nm spheres; 10^{-10} M 40 nm spheres; 10^{-9} M 40 nm rods; 10^{-9} M 40 nm stars) were placed into a 1.5 mL low-binding plastic tube. The materials were irradiated with a 785 nm laser. The laser used was a NanoPhotontec Berlin®, model FC-D-785. The distance between the laser and the samples was set at 1.5 cm, which can be translated into 1980 mW/cm². The laser was on during 30 min, then off for another 30 min. This process was repeated in triplicate for each sample. The variation of the solution temperature was recorded with a FLIR E53 thermal camera. The distance between the sample and the camera was set at 35 cm. The irradiation curves were recorded in mp4 video format with the camera. In the posterior analysis, the temperature values were manually extracted from the video and plotted with GraphPad Prism 9.3 software.

3.5 Main remarks, conclusions and future perspective

Very thin NGs have been successfully prepared and used for the protection of isotropic and anisotropic AuNPs. These materials have been the results of the development of novel technology based on the previously reported single-enzyme NGs strategy. The thin mantle NGs shell for AuNPs have been prepared with different monomers, such as; acrylamide, vinylimidazole, DMAPS and NIPAM. These ranges of starting materials have ended up with the preparation of neutral, zwitterionic and thermoresponsive NGs that have been grown around Au nanospheres, nanorods and nanostars preserving their original size and shape. High-resolution TEM and AFM have allowed the characterization of the thin NG mantle in terms of size and mechanical properties, corroborating the presence of thin NGs with a thickness of 2 - 4 nm.

When these materials have to face biological fluids, like salts and proteins (with BSA as a model protein), it has been found that the mantle NGs improve the stability of AuNPs along the time. Improving their lifetime represents a turning point in the ability of AuNPs as therapies of tomorrow's medicine. And, these NGs pave the way to achieving that goal. In particular, p-acrylamide and p-vinylimidazole NGs are very promising candidates to improve the stability of AuNPs in presence of proteins. Moreover, in complex systems like mucin, p-DMAPS NGs have demonstrated the lowest interaction with mucin in spherical-like shapes (spheres and stars). Though, for rods-shape p-DMAPS NGs have been found to be the ones that interact the most. These results highlight that the shape of the AuNP plays a decisive role at the same level as the polymeric shell. On contrary, p-vinylimidazole NGs have reported strong affinities with mucin for all the shapes of AuNPs. The hydrophobic behaviour from this polymer is probably promoting strong physical interactions with the mucin.

The thin NGs prepared in this chapter have also proven their value during the photothermal conversion capacity of anisotropic AuNPs. All of them have improved the stability of the AuNPs during their NIR laser conversion into heat. The typical undesired effect of Au atoms sublimation, which use to happen during the photothermal conversion and destabilizes the particles, has been notably decreased with these NGs. In fact, p-acrylamide and p-vinylimidazole NGs are the ones that have preserved the AuNPs the most.

As a general conclusion, it has been prepared a complete library of thin mantle NGs that can absorb AuNPs and improve their stability in many

biological scenarios. With the same protocol, different polymers can be used, which facilitates a controlled modulation over the synthetic material. This supposes an “à la carte” development of Au materials that can be beneficial depending on the disease to be treated.

Despite the promising results already achieved, there is still a lot of work to be done to bring these materials to the clinics. That idyllic scenario that looks so far away, will be the result of successive researchers joining forces. Until then, the next step to be taken contemplate the study of cell penetration and tumour damage capacity. If these cell culture studies would be satisfactory, *In-vivo* studies could be continued. From the material point of view, this thin mantle NG technology should be exploited to increase the stability of even more complex AuNPs that are assumed as a great challenge nowadays. For example, Au nanocages with pores in their structure, can be used to hide small molecules. Nevertheless, they have faced a lack of stability during many years. Also, chiral AuNPs have lost their chirality properties during their stabilisation. In the following months, these thin NGs would be explored for the eradication of these issues.

3.6 References – Chapter III

- [1] R. Liang, M. Wei, D. G. Evans, X. Duan, *Chem. Commun.* **2014**, 50, 14071.
- [2] H. Laroui, D. S. Wilson, G. Dalmasso, K. Salaita, N. Murthy, S. V. Sitaraman, D. Merlin, *Am. J. Physiol. - Gastrointest. Liver Physiol.* **2011**, 300, 371.
- [3] R. A. Sperling, P. Rivera Gil, F. Zhang, M. Zanella, W. J. Parak, *Chem. Soc. Rev.* **2008**, 37, 1896.
- [4] B. Karmakar, *Fundamentals of Glass and Glass Nanocomposites*, Elsevier Inc., **2016**.
- [5] R. D. Tweney, *Perspect. Sci.* **2006**, 14, 97.
- [6] J. Kimling, M. Maier, B. Okenve, V. Kotaidis, H. Ballot, A. Plech, *J. Phys. Chem. B* **2006**, 110, 15700.
- [7] N. Elahi, M. Kamali, M. H. Baghersad, *Talanta* **2018**, 184, 537.
- [8] V. Amendola, R. Pilot, M. Frascioni, O. M. Maragò, M. A. Iatì, *J. Phys. Condens. Matter* **2017**, 29, 203002.
- [9] A. Sánchez-Iglesias, J. Barroso, D. M. Solís, J. M. Taboada, F. Obelleiro, V. Pavlov, A. Chuvilin, M. Grzelczak, *J. Mater. Chem. A* **2016**, 4, 7045.
- [10] H. Liao, J. H. Hafner, *Chem. Mater.* **2005**, 17, 4636.
- [11] M. D'Acunto, *Materials (Basel)*. **2018**, 11, 2.
- [12] H. G. Jin, W. Zhong, S. Yin, X. Zhang, Y. H. Zhao, Y. Wang, L. Yuan, X. B. Zhang, *ACS Appl. Mater. Interfaces* **2019**, 11, 3800.
- [13] M. Cordeiro, F. F. Carlos, P. Pedrosa, A. Lopez, P. V. Baptista, *Diagnostics* **2016**, 6, 1.
- [14] F. Chen, P. Si, A. de la Zerda, J. V. Jokerst, D. Myung, *Biomater. Sci.* **2021**, 9, 367.
- [15] M. Fan, Y. Han, S. Gao, H. Yan, L. Cao, Z. Li, X. Liang, *Theranostics* **2020**, 10, 4944.
- [16] S. Z. M. Isa, R. Zainon, M. Tamal, *Materials (Basel)*. **2022**, 15, 1.
- [17] S. Shen, H. Tang, X. Zhang, J. Ren, Z. Pang, D. Wang, H. Gao, Y. Qian, X. Jiang, W. Yang, *Biomaterials* **2013**, 34, 3150.
- [18] Y. Liu, E. Chorniak, R. Odion, W. Etienne, S. K. Nair, P. Maccarini, G. M. Palmer, B. A. Inman, T. Vo-Dinh, *Nanophotonics* **2021**, 10, 3295.
- [19] A. R. Rastinehad, H. Anastos, E. Wajswol, J. S. Winoker, J. P. Sfakianos, S. K. Doppalapudi, M. R. Carrick, C. J. Knauer, B. Taouli, S. C. Lewis, A. K. Tewari, J. A. Schwartz, S. E. Canfield, A. K. George, J. L. West, N. J. Halas, *Proc. Natl. Acad. Sci.* **2019**, 116, 18590.
- [20] H. Kang, J. T. Buchman, R. S. Rodriguez, H. L. Ring, J. He, K. C. Bantz, C. L. Haynes, *Chem. Rev.* **2019**, 119, 664.
- [21] S. E. Skrabalak, L. Au, X. Li, Y. Xia, *Nat. Protoc.* **2007**, 2, 2182.
- [22] L. Scarabelli, A. Sánchez-Iglesias, J. Pérez-Juste, L. M. Liz-Marzán, *J. Phys. Chem. Lett.* **2015**, 6, 4270.
- [23] K. B. Vu, L. G. Bach, T. Van Tran, N. T. Thuong, H. N. Giang, Q. T. P. Bui,

- S. T. Ngo, *Chem. Phys. Lett.* **2019**, 728, 80.
- [24] N. Slesiona, S. Thamm, H. L. K. S. Stolle, V. Weißenborn, P. Müller, A. Csáki, W. Fritzsche, *Nanomaterials* **2020**, 10, 1.
- [25] R. Contreras-Cáceres, A. Sánchez-Iglesias, M. Karg, I. Pastoriza-Santos, J. Pérez-Juste, J. Pacifico, T. Hellweg, A. Fernández-Barbero, L. M. Liz-Marzán, *Adv. Mater.* **2008**, 20, 1666.
- [26] F. Howaili, E. Özliseli, B. Küçüktürkmen, S. M. Razavi, M. Sadeghizadeh, J. M. Rosenholm, *Front. Chem.* **2021**, 8, 1.
- [27] W. Sun, J. Zhang, C. Zhang, Y. Zhou, J. Zhu, C. Peng, M. Shen, X. Shi, *J. Mater. Chem. B* **2018**, 6, 4835.
- [28] M. Schumacher, D. Jimenez de Aberasturi, J. Merkl, L. Scarabelli, E. Lenzi, M. Henriksen-Lacey, L. M. Liz-Marzán, H. Weller, *Adv. Opt. Mater.* **2022**, 2102635, 2102635.
- [29] Q. Li, X. Qiao, F. Wang, X. Li, J. Yang, Y. Liu, L. Shi, D. Liu, *Anal. Chem.* **2019**, 91, 13633.
- [30] A. Rodriguez-Abetxuko, P. Muñumer, M. Okuda, J. Calvo, M. Knez, A. Beloqui, *Adv. Funct. Mater.* **2020**, 30, 2002990.
- [31] A. Beloqui, A. L. Cortajarena, *Curr. Opin. Struct. Biol.* **2020**, 63, 74.
- [32] D. Jimenez de Aberasturi, A. B. Serrano-Montes, J. Langer, M. Henriksen-Lacey, W. J. Parak, L. M. Liz-Marzán, *Chem. Mater.* **2016**, 28, 6779.
- [33] W. Haiss, N. T. K. Thanh, J. Aveyard, D. G. Fernig, *Anal. Chem.* **2007**, 79, 4215.
- [34] R. D. Near, S. C. Hayden, R. E. Hunter, D. Thackston, M. A. El-Sayed, *J. Phys. Chem. C* **2013**, 117, 23950.
- [35] H. de Puig, J. O. Tam, C.-W. Yen, L. Gehrke, K. Hamad-Schifferli, *J. Phys. Chem. C* **2015**, 119, 17408.
- [36] K. Rahme, L. Chen, R. G. Hobbs, M. A. Morris, C. O'Driscoll, J. D. Holmes, *RSC Adv.* **2013**, 3, 6085.
- [37] H. Xia, S. Bai, J. Hartmann, D. Wang, *Langmuir* **2010**, 26, 3585.
- [38] H. Hinterwirth, S. K. Wiedmer, M. Moilanen, A. Lehner, G. Allmaier, T. Waitz, W. Lindner, M. Lämmerhofer, *J. Sep. Sci.* **2013**, 36, 2952.
- [39] E. S. P. Bouvier, S. M. Koza, *TrAC Trends Anal. Chem.* **2014**, 63, 85.
- [40] J. Mehne, G. Markovic, F. Pröll, N. Schweizer, S. Zorn, F. Schreiber, G. Gauglitz, *Anal. Bioanal. Chem.* **2008**, 391, 1783.
- [41] B. Li, Q. Xu, X. Li, P. Zhang, X. Zhao, Y. Wang, *Carbohydr. Polym.* **2019**, 203, 378.
- [42] E. Cazares-Cortes, C. Wilhelm, J. E. Perez, A. Espinosa, S. Casale, A. Michel, A. Abou-Hassan, C. Ménager, *Chem. Commun.* **2021**, 57, 5945.
- [43] A. La Porta, A. Sánchez-Iglesias, T. Altantzis, S. Bals, M. Grzelczak, L. M. Liz-Marzán, *Nanoscale* **2015**, 7, 10377.
- [44] E. R. Osorio-Blanco, J. Bergueiro, B. E. Abali, S. Ehrmann, C. Böttcher, A. J. Müller, J. L. Cuéllar-Camacho, M. Calderón, *Chem. Mater.* **2020**,

- 32, 518.
- [45] Y. Gao, J. Yang, Y. Ding, X. Ye, *J. Phys. Chem. B* **2014**, *118*, 9460.
- [46] R. Yadav, S. Kumar, P. Narang, P. Venkatesu, *J. Colloid Interface Sci.* **2021**, *582*, 478.
- [47] K. Pielichowski, K. Flejtuch, *Polym. Adv. Technol.* **2002**, *13*, 690.
- [48] L. Navarro, L. E. Theune, M. Calderón, *Eur. Polym. J.* **2020**, *124*, 109478.
- [49] S. A. Alsharif, L. Y. Chen, A. Tlahuice-Flores, R. L. Whetten, M. J. Yacaman, *Phys. Chem. Chem. Phys.* **2014**, *16*, 3909.
- [50] R. Pamies, J. G. H. Cifre, V. F. Espín, M. Collado-González, F. G. D. Baños, J. G. de la Torre, *J. Nanoparticle Res.* **2014**, *16*, 2376.
- [51] S. Chakraborty, P. Joshi, V. Shanker, Z. A. Ansari, S. P. Singh, P. Chakrabarti, *Langmuir* **2011**, *27*, 7722.
- [52] J. Zhu, Z. Sun, J. Li, J. Zhao, *J. Nanosci. Nanotechnol.* **2012**, 2206.
- [53] C. Gamazo, N. Martín-Arbella, A. Brotons, A. I. Camacho, J. M. Irache, *Eur. J. Pharm. Biopharm.* **2015**, *96*, 454.
- [54] J. T. Huckaby, S. K. Lai, *Adv. Drug Deliv. Rev.* **2018**, *124*, 125.
- [55] H. S. Kim, D. Y. Lee, *J. Ind. Eng. Chem.* **2021**, *102*, 122.
- [56] S. Sunoqrot, L. Hasan, A. Alsadi, R. Hamed, O. Tarawneh, *Colloids Surfaces B Biointerfaces* **2017**, *156*, 1.
- [57] N. Barbero, M. Coletti, F. Catalano, S. Visentin, *Int. J. Pharm.* **2018**, *535*, 438.
- [58] S. Mansuri, P. Kesharwani, K. Jain, R. K. Tekade, N. K. Jain, *React. Funct. Polym.* **2016**, *100*, 151.
- [59] J. Kočevár-Nared, J. Kristl, J. Šmid-Korbar, *Biomaterials* **1997**, *18*, 677.
- [60] L. M. C. Sagis, P. Fischer, *Curr. Opin. Colloid Interface Sci.* **2014**, *19*, 520.
- [61] S. Hashimoto, D. Werner, T. Uwada, *J. Photochem. Photobiol. C Photochem. Rev.* **2012**, *13*, 28.
- [62] M. R. K. Ali, P. E. Warner, A. M. Yu, M. Tong, T. Han, Y. Tang, *Bioconj. Chem.* **2022**, acs.bioconjchem.2c00011.
- [63] L. M. Maestro, E. Camarillo, J. A. Sánchez-Gil, R. Rodríguez-Oliveros, J. Ramiro-Bargueño, A. J. Caamaño, F. Jaque, J. G. Solé, D. Jaque, *RSC Adv.* **2014**, *4*, 54122.
- [64] M. Klekotko, J. Olesiak-Banska, K. Matczyszyn, *J. Nanoparticle Res.* **2017**, *19*.
- [65] S. Hashimoto, T. Katayama, K. Setoura, M. Strasser, T. Uwada, H. Miyasaka, *Phys. Chem. Chem. Phys.* **2016**, *18*, 4994.
- [66] T.-X. Zhang, X.-Y. Liu, Y. Liu, Y. Chen, *Colloids Surfaces A Physicochem. Eng. Asp.* **2018**, *551*, 25.
- [67] F. Gong, R. Peng, Q. Wu, H. Zhang, Y. Luo, Q. Cui, *Colloids Surfaces A Physicochem. Eng. Asp.* **2022**, *641*, 128608.
- [68] A. Beloqui, S. Baur, V. Trouillet, A. Welle, J. Madsen, M. Bastmeyer, G. Delaitre, *Small* **2016**, *12*, 1716.

SECTION B

CHAPTER IV:

Screening of Eudragit as
building blocks in the
preparation of
physically cross-linked
hydrogels

4.1 Introduction

Scientists have tried to improve drug delivery systems to overcome physical barriers and to make drugs achieve the desired target. As it was described in **Chapter I**, hydrogels are polymeric materials that have been developed for the encapsulation and smart controlled release of several cargos in a wide variety of applications.

Hydrogels are three-dimensional cross-linked networks with the ability to retain water inside themselves.^[1] They can be designed to respond to an external stimulus (like temperature or pH) and swell in aqueous media.^[2] Their intrinsic properties make them soft and elastic, which guarantees minimal tissue irritation and a very small propensity to attach proteins to their surface. Based on the cross-linking mechanism followed for the preparation of hydrogels, they can be divided into physical or chemical.^[3] In the first case, the polymeric chains are linked reversibly, being possible to dissolve the hydrogel. One of the main advantages of working with physically cross-linked hydrogels is the possibility of combining polymers that are already approved by FDA or EMA agencies,^{[4][5]} which guarantees biocompatibility, increases patient compliance, decreases secondary effects, and reduces the required time to transfer this technology towards the industry. Currently, hydrogels for drug delivery (buccal, oral, etc)^[6], wound dressing^[7], personal hygiene products,^[8] tissue engineering, contact lenses, among others, can be found in the market.^[9] Taking into account that nowadays, most of the main routes for therapeutic delivery are ocular^[10], buccal^[11], vaginal^[12], and nasal,^[13] the current development of materials is focused on the preparation of devices with good adhesion to these routes.

By definition, an adhesive material is a highly liquid density substance that can attach two or more substrate surfaces avoiding its separation.^[14] Consequently, adhesion means the creation of attractive forces between two substrates. If a biological tissue is involved in this process, the adhesion is called bioadhesion,^[15] which often involves the presence of a mucosa layer that is mainly formed by glycoproteins.^[16] All the delivery routes previously described have in common the presence of mucosal surface. Therefore, having a material with good mucoadhesion and/or mucopenetration properties remains a highly desired challenge. Recent studies have found that the interaction between hydrogels and the mucosa can prolong the residence time of active drugs at the application site.^[17] Consequently, it is important to design the materials to form the desired interaction with the mucin (main component of mucose) by selecting the optimal adhesive polymers. These can

be classified into two groups, namely specific and non-specific polymers.^[18] Specific polymers (e.g., lectins, fimbrin) can attach chemical structures with the biological molecules. In contrast, the non-specific ones (e.g., poly(acrylic acid) and acrylates) can attach to the cell surface and the mucus layer. Nevertheless, some general factors should be taken into consideration to select the appropriate polymer for mucus adhesion. For example, the molecular weight of polymers is a crucial one. A flexible long-chain increases the entanglement between the polymer and the mucosal layer. For the same reason, it is also important to control the cross-linking degree between chains and the hydration of the network. If the cross-linking degree is too high, the flexibility will be reduced and also their mucus adhesion capacity.^[18] Furthermore, to guarantee that the polymer will exhibit good mucoadhesive properties, it should be able to form hydrogen bonds by the presence of hydroxyl, carboxyl and amino groups in their chemical structure (e.g., poly(vinyl alcohol), polyacrylates). Likewise, polymers with charged functional groups increase the mucoadhesion effect.^{[19][20]} Hydrogels based on polymers with the previously described properties are emerging day by day with improved mucoadhesion properties.

Even though several hydrogels based on PVA or PEG have been studied over the last years, there are plenty of other polymers, widely used in pharmacy, that are not too much explored for the preparation of these materials. For instance, Eudragits^{[21][22]} is a family of versatile polyacrylate polymers, which their main property is to have a range of water solubility degrees with minimum chemical structure modifications. This property makes this family very interesting to be used as drug vehicles. Actually, Eudragits have been explored and applied during the last years for gastrointestinal release and as coating protection in pills to increase patient compliance. However, there is just a little literature about its potential application in hydrogel formulations.^[23] Some recent studies have investigated the use of pH-sensitive Eudragits to create NPs that can be loaded inside contact lens hydrogels in ophthalmic drug delivery applications.^[24] Additionally, these polymers can be chemically cross-linked with acrylic acid, in presence of methylenbisacrylamide to create a Eudragit-co-acrylic acid hydrogel as a pH-dependence smart carrier for colonic delivery.^[25] Also, it has been demonstrated that Eudragit's non-pH dependence can increase mucoadhesiveness when they are part of hydrogel formulations. In fact, Eudragit RS and S100^[26] have confirmed a notable increase in the hydrogel mucoadhesion towards vaginal and buccal mucosa. In addition, some Eudragits have been also explored for their use in physically cross-linked hydrogels for ophthalmology applications.^{[27][28][29][30][31]} In most of these

works, the application is only focused on drug delivery, without taking care of the mucosa layer and high humidity conditions that are present in the eye. Besides that, there is no comprehensive rationale for the selected Eudragit use for this application. Considering that several Eudragits formulations can be found in the market, with aqueous solubility from 0 to 100 % in function of the pH, it is necessary to complete the literature demonstrating the influence of each Eudragit when they are combined with other polymers to create a physically cross-linked hydrogel.

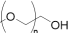
This chapter deals with the preparation of physically cross-linked hydrogels based on different Eudragits for ophthalmology applications. It is expected that the developed material will be an alternative to current ocular treatments. In fact, the corneal eye epithelium is exposed to many aggressions for being superficial. It can be self-repaired guided by Sclerocorneal limbus stem cells.^[32] These cells contain small proteins called growth factors (GF) that help in their recovery. Even though a huge amount of different GF can be found in the eye, the most important ones are Epidermal GF (EGF),^[33] Nerve GF (NGF),^[34] Hepatocyte GF (HGF)^[35] and Insulin-like GF 1 (IGF-1).^[36] EGF promotes wound healing as it can stimulate epidermal regeneration. NGF acts as a neural communication channel. Furthermore, it can also differentiate and promote somatic cells. HGF acts in the cellular cycle letting the cell division. Finally, IGF-1 can control the level of growth hormone, the development and growth of cells and cell DNA synthesis. Nevertheless, when the eye is seriously damaged, this self-repair mechanism is not enough to recover it. Nowadays, to solve this issue, patients need to undergo a surgery where amniotic membrane (AM)^[37] is grafted around the eye. Although beneficial, as the membrane contains GF that assist with the recovery, the whole procedure presents several shortcomings.

Hereby, five representative Eudragits have been explored as part of physically cross-linked hydrogels based also on polyvinylpyrrolidone (PVP), polyvinyl alcohol (PVA) and polyethylene glycol (PEG). This study aims to establish similarities and differences among five different hydrogels in regard of their matrix stability, protein and GF release profile, pore size, crystallinity, mechanical and rheological properties, *In-vitro* cytotoxicity and *In-vivo* mucoadhesion. Furthermore, the final optimized material will be loaded with GF and applied in a full ocular therapy *In-vivo*. As the five hydrogels will be based on non-water-soluble Eudragits (RSPO, RL100) or water-soluble ones (S100, L100, L100-55), the aforementioned parameters will dramatically change in function of the formulation. **Figure 4.1** shows a scheme of the hydrogel composition and the GF encapsulated.

Hydrogel based on F.D.A approved polymers:

Polyvinylpyrrolidone 50 kDa (PVP): 

Polyvinyl alcohol 100 kDa (PVA): 

Polyethylene glycol 2 kDa (PEG): 

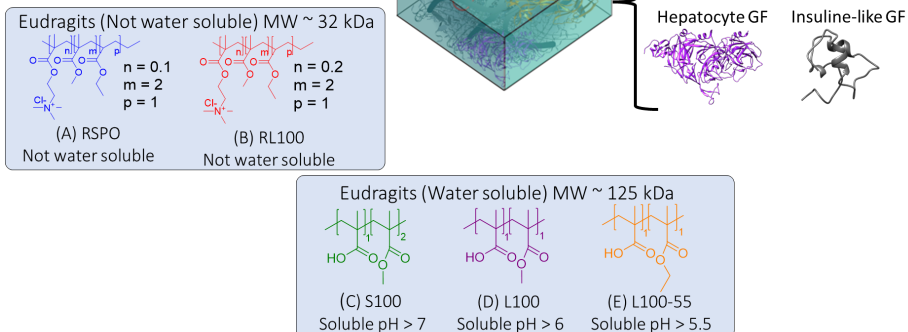


Figure 4.1. Scheme of a hydrogel composition and GF encapsulated inside the matrix (Epidermal, Nerve, Hepatocyte and Insuline GF).

Due to the complexity of the eye, to mimic its conditions, a novel release setting has been optimized during the development of this thesis. Furthermore, to decrease the number of animals required during the optimization process, a rheology technique has been optimized to measure the mucoadhesion of hydrogels towards ocular conjunctiva at a laboratory scale.

4.2 Objectives

The general objectives of Chapter IV were addressed in Chapters I (section 1.5) and II. Here, it is going to be remarked on some specific objectives of the project.

The project deals with the preparation of physically cross-linked hydrogels based on already approved polymers by regulatory agencies like the FDA or EMA. The global objective is to prepare a hydrogel that can be used as an ocular insert for the controlled release of GF. To achieve the desired material, this chapter faces the challenge of carrying out a large number of characterizations that will allow discerning the key parameter for the development of the optimal materials. The main objectives are listed as follows:

- As a first step, it is required to get a protocol that allows the preparation of physically cross-linked hydrogels in a reproducible manner, using different Eudragits.
- The prepared materials must have the capacity to swell in aqueous media while preserving their integrity. It is going to be optimized a methodology to dissolve the hydrogel in controlled conditions and follow the polymer dissolution kinetics by nuclear magnetic resonance (NMR).
- The potential application of the hydrogel will be as ocular inserts. Therefore, they should be able to tolerate certain mechanical stress. Several Eudragits, with different chemical structures, will be assayed to achieve a better mechanical tolerance.
- One of the main requirements of the formulations to be used as ocular inserts is to have good ocular mucoadhesion. Consequently, one of the challenges of this project is to be able to quantify the mucoadhesion capacity of the materials at a laboratory scale using a rheometer. Achieving this objective is crucial to optimise the formulations before getting access to *In-vivo*.
- The presence of crystals during the gelation process can have an effect on the protein-loaded stabilization. Hence, several Eudragit will be analyzed to decrease the number of crystals formed during the preparation of the film. The objective is to decrease this effect as much as possible and be

able to follow their formation by differential scanning calorimetry (DSC) and X-Ray spectroscopy.

- Another important objective of the project is to get closer to industrial scalability. Then, it should be feasible to load proteins homogeneously in a scale-up process. This will be addressed using a fluorophore chemically conjugated with a protein to have visual control over the distribution of the protein in the patch. It is also expected to be able to get different release kinetic profiles (from abrupt to sustained) of proteins by changing the Eudragit polymer.
- Attach cells to hydrogels' surfaces and let them grow healthy remains challenging. Nevertheless, as the final application of the material is biomedicine, it is a must to quantify the metabolic activity of cells in presence of the hydrogel formulations. The main specific objective of this section will be to get a protocol to demonstrate that the hydrogels are not toxic to cells at different concentrations. However, in the case of obtaining a negative result, it is expected to be able to eliminate the cytotoxic capacity by changing the film's composition.
- It is expected to achieve a final hydrogel candidate and use in pre-clinical studies in animal treatment.

4.3 Results and discussion

4.3.1 Hydrogel preparation

Five different physically cross-linked hydrogels based on PVP, PVA, PEG, Eudragit and glycerol were prepared by solution casting technique.^[38] It is expected that they could be used for the controlled release of a protein or a drug in presence of mucose and conditions of high humidity. For instance, they can be used as ocular inserts^[30], delivery vehicles inside the mouth^{[39][40]}, and vagina^[41], among others. All the formulations have three polymers in common. PVP with a molecular weight (MW) of 50 kDa, PVA with a MW of 100 kDa and PEG with a MW of 2 kDa.

The first two polymers (PVP and PVA) belong to the vinyl-based family. They display an important role in the hydrogel matrix, contributing to an increase of the mucoadhesive properties while balancing the hydrophobic/hydrophilic ratio. During the last years, PVP has been used in material development for wound dressings and drug delivery systems due to its excellent biocompatibility. Furthermore, it is also remarkable the good mechanical strength properties that have been previously reported in PVA formulations.^[42]

The last polymer, PEG, belongs to the family of polyethers and is well-known for being used in hydrogels because of its high biocompatibility, physical properties, elastic nature, non-toxicity, low recognition by the immune system and good thermal resistance.^[43]

In addition, all the formulations also contain glycerol, which acts as a plasticiser, increasing the stability of the matrix and mucoadhesivity while adding flexibility and decreasing the irritation potential.^[44] The remained used polymer is the Eudragit.

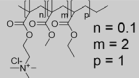
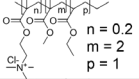
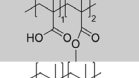
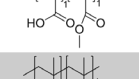
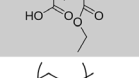
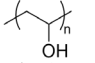
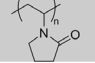
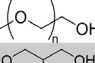
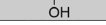
The interest of the research deals with an analysis of the Eudragit influence in hydrogel matrices formulations. Several Eudragits were analyzed in function of their pH-dependent water solubility. For that purpose, five representative Eudragits were selected as starting materials to be part of the hydrogel formulations. As pH-independent Eudragit, the formulation A contains Eudragit RSPO and the formulation B, Eudragit RL100. The chemical structure of these two polymers is composed of a triblock copolymer, based on ethyl acrylate, methyl methacrylate and low content of methacrylic acid ester with quaternity ammonium groups. The difference between Eudragit RSPO and RL100 is the number of repeating units in the block that contain the quaternary ammonium, being 0.1 units for RSPO and 0.2 units for RL100. The

ammonium group, presented as salt, makes the polymer to be very insoluble in water, with swelling capacities in aqueous solvents, cationic and non-biodegradable. Their average molar mass is around 32 kDa.^[21]

Water-soluble Eudragit were also studied. As they are pH-dependent, this behaviour could increase the drug's effectiveness and storage stability. As water soluble pH-dependent Eudragit, it has been selected Eudragit S100 (formulation C), which is water-soluble when the pH is above 7.0, Eudragit L100 (formulation D), soluble at pH above 6.0 and Eudragit L100-55 (formulation E), that is water-soluble at pH above 5.5. Their structure is based on a di-block polymer with methacrylic acid and ethyl acrylates repeating units. The structure difference between S100 and L100 is the block ratio. Being 1:2 for S100 and 1:1 for L100. In the case of L100-55, an end-methyl group from the ethyl acrylate block is changed for an end-ethyl group. In summary, they are anionic polymers with an average molar mass of around 125 kDa.^[21]

All the cited polymers have in common that they are already approved by the medicine regulation agencies (e.g., EMA and FDA).^[45] For this reason, it can be expected a hypothetical future fast process into their authorization to be used in humans. **Table 4.1** summarizes the five hydrogels' formulations and the polymers involved in their preparation.

Table 4.1. Polymers used in the hydrogel's formulations and their chemical structure.

Sample Name	Matrix Hydrogel Component	Chemical Structure	Water Solubility
Hydrogel A	Eudragit RSPO		No
Hydrogel B	Eudragit RL100		No
Hydrogel C	Eudragit S100		pH > 7
Hydrogel D	Eudragit L100		pH > 6
Hydrogel E	Eudragit L100-55		pH > 5.5
Hydrogels A - E	PVA (MW = 100 kDa)		Yes
Hydrogels A - E	PVP (MW = 50 kDa)		Yes
Hydrogels A - E	PEG (MW = 2 kDa)		Yes
Hydrogels A - E	Glycerol		Yes

The employed polymers mass was adapted during the solve casting process in order to prepare hydrogel films with a thickness of 1 mm. **Figure 4.2** shows the appearance of the hydrogels and their average thickness, measured with a digital caliper. As it is observed, the opacity varies within hydrogels, which may be an indication of crystallization during the gelation process, as it was already reported for hydrogels with PVA in their composition.^[46] This is later analysed in section **4.3.7**.

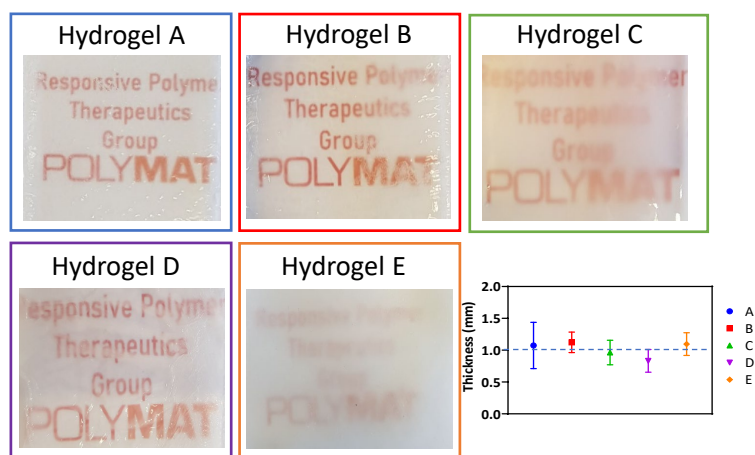


Figure 4.2. Pictures of the 5 prepared hydrogels and their average thickness (mm) measured with a caliper.

4.3.2 Hydrogels pore sizes in dried state

Many of hydrogel applications in biomedicine depend on the synthetic strategy followed during their preparation. For instance, just changing the nature of the crosslinking from chemical to physical, the internal hydrogel's pore size it is expected to be different.^[47] Recent studies have extolled that cell attachment, viability and migration, are directly correlated with the hydrogel pore size.^[48] This reveals the importance of a well-understanding of their internal structure. In the last years, the freeze-drying technique^[49] has been applied to analyse the internal structure of hydrogels by SEM. The main benefit of freeze-drying the hydrogels is that can be guaranteed the removal of the internal water by sublimation with a minimal structure modification. In addition, some studies that combine hydrophobic and hydrophilic polymers in the preparation of hydrogels have reported an effect of the hydrophobic polymer on the water retention capacity, highlighted after freeze-drying the samples. For instance, Vázquez et al.^[50] prepared acrylic hydrogels based on

2-hydroxyethyl methacrylate as hydrophilic polymer combined with different feeding ratios of 2-ethylhexyl acrylate as hydrophobic polymer. They demonstrated that an increase in the hydrophobic polymer was inverse to the swelling capacity of the hydrogel. Also, the capacity for freezing and removing the water was reduced. Therefore, if the presence of a hydrophobic polymer reduces the capacity to remove the water from a hydrogel, it is expected that the pores that can be found in the formulations analyzed in this work will be different among them. Moreover, it has been reported that the net charge of the hydrogel also influences the pore size.^[51]

In the present work, Eudragits with different water-soluble capacities have been used for the preparation of materials A – E. This, will end up in a different interaction between Eudragits with the other polymers (PVP, PVA, PEG) and therefore the pore sizes too. Here, pores size from the hydrogels matrices was measured in the dried state.^[52] **Figure 4.3** shows SEM micrographs obtained from internal hydrogel structures (transversal cut) and pore size histogram distributions obtained from the measurement of around 1000 pores from each hydrogel.

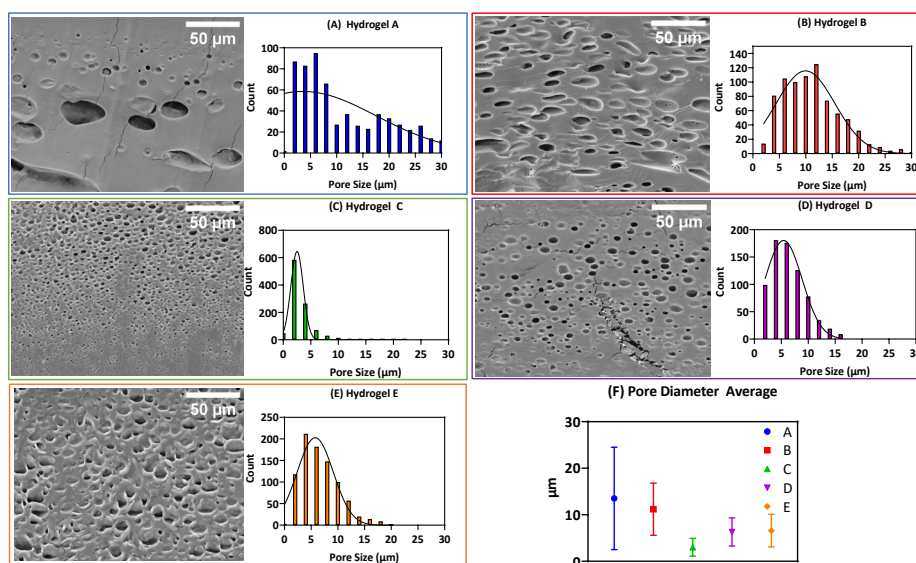


Figure 4.3. (A - E) SEM pictures and histogram distribution for the pores in the transversal cut of the five hydrogels after their freeze-drying. (F) Summary plot with the average pore diameter for the five materials. Scale bars 50 μm.

In **Figure 4.3**, a tendency in function of the type of material can be observed. Hydrogels A and B, based on non-water-soluble and positively charged Eudragits, exhibit a wider pore size distribution than hydrogels C, D

and E. Besides, the average pore diameter for materials A and B is around 11 – 14 μm . In contrast, materials C, D and E show a smaller pore diameter, with values between 3 – 6 μm with a narrower size distribution. These differences in the pore size are directly correlated with different structure compositions of the materials in terms of the number of cross-linkers and physical interactions between the polymeric chains. In fact, very small pores (1 μm) has been reported for physically cross-linked hydrogels based on PVA as a consequence of the high number of PVA crystals, that can be formed during the gelation process, and act as knots between chains. Yao *et al.*^[53] demonstrated with their carrageen-PVA hydrogels that the presence of carrageen was directly proportional to the increase in the pore size distribution as a decrease in the number of PVA crystals. Therefore, it is expected that the other polymers presented in materials A – E will reduce the presence of PVA crystals as well and increase the pore size distributions.

It is expected that the great variety of pore size distribution observed in materials A – E will have an influence on the matrix stability, mucoadhesion properties and kinetic release. These characteristics will be analyzed in detail in sections **4.3.3**, **4.3.6.2**, **4.3.8** and **4.3.9**.

4.3.3 Determination of matrix stability (I): Moisture uptake and moisture content

One of the main properties of hydrogels is their ability to retain water inside their matrices. Due to the physically cross-linked nature of the materials analyzed in this study, there is a maximum amount of water that they can retain without losing their integrity. Once this limit is reached, the polymers that compose the hydrogel start getting dissolved into the adsorbed water. To have a better understanding of the matrix stability in presence of humidity, moisture uptake (MU) and moisture content (MC) were analyzed following a reported procedure, with minimum modifications.^[54] Samples of all the hydrogels were introduced inside of a desiccator (**Figure 4.4**) in presence of a saturated solution of potassium sulphate, K_2SO_4 , (MU), that accounts for an ambient humidity of 95 %, or in presence of silica gel (MC).

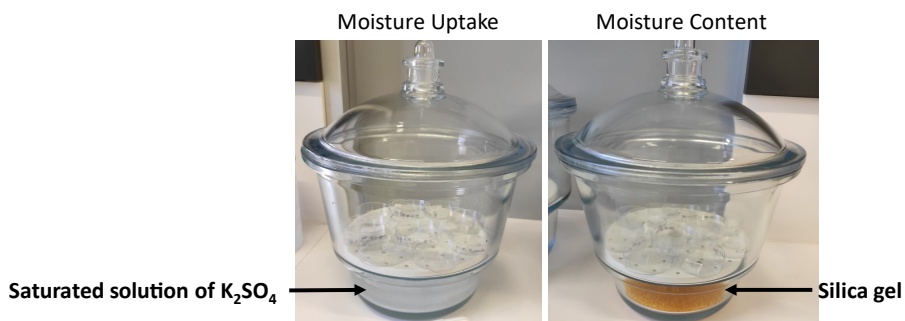


Figure 4.4. Samples of 1 x 1 cm from hydrogels A - E inside of a desiccator. Moisture uptake assay (with a saturated solution of K_2SO_4 , 95% relative humidity) and moisture content (with silica gel).

For the moisture uptake study, the K_2SO_4 can create an atmosphere with 95% of relative humidity. Once the hydrogels are exposed to this scenario, the matrices will adsorb water from the environment. Therefore, the hydrogels' weight will increase until they reach their maximum water retention capacity. Afterwards, they will start dissolving and decreasing their stability. In contrast, for the moisture content study, the silica gel can absorb the water from the environment. Then, water retained inside of the matrices will be removed. The weight of the hydrogel will decrease as a consequence of the water loss. **Figures 4.5A** and **4.5B** show the obtained results for the moisture content and moisture uptake analysis.

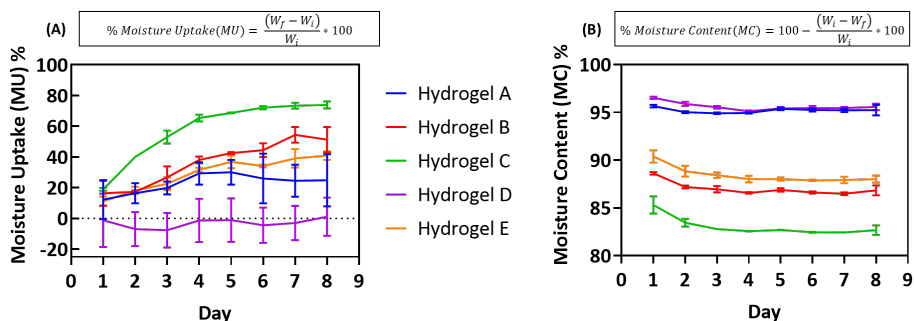


Figure 4.5. (A) Percentage of moisture uptake for all hydrogels vs. time. (B) Percentage of moisture content for all hydrogels vs. time. W_i represents initial weight; W_f is referred to the final weight.

For the MU results collected in **Figure 4.5A**, three types of behaviour were observed. The first one is correlated with a hydrogel that is totally swollen and cannot absorb more water. Therefore, it starts dissolving in the humidity absorbed from the environment and the hydrogel loses weight (hydrogel D). On the opposite behaviour, a second case is referred to a

material that can absorb water for more than one week and keep increasing its weight (hydrogel C). Intermediate behaviours were observed for hydrogels A, B and E. In these cases, the materials can absorb water for a couple of days. Afterwards, they lose their weight as a consequence of polymeric chains that are being dissolved in the environmental humidity.

In the first previously described scenario, hydrogel D cannot absorb more water. As it can be observed in the plot **4.5A**, MU for material D is negative, which means that the hydrogel is losing weight throughout the whole experiment. As it cannot absorb more water, the humidity that the material is absorbing from the K_2SO_4 solution is being used to dissolve the hydrogel, which means that the stability of the matrix is compromised in presence of humidity.

In a second scenario, hydrogel C is the one that presents more swelling capacity without losing matrix stability. Material C can absorb water for 7 – 8 days increasing its MU. In conclusion, material C is the one among the five studied materials that can absorb more water and maintain its integrity in presence of 95% of relative humidity for a longer time.

The third scenario explores an intermediate situation between the two previously described. In this scenario, followed by hydrogels A, B and E, the materials can absorb water from the environment and maintain their matrix integrity for some days. After that period, materials lose their weight and the stability of the matrix. For example, hydrogel A and E can absorb water during 4 – 5 days. After that time, the MU decreases in both materials, which means that the stability of the materials is being compromised. In contrast, hydrogel B can retain water, and preserve the stability of the matrix during 7 days. After one week, the MU also decreases.

It can be concluded that the use of different Eudragits influences the water retention capacity of the hydrogels A – E. The hydrogel that can retain more amount of water is hydrogel C, based on Eudragit S100. This Eudragit is water-soluble at physiological pH. It is possible that the acidic pH of the atmosphere humidity, generated by K_2SO_4 , avoids the solubility of the Eudragit S100, which probably also affects the solubility of the rest of the polymers. In other words, this material can swell more than the others preserving its stability. The rest of the materials have different swelling/dissolution behaviours that cannot be well-explained in this experiment. Nevertheless, it is very interesting that the different Eudragits affect the swelling capacity of the global matrix. To clarify more about the swelling capacity of hydrogel A –

E and the different dissolution kinetics of the polymers, in section **4.3.4** an advanced swelling study characterized by NMR will be performed.

The MC for materials A – E is summarized in **Figure 4.5B**. In the plot, it can be observed that all the materials are constantly losing water from their internal matrices during 3 – 4 days. The MC decay slope for hydrogels A – E is bigger during the first 4 days, which means that a big amount of water is lost during that period. Analysing the difference between the initial water percentage and the final one for each material, differences among all of them can be observed. For example, hydrogel A (based on Eudragit RSPO) and B (based on Eudragit RL100) present a decrease of 0.625% and 2.44%, respectively. Attending to the chemical structures of both Eudragits, even though both are non-water soluble, RL100 is more polar than RSPO as it contains a greater number of repeating units from the quaternary amine group. Then, it is expected that hydrogel B can retain more water than hydrogel A, which matches with the obtained MC results.

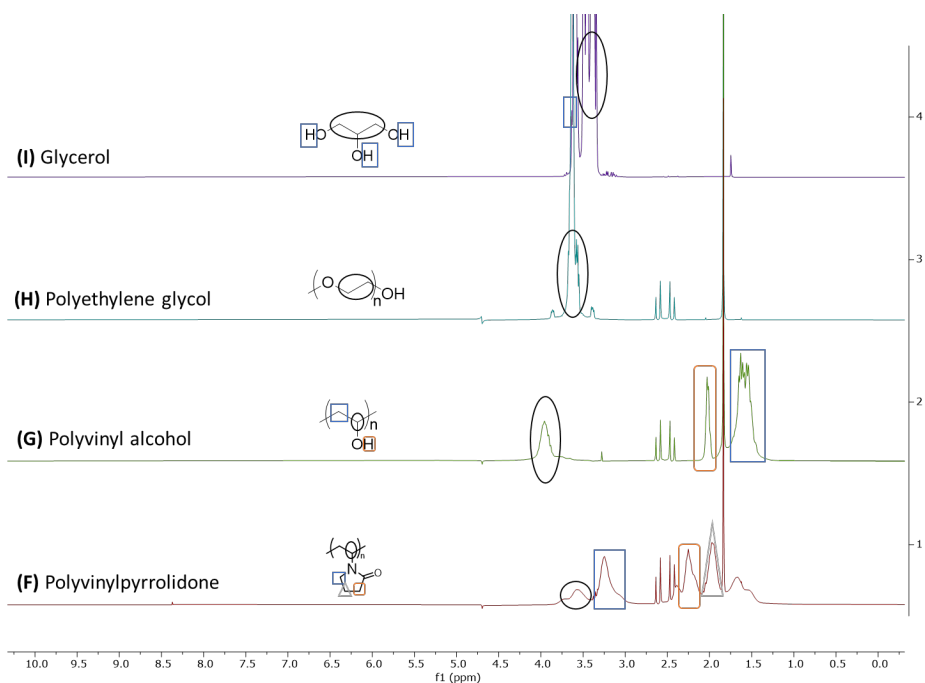
The other three materials, hydrogels C, D and E, are the ones formed by water-soluble polymers. Their different percentage of MC (initial minus final) are 3.2%, 1.8% and 3.13%, respectively. Hydrogels C and E show major water retention than hydrogels A and B, which is probably attributed to the presence of water-soluble polymers.

Hydrogel D yields only 1.8% of water retention. It could be expected a similar value to the ones obtained for hydrogels C and E. The reason for obtaining here a lower MC is related to the stability and homogeneity of this material. Hydrogel D, based on Eudragit water-soluble at pH > 6, is not mixing well with the other polymers that form the matrix. Therefore, during the drying process, this material is not homogeneous, letting the appearance of phase separation. In the end, it is not possible to properly reproduce the formulation, leading to inconsistent characterizations.

4.3.4 Determination of matrix stability (II): Kinetic of dissolution by NMR

The durability of hydrogels stabilized by physical interactions is directly correlated with the time that takes the patch to lose its properties and shape.^{[55][56][57]} In fact, MC and MU characterization have revealed the matrix stability dependency with the environmental humidity. Hence, it is very important to identify the dissolution rate profile of the materials in the humidity conditions of their particular application. In a typical procedure,^{[53][58]}

to study the dissolution rate of physically cross-linked hydrogels, a known mass of hydrogel is immersed in a defined volume of water. The initial and final weight of the material is compared to determine the possible dissolution of the polymers being released outside of the hydrogel matrix. Considering ocular inserts as a potential application for hydrogels, the stability of the materials has been investigated with a more advanced methodology. For that, hydrogels have been incubated in presence of an ophthalmic irrigation aqueous solution (BSS) at constant flow (110 $\mu\text{L}/\text{min}$) and at 36 $^{\circ}\text{C}$. The patches were held with the help of a 3D printed system. More technical details are given in section 4.4.3.3. The collected aliquots were analyzed in an NMR equipment. The signal from the different ^1H -NMR spectra, have been correlated with the corresponding polymers, with the help of the reference spectrum shown in **Figure 4.6 (A – I)**. Each spectrum has been obtained by dissolving the polymers in the BSS solution and their posterior analysis with the NMR equipment.



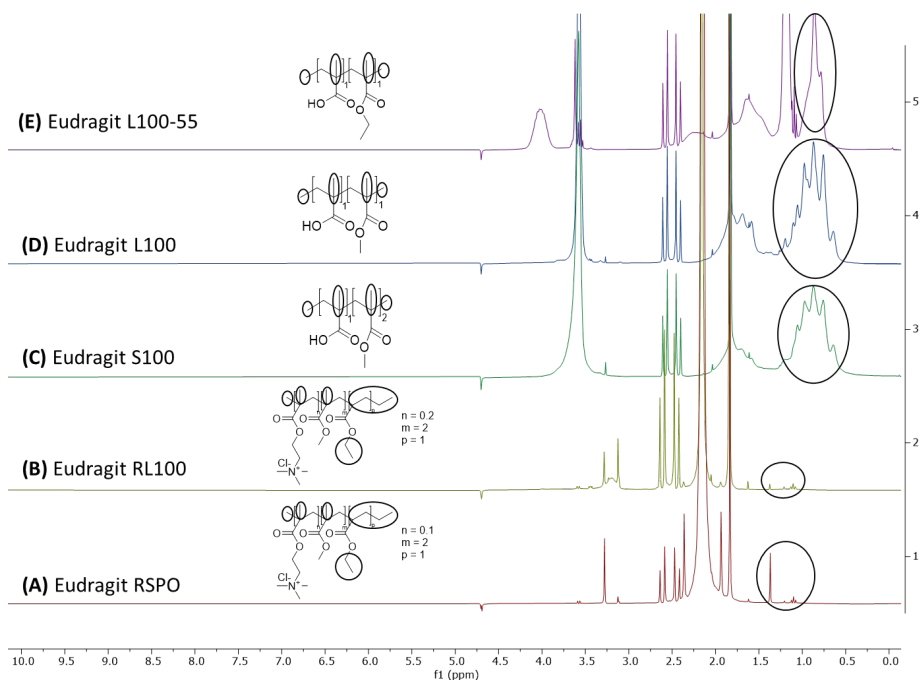


Figure 4.6. ^1H -NMR (300 MHz, BSS/ D_2O 90/10) spectra of all the polymers that are involved in the different hydrogels. A) Eudragit RSPO, B) Eudragit RL100, C) Eudragit S100, D) Eudragit L100, E) Eudragit L100-55, F) Polyvinylpyrrolidone, G) Polyvinyl alcohol, H) Polyethylene glycol and I) Glycerol.

Several aliquots were collected and quantified by ^1H -NMR to observe the dissolution kinetics of each polymer in the media. **Figure 4.7** contains the NMR spectrum obtained for the dissolution of hydrogels A and B at different times.

Screening of Eudragits as building blocks in the preparation of physically cross-linked hydrogels

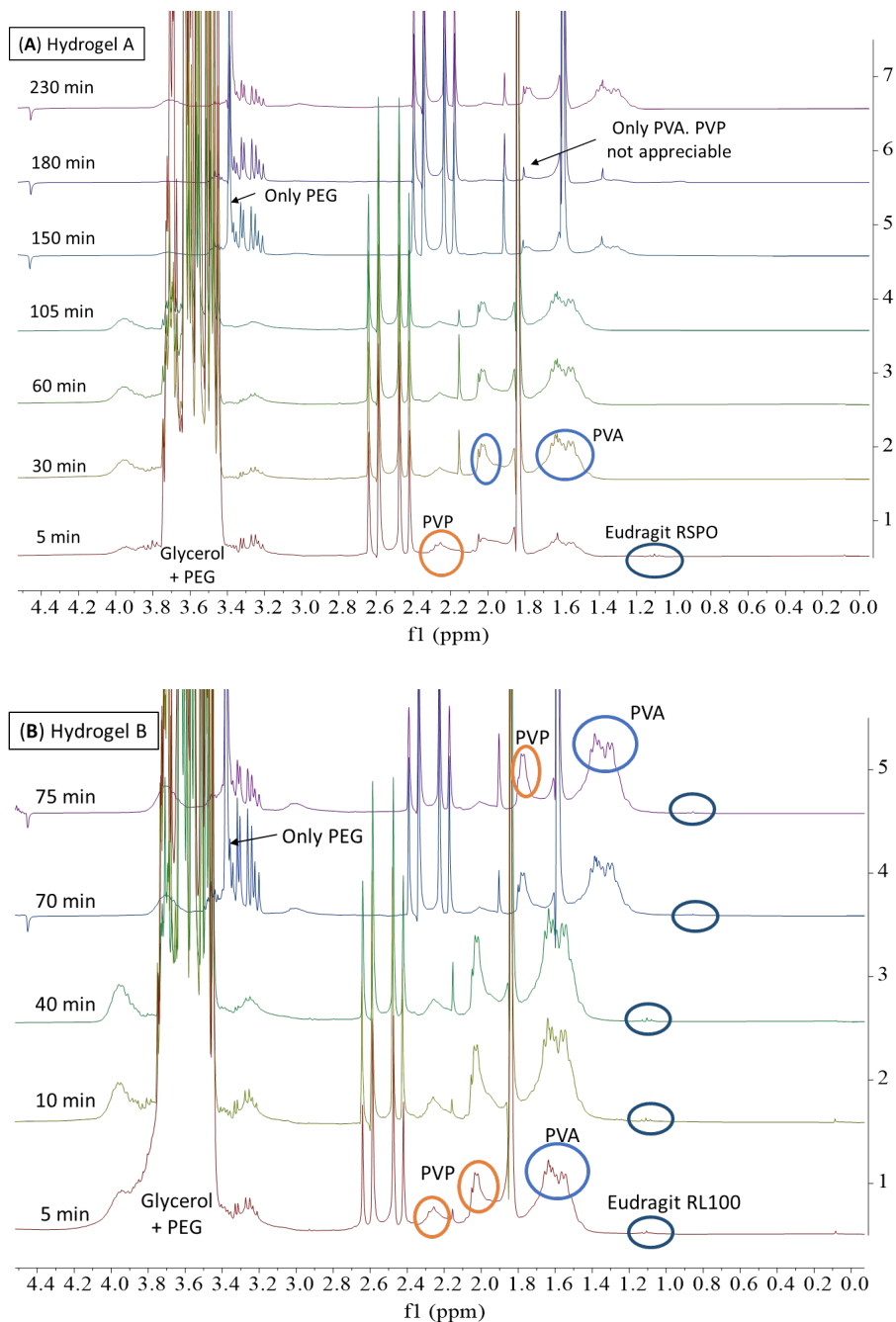
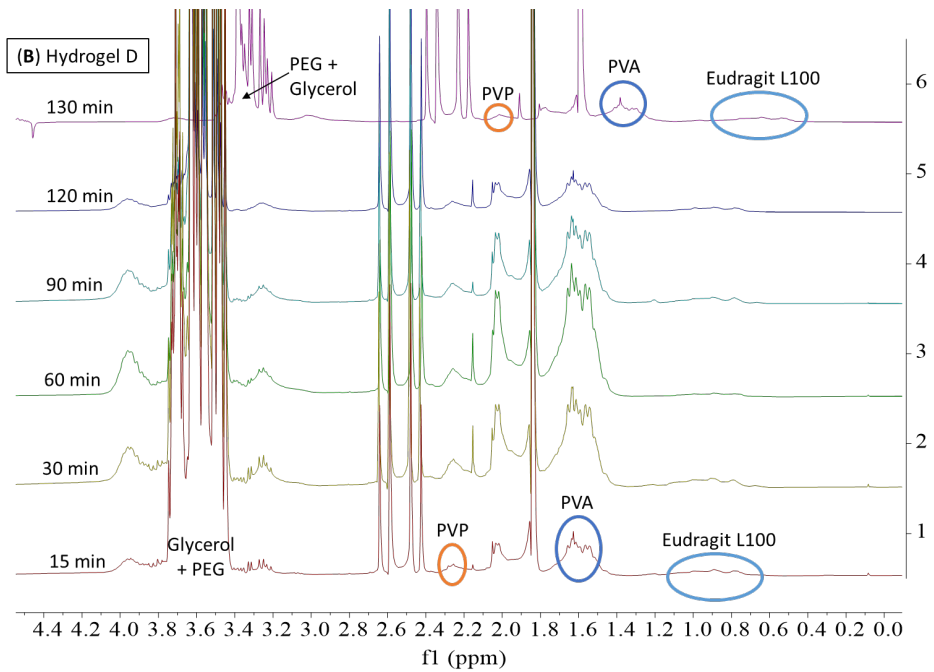
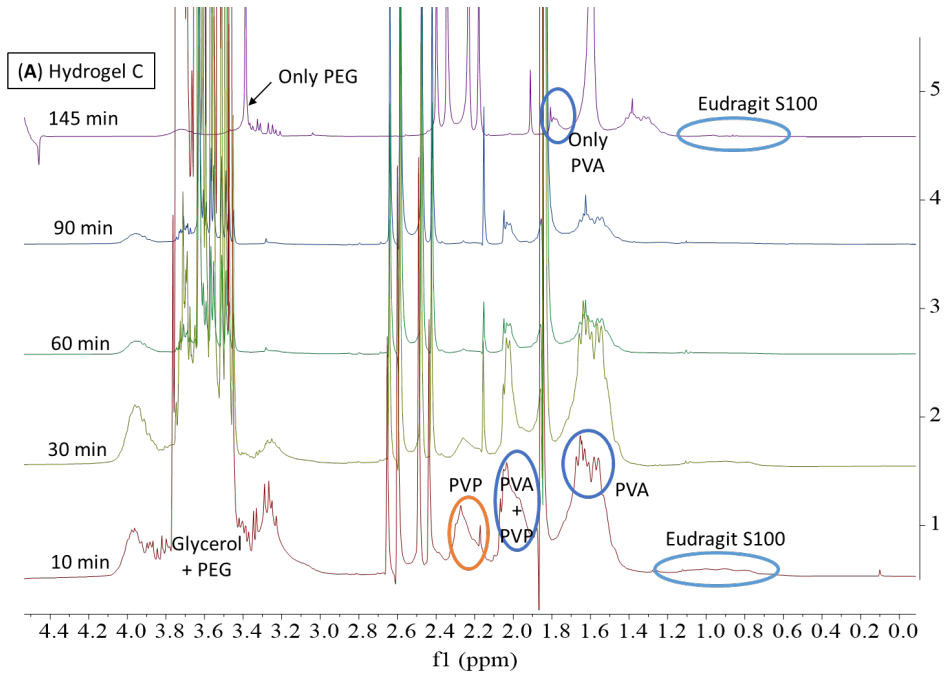


Figure 4.7. $^1\text{H-NMR}$ (300 MHz, BSS/ D_2O 90/10) spectra were obtained during the dissolution of hydrogel A (A) and hydrogel B (B). For hydrogel A (A), spectra 150 min, 180 min and 230 min have been shifted -0.24 ppm to improve signals observation. For hydrogel B (B), spectra 70 and 75 min have been shifted -0.24 ppm to improve signals observation.

Figure 4.7 compares the results obtained for the dissolution of hydrogels A and B. These materials are very similar in structure, as they are composed of hydrophobic Eudragits. As it can be appreciated in the spectra, hydrogel A (**Figure 4.7A**) needed 230 min for its complete dissolution. However, hydrogel B just needed 75 min for the same process. This difference can be explained by attending to the polarity of both Eudragits. Eudragit RL100 (which is part of hydrogel B) has 0.2 number of repeated units of the block that contains a quaternary amine, while Eudragit RSPO (part of hydrogel A) only has 0.1 number of repeated units of this block. This difference gives to the first Eudragit a higher water solubility behaviour than the other one. In **Figure 4.7A** can be appreciated the signals from all the polymers (Glycerol, PEG, PVP, PVA and Eudragit RSPO) after 5 min, which indicates that all the polymers are being dissolved in the aqueous media and been released outside of the hydrogel matrix. Conversely, at the end of the experiment (180 – 230 min), the signals from glycerol and PVP cannot be appreciated. It can be concluded that the dissolution of this matrix is not homogeneous, since the dissolution rate is different for every polymer. As a consequence, the number and strength of the physical interactions, that are stabilizing the matrix, are changing while some polymers are removed. In this case, the permeability of the matrix is decreasing as a function of the absence of glycerol and PVP, increasing the global stabilization of the matrix. This conclusion is reinforced by the results obtained for the dissolution of hydrogel B (**Figure 4.7B**). For this second case, as the global matrix is more soluble, the total time required for the hydrogel dissolution is lower than the one needed for hydrogel A. Furthermore, during the first minute of the hydrogel dissolution, it is possible to observe the signals from all the polymers (PEG, PVP, PVA and Eudragit RL100). Also, at the very end of the experiment (min 75), the signals from all the polymers can be still observed, which confirms that the dissolution of the matrix is more balance.

Hydrogels C, D and E constitute the second group as they are formed by hydrophilic Eudragits. **Figure 4.8** contains the NMR spectra obtained for the dissolution of hydrogels C, D and E.

Screening of Eudragits as building blocks in the preparation of physically cross-linked hydrogels



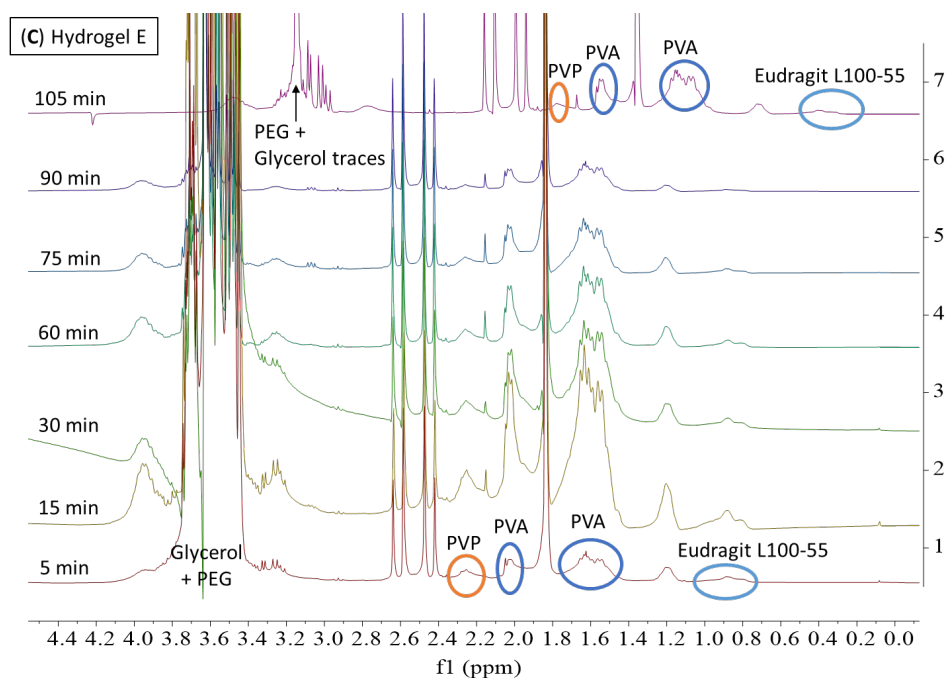


Figure 4.8. $^1\text{H-NMR}$ (300 MHz, BSS/ D_2O 90/10) spectra were obtained during the dissolution of hydrogel C (A) and hydrogel D (B) and hydrogel E (C). For hydrogel C (A), spectrum 145 min has been shifted -0.24 ppm to improve signals observation. For hydrogel D (B), spectrum 130 min has been shifted -0.24 ppm to improve observation. For hydrogel E (C), spectrum 105 min has been shifted -0.24 ppm to improve observation.

Hydrogel C (**Figure 4.8A**) is formed by Eudragit S100, which is water-soluble at a pH higher than 7. The dissolution of the materials has taken place using BSS at physiological pH ($\text{pH} = 7.4$). As both values (7 and 7.4) are quite similar, the polymer is reluctant to be dissolved, having this effect on the whole matrix. As it can be seen, the signal from PVP can be observed in min 10, as well as the signal from glycerol. Meanwhile, at the end of the experiment (min 145), the signals of both polymers cannot be observed anymore. In other words, the dissolution of the matrix is not equal for all the polymers. As in the previous case, the strength and number of physical interactions are changing along the dissolution process. The matrix stability of the hydrogel C is increasing once the PVP polymer is not present anymore, which can be seen attending to the higher required time for the total dissolution (145 min) in comparison with the required one for hydrogels D and E (130 and 105, respectively).

Hydrogels D and E (**Figure 4.8B** and **4.8C**) are formed by Eudragits that are water-soluble at pH higher than 6 and 5.5, respectively. Now, all the polymers from the matrices have similar solubility in the media. Namely, the dissolution of these two matrices is more homogeneous. Both the signals from PVP and glycerol can be seen at the beginning and at the end of the experiment. The main drawback is that also the number of physical forces decreases faster, dissolving the matrices into the media in less time.

4.3.5 Mechanical properties of the hydrogels without hydration: Tensile strain analysis

The elasticity of hydrogels was analyzed in the framework of a collaboration with Prof. Nora Aramburu (from the University of the Basque Country, UPV-EHU). The tensile stress of hydrogels A - E were characterized without further hydration, as reported in the literature.^[59] The raw data shown in this section was obtained by Prof. Aramburu, while the analysis and discussion was done by the PhD candidate.

Each hydrogel was cut in triplicate with the shape of a dogbone and set into the equipment Instron 5569. Then, strain is applied until the materials breaks. Plotting tensile stress versus the percentage of applied tensile strain, several mechanical properties from the materials can be obtained. As can be seen in **Figure 4.9**, from the slope of the elastic deformation area, the young modulus can be obtained. This modulus is directly correlated with the elasticity of the material. The smaller this value, the more elastic and less stiff the material will be. Besides, at the end of the uniform plastic deformation, it is possible to know the maximum stress that it has been applied to the materials before its fracture. Then, in the non-uniform plastic deformation zone of the plot, where the materials are already broken, it is possible to know the tensile brake. Tensile strain analysis of the five hydrogels can allow materials to be sorted based on their stiffness.

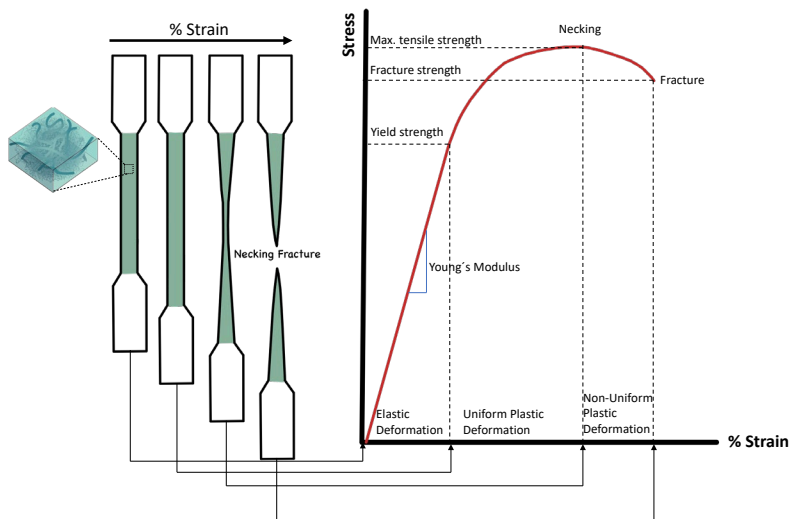


Figure 4.9. The scheme shows the dogbone stands for the hydrogel and the different information that is possible to obtain with the tensile strain analysis.

Figure 4.10 contains the achieved results when the five hydrogels (A – E) were exposed to a tensile strain deformation. In the five plots, it’s easy to observe the elastic and plastic (uniform and non-uniform) areas. It is important to notice that hydrogel C is the only one that shows a big elastic deformation region in comparison with the other hydrogels.

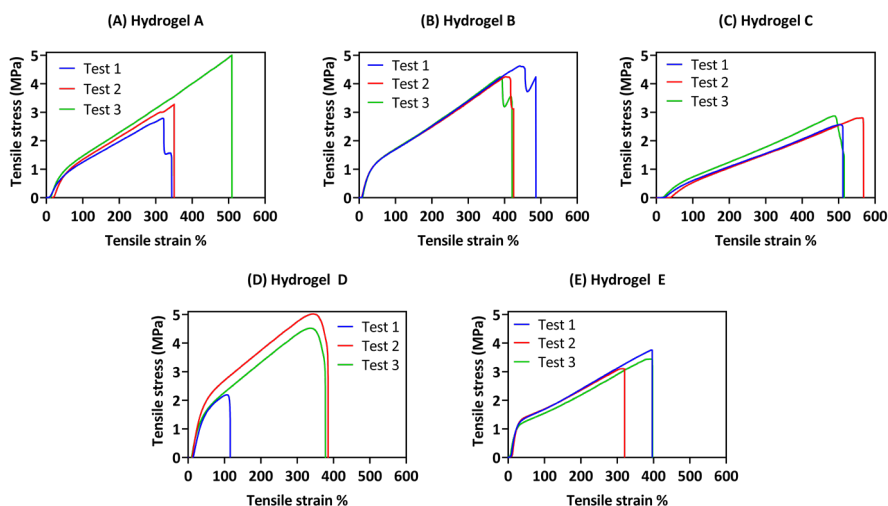


Figure 4.10 Plots of tensile stress versus percentage of tensile strain applied for hydrogels A - E.

The most relevant mechanical properties obtained from the plots shown in **Figure 4.10** are summarized in **Figure 4.11**. It can be seen the

maximum strength applied to hydrogels A – E until they break. Furthermore, the tensile break and young's modulus are also plotted.

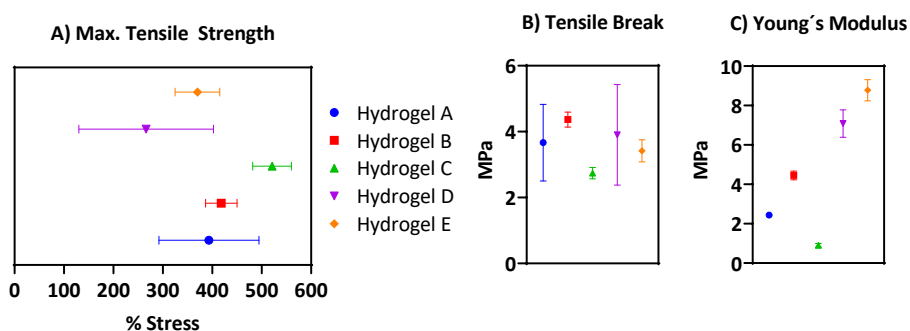


Figure 4.11 Plots showing (A) the maximum tensile strength applied until the material breaks, (B) the tensile break and (C) Young's modulus for hydrogels A – E.

As can be seen in **Figure 4.11 A**, hydrogel C shows the lowest tensile break and young's modulus. Besides, it also shows the highest value of percentage of stress to get the maximum tensile strength. Therefore, hydrogel C is the most elastic material among all of them. In opposite to this, hydrogel D reported the highest tensile break and the lowest percentage of stress to achieve the maximum tensile strength. Even though hydrogel E reports the maximum Young's modulus, the elastic behaviour of hydrogels E and D are quite similar. In between, hydrogels A and B have intermediate behaviours, which means that they are more elastic than hydrogels D and E but less than hydrogel C. Consequently, the order of stiffness according to this experiment, from less to more, is: Hydrogel C < Hydrogel A < Hydrogel B < Hydrogel D < Hydrogel E. It can be hypothesized that as hydrogel C is based on water-soluble Eudragit (at pH = 7) and the polymers mixture has been done at this pH, hydrogel C represents the most homogeneous matrix. Therefore, this material is the most elastic one. Followed by hydrogels based on non-water soluble Eudragit (A and B), which have also reported a homogeneous pre-gel mixture. Hydrogels D and E, based on Eudragits soluble at lower pH, have reported heterogeneity in the dried patch. This has been translated into an increase in the stiffness, as a consequence of not well polymer concentration distribution along the hydrogel matrix. The heterogeneity and phase segregation obtained in these 2 formulations (D and E), can lead to inconsistent measurements of Young's modulus and reduced elasticity values.

It has been mentioned before, that the final objective of the material is to be used as an ocular insert. As the eye contains a high degree of humidity,

the hydrogels will quickly swell decreasing their Young modulus. Nevertheless, hydrogel C looks like the more promising material as it has a low Young modulus even when the material is not hydrated. It is also expected, that the mucoadhesion properties of the materials with the eye mucosa will increase when they swell. To demonstrate this hypothesis, rheology measurements have been tuned to analyse the adhesion of the hydrogel to ocular conjunctiva in presence of humidity. These results are going to be discussed in the following section **4.3.6.2**.

4.3.6 Rheological characterization

In the framework of this research project, a collaboration with the rheology group was established. The raw data shown in this section was obtained by Dr. M^a Mercedes Fernandez San Martin. The analysis of the results was possible thanks to several meetings and discussions over around 3 years.

4.3.6.1 Dynamic oscillatory shear rheological analysis

After the conclusions obtained from mechanical properties analysis, where it was demonstrated the important role of Eudragits, it was necessary to continue understanding their intrinsic properties. In a similar scenario to the previous analysis, where the hydrogels are not hydrated, the dynamic oscillatory rheological analysis took place. Thanks to this experiment, it is possible to determine the temperature's influence on their structures at the dynamic molecular level. A compression deformation for hydrogels A – E has been applied in a dynamic oscillatory mode^[60] at a constant frequency of 1 Hz and a sweep of temperatures. With this assay, it is possible to analyse the thermal transitions and to distinguish the elastic behaviours that correspond to the hydrogel structure and the deformation that occurs as a matter of time, due to the viscous dissipation. **Figure 4.12** shows the scheme of this experiment and the information that can be obtained.

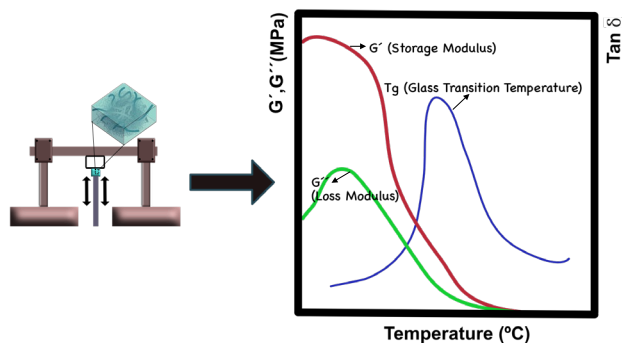


Figure 4.12 Scheme of compression dynamic oscillatory rheology analysis and the information that can be obtained. Storage modulus (G'), loss modulus (G'') and glass transition temperature ($\text{Tan } \delta$).

The results for hydrogels A – E after the compression dynamic oscillatory experiments are shown in **Figure 4.13**. It can be observed the storage modulus G' (**Figure 4.13A**), the loss modulus G'' (**Figure 4.13B**) and the $\text{tan } \delta$ loss tangent (**Figure 4.13C**).

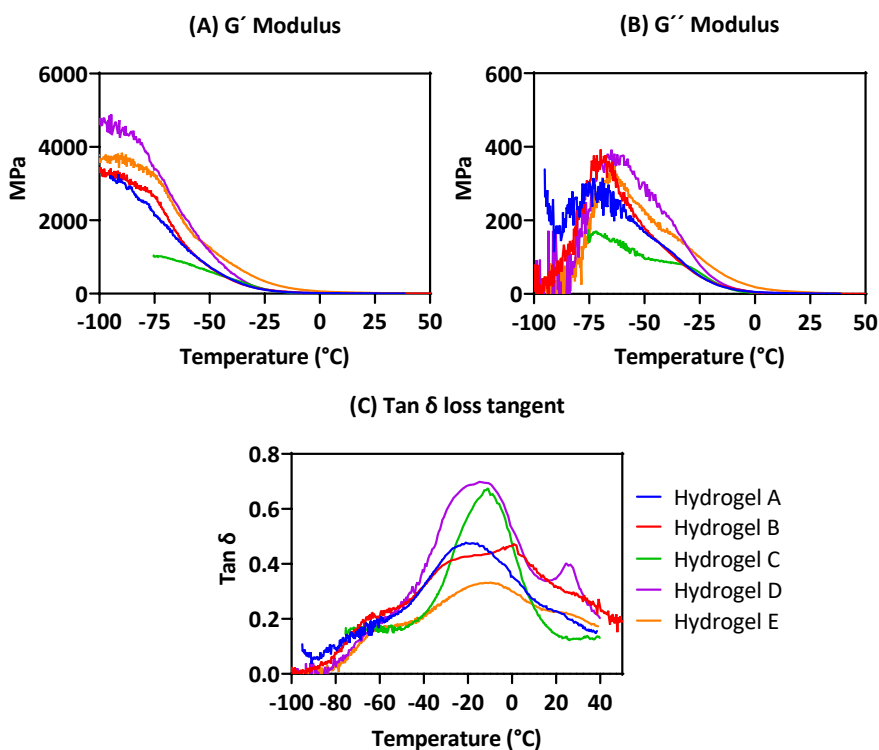


Figure 4.13 Evolution of storage modulus G' , loss modulus G'' and $\text{tan } \delta$ loss tangent at different temperatures and a constant 1 Hz oscillatory frequency compression.

From **Figures 4.13 A and B**, it is possible to observe that storage modulus (G') and loss modulus (G'') only appeared at temperatures lower than $0\text{ }^{\circ}\text{C}$, with maximum values in the range of -50 to $-70\text{ }^{\circ}\text{C}$. In these very low temperatures, the storage modulus, G' , has big values, in the range of MPa. This modulus decreases with the increase of temperature as a consequence of the increase of free movement due to the rise of thermal energy. These behaviours correspond with a gelled system, from rigid structures. The decrease in both moduli means that the hydrogels are softened at higher temperatures. It is worth it to mention that hydrogel C (green lines) show lower values of G' and G'' , which means that is the softest hydrogel among the five of them.

In **Figure 4.13 C**, with the evolution of $\tan \delta$ loss tangent, it is possible to determine the glass transition temperature (T_g) of each hydrogel as the maximum value of $\tan \delta$. The glass transition temperature is the temperature at which an amorphous polymer structure turns viscous liquid or rubbery. **Table 4.2** summarizes the T_g for hydrogels A – E.

Table 4.2 T_g values for hydrogels A – E obtained from Figure 4.13C after compression dynamic oscillatory rheology analysis.

Hydrogel	T_g ($^{\circ}\text{C}$)
A	-19
B	1
C	-11
D	-15
E	-10

As it can be concluded from **Table 4.2** is possible to change the T_g value by just changing the type of Eudragit. Nevertheless, all the values are lower than $37\text{ }^{\circ}\text{C}$, which is the body's normal temperature. Therefore, all the materials will have a viscous structure in their use for biomedical applications.

4.3.6.2 Mucoadhesive properties of hydrogels towards ocular conjunctiva

The main objective of the hydrogels prepared during this work was to use them as ocular inserts. Hence, it was necessary to quantify the

mucoadhesion properties of the materials to guarantee their attachment to the ocular conjunctiva. To quantify the mucoadhesion, a novel technique was optimized with the use of a tack experiment into an Ares rheometer equipment (**Figure 4.14**). Two disks were set into the equipment. On top, the ocular conjunctiva obtained from the rabbit's eye was attached. On the bottom, the hydrogel to be analyzed. First (**Figure 4.14 I**), both disks are getting closer at the constant speed of 0.1 mm/s until contact. Then (**Figure 4.14 II**) both disks continue in contact for 2 minutes at a constant force of 2 N. Finally (**Figure 4.14 III**), the upper disk is detached at a constant speed of 0.3 mm/s. The resistance of hydrogel to be detached from the ocular conjunctiva is registered as a function of time and disk displacement. In other words, the force required to separate the conjunctiva from the hydrogel is known as adhesion work. Plotting the force applied in the function of the disk displacement, it is possible to determine the work of adhesion as the area under the curve.

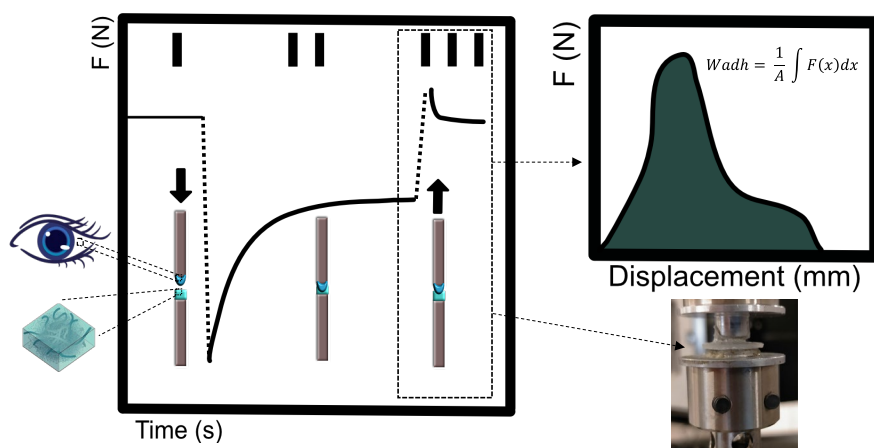


Figure 4.14 Scheme of the hydrogel's mucoadhesive measurements using an Ares instrument. (I) Conjunctiva approximates hydrogel. (II) Conjunctiva and hydrogel together during a certain time. (III) Separation conjunctiva from the hydrogel. Work of adhesion is determined with the formula shown in the figure.

As the eye contains a high degree of water, the materials were analysed in three scenarios at 37 °C (A) without any hydration, (B) after 3 and 5 days in presence of relative humidity of 95% (the same set-up used for the MU in section 4.3.3); (C) after 10 and 30 minutes of adding 20 µL of BSS ophthalmology solution on top of each hydrogel. The objective was to find the optimal scenario and material to be used as an ocular insert, guaranteeing the adhesion to the eye conjunctiva. **Figure 4.15** summarizes the processed data as work of adhesion.

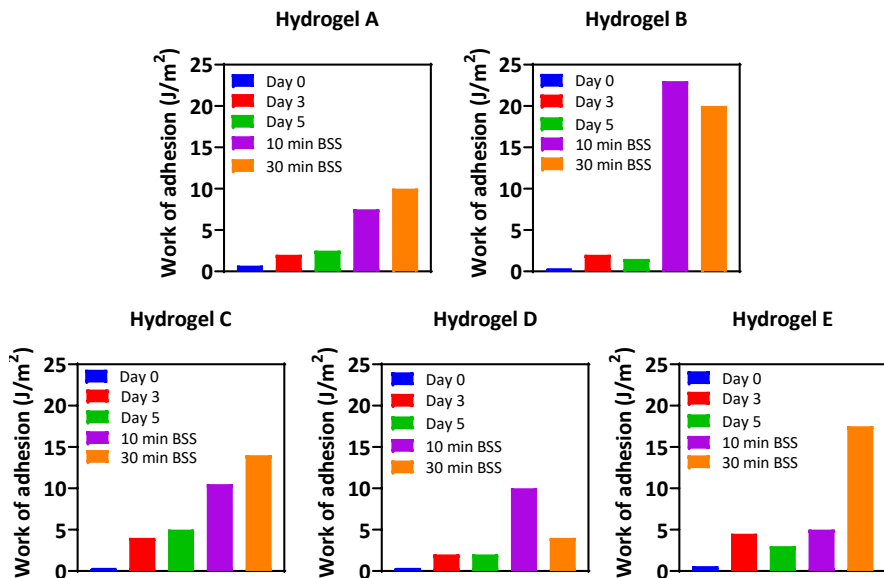


Figure 4.15 Work of adhesion obtained for hydrogels A – E. Day 0 means without hydration, after 3 days hydration being in a 95% of relative humidity, after 5 days hydration being in a 95% of relative humidity, after 10 min of hydration with 20 μL of BSS solution, after 30 min of hydration with 20 μL of BSS solution.

In **Figure 4.15**, it can be seen that all the hydrogels have negligible work of adhesion when they are not hydrated (day 0). Meanwhile, after hydration, the work of adhesion for hydrogels A – E increase with certain differences among them. As it has been reported in the literature^{[61][62]} for similar materials, the adhesion interaction is correlated with the detachment speed and the chain length of the polymers. The dissipation energy in swollen elastic materials^[63] belongs to the break of weak forces between the hydrogel and the conjunctiva, such as electrostatic interactions, interfacial bridging and background hysteresis. As a general tendency, the hydrogels hydrated with 20 μL of BSS buffer for 10 or 30 minutes, exhibit higher work of adhesion than the ones that have been hydrated under a humid atmosphere. These results reveal the great capacity of hydrogels to absorb water and swell in some minutes. As it has been demonstrated in section 4.3.4 with the NMR dissolution rates, some polymers are being dissolved while the hydrogel is hydrated. Consequently, these polymers that are abandoning the hydrogels matrix let an increase in the number of interactions between the hydrogels and the surface of the eye, increasing the mucoadhesion properties of the materials. Hydrogel B is the one that shows the highest work of adhesion, 23 J/m^2 after 10 min of hydration with BSS. Nevertheless, after 30 min of hydration, this value decreases to 20 J/m^2 . The same tendency has been

observed when the hydrogel has been hydrated in a 95% or relative humidity environment. After 3 days of hydration, the work of adhesion was 2 J/m^2 , but after 5 days of hydration, this value decreased to 1.5 J/m^2 . Hydrogel B was the fastest to be dissolved in the stability assay shown in section 4.3.4. That result matches with the decreased tendency of work of adhesion. The reduced number of polymers also decreases the number of interactions between the eye and the hydrogel, decreasing the work of adhesion. Hence, among the five hydrogels, material B is not too interesting to be used as an ocular insert.

Hydrogel D reported a similar tendency to the one observed in hydrogel B. An increase in the hydrogel's hydration produces a decrease in the work adhesive value, being 10 J/m^2 after 10 min of hydration and 4 J/m^2 after 30 min of hydration. In addition, hydrogel D has reported the minimum work of adhesion among the five hydrogels, which makes it the worst option to use in ophthalmology applications.

Hydrogels A and C look like the most promising materials to be used as ocular inserts from the mucoadhesion properties point of view. Both show a constant increase in the mucoadhesion while the hydration is growing. Nevertheless, after 30 min, hydrogel C shows 14 J/m^2 of work of adhesion, while hydrogel A only reports 10 J/m^2 , which makes the first hydrogel the possible winner.

Finally, hydrogel E shows an intermediate behaviour between all of them. After hydrating it for 10 min with BSS buffer, the work of adhesion was 5 J/m^2 , but, after 30 min it was 17.5 J/m^2 . This hydrogel shows a large increase in mucoadhesiveness after long periods of hydration. This strategy has an important drawback, the stability of the matrix could be compromised if it is hydrated for very long periods, as has been demonstrated in section 4.3.3.

It can be concluded that hydrogels A and C are the most promising candidates to be used as ocular inserts. Nevertheless, it is necessary to test their capacities as protein drug delivery and their possible cytotoxicity to confirm a potential application.

4.3.7 Thermal and X-ray diffraction characterization for hydrogels' opacity comprehension

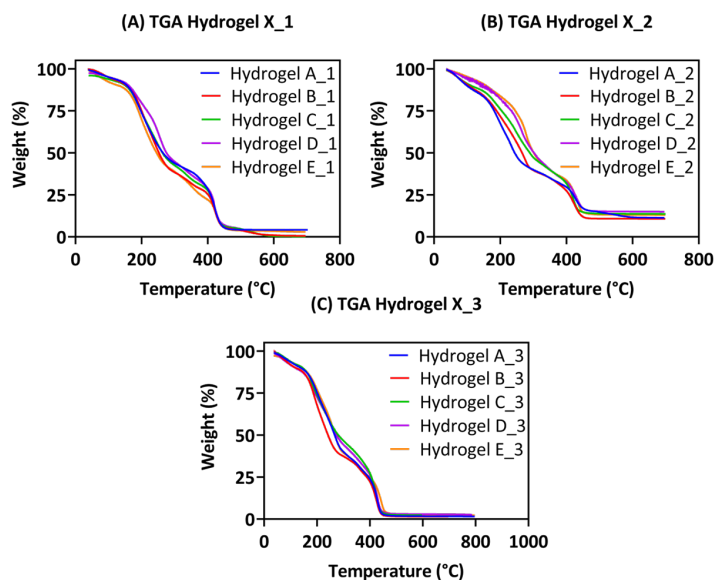
In section 4.3.1, Figure 4.2, it was observed that the opacity varies within hydrogels A – E. It has been hypothesized that this opacity is caused by crystallization during the gelation process. To prove this, X-ray studies have

taken place in collaboration with Prof. Alejandro J. Müller and Dr. Eider Matxinandiarena (from Advanced Multiphasic Materials group, Polymat, UPV-EHU) and B.Sc. Ruth Schmarsow (from Nanostructured Polymers group, Institute of Materials Science and Technology Research, INTEMA, Argentina). The raw data from thermogravimetric analysis (TGA) and differential scanning calorimetry (DSC) shown in this section was acquired by Dr. Matxinandiarena. The WAXS raw data was obtained as an external service from the University of the Basque Country. The analysis and discussion were done by the PhD candidate with external scientific support from collaborators.

A total of 15 samples were prepared and divided into three groups. A) Empty hydrogels A – E empty, named as hydrogel X_1. B) Hydrogels A – E with BSA protein encapsulated inside of them, named hydrogel X_2. C) Hydrogel A – E with BSA-FITC encapsulated inside of them, named hydrogel X_3. In the last group, C, the protein BSA was chemically labelled with the fluorophore fluorescein isothiocyanate (FITC).

4.3.7.1 Thermogravimetric analysis (TGA)

At first, TGA has been done to determine the humidity content of each material and the degradation temperatures. **Figure 4.16** contains the TGA obtained for the 15 samples in the three mentioned scenarios (**Figure 4.16 A, B and C**) and the commercial polymers and proteins used as a reference for the data analysis (**Figure 4.16 D and E**). A temperature summary of the 5, 10 and 50% of weight lost is shown in **Table 4.3**.



Screening of Eudragits as building blocks in the preparation of physically cross-linked hydrogels

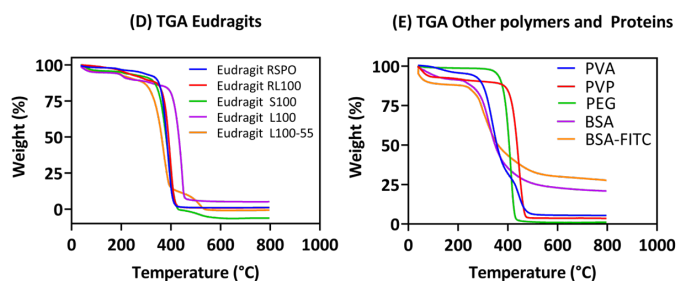


Figure 4.16. TGA plots for Hydrogels A – E in three scenarios. (A) Empty hydrogels. (B) Hydrogels with BSA. (C) Hydrogels with BSA-FITC. (D) Eudragits as controls. (E) Rest of the polymers and proteins used for hydrogel preparation.

Table 4.3 Summary of the temperatures at which 5, 10 and 50% of the total weight has been lost. Data is shown for Hydrogels A – E in the three scenarios. 1) Empty hydrogels. 2) Hydrogels with BSA. 3) Hydrogels with BSA-FITC.

Sample Code	T (°C): Loss 5 % of Weight	T (°C): Loss 10 % of Weight	T (°C): Loss 50 % of Weight
Hydrogel A_1	111.6	156.2	264.7
Hydrogel A_2	71.2	99.5	243.8
Hydrogel A_3	85.4	138.9	267.2
Hydrogel B_1	100	154.1	252.5
Hydrogel B_2	71.5	104.3	266.3
Hydrogel B_3	75.2	120.1	241.8
Hydrogel C_1	78.5	151.5	263.5
Hydrogel C_2	71.9	111.7	289.5
Hydrogel C_3	88.5	146.1	280.8
Hydrogel D_1	103.4	161.5	275.2
Hydrogel D_2	91	143.3	302.3
Hydrogel D_3	71.9	118.2	273.6
Hydrogel E_1	75.7	131	245.7
Hydrogel E_2	104.5	157.7	301.1
Hydrogel E_3	81.7	142.5	268.6
Eudragit RSPO	273.9	343.4	382.7
Eudragit RL100	213.4	297.5	390.5
Eudragit RL100	213.4	297.5	390.5
Eudragit S100	197.9	319.9	380.5
Eudragit L100	87.6	239.3	432.2
Eudragit L100-55	176.6	251.7	362.8
PVA	240.9	292	356.5
PVP	68.5	316.6	437.5
PEG	357.1	373.3	405.7
BSA	90.9	229.7	348.9
BSA-FITC	41.3	76.9	360.8

As it can be observed in **Figure 4.16** and **Table 4.3**, the temperature required for a 5% loss of weight changes dramatically from one formulation to another. In the case of empty hydrogels (scenario 1), hydrogels C and E lose 5% of their weight with temperatures in the range of 75 – 78 °C. In contrast, the rest of the materials, hydrogels A, B and D need temperatures above 100 °C for the same loss of weight. These big differences decrease when more amount of weight is lost. These results match with the temperatures needed to lose weight on the Eudragit references, which highlights the important role of this polymer in the matrix formulations. Nevertheless, when BSA is encapsulated inside of them, scenario 2, the required temperature to eliminate the 5 and 10% of a weight drops for hydrogels A – D and it rises for hydrogel E. It can be concluded that BSA protein can reinforce the physical interactions between polymers in hydrogel E, being this material more robust at higher temperatures. Attending now to the 50% of weight lost, the temperature required is higher when the BSA is present for hydrogels B – E and lower for hydrogel A. Therefore, this confirms that BSA protein can increase the stability of hydrogels, at least in the case of more hydrophilic formulations (hydrogels C, D and E). Hydrogel A has the most hydrophobic formulation. It is quite probable that after losing half of the weight of this material, the instability achieved could compromise the interactions between the BSA and the polymeric chains. Therefore, this will end up in a decrease in the global heating temperature in this particular case.

Scenario 3 raises the presence of BSA chemically conjugated with a hydrophobic fluorophore (FITC). Hence, the tendencies observed are different from the previous case. The presence of a hydrophobic small molecule reinforces the polymeric physically cross-linked chain in hydrogels A, C and E. In these three cases, the temperature to remove half of the weight is higher than the one required when the hydrogels are empty. For hydrogels B and D the temperature needed for loss of half of the weight decreases a little bit, but with similar values to the empty hydrogels.

To shed light on the obtained results, the first derivative of the TGA curve was plotted to determine inflexion points useful for in-depth interpretations and differential thermal analysis understanding. **Figure 4.17** contains the first derivative of the TGA curve for hydrogels A – E in the three scenarios previously discussed. Furthermore, the figure also contains the first derivative for the TGA curve for Eudragits, PVA, PVA, PEG, BSA and BSA-FITC to be used as references in the rationale discussion of the results. **Table 4.4** summarize the maximum peaks obtained from the first derivative curve for

each analysis. To simplify, the table has been divided into two regions. Region 1 (100 – 350 °C), region 2 (350 – 700 °C).

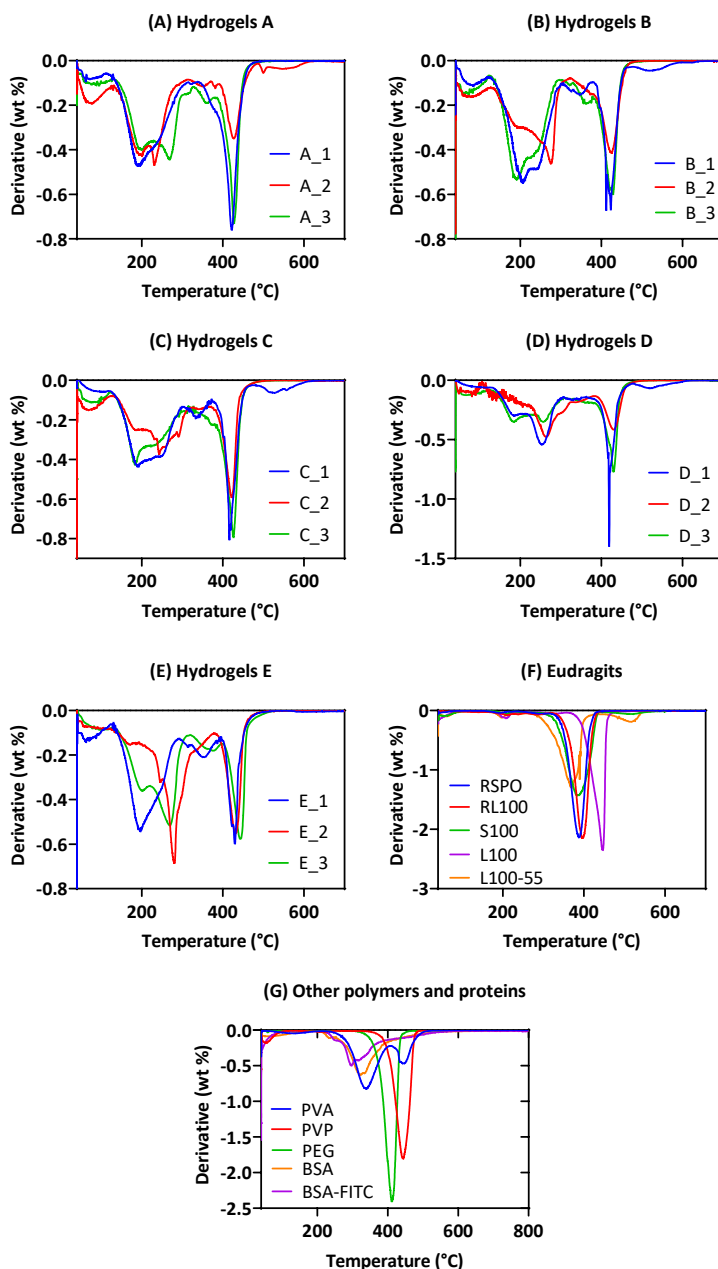


Figure 4.17. (A – E) First derivative of the TGA curve for hydrogels A – E. (X_1) Empty hydrogels. (X_2) Hydrogels with BSA. (X_3) Hydrogels with BSA-FITC. (F) First derivative of the TGA curve for Eudragits pure polymers. (G) First derivative of the TGA curve for the rest of polymers and proteins used for hydrogel's preparation.

Table 4.4 Summary of the temperatures from the maximum peak obtained from the first derivative of the TGA curve.

Sample Code	(Region 1) Max. Peak T (°C)	(Region 2) Max. Peak T (°C)
Hydrogel A_1	190	-
Hydrogel A_2	198	231
Hydrogel A_3	195	266
Hydrogel B_1	205	-
Hydrogel B_2	275	-
Hydrogel B_3	190	-
Hydrogel C_1	188	-
Hydrogel C_2	241	-
Hydrogel C_3	183	-
Hydrogel D_1	181	250
Hydrogel D_2	266	-
Hydrogel D_3	180	255
Hydrogel E_1	195	-
Hydrogel E_2	279	-
Hydrogel E_3	199	269
Eudragit RSPO	-	-
Eudragit RL100	-	-
Eudragit S100	-	-
Eudragit L100	-	-
Eudragit L100-55	-	-
PVA	337	-
PVP	-	-
PEG	-	-
BSA	322	-
BSA-FITC	295	-

The region obtained between 40 and 100 °C belongs to water evaporation and dehydration of the materials. Consequently, data below 100 °C will not be taken into account for the following discussion.

In **Figure 4.17 A – E**, it is easy to observe that region 2 always contains an intense band in comparison with region 1. To explain this, it is enough to have a look into the calcination temperature for neat polymers, **Table 4.4**, where it can be seen that all of them have it around 400 °C. The peaks observed in region 1 correspond to BSA and PVA. Furthermore, as can be corroborated in **Table 4.4**, the maximum temperature values are correlated with the hydrogels and BSA-FITC encapsulated in them. So, as it was concluded before, the presence of a hydrophobic small molecule reinforces the polymeric physically cross-linked chain of the hydrogels. Nevertheless, the temperature is also higher when the BSA is encapsulated inside the hydrogel

than when they are empty. This also reaffirms that proteins can increase the global stability of the hydrogels, increasing the number of physical forces that are forming the polymeric network.

4.3.7.2 Differential Scanning Calorimetry (DSC)

Even though with the TGA analysis it has been concluded that Eudragits polymers and proteins play an important role in the thermal hydrogel stabilization, it was not possible to prove the formation of crystals during the gelation process. To try to discern the presence or absence of crystals inside the hydrogels, non-isothermal DSC experiments have been carried out. This technique is a thermal analysis in which the heat flow into or out of a sample is measured as a function of temperature or time. This can be used to characterize and identify the different transitions. **Figure 4.18** shows the heating and cooling scans for hydrogel A in the three scenarios previously described. Scenario_1 empty hydrogel A, scenario_2 hydrogel A with encapsulated BSA and scenario_3 hydrogel A with encapsulated BSA-FITC. Moreover, the experiment has been replicated after 24 h in tandem, starting from the material previously heated twice the day before. The heating and cooling rate was 20 °C/min. **Table 4.5** summarises the temperature at which endothermic peak (T_p) is obtained and the observed enthalpy of the melting endotherms (ΔH_p).

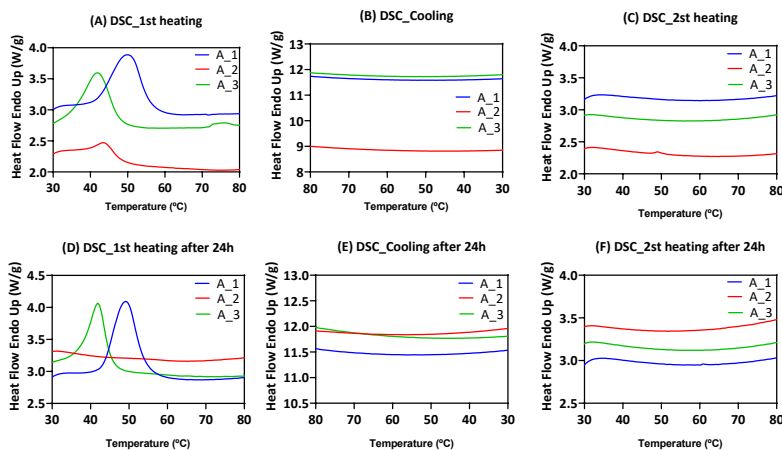


Figure 4.18 (A) DSC results of the first heating for hydrogel A. A_1 empty hydrogel A. A_2 hydrogel A with BSA. A_3 hydrogel A with BSA-FITC. (B) DSC of the cooling curve. (C) DSC of the second heating curve. (D) DSC of the first heating curve after 24 hours. (E) DSC of the cooling curve in the second experiment. (F) DSC of the second heating curve in the second experiment. The heating and cooling rate for all the cases are 20 °C.

Table 4.5 Summary of the endothermic peak T_p and the enthalpy of the melting endotherms for hydrogels A. A_1 empty hydrogel. A_2 hydrogel A with BSA. A_3 hydrogel A with BSA-FITC. Data obtained from DSC analysis.

Sample Code	T_p , peak ($^{\circ}\text{C}$) (1 st heating)	ΔH_m (J/g)
Hydrogel A_1	50.1	24.8
Hydrogel A_2	43.6	4.8
Hydrogel A_3	42	16.1
Hydrogel A_1 (after 24 h)	49	24.7
Hydrogel A_2 (after 24 h)	-	-
Hydrogel A_3 (after 24 h)	42	16.1

In the DSC results corresponding to the first heating curves for hydrogel A with and without BSA proteins, **Figure 4.18A** can be seen peaks for the three samples. In addition, the melting temperatures are achieved at a lower temperature for hydrogels A_2 (43.6 $^{\circ}\text{C}$) and A_3 (42 $^{\circ}\text{C}$), than the ones that do not contain BSA protein as hydrogel A_1 (50.1 $^{\circ}\text{C}$). This reinforces the important role that proteins play in the physical interactions of the material. However, after cooling down (**Figure 4.18B**) and heating the material again (**Figure 4.18C**), it is not possible to observe any peak. It was hypothesized that the reason could be that there is no crystal formation during the gelation process. To prove it, the resulting material after the second heating was stored and re-heated after 24 h (**Figure 4.18D**). Then, the maximum peaks were observed again for hydrogels A_1 and A_3, with similar values to 24 h before. Thus, it is concluded that physically cross-linked hydrogels need several hours to form the hydrogel (with crystals) again after their dissolution. This is the reason why in the second heating curve it is not possible to observe any transition.

Table 4.5 collects the enthalpy of melting endotherms calculated from the DSC data, which gives an idea of the strength forces that are forming the hydrogels. For empty hydrogel A_1, ΔH_m is 24.8 J/g. When BSA is encapsulated inside this hydrogel, ΔH_m decrease to 4.2 J/g. However, when the BSA is modified with FITC, ΔH_m increase from 4.2 to 16.1 J/g. These values highlight that the cohesive energies are influenced by the presence of the protein. It is surprising that when FITC is also present, the enthalpy values increase considerable, meanwhile, when the BSA is not modified with FITC, the enthalpy values are even lower. As FITC is a small hydrophobic molecule, and hydrogel A is based on Eudragit RSPO, which is also hydrophobic, FITC may increase the number of physical interactions between polymeric chains.

Therefore, the bonds are strengthened, increasing the melting enthalpy values, even when BSA is also present.

The crystals that might be formed during the gelation process are PVA and PEG. According to the literature, the melting endotherms that correspond to net crystals formed by these polymers are 138.60 J/g (PVA) and 173.21 J/g (PEG).^{[64][65]} Applying formula (**Equation 4.1**), it is possible to determine the crystal fractions obtained (X_c) for each material. **Table 4.6** summarizes the crystal fractions observed by DSC.

$$X_c = \frac{\Delta H_m \text{ experimental}}{\Delta H_m \text{ net PVA} + \Delta H_m \text{ net PEG}} * 100 \text{ (Equation 4.1)}$$

Table 4.6 Summary of the crystal fractions obtained by DSC for hydrogel A, scenarios 1 – 3.

Sample Code	Xc (%)
Hydrogel A_1	7.95
Hydrogel A_2	1.54
Hydrogel A_3	5.16

As the PVA and PEG crystals fractions (**Table 4.6**) are very low in comparison with the big peaks observed in **Figure 4.18**, it can be concluded that melting endotherms are influenced by two components. On the one hand the presence of PVA and PEG crystals. On the other hand, endotherms from the gel transition to sol (liquid). One might mention that the crystal fraction is reduced when the hydrogel is loaded with BSA (from 7.95% to 1.54%). The BSA has a water solubility of 40 g/L, demonstrating that it is a high hydrophilic biomolecule. Thus, when it is inserted during the gelation process of the hydrogels, it increases the global solubility of the matrix, decreasing the appearance of crystals. In contrast, when the BSA is chemically conjugated with the fluorophore FITC, the small molecule increases the global hydrophobicity of the matrix. This tendency to decrease the dissolution capacity of the polymeric chains has as a consequence an increase in the number of crystals that are formed during the gelation process. This effect can be observed attending to the crystal fraction. When the hydrogel is loaded with BSA-FITC, the crystal fraction is 5.16%, which is a similar value to the one obtained for empty hydrogels. Besides, it might be present crystals from other polymers. However, to clarify this it will be necessary X-ray diffraction analysis (section **4.3.7.3**).

The same DSC study has been done for hydrogels B – E. **Figure 4.19** contains the resulting plots for this analysis. **Table 4.7** summarises the melting temperature at which peak maximum (T_m) is obtained, the observed enthalpy of the melting endotherms (ΔH_m) for hydrogels B – E and the crystal fraction.

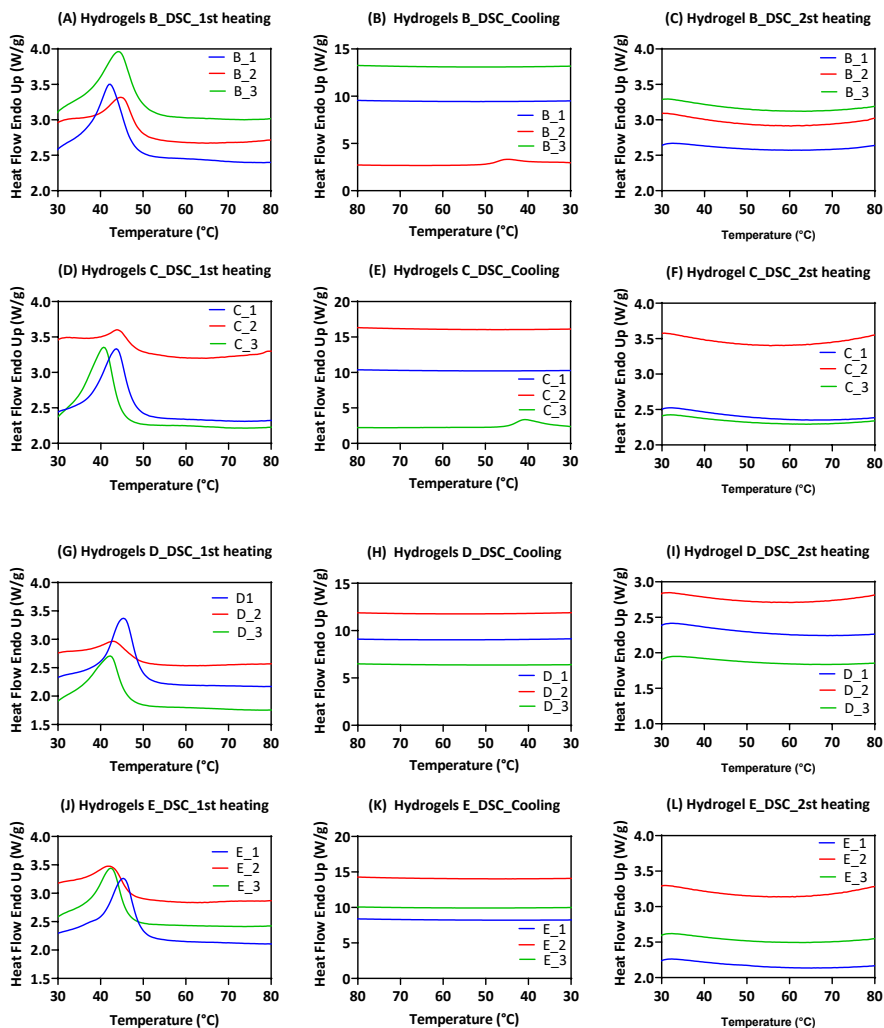


Figure 4.19. X_1 empty hydrogel A. X_2 hydrogel A with BSA. X_3 hydrogel A with BSA-FITC. (A, D, G, J) DSC of the first heating for hydrogels B, C, D and E respectively. (B, E, H, K) DSC of the cooling curve for hydrogels B, C, D and E respectively. (C, F, I, L) DSC of the second heating curve for hydrogels B, C, D and E respectively. The heating and cooling rate for all the cases are 20 °C.

Table 4.7 Summary of the temperatures at maximum peak, the enthalpy of the melting endotherms and the crystals fraction for hydrogels B - E. X_1 empty hydrogel. X_2 hydrogel with BSA. X_3 hydrogel with BSA-FITC. Data obtained from DSC analysis.

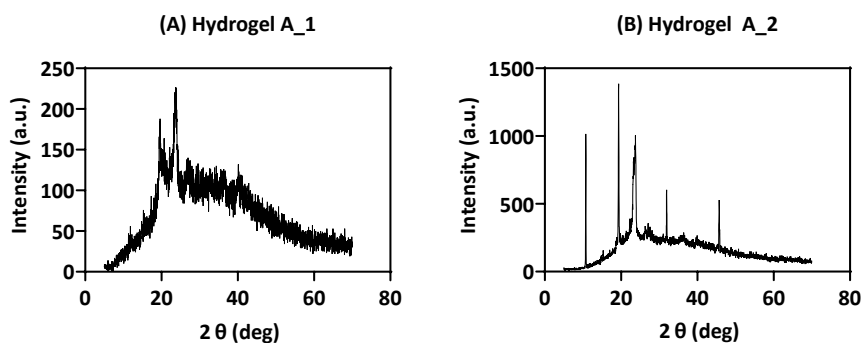
Sample Code	T _m , peak (°C) (1 st heating)	ΔH _m (J/g)	X _c (%)
Hydrogel B_1	42.4	19.4	6.22
Hydrogel B_2	44.9	9.5	3.05
Hydrogel B_3	44.4	17.5	5.61
Hydrogel C_1	43.7	19.6	6.28
Hydrogel C_2	43.9	5.3	1.7
Hydrogel C_3	40.7	24.7	7.92
Hydrogel D_1	45.4	21.9	7.02
Hydrogel D_2	42.9	7.9	2.53
Hydrogel D_3	42.3	22.2	7.12
Hydrogel E_1	45.4	20.2	6.48
Hydrogel E_2	42.3	15.5	4.97
Hydrogel E_3	42.4	17.4	5.58

In **Figure 4.19 C, F, I, L** it can be observed that the second heating scan of DSC analysis does not show any peak. As it happened in the previous case for hydrogel A, after the first heating curve, hydrogels need more time to form again the matrix. Nevertheless, in the first heating curve (**Figure 4.19 A, D, G, J**) it is possible to observe peaks for empty hydrogels B – E and with BSA, BSA-FITC. Therefore, it can be confirmed that the largest transition observed in these conditions, for these samples, is related to the heat exchange involved in the crystal melting process and the gel-sol transitions. These crystals appeared during the gelation process and they are partially presumably responsive to the opacity observed in the hydrogels. In **Table 4.7** a similar tendency for the enthalpy values to the ones analysed for hydrogel A can be observed. When the BSA is encapsulated inside the hydrogels, the enthalpy of the melting endotherms decreases to more than half of the enthalpy for empty hydrogels in B – D samples. This affects the crystal fraction, similarly to the previous reported hydrogel A. Now, for hydrogel B, it drops from 19.4 to 9.5 J/g, and the crystal fraction is decreased to half. For hydrogel C from 19.6 to 5.3 J/g, which influences 3.7 times less amount of crystal fraction. For

hydrogel D from 21.9 to 7.9 J/g, 2.7 times less amount of crystal fractions. However, for hydrogel E, the enthalpy only decreases from 20.2 to 15.5 J/g, which can be translated into 1.3 times less crystal fraction. Attending **Table 4.7**, it has found more crystal fractions when the BSA was conjugated with FITC than when it not was. In the case of hydrogel B, with BSA it has been found 3.05% of crystal fraction and with BSA-FITC, 5.61%. For hydrogel E, the jump has been from 4.97% to 5.58%. In hydrogels formed by more hydrophilic matrices (like hydrogel C and D), the enthalpy of the melting endotherms increases from 19.6 to 24.7 (from 6.28% of crystal fraction to 7.92%) and 21.9 to 22.2 J/g (from 7.02% of crystal fraction to 7.12%), respectively. These experimental data reaffirm the growth of more crystals when the gelation process takes place in presence of a hydrophobic molecule. In addition, as was observed for hydrogel A, the enthalpy endotherms are also influenced by a combination between the melting crystals and the gel-sol transitions.

4.3.7.3 Wide-angle X-ray scattering (WAXS)

To further characterize the crystals formed inside the hydrogels during the gelation process, wide-angle X-ray scattering (WAXS) measurements were performed. WAXS X-ray crystallography is based on the analysis of Bragg peaks scattered to wide angles. To clarify, Bragg peak, discovered by William Henry Bragg in 1903, is an intense peak in the Bragg curve, which plots the energy lost during ionizing radiation. These peaks appear immediately before the particles relax. WAXS measurements were performed with empty hydrogels A and C and with BSA and with BSA-FITC to confirm the presence or absence of crystals. **Figure 4.20** shows the obtained results after WAXS analysis. One might mention that hydrogels mainly show an amorphous halo with several crystalline signals.



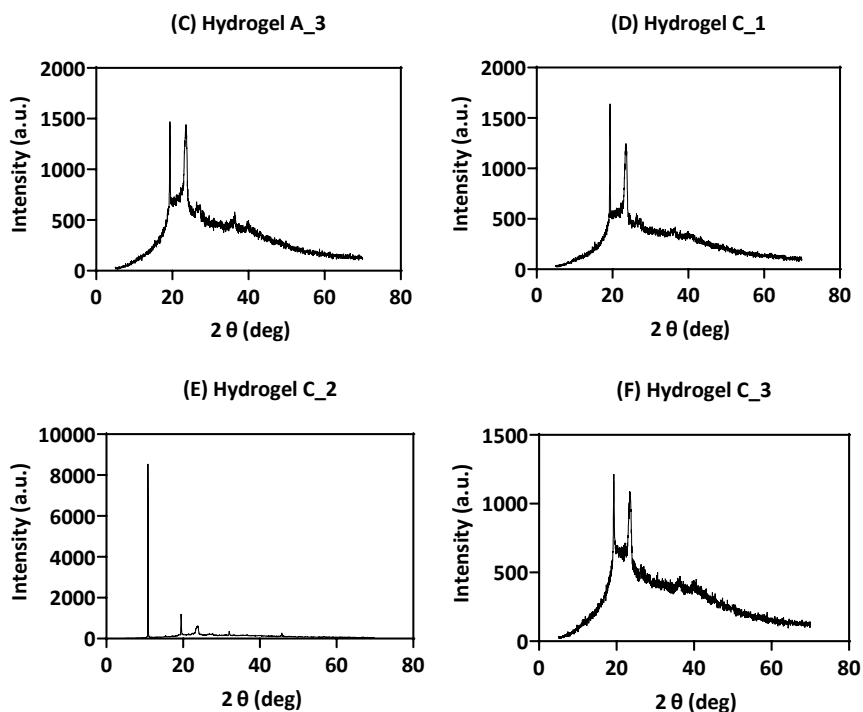


Figure 4.20 WAXS analysis of (A) empty hydrogel A. (B) hydrogel A with BSA. (C) hydrogel A with BSA-FITC. (D) empty hydrogel C. (E) hydrogel C with BSA. (F) hydrogel C with BSA-FITC.

In **Figure 4.20** Bragg peaks at 19 and 23 degrees for the six formulations can be seen. Formulations with BSA (**Figure 4.20 B and E**) also show Bragg peaks at 10, 31 and 45 degrees. The reason for this is that BSA has been dissolved in the PBS buffer. This buffer is made of NaCl, KCl, Na₂HPO₄ and KH₂PO₄. During the gelation process, the inorganic salts are dried, thereby forming crystals. Nevertheless, it is also worth to mention that the intensity of signals at 19 and 23 degrees are reduced for hydrogels A₂ and C₂, in comparison with the other formulations. For materials A₁, C₁, A₃ and C₃, there are no inorganic salts used during the gelation process. Therefore, signals at 19° and 23° belong to polymeric crystals. According to literature, polyvinyl alcohol^[64] crystallizes giving a peak at 19 degrees in WAXS profiles. Therefore, some of the signals that appeared during the gelation process are PVA crystals. The Bragg peak at 23 degrees belongs to PEG polymer, as has been reported in previous studies.^[65]

It is possible to determine the crystal fraction from WAXS measurements by integrating the area under the curve for each peak and

dividing this number by the total area. **Table 4.8** contains the crystal fraction for PVA and PEG crystals for scenarios 1 and 3. The signals obtained for scenario 2 could not be integrated properly.

Table 4.8 Summary of PVA and PEG percentage of crystals presented in hydrogels A_1, A_3, C_1 and C_3.

Sample Code	Xc% (PVA)	Xc% (PEG)
Hydrogel A_1	1.58	2.06
Hydrogel A_3	1.69	4.09
Hydrogel C_1	1.61	3.42
Hydrogel C_3	1.52	2.35

From **Table 4.8**, it can be concluded that the number of crystals is quite low. Besides, in all the formulations there are more amount of PEG crystals than PVA. Also, as observed by DSC, for hydrophobic formulations (hydrogel A), a hydrophobic molecule (FITC, scenario 3) promotes the appearance of crystals. However, in hydrophilic hydrogels (hydrogel C), the FITC reduces the number of crystals that can be formed during the gelation process. However, when the BSA is not modified with FITC, it is possible to observe an increase in the global hydrophilicity of the matrices, reducing the number of crystals, which can be seen in a reduction of the Bragg's peaks intensity in WAXS analysis.

4.3.8 Encapsulation and release of bovine serum albumin

Proteins, that are long chains of amino acids and can be found in all living organisms, have been used recently as therapeutic agents thanks to their multiple applications.^[66] For instance, they can catalyse bioreactions in misfolding diseases (e.g., cystic fibrosis),^[67] block antibodies in pulmonary delivery,^[68] or be one of the fundamental components of the most newer vaccines.^[69] However, their lack of stability during the delivery, combined with the necessary to address many biological barriers (e.g., mucosa layer, blood brain barrier), represents a bottleneck for their biomedical applications.^{[70][71][72]} Nowadays, scientifics have overcome these problems by developing smart vehicles that are able to carry the protein to the desired place, decreasing the negative effects and improving the therapeutic

efficacy.^{[73][74]} In particular, hydrogels have raised researchers' interest to act as protein delivery vehicles due to their excellent biocompatibility.^{[75][76]}

It can be expected that the hydrogels developed in this work can load proteins inside their matrices to release them afterwards. To prove it, fluorescently labelled Albumin (BSA-FITC) has been encapsulated. This protein is widely used as a model for encapsulation due to its low cost, biodegradability, low toxicity and high stability.^[77] The use of a fluorophore-modified protein allows the observation of the encapsulation homogeneity in the hydrogel film. Moreover, the fluorophore also improves the subsequent release analysis by the quantification with UV-Visible and fluorescence spectrophotometry.^[78] **Figure 4.21** shows the aspect of the five hydrogels after the BSA-FITC encapsulation (top) and the aspect after irradiation with light with a 254 nm wavelength (bottom).

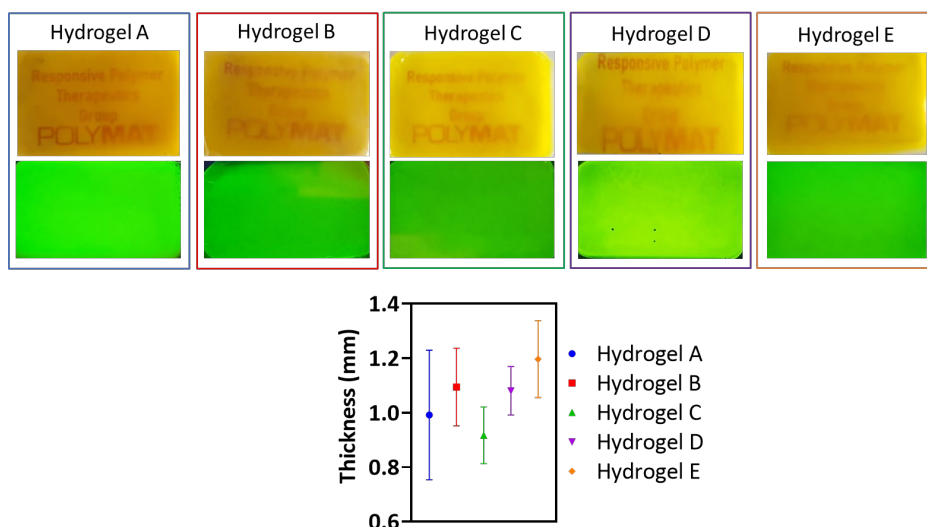
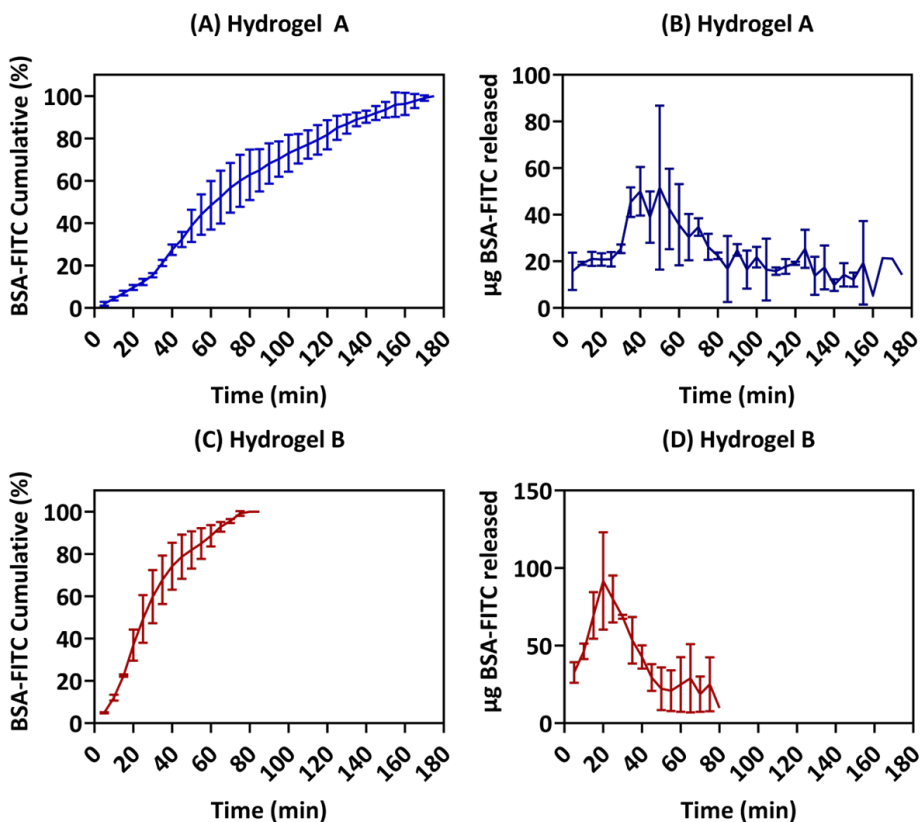


Figure 4.21. Hydrogels A – E with BSA-FITC protein encapsulated inside the materials and their average thickness (mm). The aspect of the materials with direct observation (top) and aspect after irradiation with 254 nm wavelength (bottom).

The orange appearance of the materials corresponds to the BSA-FITC. For the same reason, a green colour after irradiating the material with light of 254 nm can be observed. As the green colour is homogeneously distributed along with the whole hydrogel film, it can be concluded that the BSA protein is well dispersed. In other words, hydrogels A – E are good materials to be used as protein carriers.

For the release of BSA-FITC from hydrogels A – E, the same methodology used in section 4.3.4 has been applied. A 3D-printed mould has held the hydrogel while a constant flow of BSS runs over the surface. As it has been observed in the previous section, the dissolution rate for the hydrogels is different between them. Therefore, a difference in the kinetics of protein release for the five materials can be expected. **Figure 4.22** contains the released obtained as a percentage of accumulated released and μg of protein released along the time. **Table 4.7** shows the min at which the 50%, 80% and 100% and maximum BSA-FITC protein is released from hydrogel A – E.



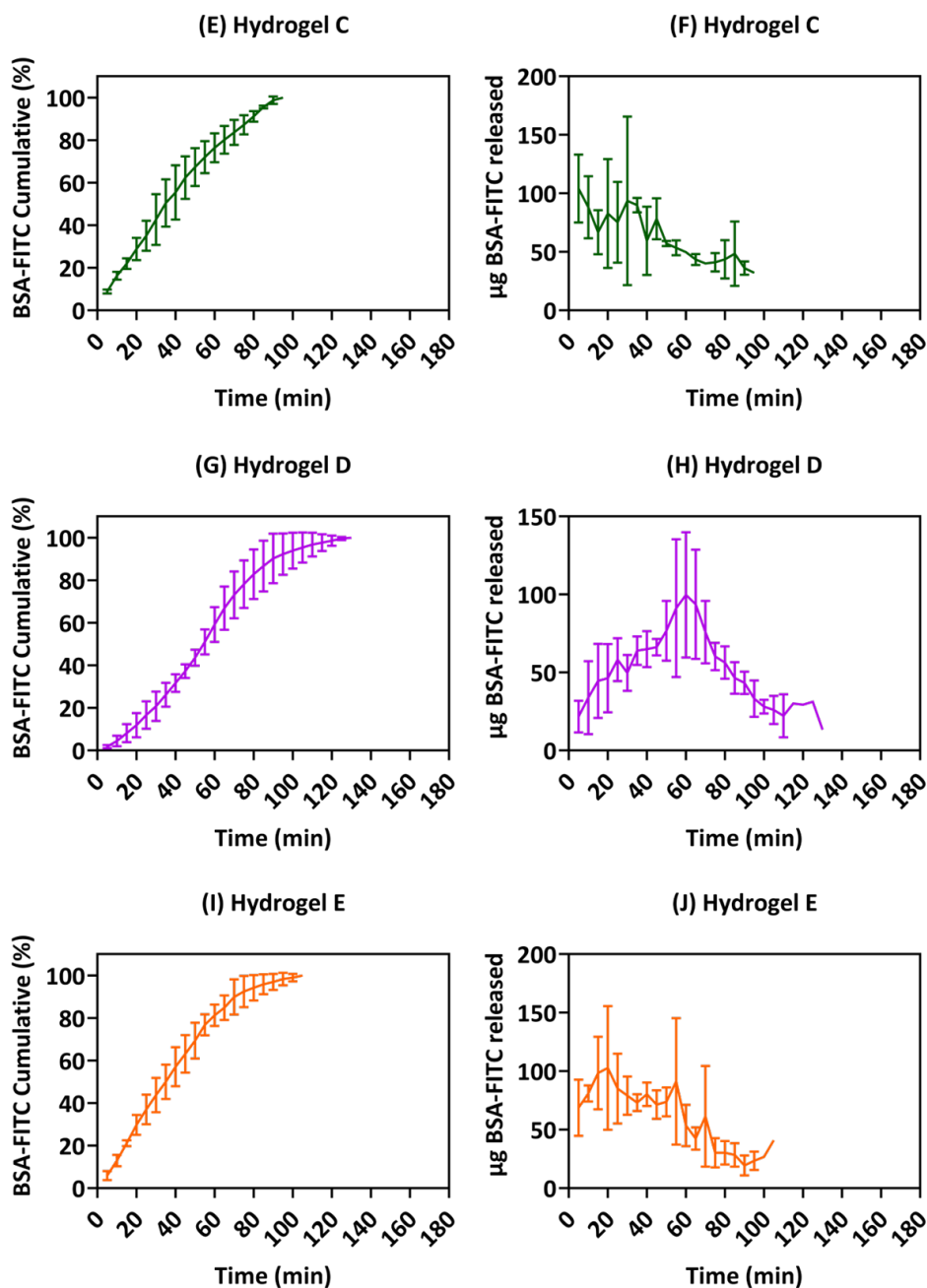


Figure 4.22. BSA-FITC release kinetics obtained from hydrogels A – E. Results represented as a percentage of accumulative released (A, C, E, G, I) and as BSA µg released (B, D, F, H, J).

Table 4.9. Summary of the principal data obtained from the BSA-FITC release kinetic from hydrogels A – E.

Hydrogel	50% BSA (min)	80% BSA (min)	100% BSA (min)	Max. μg BSA (min)
A	63	120	175	50
B	25	50	85	20
C	35	65	95	5
D	54	77	130	60
E	35	59	105	20

From **Figure 4.22** and **Table 4.9**, the release kinetic for hydrogels A and B can be compared. The first material needed 65 min to release the half amount of protein and 180 min to release the total. The maximum peak of protein μg released was achieved at the min 50. By contrast, in hydrogel B, it is only required 25 min to release the half amount of protein and 85 min to release the total. Likewise, the peak of maximum protein μg released has been obtained after 20 min. As was demonstrated in the matrix stabilization section, the physical interactions in hydrogel A are stronger than the ones in hydrogel B. The BSA is highly hydrophilic, which affects the permeability of the matrices. Therefore, due to the presence of the Eudragit polymer, there are big differences between hydrogel A and B that affect the release. The second one, has a more polar matrix, which makes it to have a burst release. On contrast, hydrogel A exhibits sustained release.

Attending now to the other sub-group of materials (hydrogels C, D and E), hydrogel C exhibits a burst release with a maximum amount of protein released after 5 min. To release half of the amount of protein, it is necessary 35 min and for the total amount 95 min. On the contrary, hydrogel D shows a sustained release, where now it is required 60 min to reach the peak of the maximum amount of protein released. Also, the time required to release half of the amount of protein has increased to 55 min and for the total amount to 130 min. Finally, hydrogel E displays an intermediate behaviour between C and D. The maximum amount of protein released for this case is reached after 20 min. To release half of the amount of protein from the hydrogel film, it is required 35 min and for the total amount 100 min. As can be observed, it is

possible to find different materials with different profiles, from sustained to burst release, that can be selected in function of the requirements.

In a typical release experiment, while working with hydrogels, it is possible to predict^[79] the release profile using Peppas's model equation.^[80] Two scenarios can be applied, known as Fickian diffusion or Case-II transport. The main requirement to fit this equation is that the release must be done by immersing the hydrogel in a defined volume of liquid. Here, the materials are dissolved after the release study and also, it has been used a continuous BSS flow for the experiment. Therefore, it is not possible to compare the experimental results with the predicted ones. Results obtained after applying Peppas's model equation, showed a mix between Fickian diffusion, anomalous transport and Case-II transport, with a huge variance. Therefore, theoretical calculations using experimental data to determine the release mechanism are not presented here.

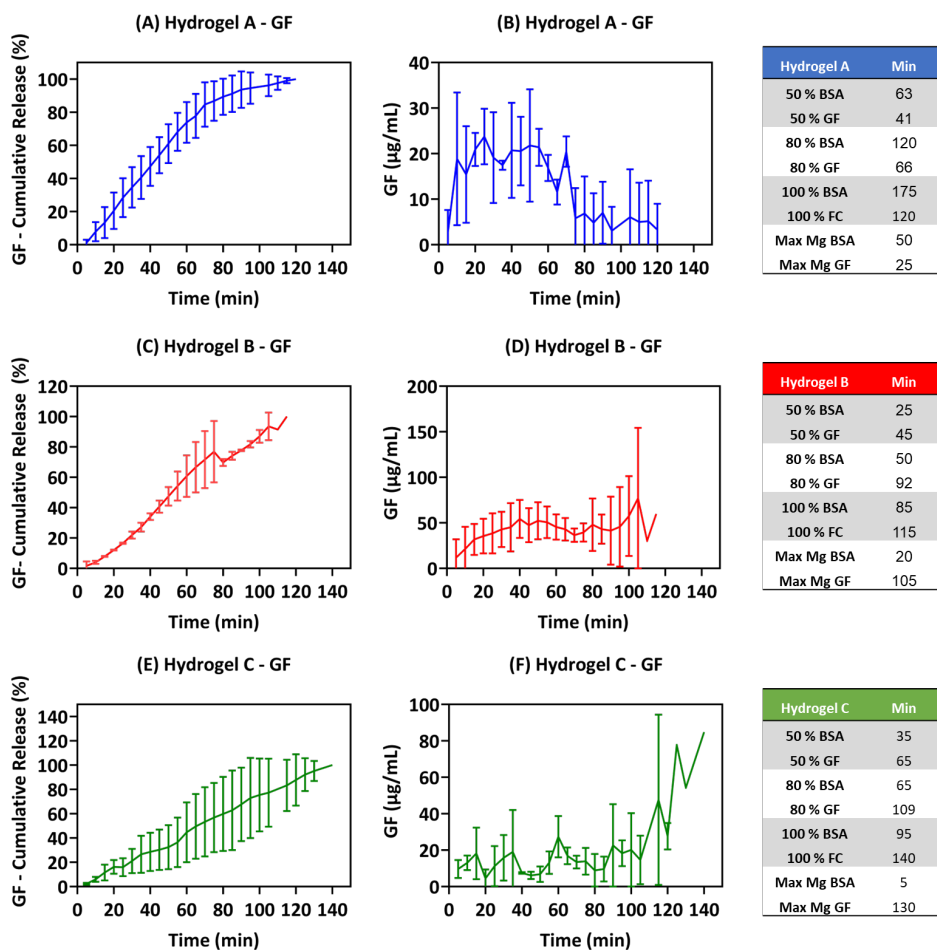
4.3.9 Encapsulation and release of growth factors (GF)

Eye epithelium is exposed to many aggressions every day. In general, it is self-repaired guided by Sclerocorneal limbus stem cells that contain several growth factors (GF). Nevertheless, when the eye is seriously damaged, this repair mechanism could be not enough to totally recover the epithelium and the patient needs to go into surgery. Nowadays, to promote the ocular re-epithelization, a section of an amniotic membrane (AM) is grafted around the eye. The AM is rich in growth factors (GF) and during one month, they help with the eye recovery. Even though this methodology is efficient, it is also highly uncomfortable for the patient and it has a high economic cost. To overcome these issues, it has been decided to encapsulate GF into hydrogels A – E to find a promising material that can be used for GF controlled delivery in ophthalmology applications.

After demonstrating that the hydrogels investigated in this chapter can encapsulate and release BSA, the encapsulation and release profile of GF have been investigated from hydrogels A – E. In the framework of a collaboration, the GF have been extracted from AM by Dr. Arantxa Acera (from the experimental ophthalmology group, University of the Basque Country) with the ethical approval CEIC E20/05 from Cruces for the use of AM. Later, the concentrated aliquots have been lyophilized and stored at -80°C until their encapsulation inside the hydrogels A – E. The obtained powder is rich in several growth factors. The four more interesting GF (EGF, NGF, HGF, EGF-1)

have been identified by ELISA characterization to guarantee their presence (data not shown here).

Release kinetics for hydrogels A - E were quantified as total protein concentration, measured with the indirect quantification kit EZQ[®].^[81] This kit, similar to Bradford, allows the quantification of proteins with just 1 μL of the sample by fixing the proteins onto a paper that is later stained with EZQ[®] reagent. The final product is analyzed by fluorescence. The data, obtained every 5 minutes, have been collected with the same methodology used for the BSA release quantification. **Figure 4.23** shows the release kinetic obtained for hydrogels A – E as a percentage of accumulated protein release and $\mu\text{g}/\text{mL}$ of total protein released along the time.



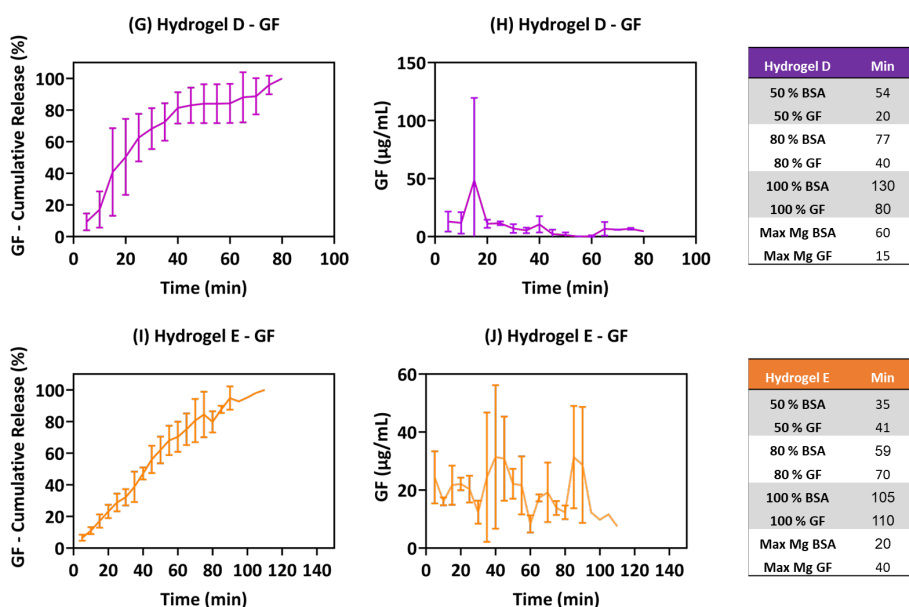


Figure 4.23. Grow Factor release kinetics obtained from hydrogels A – E. Results represented as a percentage of cumulative release (A, C, E, G, I) and as BSA $\mu\text{g/mL}$ released (B, D, F, H, J). Table summarizing the time for 50%, 80%, 100% and max mg released is also represented for each hydrogel and compared with the value obtained from BSA release studies.

From the data shown in **Figure 4.23**, in **A** and **B**, the total time required for 100% release of GF from hydrogel A is 120 min as can be seen. Among the five hydrogels, material A is the most hydrophobic one. Considering that 175 min was required to release all the BSA from it, and now, for GF, that time has been reduced to 55 min, it can be assumed that GF are more hydrophilic than BSA. Also, the maximum amount of GF released has been achieved after 25 min, instead of the 50 min that was required in the case of BSA. These results reinforce the observed tendency. The more hydrophilic the encapsulated molecule, the smaller the number of physical interactions with hydrophobic polymer will be. Therefore, the stability of the matrix is being reduce in presence of an aqueous liquid.

The presumably great hydrophilicity of the GF is verified by the results obtained for hydrogels B, C and E. For these materials, the time required for 50%, 80%, 100% and the peak of maximum GF released is higher than the one required for BSA. It is worth it to notice the differences between hydrogels B, C and E.

Hydrogel B is based on Eudragit RL100, even though this Eudragit is hydrophobic, it is more permeable^[82] than Eudragit RSPO, as it contains a higher amount of quaternary amines. The GF can easily penetrate through the polymeric chains of the matrix, reinforcing the number of physical interactions, which end up in an increase in its stability. As a consequence, the time required for the total release of GF from hydrogel B increased by 25% as compared with the BSA release. To release the half, it increases by 45%. And, to achieve the maximum GF released, this value increased by 80%.

Hydrogel C is formed with the water-soluble Eudragits family, like materials D and E. Nevertheless, hydrogel C is based on Eudragit S100, which is the only one with an aqueous-soluble Eudragit at the physiological pH. For the other two materials, hydrogel D is based on Eudragit L100, soluble at $\text{pH} > 6$. And, hydrogel E, based on Eudragit L100-55 is based on Eudragit L100-55, soluble at $\text{pH} > 5.5$. Considering that an ophthalmological buffer (at physiological pH) has been used for the release studies, it is expected to find better results for material C than for D and E. The reported data have shown that to release the total amount of GF, 140 min was required, while for BSA it was only 95 min. This is an increase of 35%. The same experiment for hydrogel E has reported only an increase of 5% in the time required for the total release of GF (110 min) in comparison with the required for the total release of BSA (105 min). To release 50% or 80%, for hydrogel C, the increase for GF than BSA is around 40 – 45%. In contrast, for hydrogel E, this increase is only 15%. Finally, the maximum amount of GF released is achieved after 130 min for GF, which represents a 99% of time increase, as for BSA it was achieved after 5 min. This more amount of time required is also decreased for material E. In that case, the maximum amount of GF has been released in the min 40, vs. the 20 min that was required for BSA. This is an increase of just 50%. All these results reveal that hydrogel C is more suitable for a controlled release of GF under physiological conditions.

The last material to be discussed, hydrogel D, shows unexpected results. Initially, a similar tendency to materials C and E could be expected. That is to say, a lower GF release kinetic, considering that it is also based on water-soluble polymers. Nonetheless, it has been found exactly the opposite. To release the total amount of GF, it is required 80 min, meanwhile for BSA it is necessary 130 min. In other words, it is required a 60% less time, similar to the tendency observed for material A. To release 50% and 80% of GF from material D, it was required 52 and 36% less time than the same experiment with BSA. The reason to explain these values is that it was not possible to prepare a homogeneous hydrogel D with GF encapsulated. The thickness of

the material and its surface were irregular, even though it was prepared in triplicate. Probably, the high hydrophilicity observed in GF and the number of attractive physical forces that these pools of proteins are having with the polymeric chains are making the hydrogel matrix unstable. The hydrogel is formed by the solve-casting technique, where it is necessary to evaporate the solvent. For hydrogel D with GF, it was observed that it is not possible to remove all the solvent, being impossible its preparation with the same methodology used when the material was empty. Therefore, material D is not a good option to encapsulate GF, as it was also concluded in the matrix stability studies (sections 4.3.3 and 4.3.4).

4.3.10 Metabolic activity of MRC-5 cells in presence of hydrogels A

The cytotoxicity of hydrogels A – E has been analyzed in collaboration with Dr. Aitor Larrañaga (from Mining-Metallurgy Engineering and Materials Science, Polymat, Faculty of Engineering in Bilbao, University of the Basque Country). In the applied methodology, hydrogels have been dissolved in BSS buffer at different dissolution degrees. The obtained aliquots have been mixed with cell medium and incubated with the cells to observe their viability. Each formulation has required a different dissolution time. E.g., hydrogel A 480 min, hydrogel B 135 min, hydrogel C 150 min, hydrogel D 130 min and hydrogel E 135 min. Samples were also acquired at different degrees of dissolution (i.e., 25 and 50%) to study the potential cytotoxicity of different polymers concentrations in the BSS solution. The obtained dissolutions were incubated with MRC-5 cells and their metabolic activity was subsequently determined after 24 and 48 h. **Figure 4.24** shows the metabolic activity of human fetal lung fibroblast (MRC-5) cells in presence of each aliquot after 24 and 48 h respectively.

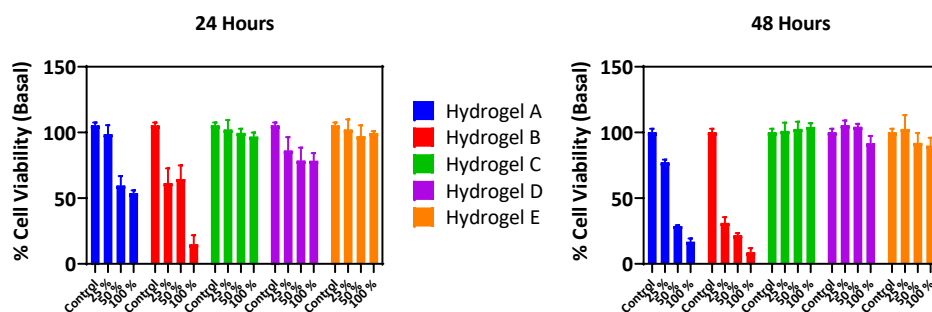


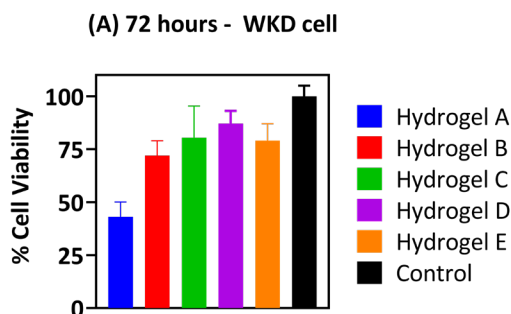
Figure 4.24. Metabolic activity of MRC-5 cells was obtained after 24 and 48 h of incubation with different dissolution degrees (25, 50 and 100%) of hydrogels A – E with the cells.

The metabolic activity of MRC-5 cells, measured with AlamaBlue®, shown in **Figure 4.24**, has been reduced in the presence of hydrogels A and B. Accordingly, the metabolic activity of MRC-5 cells after 48 h decreased from 100% to 17% and 9% for formulations A and B (100% dissolution), respectively. The cytotoxic effect was particularly relevant for formulation B, in which the metabolic activity after 24 h was reduced to 61% even when this sample had undergone only 25% of its complete dissolution. This can be ascribed to the presence of quaternary amines, from Eudragits RSPO and RL100, in both formulations. As recently reported in a multiparametric study^[83], cationic functionalities induce an inflammatory response in cells. The other formulations, hydrogels C, D and E, did not elicit any significant cytotoxic effect on cells, being the metabolic activity similar to the control in all the cases.

Accordingly, it can be concluded that these three formulations may be potentially considered for biomedical applications. Therefore, as ophthalmology applications have been the final objective of these studies, it has been decided to analyze the metabolic activity of conjunctive cell lines in presence of hydrogels A – E. These cells are economically more expensive than MRC-5, therefore the use of general cell lines for toxicology studies in the first case is justified. The obtained results are detailed in the following section, **4.2.10**.

4.3.11 Metabolic activity of WKD ocular conjunctiva cells in presence of hydrogels A – E

The cytotoxic effect of hydrogels A – E in Wong Kilbourne derivate of Chang conjunctiva epithelial cell line (WKD; clon 1-5c-4, American type culture collection) was evaluated in a collaboration with the same research group thyalurot extracted the GF from AM. The five hydrogels were dissolved in 2 mL of BSS solution. The resulting aliquots were incubated with WKD cells for 72 h. **Figure 4.25** shows the metabolic activity of WKD cells, determined with Kit XTT II, in presence of each hydrogel's aliquot after 72 h.



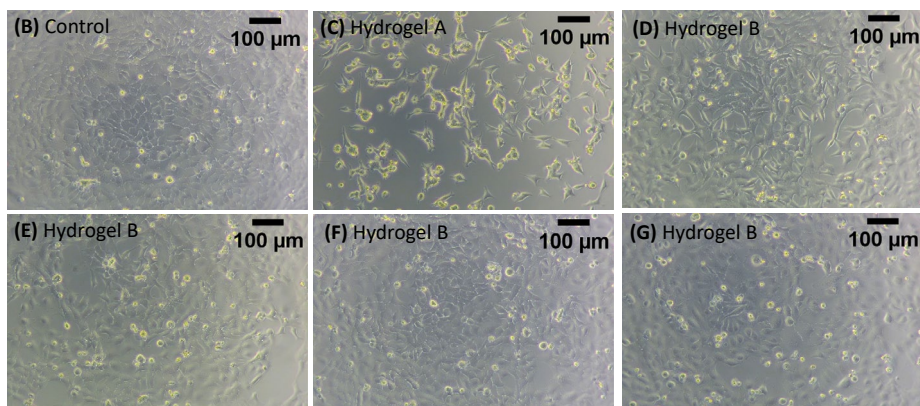


Figure 4.25. Metabolic activity of WKD Chang conjunctiva epithelial cells was obtained after 72 h of incubation of hydrogels A – E with the cells. (A) Summary of the cell viability. (B – G) Optical microscopy pictures of the cell's aspect.

In **Figure 4.25**, can be observed that hydrogels A and B are the ones that inhibit the cell growth the most. This tendency is similar to the one obtained when the materials were incubated with MRC-5 cells. For hydrogel A, 45% of cell growth and around 70% for hydrogel B has been achieved. These two hydrogels are based on the tri-block Eudragit, which contains a quaternary amine group that increases the toxic behaviour. Contrarily, the results from hydrogels C – E are more promising for ophthalmology applications. This group of hydrogels are based on di-block Eudragits, where the quaternary amine block is not present. Therefore, they do not inhibit cell proliferation at the studied concentration.

As hydrogels C – E do not inhibit cell growth *In-vitro* assays, the materials are going to be tested in pre-clinical analysis with animal models. The obtained results are going to be described in sections **4.3.12**, **4.3.13** and **4.3.14**.

4.3.12 *In-vivo* eye-adhesion study

In section **4.3.6.2** was been demonstrated that hydrogels A – E show mucoadhesion properties towards ocular conjunctiva. The experiments reported in that section were at a laboratory scale using a rheometer. To move towards the next step, hydrogels A – E have been analysed in an animal model. To confirm the mucoadhesion properties, empty hydrogels A – E were pre-hydrated with 200 μ L of BSS during 5 – 10 min. Afterwards, the materials were set into a rabbit's eye. Then, the eyelid was closed for 2 min and opened

several times to corroborate if the hydrogel film (0.4 x 0.4 x 0.1 cm) remains in contact with the conjunctiva. The eyelid was opened during 15 s, closing again for 1 min and opened again during another 15 s. This operation was done in triplicate.

All the *In-vivo* experiments shown in Chapter IV (sections **4.3.12**, **4.3.13** and **4.3.14.3**) were performed in collaboration with Dr. Arantxa Acera and Ayla Basasoro (part of the data is shared with Ayla's doctoral thesis) from the University of the Basque Country (UPV/EHU) and the Department of Ophthalmology, Hospital Universitario, Donostia- San Sebastián, with the ethical permission from diputación general de Gipuzkoa (code PRA-AR-SS-196) and animal experimentation committee (code CEEA20/15).

Figure 4.26 shows the pictures obtained when hydrogel A was applied to the eye's surface.

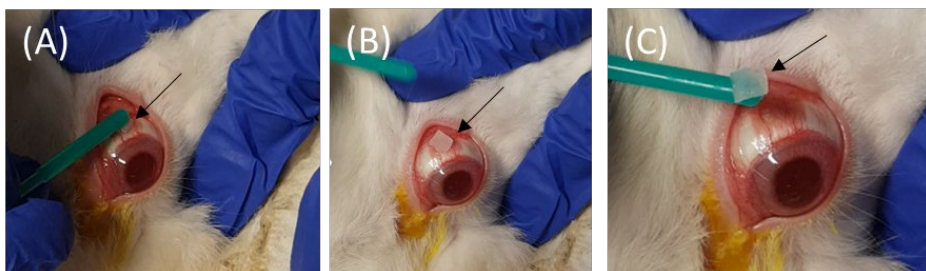


Figure 4.26. (A) Hydrogel A with dimensions 0.4 x 0.4 x 0.1 cm onto the ocular surface. (B) Hydrogel A onto the ocular surface. (C) A few seconds after, the material is not attached to the conjunctiva and can be easily removed.

In **Figure 4.26A**, it can be observed how the hydrogels are placed in contact with the conjunctiva. Even though the material looks like it is attached to the conjunctiva (**Figure 4.26 B**), after closing and opening again the eyelid, it can be seen that the hydrogel is no longer in contact with the conjunctiva. In other words, the mucoadhesive capacity of the hydrogel is not enough. Similar results were obtained for hydrogel B.

Figure 4.27 reports the results obtained after setting hydrogel C onto the rabbit's eye.



Figure 4.27. (A) Hydrogel C with dimensions 0.4 x 0.4 x 0.1 cm onto the ocular surface. (B) Hydrogel C outside ocular conjunctiva after closing and opening again the eyelid.

In **Figure 4.27**, it can be seen that after setting the hydrogel C onto the conjunctiva (**Figure 4.27 A**) the material does not remain in contact with it after some min (**Figure 4.27 B**). The mucoadhesion forces between the hydrogel and the ocular conjunctiva are not enough to maintain the hydrogel attached along the time. Similar results were obtained for hydrogels D and E.

Even though hydrogels A – E reported mucoadhesion properties with conjunctiva on a laboratory scale (section **4.3.6.2**), the *In-vivo* mucoadhesion assays have demonstrated that this mucoadhesion is not enough to maintain the hydrogels onto the conjunctiva. Therefore, it can be concluded optimization of hydrogels' formulations is necessary to increase the mucoadhesion properties. A good mucoadhesion behaviour is a mandatory requirement to guarantee that the hydrogel remains on the eye while releasing the GF.

4.3.13 Hydrogels optimization: Improvement of their mucoadhesion properties

The *In-vivo* assays shown in section **4.3.12** demonstrated that there is a lack adhesion capacity of the hydrogels to the conjunctiva. Consequently, it is imperative to improve the mucoadhesion capacity of the materials with minimum modifications that can guarantee biocompatibility while preserving the properties of the developed hydrogels. To achieve these objectives, formulation C has been modified with hyaluronic acid (HA) with molecular weight of 750 kDa and hydroxypropyl cellulose (HPC) with molecular weight of 100 kDa. This material has been demonstrated to be a good candidate in every characterization. Besides, it has also reported good WKD cells viability,

which makes it ideal for ocular applications. **Figure 4.28** shows the chemical structure of both polymers. As they are biopolymers commonly used in pharmaceutical formulations, it is expected that cytocompatibility, biodegradability, ocular tolerability, mechanical strength and an enhancement in the ocular penetration are guaranteed.^[84] Actually, HA is present in the aqueous and vitreous humour of the eye. Thanks to the presence of carboxyl groups in its chemical structure, it can create hydrogen bonds that interact with biological substrates. Hence, good mucoadhesive properties have been reported for this polymer.^[85] As a recent example, Marto, et al. reported an increase of around 300% of mucoadhesive index towards mucin in NPs when they added HA to the formulations.^[86] In addition, HPC is a non-ionic water-soluble cellulose that can form intermolecular hydrogen bonds with mucosa layers thanks to the presence of hydroxyl groups in its structure.^[87] Recent studies have proved the capacity of HPC to be used as adhesive towards mucus layer in comparison with other polymers (Carbopol, chitosan and carboxymethyl cellulose). For all the cases, HPC has reported bigger values of mucoadhesion than the other three polymers.^[88]

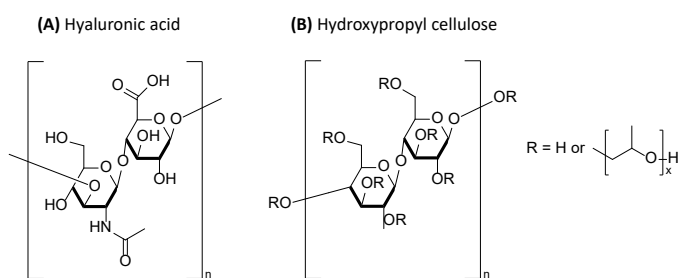


Figure 4.28. Chemical structures of (A) HA and (B) HPC.

Hydrogel C has been modified with different degrees of HA and HPC to test several formulations and find the mucoadhesive requirements for ocular applications. Hence, the material has been modified with 30% wt. of HA and 2% wt., 10% wt., 20% wt., 30% wt. and 50% wt. of HPC. The materials have been pre-hydrated for 10 and 30 min with BSS ophthalmological solution to replicate the protocol used *In-vivo*. **Figure 4.29** shows the obtained results of work of adhesion towards the ocular conjunctiva measured with a rheometer.

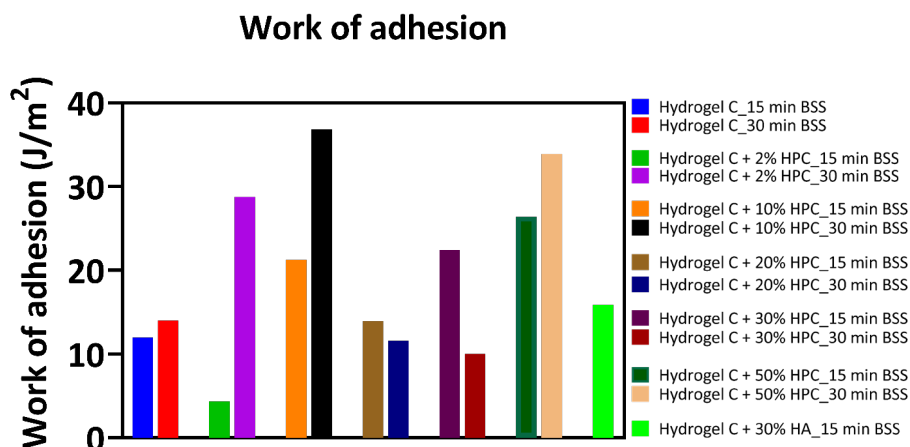


Figure 4.29. Work of adhesion of the hydrogels to the ocular conjunctiva obtained after 15 and 30 min of hydrogels pre-hydration with BSS.

From the samples analyzed in **Figure 4.29**, it can be observed that incorporation of 2%, 10% and 50% of HPC in hydrogel C increase the work of adhesion to more than triple in comparison with the same material without HPC. Nevertheless, the modification adding 20%, 30% and 50% of HPC, generates a heterogeneous hydrogel with phase segregation between polymers during the drying process. In addition, the material is also quite rigid even after being swollen. Therefore, hydrogel C with 20%, 30% and 50% of HPC are not further considered. Hydrogel C modified with 30% of HA also reported an improvement in the work of adhesion. For this formulation, it was not possible to measure it with 30 min of BSS hydration due to technical issues.

The three most relevant formulations, hydrogel C combined with 2% and 10% of HPC and 30% of HA have been analyzed *In-vivo* to select the final candidate for *In-vivo* treatment assays. **Figure 4.30** shows the pictures obtained after placing these three formulations on the eye, closing the eyelid and opening it again.

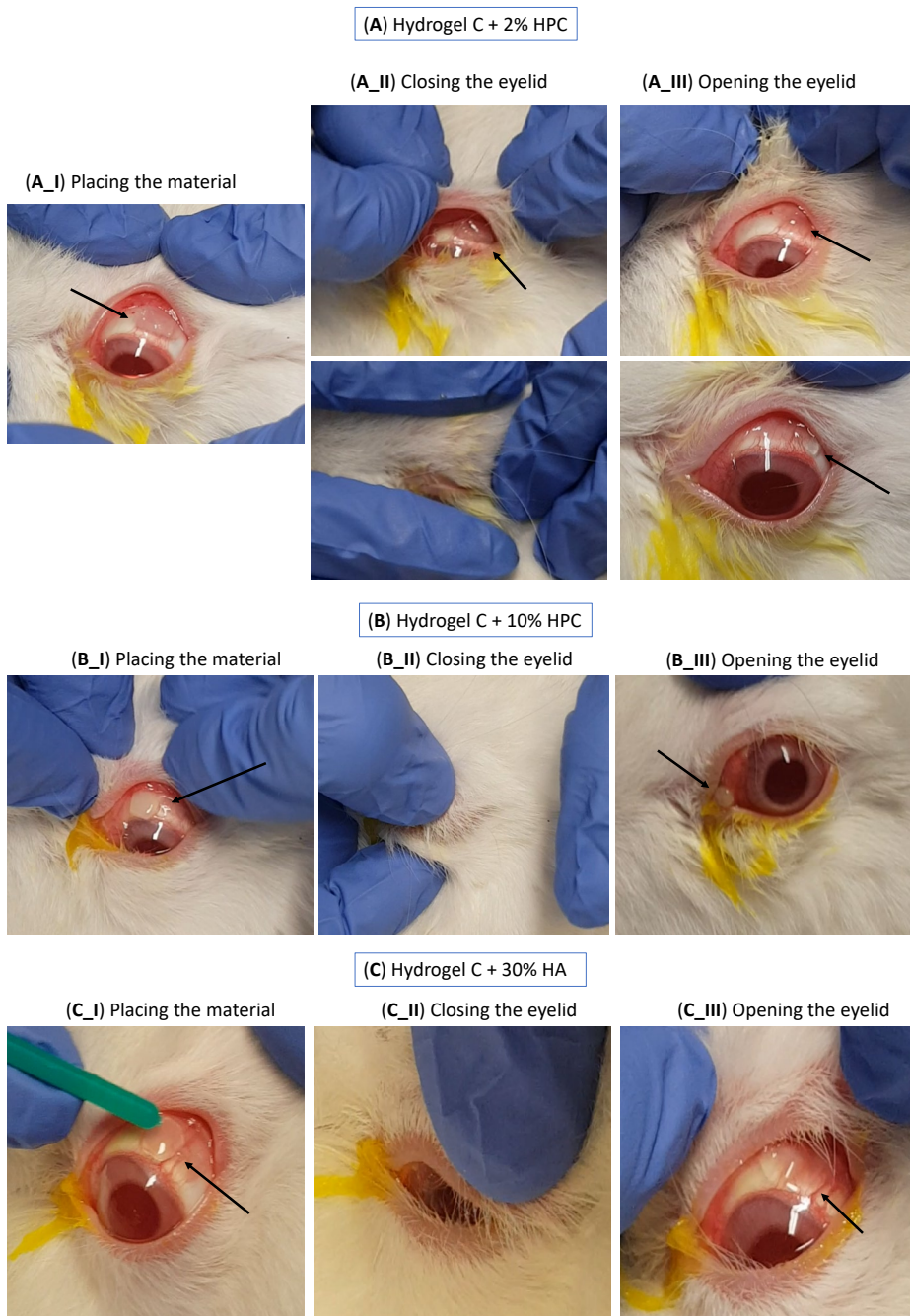


Figure 4.30. Mucoadhesion test *In-vivo* of hydrogel C with three composition modifications. (A) Hydrogel C + 2% HPC. (B) Hydrogel C + 10% HPC. (C) Hydrogel C + 30% HA. For all the cases, (I) placing the material. (II) closing the eyelid. (III) opening again the eyelid.

From **Figure 4.30**, it can be concluded that only hydrogel C modified with 2% of HPC or with 30% of HA remains on the eye after closing and opening again the eyelid. In other words, these two formulations are the only ones that exhibit good enough mucoadhesion properties towards the ocular conjunctiva. In contrast, hydrogel C modified with 10% of HPC cannot stick to the ocular surface. Therefore, after closing and opening again the eyelid, the hydrogel does not remain on the eye.

Among the two promising candidates (hydrogel C modified with 2% of HPC or 30% HA), the second one was selected as the material for the next round of *In-vivo* experiments, now with GF encapsulated inside the hydrogel. The main reason is that hydrogel C modified with HA can be reproduced with good homogeneity. On the contrary, hydrogel C modified with 2% of HPC allows the appearance of small phase segregation and heterogeneity during the drying process. These undesired effects cannot guarantee the good distribution of GF along with the patch and neither the good reproducibility and scale-up of the material.

The selected candidate, hydrogel C modified with 30% of HA, is going to be prepared and loaded with GF for a pre-clinical analysis. GF kinetic release and material stability, followed by NMR, will be described as well in the section **4.3.14**.

4.3.14 Material candidate: GF release, matrix stability and efficacy studies

The final candidate has been prepared with a similar methodology to the one previously described. 30% w/w of HA was added to the pre-gel solution and the material was prepared by the solve-casting technique. The GF were added to the pre-gel solution as well. Taking advantage of the fact that GF need to be kept frozen, once the film was dried after 3 days, the patch was frozen and thawed 3 times, which allowed reinforcing the physical interaction between polymers. This post-treatment methodology has been described in the literature to improve the stability of physically cross-linked hydrogels based on PVA.^[89] It is expected that this material will have better stability and control over the GF release than hydrogel C without HA modification and without post-treatment.

4.3.14.1 Matrix stability followed by NMR

The same methodology described in section 4.3.4 was applied here. The hydrogel was dissolved in a constant flow of BSS solution (110 $\mu\text{L}/\text{min}$) and the collected samples were analyzed by NMR. **Figure 4.31** shows the obtained spectra for the hydrogel C modified with 30% of HA and with a frozen post-treatment. Besides, the figure also shows the previously reported spectra for hydrogel C as a comparison.

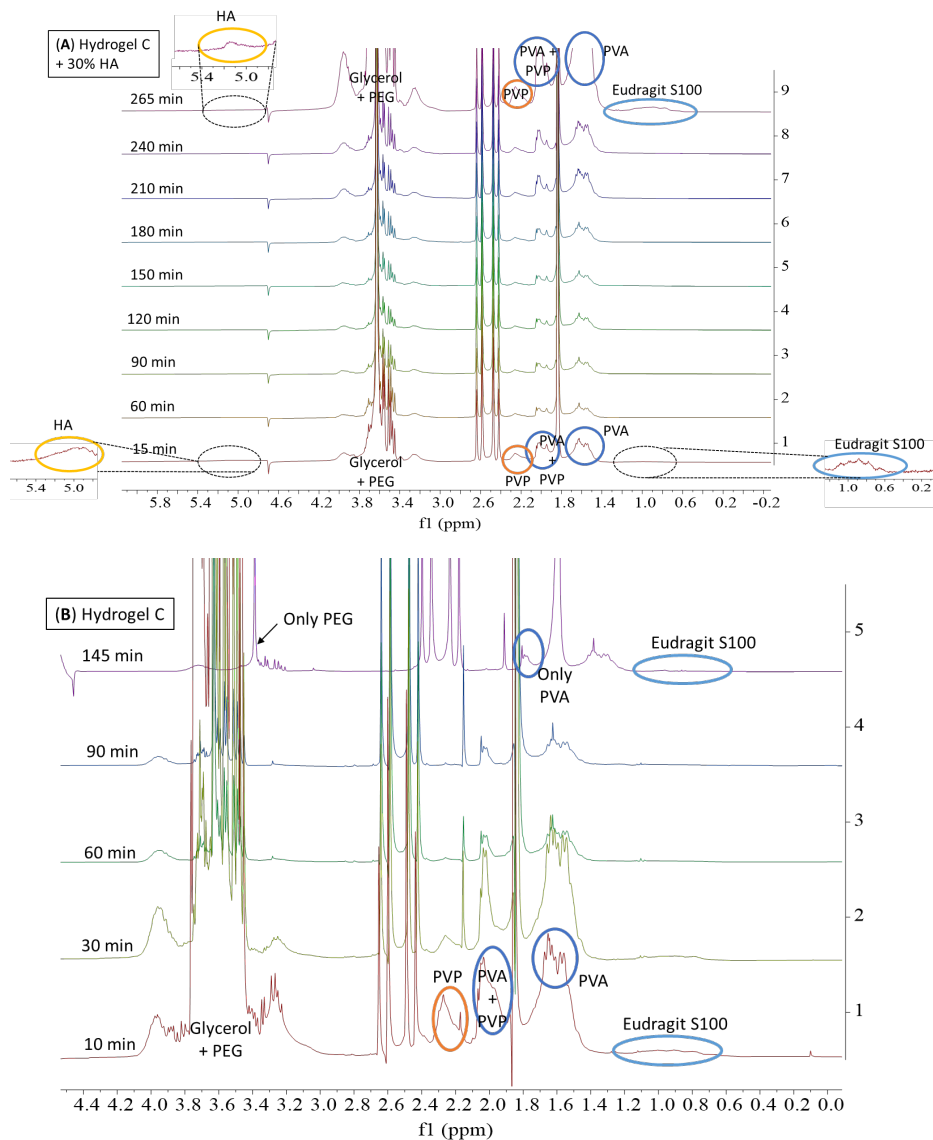


Figure 4.31. ^1H -NMR (300 MHz, BSS/ D_2O 90/10) spectra were obtained during the dissolution of hydrogel C modified with (A) 30% of HA and (B) hydrogel C without modifications.

From **Figure 4.31**, it can be seen that the modification of the hydrogel C with 30% of HA has two main benefits. On the one hand, to dissolve the hydrogels, now it is required 265 min instead of 145 min which was required for the non-modified hydrogel C. This big increase in the matrix stability is due to a double component. From one side, the presence of HA increases the number of physically cross-linkers interactions between the polymeric chains. On the other side, freeze-thaw post-treatment cycles also increment the number of physical interactions between the polymeric chains. In addition, the $^1\text{H-NMR}$ signals from all the polymers can be seen during the whole experiment once the HA is present (**Figure 4.31A**). In fact, PVP and glycerol are still present after 265 min. However, their signals cannot be observed after 145 min for the non-modified hydrogel (**Figure 4.31B**). One might mention that the intensities of the polymers increase significantly during the last mins of the experiment for the hydrogel C modified with HA. That is to say, the cross-linkers degree between chains is higher when the HA is present and the material has been frozen and thawed 3 times. It is expected that this will affect the GF release. Hence, the GF kinetic release from hydrogel C modified with HA will be slower than the same material without modifications. This is going to be analyzed in section **4.3.14.2**.

4.3.14.2 GF release profile from hydrogel C modified with HA

GF were encapsulated and released from hydrogel C modified with HA using the same protocol applied in section **4.3.9**. **Figure 4.32** shows the release kinetic obtained as total accumulation percentage released and μg of GF released versus time. Moreover, **Table 4.10** collects the most important data and its comparison with the GF release obtained from hydrogel C (without modifications).

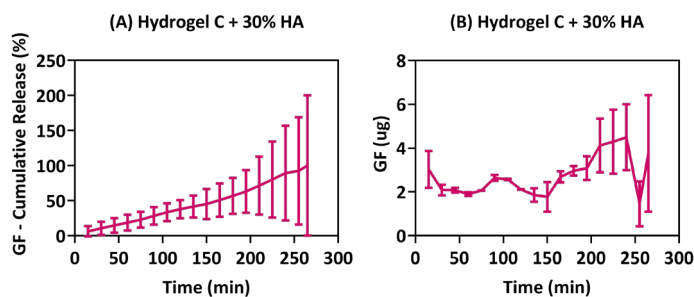


Figure 4.32. Grow Factor release kinetics obtained from hydrogels C modified with 30% of HA. (A) Percentage of cumulative release vs time. (B) μg of GF released vs time.

Table 4.10. Summary of the most relevant data obtained from GF release kinetics from hydrogel C modified with 30% of HA and hydrogel C without modifications.

Released	Hydrogel C + 30% HA [Min]	Hydrogel C [Min]
50 %	165	65
80 %	225	109
100 %	265	140
Max μg of GF released	241	130

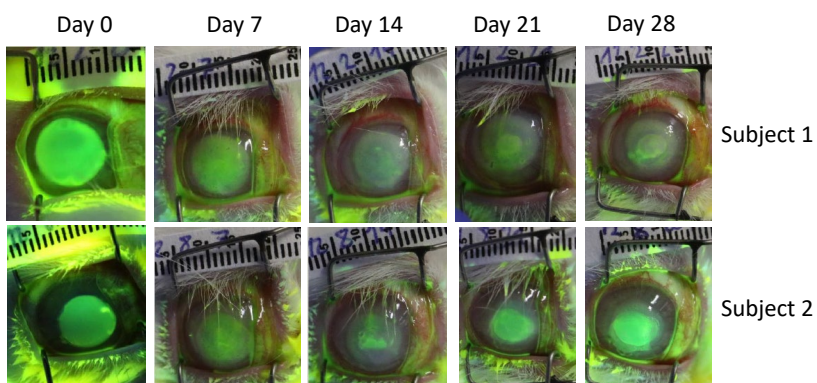
As it can be seen in **Figure 4.32** and **Table 4.10**, the double-time is required to release the total amount of GF from hydrogel C modified with HA and reinforced with a frozen post-treatment than the one needed for a non-modified hydrogel C. Besides, to release the 50% and 80% of GF, it is required more than the double of time when the hydrogel C is modified. These results highlight the importance of a post-treatment reinforcement of the physical cross-linkers to guarantee that the material can release GF for more time. Taking into account the success of the material's optimization, the therapeutic efficacy of hydrogel C modified with 30% of HA is going to be tested in rabbits as a model. These results are summarized in section **4.3.14.3**.

4.3.14.3 Efficacy assays of final hydrogel candidate

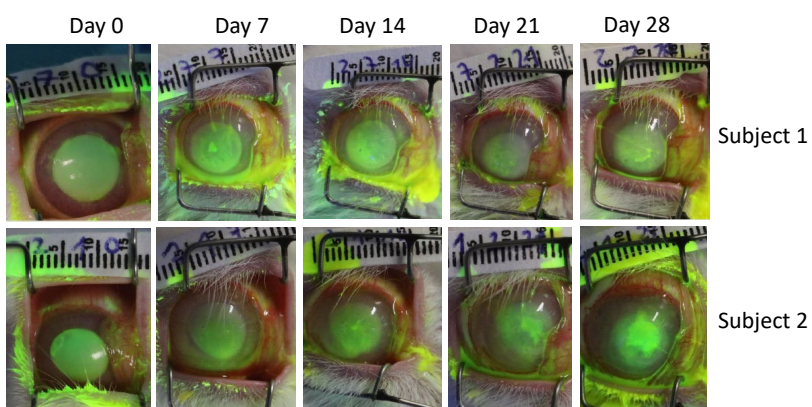
For the efficacy assays, rabbits' eyes have been injured with NaOH under general anaesthesia, creating a controlled ocular ulcer as reported in the literature.^[90] A total of 27 rabbits have been used for these experiments divided into three groups. Group A was treated with Tobradex® as a negative control. This component is a commercial anti-inflammatory and antibiotic liquid that has also been applied in the eye treated with hydrogel. Group B was treated with AM and Tobradex®, as a positive control, replicating the actual human treatment. Lastly, group C was treated with hydrogel C modified with 30% of HA and loaded with GF. One material has been set into the rabbit's eye every 12 h for 7 days in a total of 9 rabbits. **Figure 4.33** show the eyes of two rabbits for each group after 0, 7, 14, 21 and 28 days. The **Figure 4.34** summarizes in two plots the data obtained from the eyes. **Figure 4.34A** shows the median epithelial defect area and **Figure 4.34B** shows the ocular epithelial wound closure.

Screening of Eudragits as building blocks in the preparation of physically cross-linked hydrogels

(A) Negative control - Tobradex



(B) Positive control – AM + Tobradex (Actual treatment)



(C) Hydrogel (C + 30% HA) + Tobradex

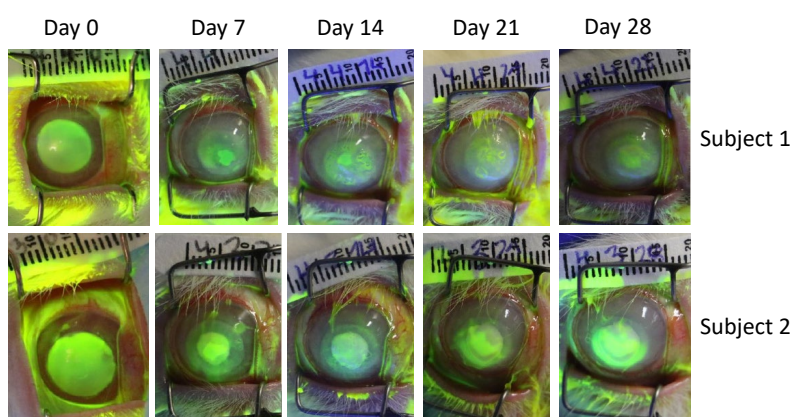


Figure 4.33. Evolution of the eye injury after 0, 7, 14, 21 and 28 days of two random rabbits treated with (A) Tobradex as a control. (B) AM and Tobradex as a positive control. (C) Hydrogel C + 30% HA and Tobradex.

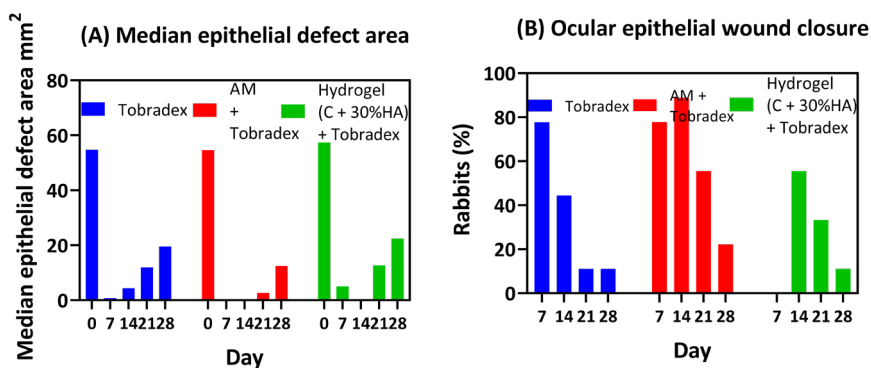


Figure 4.34. (A) Median epithelial defect area (mm²) after 0, 7, 14, 21 and 28 days of the injured eye with Tobradex (blue), AM and Tobradex (red) and hydrogel C + 30% HA candidate and Tobradex (green). (B) Ocular epithelial wound closure as a percentage of total rabbits' complete closure after 0, 7, 14, 21 and 28 days of the injured eye with Tobradex (blue), AM and Tobradex (red) and hydrogel C + 30% HA candidate and Tobradex (green).

The treatment with Tobradex, AM and hydrogel consisted of 7 days of treatment with doses every 12 h. As can be seen in **Figures 4.33** and **4.34A** the Tobradex can almost close the epithelial defect after 7 days, reducing the wound from 54 to 0.7 mm². Later, the wound is reopened until 20 mm² after 28 days, which means that the treatment with Tobradex® was not successful at all. In the case of the treatment with AM, actual human treatment, the wound is closed after the 7 days of the treatment and it continues closed for more than 14 days. After 21 days, the wound is reopened again and it grows to 12 mm² after 28 days. Finally, the treatment with the hydrogel reduces the median epithelial defect from 57 mm² to 5 mm² after 7 days. This reduction is lower than the positive and negative control, which means that the treatment is not working well enough. However, after 14 days, the wound disappears. Nevertheless, the epithelial defect area treated with the hydrogel reopen to 12 mm² after 21 days (better than negative control) and to 22 mm² after 22 days. It can be hypothesized that even though the material has mucoadhesive properties, it might be not good enough, which allows the hydrogel to move along the ocular surface and reopen the wound. Also, maybe the GF concentration loaded are not high enough to close the epithelial defect. Hence, it can be speculated that using hydrogels as an ocular insert to cure wounds could be a good approach but it requires the development of a material with good mucoadhesion properties that avoid the free movement. Besides, higher loading of GF concentration should be explored as well.

Figure 4.34B summarizes the percentage of rabbits with the total ocular epithelial wound closure. With the Tobradex treatment, around 80% of the rabbits have the wound closed after 7 days. Nevertheless, after 14 days, only 44% of the rabbits have the eye wound closed. This percentage reduces to 11% after 21 days. For the positive control, treatment with AM, 77% of the rabbits have the eye wound closed after 7 days. After 14 days, this percentage rises to 89%. Then, it decreases to 55% after 21 days and 22% after 28 days. Lastly, the treatment with the hydrogel manages to close the wound in 55% of the rabbits after 14 days. This treatment is better than the negative control (Tobradex) but worse than the positive control (AM). A similar scenario can be found after 21 days, where 33% of the rabbits have the eye wound closed with the hydrogel treatment. This value is better than the negative control after the same time (11%) but worse than with the AM treatment (55%). Finally, after 28 days, only 11% of the rabbits treated with hydrogel have the eye wound closed. As it was concluded before, the feasible free movement of the hydrogel on the eye promotes the re-opening of the wound. On the other side, it is possible that the concentration of GF loaded in the hydrogel is not as high as the GF concentration in the AM. From a future perspective, it should be considered to increment the loaded amount of GF, change the administration plan, etc.

4.4 Materials and methods

The starting materials were purchased from the following suppliers: Polyethylene glycol (PEG) 2 KDa, Albumin-fluorescein isothiocyanate conjugate and phosphate buffer saline pH = 7.4 were obtained from Merck®. Polyvinylalcohol (PVA) 100 KDa and Polyvinylpyrrolidone (PVP) 50 KDa were from Acros Organics®. Eudragit RSPO, RL100, S100, L100 and L100-55 were obtained for free from Evonik®. Hyaluronic acid (HA) 700 KDa was purchased from Contipro®. Hydroxypropyl cellulose (HPC) 100 KDa was bought from FisherScientific®. 99.8% D₂O NMR solvent, 99.5% Glycerol and ACS grade Potassium sulphate (K₂SO₄) were bought in Scharlab®. Balanced Salt Solution (BSS) for eye irrigating tissues was from AJL Ophthalmic®. All the reagents were used as received, without any further purification. The water used for the experiments was the type I quality (ultrapure water), obtained from a purification system (18.2 MΩcm). Dulbecco's modified Eagle's medium (DMEM), fetal bovine serum (FBS), penicillin-streptomycin solution (P/S) and AlamarBlue® cell viability reagent were purchased from ThermoFisherScientific.

4.4.1 Hydrogel preparation

All the physically cross-linked hydrogels matrices were prepared by casting polymers solutions, as reported in the literature^{[28][29]} with minimum modifications. For all the formulations PVP (12 % w/w) and PVA (27% w/w) were mixed at 90 °C^[91] in ultra-pure H₂O (100 mL) for 2 h. Afterwards, the solution was cooled down to room temperature (25 °C). PEG (27 % w/w) and glycerol (27 % w/w) were introduced into the mixture. Then, Eudragits were added in a final concentration of 7 % w/w, according to **Table 4.1** (from the results section **4.3.1**), to prepare the different hydrogels. In the case of Eudragit RL100, Eudragit RSPO and Eudragit L100-55 were necessary for a previous dissolution in 2 mL of acetone for the first case and ethanol for the two remainings. The pH of the pre-gel solutions was stabilized to 7.4 with the help of a phosphate buffer solution of 10 mM and NaOH/HCl 1 M. Finally, the gel was obtained by drying the mixture at 50 °C in an oven until a constant weight was achieved. The final thickness was about 1 mm.

For the preparation of hydrogels with HPC or HA, the corresponding polymer was added to the pre-gel solution after the glycerol. For the loaded hydrogels with BSA or GF, the cargo was added after the pH was stabilized to 7.4. The drying process took place at 35 °C to avoid protein denaturalization.

4.4.2 Hydrogels pore sizes in dried state

The internal morphology of the hydrogels was observed by accessing their cross-sections. For that, hydrogels were cut into pieces, frozen with liquid nitrogen and lyophilized. The freeze-dried materials were gold-coated with a Bio-Rad SC500 sputter coater for 2 min and analyzed in a Hitachi TM3030 SEM microscope at 15 KeV.

4.4.3 Matrices stability under several conditions

4.4.3.1 Moisture uptake

The percentage of moisture absorption was determined to analyse the stability of the hydrogels in high humid conditions. Hydrogels were cut into pieces of 1 x 1 x 0.1 cm and incubated in a desiccator containing saturated solutions of K₂SO₄ that provides a relative humidity of 97 % for a range of temperatures 20 – 25 °C.^[92] Samples were weighed every 24h until constant weight. The moisture uptake percentage was calculated according to formula (**Equation 4.2**). W_f is the weight of the sample measured every 24h, W_i is the initial weight of the sample. This procedure was carried out in triplicate.

$$\% \text{ Moisture Uptake}(MU) = \frac{(W_f - W_i)}{W_i} * 100 \quad (\text{Equation 4.2})$$

4.4.3.2 Moisture content

The water content that hydrogels have taken from the environmental laboratory conditions (25 °C, 30% – 50% humidity) was quantified. All the hydrogel patches (with dimensions 1 x 1 x 0.1 cm) were introduced inside of a desiccator with silica-gel in triplicate. Every 24h, the samples were weighed individually and kept back in the desiccator immediately until constant weight. The moisture content percentage was calculated according to formula (**Equation 4.3**), where W_i is the initial weight of each hydrogel and W_f is the final weight of the materials.

$$\% \text{ Moisture Content}(MC) = 100 - \frac{(W_i - W_f)}{W_i} * 100 \quad (\text{Equation 4.3})$$

4.4.3.3 Kinetic of dissolution by NMR

The designed system for simulating eye conditions consists of a 3D printed mould that holds a hydrogel sample at a 45° angle (**Figure 4.35**). The hydrogel is exposed to the environment and a buffer is dosed at the upper end that flows along the surface of the material. This liquid is finally collected as aliquots every 5 min. As the hydrogel is stabilized with physical interactions, the liquid can dissolve the polymers that confer the matrix, dissolving the hydrogel. As a liquid, it has been used an eye irrigating isotonic salt solution (BSS). In a normal eye, the tear flow rate is 2.2 μl per minute^[93]. As this value is too low for a laboratory experiment, it has been used 50 times more, 110 μl per minute as the speed. Furthermore, the systems were set inside an oven with a constant temperature of 35.5 ± 1 °C. A rectangle of 1.5 x 0.5 x 0.1 cm from each hydrogel (A – E and their corresponding varieties) were set inside of the 3D printed mould. The whole system was set up inside the oven with a constant temperature of 35.5 ± 1 °C. The collected aliquots were analyzed in a Bruker Fourier 300 MHz Bruker Fourier 300 NMR using BSS/D₂O 90/10 as a solvent and the data were processed with MestReNova 14.2 software. The measurement conditions were ¹H-NMR, 128 scans with 1 s of relaxation time in water suppress mode.

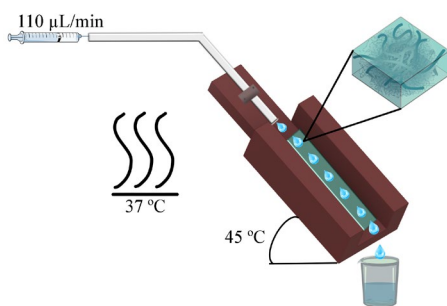


Figure 4.35. Scheme of stability assays set-up.

4.4.4 Hydrogel's mechanical properties: Tensile strain

The hydrogel's tensile strain has been measured without hydration by cutting the hydrogel, in triplicate, with the shape of a dogbone. The equipment used was Instron 5569 universal testing machine. The test specimens were cut with the appropriate shape and dimensions (dogbone shape) according to ASTM D-638 (type V, thickness of 200 μm). A strain was applied until the materials broke. The mechanical properties have been obtained by plotting tensile stress versus the percentage of applied tensile strain. Young's modulus,

maximum tensile strength and tensile break were measured as the elongation at break. The crosshead speed was 10 mm/min. The data have been analyzed with the software Microsoft Excel 2021 and GraphPad Prism 9.3.

4.4.5 Hydrogel's rheological characterizations

4.4.5.1 Dynamic oscillatory

Dynamic oscillatory measurements took place using an Ares-G2 rheometer (TA instrument). The experiment was done at a constant frequency of 1 Hz in a range of temperatures from – 100 to + 50 °C. The curves obtained were the G' , G'' and $\tan \delta$ loss tangent. The last one allows the quantification of the T_g . The data was collected using TRIOS software and processed afterwards with Microsoft Excel 2021 and GraphPad Prism 9.3.

4.4.5.2 Mucoadhesive rheological characterization

The mucoadhesion of hydrogels has been quantified using an Ares-G2 rheometer (TA instrument) with an optimized methodology. The instruments have two disks. On the upper disk, the ocular conjunctiva was attached using a drop of glue. On the lowest disk, the material was held. Disks were getting closer at a constant speed of 0.1 mm/s until contact. Then, both disks continue in contact for 2 minutes at a constant force of 2 N. Finally, the upper disk is detached at a constant speed of 0.3 mm/s. The data was collected using TRIOS software and processed afterwards with Microsoft Excel 2021 and GraphPad Prism 9.3.

4.4.6 Thermal and X-ray diffraction characterization for hydrogels' opacity comprehension

4.4.6.1 Thermogravimetric analysis (TGA)

Hydrogels A-E (10 mg) were heated from 30 – 700 °C at a heating rate of 10 °C/min in aluminium oxide crucibles under a pure nitrogen atmosphere. Mass changes were measured using a Thermal Gravimetric Analyzer (Perkin Elmer™, STA 6000). The data was processed afterwards with the software Origin 2021 Pro and GraphPad Prism 9.3.

4.4.6.2 Differential Scanning Calorimetry (DSC)

DSC experiments were performed on a PerkinElmer 8500 DSC equipped with an Intracooler III, calibrated for temperature and heat flow using an indium standard. Non isothermal experiments were made. Samples (about 3 mg) were placed in non-recyclable aluminium hermetic pans and analyzed under a nitrogen atmosphere by heating and cooling scans at 20 °C/min. First, the samples were heated from 30 to 90 °C, kept isothermally for 3 min to erase the thermal history, and cooled down to 30 °C. Subsequently, a heating scan was made for all the samples. Data have been processed with the software Origin 2021 Pro and GraphPad Prism 9.3.

4.4.6.3 Wide-angle X-ray scattering (WAXS)

X-ray powder diffraction patterns were collected by using a Philips X'pert PRO automatic diffractometer operating at 40 kV and 40 mA, in theta-theta configuration, secondary monochromator with Cu-K α radiation ($\lambda = 1.5418 \text{ \AA}$) and a PIXcel solid state detector (active length in 2θ 3.347°). Data were collected from 5 to 70° 2θ , step size of 0.026° and time per step of 180s at RT (total time 30 min). A variable divergence slit giving a constant 8 mm area of sample illumination was used. The data was processed afterwards with GraphPad Prism 9.3.

4.4.7 Bovine Serum Albumin as a model for encapsulation and release studies

Bovine Serum Albumin chemically conjugated with the fluorophore fluorescein isothiocyanate (BSA-FITC) was encapsulated inside the 5 different hydrogels (A – E). 5 mg of BSA-FITC were added to a pre-gel solution of each hydrogel to prepare samples of 5.5 x 3.5 x 0.1 cm in a silicone mould.

For the release studies, a piece of 1.5 x 0.5 x 0.1 cm was cut and set in the 3D mould release system. The same methodology as the one detailed in section **4.4.3.3** was applied. The generated aliquots were collected every 5 min and quantified by measuring the maximum absorbance from the FITC at 494 nm in a NanoPhotometer NP80 from Implen® processed afterwards with GraphPad Prism 9.3.

4.4.8 Growth Factors encapsulation and release studies

Powder lyophilized GF (obtained from AM, ethically approved CEIC E20/05 from Cruces) were encapsulated inside hydrogels A – E. 1 mL of GF stock solution (5 mg/mL in PBS 0.001M, pH = 7.4) were added to a pre-gel solution of each material to prepare samples of 5.5 x 3.5 x 0.1 cm in a silicone mould.

For the release studies, a piece of 1.5 x 0.5 x 0.1 cm was cut and set in the 3D mould release system. The same methodology as the one detailed in section 4.4.3.3 was applied. The generated aliquots were collected every 5 min and mixed with the EZQ reagent. Indirect quantification was done by measuring the EZQ fluorescence in a BioTek Synergy Neo 2 multi-mode reader. The data have been collected with the software GEO 5 3.1 and interpolated into a calibration curve to get the amount of GF released. The final data were processed with GraphPad Prism 9.3.

4.4.9 Metabolic activity of MRC-5 cells. *In-vitro* studies

The different formulations of hydrogels were dissolved at different degrees (25%, 50% and 100% dissolution) by placing a sample of the hydrogel (1.5 x 0.5 x 0.1 cm) in 2 mL of BSS. The resulting solution was mixed (1:1 ratio) with complete media and subsequently sterile-filtered. To determine the cellular metabolic activity in response to the different hydrogel formulations, human fibroblasts (MRC-5, ATCC) were seeded at a density of 5,000 cells/well on 96-well plates with complete medium (DMEM + 10% FBS + 1% P/S) and incubated overnight to allow cell adherence to the tissue culture plastic. Then, complete media was aspirated and replaced by the aforementioned solutions containing the hydrogel degradation byproducts. The metabolic activity was determined after 24 and 48 with AlamaBlue® following a previously reported protocol^[94]. In this experiment, BSS mixed with complete media (1:1 ratio) was used as a control. The data were processed with the software Microsoft Excel 2021 and GraphPad Prism 9.3.

4.4.10 Metabolic activity of WKD conjunctiva cells. *In-vitro* studies

The different formulations of hydrogels were dissolved by placing a sample of the hydrogel (1.5 x 0.5 x 1 cm) in 2 mL of BSS. The resulting solution was mixed (1:1 ratio) with complete media and subsequently sterile-filtered. To determine the cellular metabolic activity in response to the different

hydrogel formulations, The Wong Kilbourne derivate of Chang conjunctiva epithelial cell line (WKD; clon 1-5c-4, American Type Culture Collection, [ATCC, Manassas, VA] certified cell line [CCL], 20.2) were seed at a density of 15,000 cells/well on 96-well plated with medium (M199) supplemented with 50 mg/mL of penicillin-streptomycin and 10 % of fetal bovine serum. The culture took place at 95 % of humidity, 5 % of CO₂ and 37 °C. The metabolic activity was determined after 72 h with cell proliferation Kit XTT II. In this experiment, the control was WKD cells with a culture medium (M199, FBS 10x, penicillin-streptomycin 1x). The data were processed with the software Microsoft Excel 2021 and GraphPad Prism 9.3.

4.4.11 *In-vivo* assays (I): Eye-adhesion study

The *In-vivo* experiments were carried out with ethical permission from diputación general de Gipuzkoa (PRA-AR-SS-196) and the animal experimentation committee approved (CEEA20/15). Hydrogels were cut into pieces of 0.4 x 0.4 x 0.1 cm and sterilized with a UV germicidal lamp of 254 nm, 15W for 30 min for each side. Hydrogels were pre-hydrated with BSS (10 µL) for 15 min before they were placed on the eye. In addition, the rabbit's eye was anaesthetized prior to implant placement. After placing the implant, the eyelid was closed on holding for 2 min. Then, the eyelid was opened and closed multiple times to corroborate if the hydrogel was still on the ocular surface.

4.4.12 *In-vivo* assays (II): Efficacy studies

An epithelial defect area was created on the eye's surface of rabbits with 1M NaOH under general anaesthesia. A total of 27 rabbits were necessary for the whole experiment. 9 rabbits were treated with Tobradex (commercial anti-inflammatory and antibiotic solution) as a negative control. Another 9 rabbits were treated with AM transplanted around the eye as a positive control. The remaining 9 rabbits were treated with the hydrogel candidate loaded with GF. A patch of 0.4 x 0.4 x 0.1 cm was placed on the eye every 12h for 7 days. Pictures were taken with a camera after 7, 14, 21 and 28 days to measure the dimension of the epithelial defect. Data were processed with GraphPad Prism 9.3.

4.5 Main remarks, conclusions and future perspective

Physically cross-linked hydrogels have been prepared based on PVP, PVA, PEG, glycerol and five types of Eudragits (RSPO, RL100, S100, L100 and L100-55) by solve casting technique. All the formulations have been prepared homogeneously and a reproducible protocol has been generated. Hydrogel C, based on Eudragit S100, has turned out to be the most promising material among the five films. First of all, this hydrogel is the one that has been prepared with greater homogeneity and reproducibility. Besides, it shows the smallest pore size and the best-swollen capacity while preserving its integrity. The mechanical analysis has reported that hydrogel C is also the one with the smallest young's modulus but the biggest tensile strength, which highlights the great elastic behaviour of the material with optimal behaviour to resist ocular mechanical stress. Moreover, hydrogel C is the only one with a big sustained BSA and GF release, where the maximum amount of GF are released in the last 30 min. This guarantees a constant presence of GF concentration in the eye. The modification of hydrogel C with HPC or HA have reported an increase in the mucoadhesion capacities. This has let the preparation of a final hydrogel candidate with promising pre-clinical results. The *In-vivo* assays have concluded a better epithelial defect closure after 14 and 21 days in comparison with the negative control. Even though the positive control has reported better therapeutic results, the hydrogel can be placed without surgery. Therefore, it can be concluded that the hydrogel can reduce the risk for the patient, compared to the current treatment with AM, while improving patient compliance.

One might mention that the therapeutic effect achieved with the hydrogel C modified with HA in the efficacy studies is promising despite being still preliminary. Hence, from a future perspective, it is expected to keep improving the formulation to get closer to a material that can be studied in a clinical set up. The global goal is to find a formulation that ends up replacing the current treatment based on the transplant of the AM. Consequently, future research will be focused on optimizing ring-shaped 3D printed hydrogels that avoid free movement of the material in the eye. In addition, the chemically cross-linked of the hydrogel will also be investigated to reinforce its structure.

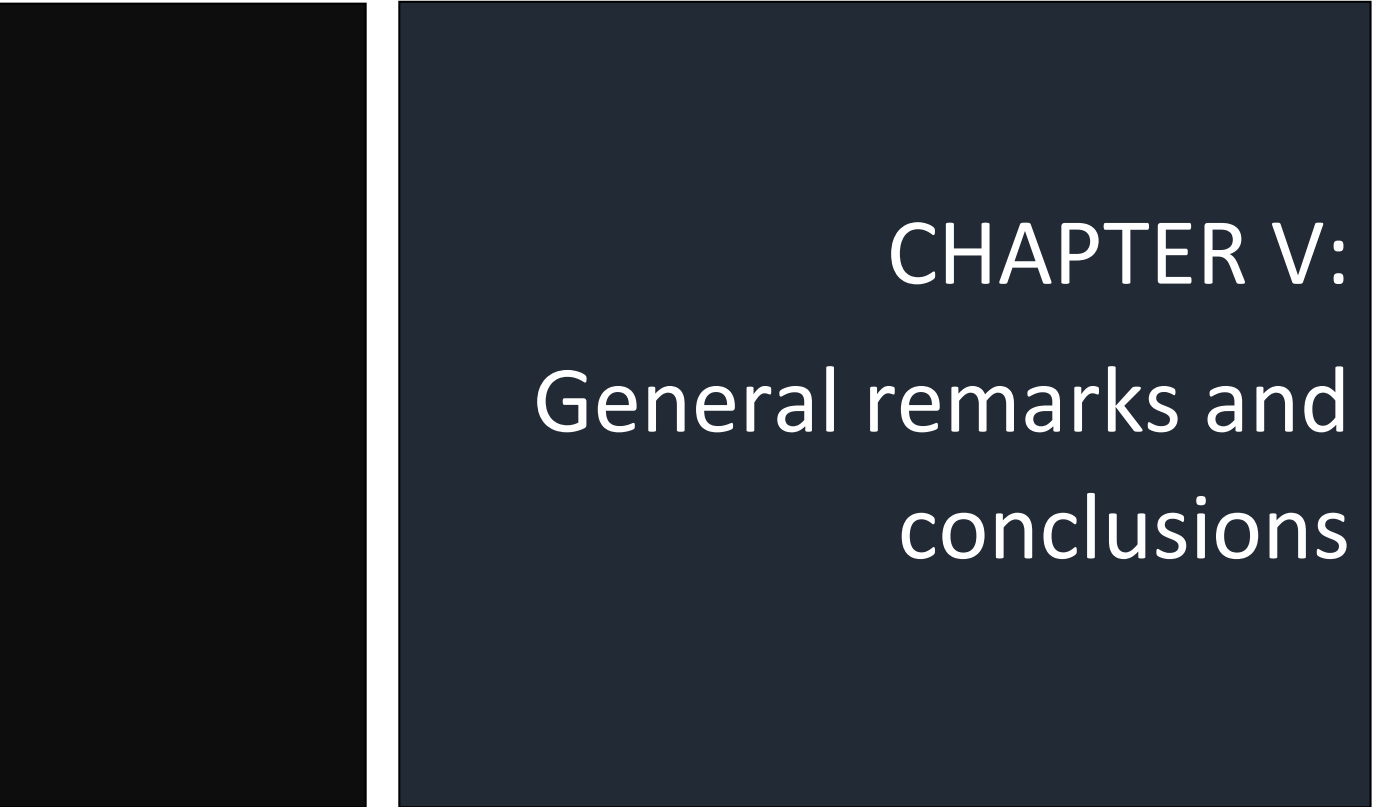
4.6 References – Chapter IV

- [1] M. Mahinroosta, Z. Jomeh Farsangi, A. Allahverdi, Z. Shakoori, *Mater. Today Chem.* **2018**, *8*, 42.
- [2] S. Amin, S. Rajabnezhad, K. Kohli, *Sci. Res. Essays* **2009**, *4*, 1175.
- [3] M. F. Akhtar, M. Hanif, N. M. Ranjha, *Saudi Pharm. J.* **2016**, *24*, 554.
- [4] R. C. Cooper, H. Yang, *J. Control. Release* **2019**, *306*, 29.
- [5] S. C. Lee, I. K. Kwon, K. Park, *Adv. Drug Deliv. Rev.* **2013**, *65*, 17.
- [6] Z. Sun, C. Song, C. Wang, Y. Hu, J. Wu, *Mol. Pharm.* **2020**, *17*, 373.
- [7] M. Kumari, A. Dhasmana, *Adv. Tissue Eng. Regen. Med.* **2020**, *6*, 20.
- [8] A. Bashari, A. Rouhani Shirvan, M. Shakeri, *Polym. Adv. Technol.* **2018**, *29*, 2853.
- [9] S. Cascone, G. Lamberti, *Int. J. Pharm.* **2020**, *573*, 118803.
- [10] K. Y. Seo, S. J. Han, H.-R. Cha, S.-U. Seo, J.-H. Song, S.-H. Chung, M.-N. Kweon, *J. Immunol.* **2010**, *185*, 3610.
- [11] S. Jacob, A. B. Nair, S. H. S. Boddu, B. Gorain, N. Sreeharsha, J. Shah, *Pharmaceutics* **2021**, *13*, 1.
- [12] H. M. Vanbenschoten, K. A. Woodrow, *Adv. Drug Deliv. Rev.* **2021**, *178*, 113956.
- [13] R. Lombardo, T. Musumeci, C. Carbone, R. Pignatello, *Pharm. Dev. Technol.* **2021**, *26*, 824.
- [14] A. J. Kinloch, *J. Mater. Sci.* **1982**, *15*, 2141.
- [15] J. Woodley, *Clin. Pharmacokinet.* **2001**, *40*, 77.
- [16] A. Allen, D. Snary, *Gut* **1972**, 666.
- [17] V. V. Khutoryanskiy, *Macromol. Biosci.* **2011**, *11*, 748.
- [18] S. Roy, K. Pal, A. Anis, K. Pramanik, B. Prabhakar, *Des. Monomers Polym.* **2009**, *12*, 483.
- [19] G. S. Asane, S. A. Nirmal, K. B. Rasal, A. A. Naik, M. S. Mahadik, Y. M. Rao, *Drug Dev. Ind. Pharm.* **2008**, *34*, 1246.
- [20] R. S. Dave, T. C. Goostrey, M. Ziolkowska, S. Czerny-Holownia, T. Hoare, H. Sheardown, *J. Control. Release* **2021**, *336*, 71.
- [21] S. Singh, Neelam, S. Arora, Y. P. Singla, *Asian J. Pharm. Clin. Res.* **2015**, *8*, 1.
- [22] V. Nikam, K. Kotade, V. Gaware, R. Dolas, K. Dhamak, S. Somwanshi, A. Khadse, V. Kashid, *Pharmacologyonline* **2011**, *1*, 152.
- [23] S. Thakral, N. K. Thakral, D. K. Majumdar, *Expert Opin. Drug Deliv.* **2013**, *10*, 131.
- [24] P. Franco, I. De Marco, *Polymers (Basel)*. **2021**, *13*, 1102.
- [25] S. Mahmood, M. A. Buabeid, K. Ullah, G. Murtaza, A. Mannan, S. A. Khan, *Curr. Drug Deliv.* **2019**, *16*, 548.
- [26] P. D. S. Chaves, L. A. Frank, A. G. Frank, A. R. Pohlmann, S. S. Guterres, R. C. R. Beck, *Am. Assoc. Pharm. Sci.* **2018**, *19*, 1637.
- [27] K. M. Manjunatha, G. T. Kulkarni, M. Ismail, *Int. J. Pharm. Sci. Res.* **2012**, *3*, 3915.

- [28] Z. Jafariazar, N. Jamalnia, F. Ghorbani-bidkorbeh, S. Alireza Mortazavi, *Iran. J. Pharm. Res.* **2015**, *14*, 23.
- [29] S. Mirzaeei, M. Alizadeh, *J. Reports Pharm. Sci.* **2017**, *6*, 123.
- [30] A. Ludwig, *Adv. Drug Deliv. Rev.* **2005**, *57*, 1595.
- [31] L. I. Tártara, S. D. Palma, D. Allemandi, M. I. Ahumada, J. M. Llabot, *Recent Patents Drug Deliv. Formul.* **2014**, *8*.
- [32] H. S. Dua, A. Azuara-Blanco, *Surv. Ophthalmol.* **2000**, *44*, 415.
- [33] M. Inobe, S. Takeda, *J. Biol. Chem.* **2000**, *265*, 2116.
- [34] R. Levi-Montalcini, P. U. Angeletti, *Physiological Rev.* **1968**, *48*, 534.
- [35] G. K. M. R. Zarnegat, *AASLD Hepatol.* **1992**, *15*, 149.
- [36] D.J.Hill, R. D. G. Milner, *Pediatr. Res.* **1985**, *19*, 879.
- [37] D. Meller, M. Pauklin, H. Thomasen, H. Westekemper, K.-P. Steuhl, *Dtsch. Aertzblatt Int.* **2011**, *108*, 243.
- [38] S. M. Pawde, K. Deshmukh, *J. Appl. Polym. Sci.* **2008**, *109*, 3431.
- [39] L. Martin, C. G. Wilson, F. Koosha, I. F. Uchegbu, *Eur. J. Pharm. Biopharm.* **2003**, *55*, 35.
- [40] M. E. de Vries, H. E. Boddé, H. J. Busscher, H. E. Junginger, *J. Biomed. Mater. Res.* **1988**, *22*, 1023.
- [41] A. M. dos Santos, S. G. Carvalho, V. H. S. Araujo, G. C. Carvalho, M. P. D. Gremião, M. Chorilli, *Int. J. Pharm.* **2020**, *590*, 119867.
- [42] I. A. Alsarra, A. Y. Hamed, G. M. Mahrous, G. M. El Maghraby, A. A. Al-Robayan, F. K. Alanazi, *Drug Dev. Ind. Pharm.* **2009**, *35*, 352.
- [43] A. S. Ahmed, U. K. Mandal, M. Taher, D. Susanti, J. M. Jaffri, *Pharm. Dev. Technol.* **2018**, *23*, 751.
- [44] L. Li, S. Guan, L. Yang, X. Qin, W. Feng, *Chem. Res. Chinese Univ.* **2018**, *34*, 311.
- [45] C. M. Dawidczyk, C. Kim, J. H. Park, L. M. Russell, K. H. Lee, M. G. Pomper, P. C. Searson, *J. Control. Release* **2014**, *187*, 133.
- [46] R. Ricciardi, F. Auriemma, C. Gaillet, C. De Rosa, F. Lauprêtre, *Macromolecules* **2004**, *37*, 9510.
- [47] X. Xue, Y. Hu, S. Wang, X. Chen, Y. Jiang, J. Su, *Bioact. Mater.* **2022**, *12*, 327.
- [48] J. Grenier, H. Duval, F. Barou, P. Lv, B. David, D. Letourneur, *Acta Biomater.* **2019**, *94*, 195.
- [49] S. hee Kim, C. C. Chu, *J. Biomed. Mater. Res.* **2000**, *53*, 258.
- [50] B. Vázquez, J. San Roman, C. Peniche, M. E. Cohen, *Macromolecules* **1997**, *30*, 8440.
- [51] S. Garg, A. Garg, *Asian J. Biomater. Res.* **2016**, *2*, 163.
- [52] M. Naeimi, R. Tajedin, F. Farahmandfar, M. Naeimi, M. Monajjemi, *Mater. Res. Express* **2020**, *7*.
- [53] Y. Zhang, L. Ye, M. Cui, B. Yang, J. Li, H. Sun, F. Yao, *RSC Adv.* **2015**, *5*, 78180.
- [54] S. Lefnaoui, N. Moulai-mostefa, M. M. Yahoum, S. N. Gasmí, S.

- Lefnaoui, N. Moulai-mostefa, M. M. Yahoum, S. N. Gasmi, *Drug Dev. Ind. Pharm.* **2018**, *44*, 432.
- [55] S. Lefnaoui, N. Moulai-Mostefa, M. M. Yahoum, S. N. Gasmi, *Drug Dev. Ind. Pharm.* **2018**, *44*, 432.
- [56] Y. Huang, H. Yu, C. Xiao, *Carbohydr. Polym.* **2007**, *69*, 774.
- [57] I. M. El-Sherbiny, R. J. Lins, E. M. Abdel-Bary, D. R. K. Harding, *Eur. Polym. J.* **2005**, *41*, 2584.
- [58] P. Karacan, H. Cakmak, O. Okay, *J. Appl. Polym. Sci.* **2013**, *128*, 3330.
- [59] M. Safari, I. Otaegi, N. Aramburu, G. Guerrica-Echevarria, A. M. De Ilarduya, H. Sardon, A. J. Müller, *Polymers (Basel)*. **2021**, *13*, 1.
- [60] M. Tahsin, S. Karaman, H. Cankurt, A. Kayacier, O. Sagdic, *J. Food Eng.* **2011**, *103*, 197.
- [61] M. K. Chaudhury, *J. Phys. Chem. B* **1999**, *103*, 6562.
- [62] A. Ghatak, K. Vorvolakos, H. She, D. L. Malotky, M. K. Chaudhury, *J. Phys. Chem. B* **2000**, *104*, 4018.
- [63] J. Li, A. D. Celiz, J. Yang, Q. Yang, I. Wamala, W. Whyte, B. R. Seo, N. V. Vasilyev, J. J. Vlassak, Z. Suo, D. J. Mooney, *Science* **2017**, *357*, 378.
- [64] S. Lin, X. Liu, J. Liu, H. Yuk, H. Loh, G. A. Parada, C. Settens, J. Song, A. Masic, G. H. Mckinley, X. Zhao, *Sci. Adv.* **2019**, 1.
- [65] M. K. Barron, T. J. Young, K. P. Johnston, R. O. Williams, *AAPS PharmSciTech* **2003**, *4*, 1.
- [66] B. Leader, Q. J. Baca, D. E. Golan, *Nat. Rev. Drug Discov.* **2008**, *7*, 21.
- [67] F. E. Cohen, J. W. Kelly, *Nature* **2003**, *426*, 905.
- [68] C. Rothe, A. Skerra, *BioDrugs* **2018**, *32*, 233.
- [69] H. Singh, R. Jakhar, N. Sehrawat, *Heliyon* **2020**, *6*, e05528.
- [70] L. R. Brown, *Expert Opin. Drug Deliv.* **2005**, *2*, 29.
- [71] J. Liu, Z. Bian, A. M. Kuijpers-Jagtman, J. W. Von Den Hoff, *Orthod. Craniofacial Res.* **2010**, *13*, 11.
- [72] Y. Chen, L. Liu, *Adv. Drug Deliv. Rev.* **2012**, *64*, 640.
- [73] S. Hossen, M. K. Hossain, M. K. Basher, M. N. H. Mia, M. T. Rahman, M. J. Uddin, *J. Adv. Res.* **2019**, *15*, 1.
- [74] D. Lombardo, M. A. Kiselev, M. T. Caccamo, *J. Nanomater.* **2019**, *3702518*, 26.
- [75] J. Maitra, V. K. Shukla, *Am. J. Polym. Sci.* **2014**, *4*, 25.
- [76] F. Stapleton, S. Stretton, E. Papas, C. Skotnitsky, D. F. Sweeney, *Ocul. Surf.* **2006**, *4*, 24.
- [77] M. W. Sabaa, D. H. Hanna, M. H. Abu Elella, R. R. Mohamed, *Mater. Sci. Eng. C* **2019**, *94*, 1044.
- [78] C. Wischke, H. Borchert, *Pharmazie* **2006**, *61*, 770.
- [79] S. Sheth, E. Barnard, B. Hyatt, M. Rathinam, S. P. Zustiak, *Front. Bioeng. Biotechnol.* **2019**, *7*, 1.
- [80] P. L. Ritger, N. A. Peppas, *J. Control. Release* **1987**, *5*, 37.
- [81] B. J. Agnew, D. Murray, W. F. Patton, *Electrophoresis* **2004**, *25*, 2478.

- [82] J. Dos Santos, G. S. da Silva, M. C. Velho, R. C. R. Beck, *Pharmaceutics* **2021**, *13*, 1.
- [83] A. Gallud, M. Delaval, P. Kinaret, V. S. Marwah, V. Fortino, J. Ytterberg, R. Zubarev, T. Skoog, J. Kere, M. Correia, K. Loeschner, Z. Al-Ahmady, K. Kostarelos, J. Ruiz, D. Astruc, M. Monopoli, R. Handy, S. Moya, K. Savolainen, H. Alenius, D. Greco, B. Fadeel, *Adv. Sci.* **2020**, *7*, 1.
- [84] A. K. Sharma, A. Arya, P. K. Sahoo, D. K. Majumdar, *Mater. Sci. Eng. C* **2016**, *67*, 779.
- [85] X. Zhang, D. Wei, Y. Xu, Q. Zhu, *Carbohydr. Polym.* **2021**, *264*, 118006.
- [86] A. Graça, L. M. Gonçalves, S. Raposo, H. M. Ribeiro, J. Marto, *Pharmaceutics* **2018**, *10*.
- [87] H. C. Arca, L. I. Mosquera-Giraldo, V. Bi, D. Xu, L. S. Taylor, K. J. Edgar, *Biomacromolecules* **2018**, *19*, 2351.
- [88] C. A. Lee, B. S. Kim, C. W. Cho, *J. Pharm. Investig.* **2016**, *46*, 189.
- [89] N. A. Peppas, N. K. Mongia, *Eur. J. Pharm. Biopharm.* **1997**, *43*, 51.
- [90] L. Ahmed Naeem, *IAJMR.* **2017**, *3*, 984, 991.
- [91] S. Venkatraman, R. Gale, *Biomaterials* **1998**, *19*, 1119.
- [92] L. Greenspan, *J. Res. Natl. Bur. Stand.* **1977**, *81A*, 89.
- [93] E. C. Kim, S. H. Doh, S. Y. Chung, S. Y. Yoon, M. S. Kim, S. K. Chung, M. C. Shin, H. S. Hwang, *Acta Ophthalmol.* **2017**, 314.
- [94] E. Marin, C. Tapeinos, S. Lauciello, G. Ciofani, J. R. Sarasua, A. Larrañaga, *Mater. Sci. Eng. C* **2020**, *117*, 111349.



CHAPTER V:
General remarks and
conclusions

5.1 General remarks and conclusions

Human life expectancy has been seen to grow year by year. Some years ago, people could not even get to know their grandchildren, nowadays many of them are meeting their great-grandson. Besides, the lifestyle is also changing every day. From developing novel and powerful technology, to improve therapeutic treatments. If polymers were developed to be used as therapeutics in the XX century, NPs have been widely explored in the XXI century to promote polymers to a new revolution. The use of smart polymers, hybrid systems, a better understanding of the biointerface or mimicking of biological surroundings are just a few of examples of the science behind all of these achievements. The most recent and promising technologies for novel therapies have been reviewed in **Chapter I** and the introduction sections of **Chapters III** and **IV**. The work that has been presented in this PhD thesis has aimed to increase the scientific knowledge about the mechanism that materials (at nano and microscale) are following to interact with biomolecules. For that, the work has been divided into two sections.

Section A has come as a breath of fresh air to NGs. It has been demonstrated that hybrid materials can be considered as a new class of nanodevices that combine the best of two worlds. For that, organic NPs have been used as a layer where inorganic ones can be hidden. This has a double benefit, while decreasing the underside toxicological effect, it also provides new functionalities to the inorganic NPs. An encapsulation of inorganic NPs inside of NGs has emerged as a promising strategy. Nevertheless, the big thickness that NGs typically have in comparison with the small diameter of inorganic NPs could have a negative effect. As their great optical properties are being depleted as a consequence of the big polymeric thickness. Which can be translated into a decrease on their potential applications when interacting with biological environments. To eliminate this “unfair” balance of organic and inorganic material, **Chapter III** has shown a novel methodology to prepare a thin mantle NG onto AuNPs. To highlight the promising potential of these novel systems, four different AuNPs were explored. Au nanospheres with diameters of 13 and 40 nm, together with nanorods and nanostars with diameter of 40 nm were prepared. The technology optimized along this work, allowed the encapsulation of AuNPs into a thin polymeric mantle NG, increasing their total diameter in just 2 – 6 nm, while keeping the original shape of the inorganic cores. The protocols were optimized, with minimum modifications, for isotropic and anisotropic AuNPs demonstrating their easy adaptability. Besides, it has been demonstrated that the protocols work with neutral, zwitterionic and thermoresponsive polymers with identical synthetic

yield and morphological results. Therefore, the surface charge of the NGs and their hydrophilicity has been very easy to modulate.

To raise the applicability of these materials, they have been exposed to proteins, mucin and salts. In general, it has been found that thanks to the NGs, the stability of AuNPs have been improved and the interaction with the mucin controlled. Varying the surface charge and hydrophilicity degree of the NG, it is possible to decrease the protein corona effect, which had been translated into stability improvement of the AuNPs. In fact, p-acrylamide and p-vinylimidazole NGs have had the least interaction with the BSA. Nevertheless, the effect with the mucin had been the opposite, being these two NGs the ones with stronger interactions. By comparison, zwitterionic Au-NGs based on p-DMAPS have proven the opposite behaviour, with fewer interactions with mucin but more affinity for the appearance of PC, which decrease the AuNPs stability. Thin NGs developed in this work have also represented a step forward in the stability of AuNPs when irradiated with a laser. In summary, these NGs have opened up a world of possibilities that allows tuning a chemically cross-linked shell while keeping the original size and shape of AuNPs. In the end, better stabilities have been achieved, new functionalities have been offered which have led to a substantial improvement in the responses of the materials to the biointerface.

This **A** section have been at the forefront of research with the development of a new methodology to reduce the thickness of NGs around inorganic NPs. Drawing from the premise of established methodologies for enzymes, a new and re-imagined branch of materials had been opened.

Section B have explored the biointerface at the microscale with the preparation of physically cross-linked hydrogels based on several Eudragit polymers. Even though Eudragit is a family of well-known polymers used in several pharmaceutical formulations, understanding their behaviour inside of a hydrogel matrix was still challenging. **Chapter IV** has tried to get some light into the darkness by preparing several hydrogel formulations with a broad set of Eudragits and performing deep characterizations. The combination of Eudragit S100, soluble at physiological pH, with PVP, PVA, PEG and hyaluronic acid have led to preparing a hydrogel with the capacity to release GF in the eye. To achieve that goal, the material faced the ocular biointerface showing quite promising mucoadhesion properties. The developed hydrogel has remained in the eye, in contact with the conjunctiva and mechanically held with the eyelid as extra support. This goal has been achieved after exploring many formulations until one with a small Young's modulus, good control over

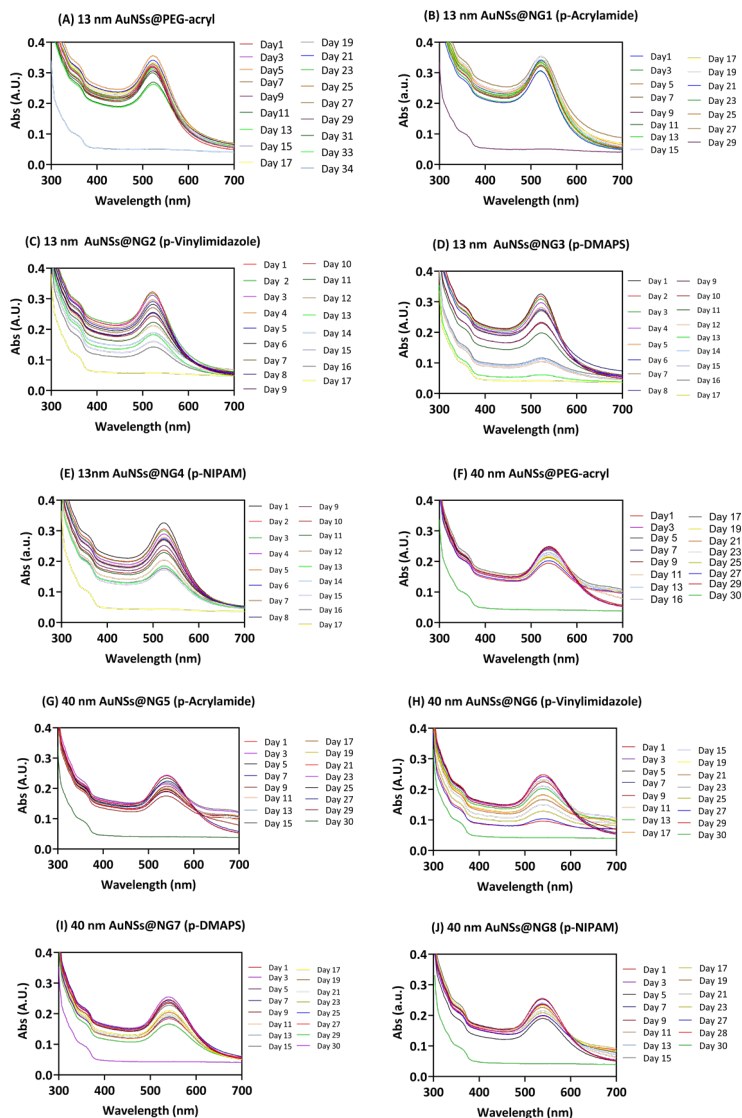
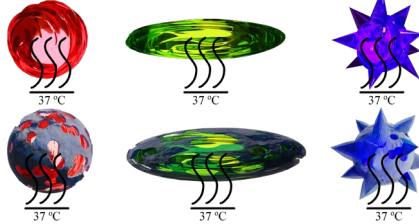
the thickness and pore size distribution, good stability at ocular conditions, sustained GF release and no cell toxicity was achieved. The maturity of the material has made it possible to jump into pre-clinical studies, using rabbits as animal models. Although the results are yet preliminary, it has been possible to eliminate the epithelial defect after 14 days of treatment. Taking into account that the current alternative treatment involves transplanting an AM around the eye, placing a hydrogel every 12 h for 2 weeks promises to revolutionize medicine. However, one should be aware that there is still a lot of work to be done to bring this material into the clinics. Even so, the work done in **section B** of this PhD thesis can be considered the first “little grain of sand” for tomorrow’s ophthalmological treatments.

In summary, this thesis has demonstrated that it is possible to fine-tuning the interactions between hybrid materials and biological fluids. In fact, the stability of AuNPs in presence of biological fluids have been notably improved thanks to their encapsulation in NGs. Also, hybrid hydrogels have demonstrated the feasibility to tune their interaction with ocular mucin and their capacity to release GF directly into the eye.

ANNEXES

Annex I: UV-VIS spectra showing the plasmon band evolution of AuNPs at 37 °C

Scenario I: AuNPs incubated at 37 °C



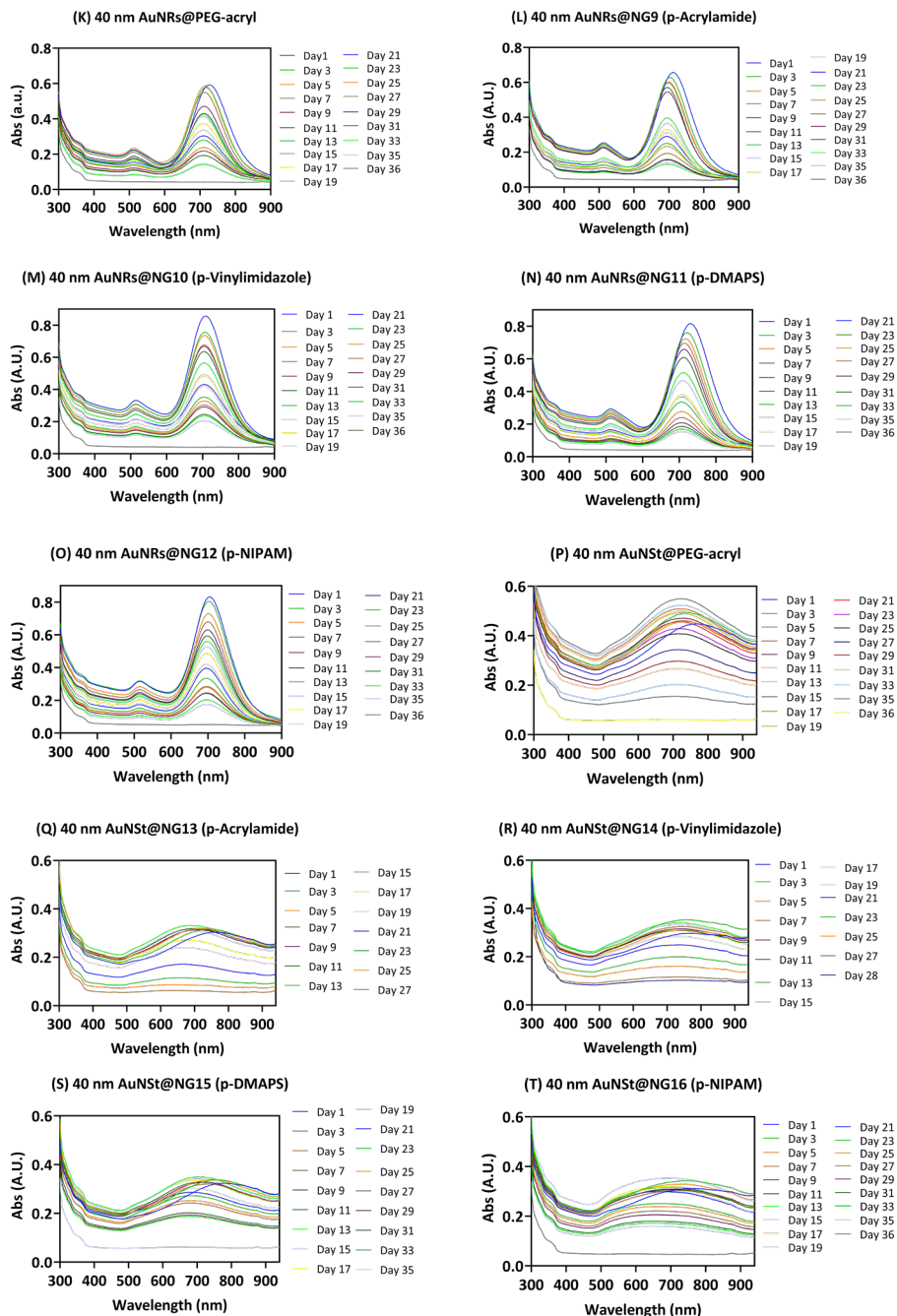
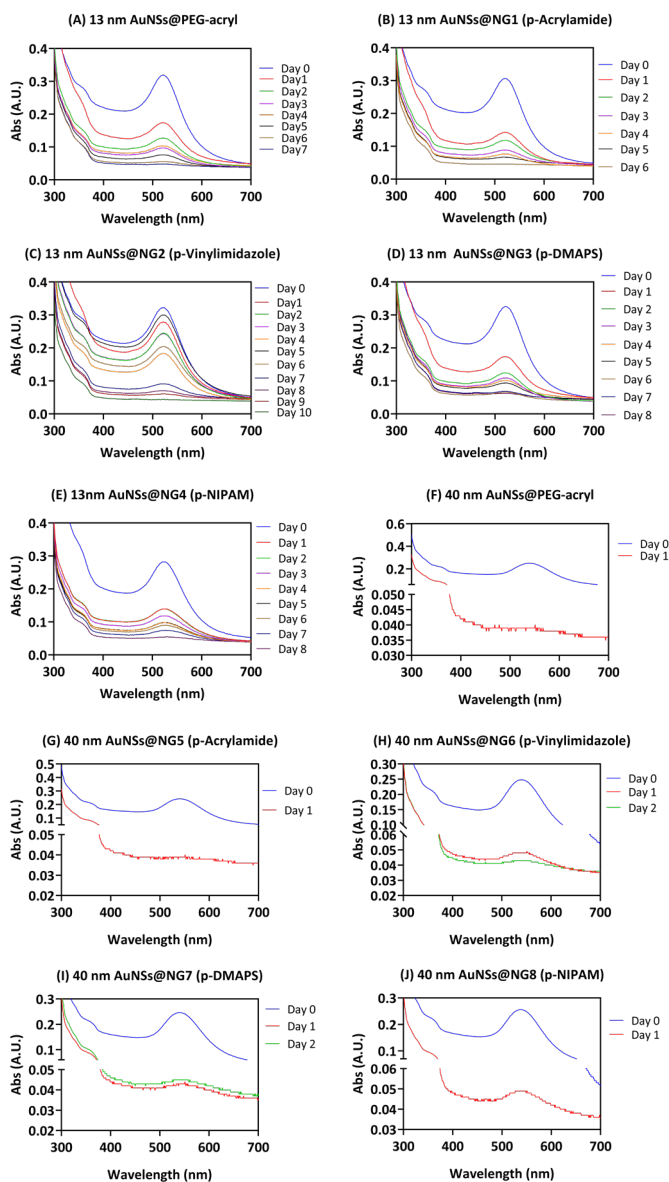
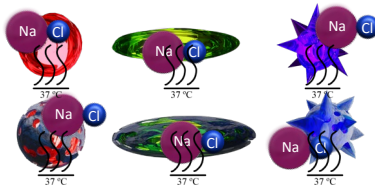


Figure Annex I. (Scenario I) Evolution of the UV-VIS spectra along the time obtained incubating the materials at 37 °C for NPs grafted with PEG-acryl and encapsulated into p-acrylamide, p-vinylimidazole, p-DMAPS and p-NIPAM. (A - E) 13 nm Au nanospheres. (F - J) 40 nm Au nanospheres. (K - O) 40 nm Au nanorods. (P - T) 40 nm Au nanostars.

Annex II: UV-VIS spectra showing the plasmon band evolution of AuNPs at 37 °C in presence of NaCl

Scenario II: AuNPs incubated at 37 °C with NaCl



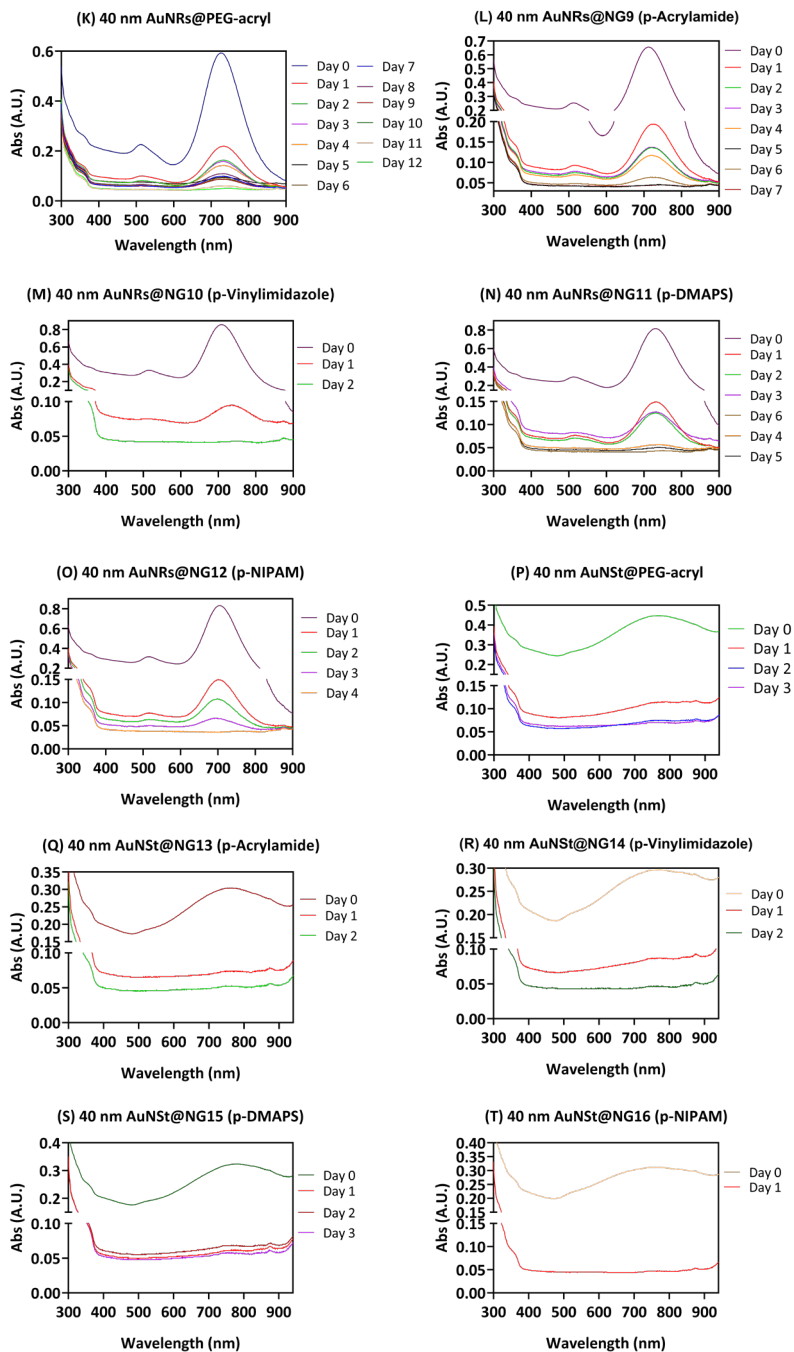
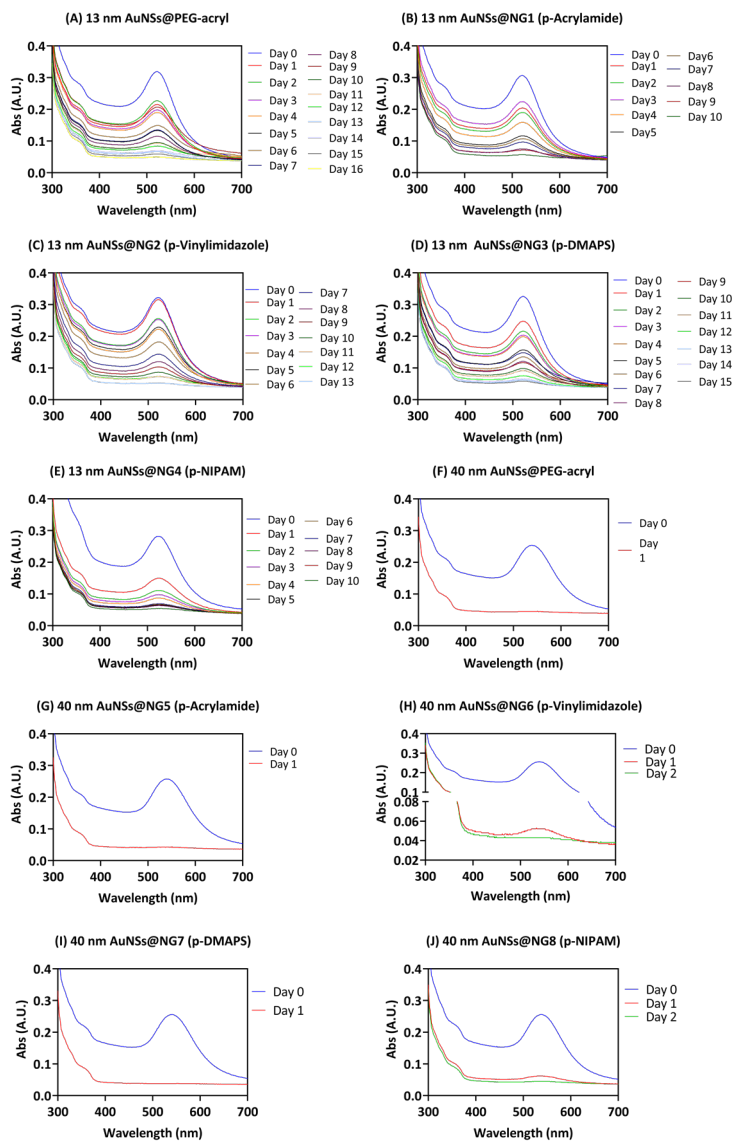
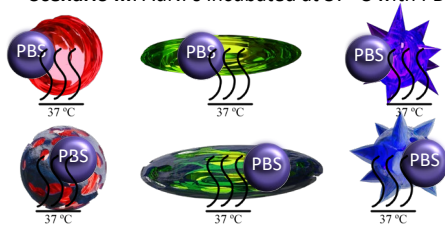


Figure Annex II. (Scenario II) Evolution of the UV-VIS spectra along the time obtained incubating the materials at 37 °C with NaCl 2M for NPs grafted with PEG-acryl and encapsulated into p-acrylamide, p-vinylimidazole, p-DMAPS and p-NIPAM. (A - E) 13 nm Au nanospheres. (F - J) 40 nm Au nanospheres. (K - O) 40 nm Au nanorods. (P - T) 40 nm Au nanostars.

Annex III: UV-VIS spectra showing the plasmon band evolution of AuNPs at 37 °C in presence of PBS

Scenario III: AuNPs incubated at 37 °C with PBS



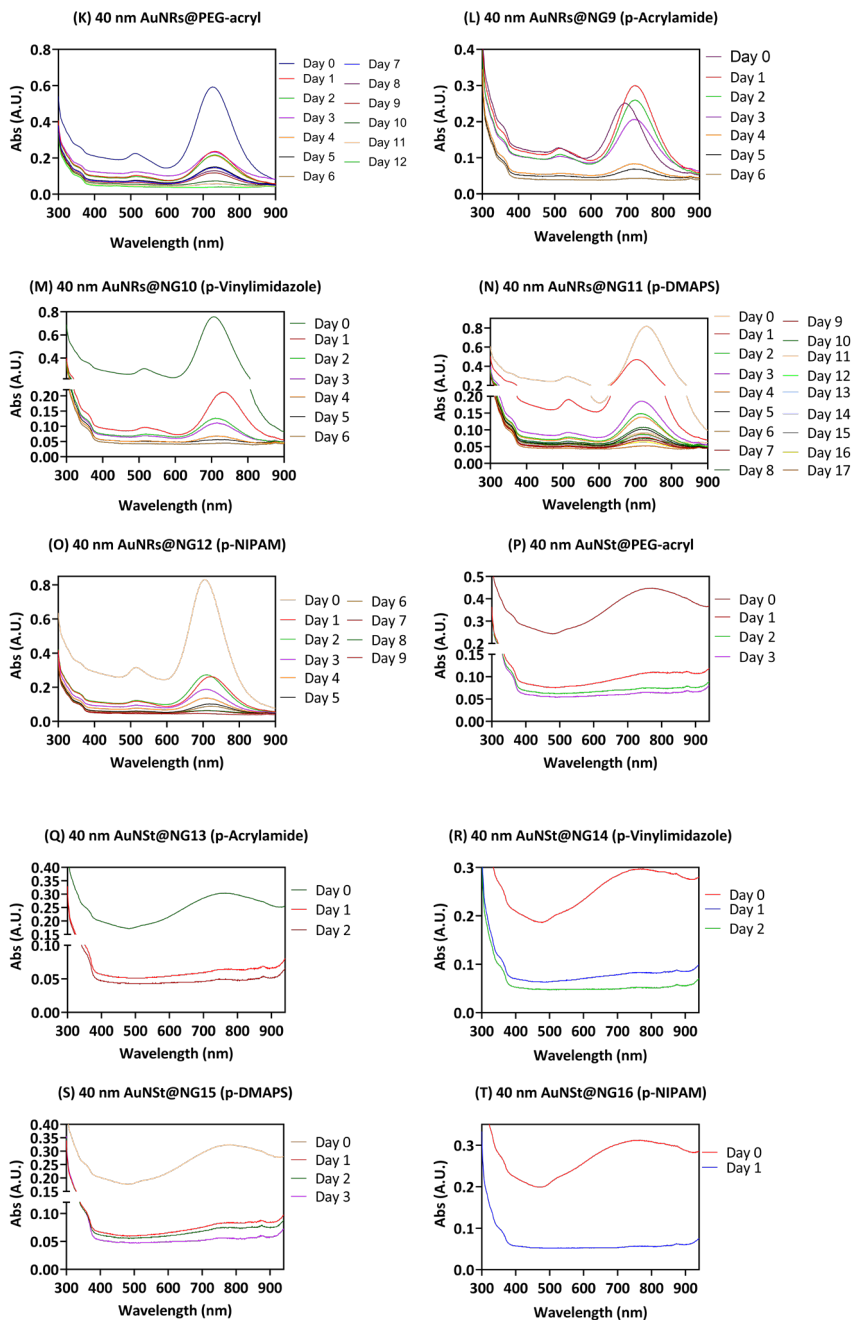
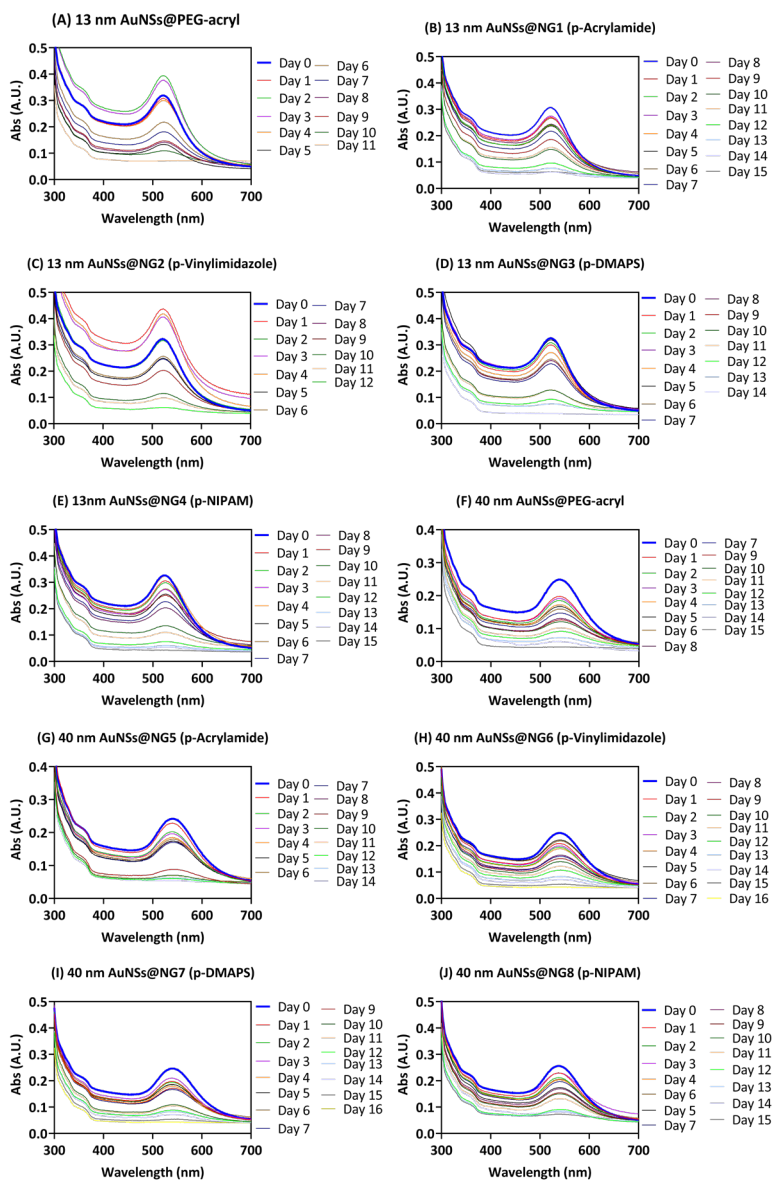
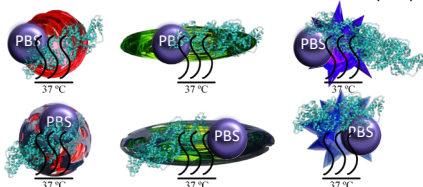


Figure Annex III. (Scenario III) Evolution of the UV-VIS spectra along the time obtained incubating the materials at 37 °C with PBS 10mM for NPs grafted with PEG-acryl and encapsulated into p-acrylamide, p-vinylimidazole, p-DMAPS and p-NIPAM. (A - E) 13 nm Au nanospheres. (F - J) 40 nm Au nanospheres. (K - O) 40 nm Au nanorods. (P - T) 40 nm Au nanostars.

Annex IV: UV-VIS spectra showing the plasmon band evolution of AuNPs at 37 °C in presence of BSA

Scenario IV: AuNPs incubated at 37 °C with BSA (PBS)



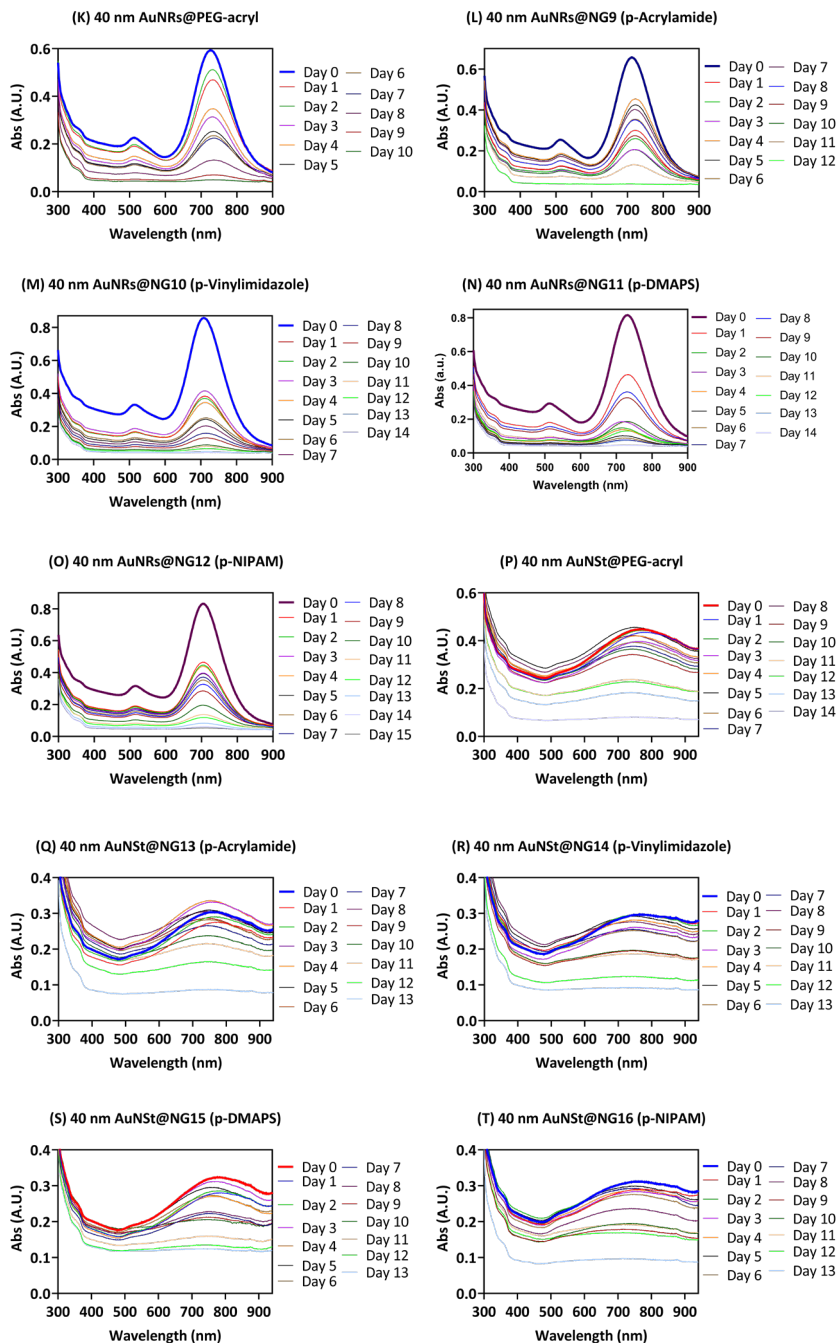


Figure Annex IV. (Scenario IV) Evolution of the UV-VIS spectra along the time obtained incubating the materials at 37 °C with BSA 1 mg/mL (in PBS 10 mM) for NPs grafted with PEG-acryl and encapsulated into p-acrylamide, p-vinylimidazole, p-DMAPS and p-NIPAM. (A - E) 13 nm Au nanospheres. (F - J) 40 nm Au nanospheres. (K – O) 40 nm Au nanorods. (P – T) 40 nm Au nanostars.

Annex V: Curriculum Vitae

- October 2018 – September 2022
(San Sebastián – Spain)
- Berc Polymat (Responsive Polymer Therapeutics Group; Prof. Marcelo Calderón)**
PhD Student Researcher
Principal Research Lines:
- Gold nanoparticles-based thin nanogels as smart nanocarriers and their study at the biointerface
 - Ophthalmic hydrogels based on FDA approved polymers to help into epithelial eye's recovery
 - Functionalized mesoporous nanoparticles nanocarriers as a key tool in a novel cancer/covid diagnosis device
- October 2017 – September 2018
(Zaragoza – Spain)
- Nanoscience and Materials Institute of Aragón (Bionanosurf Group; Prof. J. Martínez de la Fuente)**
Graduate Researcher
Synthesis and characterization of micelles and vesicles based on a tri-block co-peptides for biomedical applications
- November 2016 – September 2017
(Zaragoza - Spain)
- Nanoscience and Materials Institute of Aragón (Bionanosurf Group; Prof. J. Martínez de la Fuente)**
Undergraduate Researcher / Initial Research Fellow
Synthesis and characterization of derivative-polyetilenoglicol polymers to act as gold nanoparticles stabilizers for biomedical applications

Academic Degrees

In Course **PhD Degree in Applied Chemistry and Polymeric Materials**

Basque Country University (San Sebastián, Spain)

2018 **Master Degree in Nanostructures Materials for Nanotechnology Applications**

University of Zaragoza (Zaragoza, Spain)

2017 **Bachelor Degree in Chemistry**

University of Zaragoza (Zaragoza, Spain)

Software

Blender	Cinema 4D
Origin	NanoScope
GraphPad	Affinity Designer
MestReNova	SpectraGryph
ChemDraw	Trios Rehometer
Image J	Zetasizer



❖ Academic Publications

- “Nanocarriers for Skin Applications: Where Do We Stand?” N.Tiwari, E.Osorio-Blanco, A.Sonzogni, D.Esporrín-Ubieto, H.Wang, M.Calderon. **Angew. Chem. Int. Ed**, 2022, 61, e202107960 (1-26) .
<https://doi.org/10.1002/anie.202107960>



❖ International Stays

- Stay as PhD student researcher at the Freie Universität Berlin, FB Biologie, Chemie, Pharmazie, Institut für Pharmazie (**Berlin, Germany; 1.10.2018 – 31.12.2018**).



❖ Advance Characterization Equipment – Self user

- Scanning Electron Microscopy (SEM)
- Environmental Electron Microscopy (ESEM)
- Transmission Electron Microscopy (TEM)
- Atomic Force Microscopy (AFM)
- High Liquid and Permeation Chromatography (HPLC-GPC)
- Rheometer (Rheology measurements)
- Nuclear Magnetic Resonance (NMR)
- Dynamic Light Scattering (DLS)
- Zeta Potential (Z)
- Infrared Spectroscopic ATR (FT-IR-ATR)
- Fluorescence Spectroscopy
- Plate Reader
- Nitrogen Absorbance Isotherm
- Lyophilizer Maintenance Equipment



❖ Congresses

- **As part of the organizing committee:**
 - Virtual International Symposium on Nano/Microgels. 24 April 2020, on-line.
 - European Researchers Night, Zaragoza, Spain, September 2017
Scientific work-shop for children: “Nanoscience”
- **As main author:**
 - XXXVIII Reunión Bienal RSEQ, Granada, Spain, 27 – 30 June 2022
Oral communication: “Decorating gold nanoparticles Surface with thin nanogels: A novel stabilization strategy for inorganic nanoparticles in nanomedicine”

- GEP-SLAP, San Sebastián-Donostia, Spain, 8 – 12 May **2022**
Oral communication: “Eudragits: Versatile polymers for the preparation of physical-crosslinked hydrogels with mucus adhesion. From bench to animal model assays”.
- Controlled Release Society - Virtual Annual Meeting (Las Vegas-online), 29 June – 2 July **2020**
Poster Session: “In-depth study of the influence of different Eudragit families on ophthalmic-hydrogel formulations”.
- JICI V Reunión de Jóvenes Investigadores en Coloides e Interfases. Zaragoza, Spain, 2 – 4 Marzo **2020**
Oral communication: “Gold nanoparticles as future medicines: avoiding protein corona to combat cancer with photothermal therapy”.
- 9º Encuentro de Vidas Científicas. San Sebastián, Spain, 21 October de 2019 and 4 November **2019**
Oral Communication and Poster Session: “Nanotecnología y Química: la fusión perfecta en el tratamiento de enfermedades”.
- o **As Co-author:**
- European Association for Vision and Eye Research (EVER), Valencia, Spain, 2022
Poster Session: Use of new biomaterials with amniotic membrane growth factors in corneal regeneration *in vivo*
Poster Session (2): The effect of amniotic membrane proteins released by ocular inserts containing self-healing hydrogels
- GEP-SLAP, San Sebastián-Donostia, Spain, **2022**
Oral Communication: “Viscoelastic behaviours and bioadhesion of hydrogels to optimize ophthalmic drug delivery application.”
- Materialen Zientzia eta Teknologia V. Kongresua, Bilbo, Spain **2021**
Oral Communication: “Begiaren Azaleraren Gaitzak Sendatzeko Hidrogel Birsortzaileen. Azterketa erreologikoa”
- Spanish Conference on Biomedical Applications of Nanomaterials (SBAN) on-line, **2020**

Poster Session: “Nanocomposites containing nanoparticles into hydrogels matrixes for the encapsulation and release of proteins in ophthalmic applications”



❖ **Teaching Experience**

- University Experimental session for third-year undergraduate students. Chemistry Bachelor, University of the Basque Country, September **2019**.



❖ **Co-author in project proposals that have been approved**
(Drafting and development task)

- Elkartek Program, **2019**. Basque Government, Departamento de Desarrollo Económico e infraestructura. (KK-2019/00086) “Amniogel – Biomateriales de última generación en medicina regenerativa oftalmológica”. 99.767€. (04.2019 – 12.2019). Role as researcher.
- Programa de red Guipuzcoana de Ciencia, Tecnología e Innovación, **2019**. “Programa de apoyo a la red guipuzcoana de ciencia, tecnología e innovación. – Proyectos de inversión en equipamiento e infraestructuras científico-tecnológicas avanzadas”. 45.125€. Role as researcher.
- Elkartek Program, **2019**. Gobierno Vasco, Departamento de Desarrollo Económico e Infraestructura. Proyectos de Investigación Fundamental Colaborativa. Presupuesto concedido: 77.0000€. (04.2020 – 12.2021) Role as researcher.
- Contract of collaboration with I+Med, **2019-2021**, Biotechnology for Health. Title: “Synthesis, modification and characterization of polymers for biomaterials”. 40,000€. Role as researcher.
- Ayudas a Proyectos de Investigación y Desarrollo en Salud. Departamento de Salud, Basque Government. **2020**. “Rapid and Economic Point-of-care (POC) Viral Test for the detection of SARS-CoV-2: (REPViT)”. 23,974.88€ (01.2020 – 12.2020). Role as researcher.
- Ayudas a Proyectos de Investigación y Desarrollo en Salud de Carácter Estratégico (2021333042). Departamento de Salud, Basque Government. **2021**. “Rapid and Economic Point-of-care (POC) Viral Test for the detection of SARS-CoV-2: (REPViT)”. 45,325.80€ (01.2021 – 12.2021). Role as researcher.



❖ **Additional Courses and Training**

- Basic Experience working in cell laboratories. Cell toxicity assays.
- Academic Courses:

- Manejo del Sistema HPLC Nexera Lite con detector PDA, RID y RF acoplado al colector de fracciones FRC-10A de Shimadzu, 30h, November **2021**.
- Course “A complete introduction to scientific writing in English” – October 2020 – June **2021**.
- Emulsion Polymerization Processes Course – (Fundación Polymat, **2020**)
- Fiji/ImageJ Course (University of the Basque Country) – April **2020**
- Laboratory Rules Course (University of the Basque Country, **2019**)
- Designing and building a Critical State of the Art for Research (University of the Basque Country, **2019**)
- Introduction to the structure and properties of polymers (Polymat, **2019**)
- Effective Research Communication (Universidad del País Vasco, **2019**)
- Bibliography sources course (University of Zaragoza, **2012**)
- Experience setting up a research laboratory and its maintenance (Berc Polymat; 2018 – **2022**).



❖ **Extra Skills**

- Professional experience level in several operating systems: Windows, Linus, Android, IOS, Mac OS.
- Medium-high experience in the manipulation, recovery, cleaning and maintenance of computer motherboards, data recovery.

